
**Structure/function analysis of hRme-6, a Rab5 GEF that
integrates trafficking and signalling**

Zhou Zhu

Thesis submitted for the Degree
Of Doctor of Philosophy at the
Biomedical Science Department,
University of Sheffield

September 2016

This thesis is dedicated to my parents, my grandpa and my grandma



Table of contents

Table of contents	- 1 -
List of Figures.....	- 8 -
List of abbreviations	- 11 -
Acknowledgements	- 14 -
Summary -	16 -
1. Introduction.....	- 18 -
1.1 General introduction	- 18 -
1.2 Pathways of endocytosis	- 18 -
1.3 Rab proteins	- 24 -
1.4 Rab5	- 26 -
1.5 Endocytosis and signalling.....	- 30 -
1.5.1 Endocytosis regulates Signalling.....	- 30 -
1.5.2 Singnalling regulates endocytosis	- 33 -
1.6 Ras	- 34 -
1.7 Ras and Rab5	- 35 -
1.8 Rme-6	- 37 -
1.8.1 hRme-6 and Tfn endocytosis.....	- 39 -
1.8.2 hRme-6 and EGFR endocytosis.....	- 40 -
1.8.3 Rme-6 and insulin.....	- 41 -
1.8.4 hRme-6 and signalling	- 43 -
1.8.5 hRme-6 and other Rab5 GEFs.....	- 44 -
1.9 The Sorting Nexin 9 and Sortin Nexin 24.....	- 46 -
1.10 IQ motif containing GTPase activating protein 1 (IQGAP1).....	- 47 -
1.11 The key unanswered questions about hRme-6	- 47 -
1.12 Aims and objectives of this work.....	- 48 -

2. Materials and methods	50 -
2.1 Reagents	50 -
2.2 Antibodies	51 -
2.2.1 Primary antibody.....	51 -
2.2.2 Secondary antibodies.....	52 -
2.3 Primers used.....	53 -
2.4 Common buffers.....	54 -
2.4.1 PBS.....	54 -
2.4.2 TBS.....	54 -
2.4.3 KSHM buffer	54 -
2.4.4 5XSDS gel loading buffer	55 -
2.4.5 SDS electrophoresis running buffer.....	55 -
2.4.6 Western blotting transfer buffer	55 -
2.4.7 TAE.....	55 -
2.4.8 HBS	55 -
2.4.9 4xNative PAGE sample buffer	55 -
2.4.10 Native PAGE running buffer.....	55 -
2.4.11 Native PAGE dark blue Cathode buffer.....	56 -
2.4.12 Native PAGE light blue Cathode buffer.....	56 -
2.4.13 Native PAGE Coomassie R-250 stain solution.....	56 -
2.4.14 Ponceau S stain solution.....	56 -
2.4.15 SDS trapping buffer	56 -
2.4.16 10x GAP assay nucleotide loading buffer	56 -
2.4.17 γ -P ³² GTP dilution buffer.....	56 -
2.4.18 GEF assay preloading buffer	56 -
2.4.19 GEF assay reaction buffer	57 -
2.4.20 GEF assay stop buffer	57 -

2.4.21	CK2 assay enzyme buffer	- 57 -
2.4.22	PLA assay wash buffer A	- 57 -
2.4.23	PLA assay wash buffer B	- 57 -
2.5	Molecular biology techniques	- 57 -
2.5.1	Transforming competent bacteria	- 57 -
2.5.2	Preparation of glycerol stocks of bacteria for freezing	- 58 -
2.5.3	Isolation and purification of DNA (Mini prep protocol)	- 58 -
2.5.4	Purification of DNA (Maxi prep protocol)	- 59 -
2.5.5	DNA Agarose gel electrophoresis	- 59 -
2.5.6	Purification of DNA from agarose gels	- 60 -
2.5.7	Restriction enzyme digests	- 60 -
2.5.8	DNA ligation	- 60 -
2.6	Mammalian cell culture techniques	- 61 -
2.6.1	Culture conditions	- 61 -
2.6.2	Mammalian cell transfection strategies	- 61 -
2.7	Insect cell culture techniques	- 62 -
2.7.1	Sf21 cell Culture	- 62 -
2.7.2	Baculovirus infection of Sf21 cells	- 62 -
2.8	Protein techniques	- 62 -
2.8.1	Bradford assay	- 62 -
2.8.2	SDS-polyacrylamide gel electrophoresis	- 63 -
2.8.3	Coomassie blue staining of gels	- 63 -
2.8.4	Immunoblotting	- 63 -
2.8.5	Bis-Tris Native PAGE electrophoresis	- 64 -
2.8.6	Coomassie staining of native PAGE	- 64 -
2.8.7	Native PAGE western blot	- 64 -
2.9	Protein purification	- 65 -

2.9.1	Purification of GST fusion proteins.....	65 -
2.9.2	Purification of GST-Rab5 protein.....	66 -
2.9.3	Purification of his-SNX9 and his-SNX24 proteins from bacteria.....	66 -
2.9.4	Purification of Flag-hRme-6 from insect cells and HEK293 cells	67 -
2.10	Immunoprecipitation	68 -
2.11	In-vitro Ras GTPase stimulating assays (GAP assay).....	68 -
2.12	In-vitro GEF assay	69 -
2.13	Gel filtration	70 -
2.14	Electron Microscopy.....	70 -
2.14.1	Electron Microscopy hardware.....	70 -
2.14.2	Negative staining.....	71 -
2.15	Fluorescence Microscopy.....	72 -
2.15.1	Coverslip preparation	72 -
2.15.2	Preparation of paraformaldehyde.....	72 -
2.15.3	Immunofluorescence protocol.....	72 -
2.16	Proximity ligation assays	73 -
2.17	Mass spectrometry.....	74 -
2.17.1	Gel fragment preparation and destaining.....	74 -
2.17.2	Reduction and Alkylation	74 -
2.17.3	Trypsin Digestion	75 -
2.17.4	Peptide recovery and solid phase extraction	75 -
3.	Chapter 3 Exploration of the functional domains of hRme-6.....	77 -
3.1	Introduction.....	77 -
3.2	Investigating the GAP domain of hRme-6 Ras GAP activity	78 -
3.3	Investigating hRme-6 Rab5 GEF activity.....	80 -
3.4	hRme-6 may interact with phosphorylated p42/44.....	83 -
3.5	Overexpression Flag-hRme-6 in HeLa cells affects EGF signalling-	86

-

3.6	CK2 but not non-phosphorylated p42/44 can phosphorylate hRme-6.....	- 88 -
3.7	In HeLa cells treated with a CK2 inhibitor, phosphorylation of p42/44 increases while the phosphorylation of Akt decreases during EGF stimulation	- 89 -
3.8	Discussion.....	- 91 -
3.8.1	Analysis of the activities of hRme-6	- 91 -
3.8.2	Identification of the function of hRme-6 in signal transduction	- 92 -
3.8.3	Phosphorylation of hRme-6 by CK2.....	- 93 -
4.	Chapter 4 Structural studies on hRme-6.....	- 95 -
4.1	Introduction.....	- 95 -
4.2	hRme-6 exists in an SDS resistant form.....	- 97 -
4.3	hRme-6 can assemble into oligomeric structures in cells.....	- 99 -
4.4	Gel filtration shows that hRme-6 exists in multimeric forms ...	- 100 -
4.5	Native gels reveal two higher molecular weight conformations of hRme-6.....	- 104 -
4.6	Native gels confirmed that hRme-6 exists in multimers in HeLa cells	- 105 -
4.7	Mass spectrometry analysis of hRme-6 multimers.....	- 107 -
4.8	Sec-malls experiment estimate the molecular weight of hRme-6 monomers	- 110 -
4.9	Gel filtration separates the 720 and 480 KD conformations of Flag-hRme-6 purified from insect cells	- 111 -
4.10	Negative staining reveals the basic shape of hRme-6.....	- 114 -
4.11	Single particle reconstruction of the structure of hRme-6	- 117 -
4.12	Nanogold labeling of His-hRme-6	- 122 -
4.13	Domain interaction test	- 126 -
4.14	CK2 inhibition changes the conformation of hRme-6 in EGF stimulated HeLa cells.....	- 128 -
4.15	Discussion.....	- 129 -

4.15.1	hRme-6 forms multimers in vitro and in vivo	- 129 -
4.15.2	Determination of the size of hRme-6 monomers.....	- 130 -
4.15.3	Rme-6 exists in several multimeric forms	- 132 -
4.15.4	Towards an EM reconstruction of hRme-6.....	- 135 -
4.15.5	The domain interaction test.....	- 138 -
4.15.6	Benefits of a multimeric structure	- 138 -
5.	Chapter 5 Identification of interacting partners of hRme-6	- 140 -
5.1	Introduction.....	- 140 -
5.2	SILAC experiments to identify proteins that interact with hRme-6 ...- 141 -	
5.3	Mass Spectrometry data further analysis	- 148 -
5.4	Verification of mass spectrometry 'hits' by in vitro binding assays ...- 155 -	
5.4.1	Interaction test between hRme-6 and SNX24.....	- 156 -
5.4.2	Interaction test between hRme-6 and SNX9	- 158 -
5.4.3	Interaction test between hRme-6 and IQGAP1.....	- 160 -
5.5	Validation of the mass spectrometry 'hits' in cells	- 163 -
5.6	Proximity ligation assay to validate hRme-6 interactions in cells.- 165 -	
5.6.1	PLA assay between hRme-6 and SNX9	- 167 -
5.6.2	PLA assay between hRme-6 and CIP4	- 169 -
5.6.3	PLA assay between hRme-6 and IQGAP1.....	- 171 -
5.6.4	PLA assay to test the interaction between cargo receptors and hRme-6. ...- 173 -	
5.6.5	The interaction between CIP4 and EGFR is enhanced following overexpression of Flag-hRme-6.....	- 178 -
5.7	Discussion.....	- 182 -
5.7.1	SILAC experiment to find the interaction partners of hRme-6.....	- 182 -
5.7.2	The interaction between hRme-6 and SNX24	- 185 -

5.7.3	The interaction between hRme-6 and SNX9	- 185 -
5.7.4	The interaction between hRme-6 and CIP4.....	- 186 -
5.7.5	The interaction between hRme-6 and IQGAP1	- 187 -
5.7.6	The interaction between hRme-6 and receptors	- 189 -
6.	Chapter 6 Conclusion and future perspectives	- 192 -
6.1	Discussion.....	- 192 -
6.2	Future perspectives.....	- 196 -
7.	References	- 198 -

List of Figures

Figure 1.1 Multiple Endocytic trafficking pathways

Figure 1.2 Rabs switch and its circuitry

Figure 1.3 hRme-6 structure and comparison with Rabex-5

Figure 1.4 Predicted structure of hRme-6

Figure 1.5 hRme-6 regulate p38 and p42/44 signalling

Figure 3.1 Purification of GST-hRme-6-GAP domain and GST-Ras from *E.coli*

Figure 3.2 Ras GAP domain of hRme-6 exhibits GAP activity

Figure 3.3 purified Flag-hRme-6 from insect cells and GST-Rab5 from *E.coli*

Figure 3.4 hRme-6 exhibit GEF activity

Figure 3.5 hRme-6 binds phosphorylated p42/44 MAPK

Figure 3.6 Levels of hRme-6 affect phosphorylation of Akt and p42/44 MAPK

Figure 3.7 CK2 but not p42/44 MAPK phosphorylated hRme-6

Figure 3.8 CK2 inhibition altered signalling in EGF stimulated HeLa cells

Figure 4.1 Hypothesis I for the structure/function relationship of hRme-6

Figure 4.2 Hypothesis II for the structure/function relationship of hRme-6

Figure 4.3 hRme-6 exists in SDS resistant form

Figure 4.4 hRme-6 forms multimers in cells

Figure 4.5 hRme-6 exists in multimeric forms

Figure 4.6 Overexpressed HA-tagged hRme-6 exists as a higher order oligomer

Figure 4.7 Different conformations of hRme-6 show different SDS resistance

Figure 4.8 hRme-6 exists in multimeric forms

Figure 4.9 Endogenous hRme-6 exists in a higher molecular weight conformation in HeLa cells independent of EGF stimulation

Figure 4.10 Endogenous hRme-6 appears as a lower molecular weight conformation following freezing of HeLa cell lysates

Figure 4.11 hRme-6 elution profile and peak positions in sec malls experiment

Figure 4.12 Gel filtration separates different conformations of hRme-6

Figure 4.13 Negative staining for of different conformations of hRme-6

Figure 4.14 Direct alignments of all the particles

Figure 4.15 A selection of the final images used to reconstruct the structure of hRme-6

Figure 4.16 A reconstruction of hRme-6

Figure 4.17 Purified Flag-hRme-6 and Flag-hRme-6-his from HEK cells

Figure 4.18 Ni-NTA-Nanogold labeling of hRme-6

Figure 4.19 The GEF domain of hRme-6 can interact with full length HA-hRme-6

Figure 4.20 Inhibiting CK2 changes the conformation of hRme-6 in EGF stimulated HeLa cells

Figure 5.1 different cell lysis buffers led different protein extraction efficiency

Figure 5.2 Triple labeling SILAC experiment protocol

Figure 5.3 Protein ratio distributions in M/L and H/L

Figure 5.4 Protein ratio distribution of H/M following triple label SILAC experiment

Figure 5.5 Purification of His- SNX24 from *E.coli*

Figure 5.6 His-SNX24 and Flag-hRme-6 interact directly in vitro

Figure 5.7 Purification of His- SNX9 from *E.coli*

Figure 5.8 His-SNX9 and Flag-hRme-6 directly interact in vitro

Figure 5.9 Purification of GST and GST-IQGAP1 from *E.coli*

Figure 5.10 GST-IQGAP1 and Flag-hRme-6 interact in vitro

Figure 5.11 Immunofluorescence shows that SNX9, CIP4 and hRme-6 were largely cytoplasmic following overexpression.

Figure 5.12 PLA assay primary antibody control test

Figure 5.13 PLA assay tested an in vivo interaction between hRme-6 and SNX9

Figure 5.14 PLA assay tested the in vivo interaction between hRme-6 and CIP4 in Tfn incubation and EGF stimulation

Figure 5.15 PLA assay tested the in vivo interaction between hRme-6 and IQGAP1 in Tfn

incubation and EGF stimulation.

Figure 5.16 Quantification of the PLA assay signal between hRme-6 and IQGAP1 in Tfn

incubation and EGF stimulation.

Figure 5.17 PLA assay tested the in vivo interaction between hRme-6 and TfnR following different times of serum starvation during uptake of Tfn

Figure 5.18 Quantification of the PLA assay signal between hRme-6 and TfnR in Tfn incubation

Figure 5.19 PLA assay tested the in vivo interaction between hRme-6 and EGFR

Figure 5.20 Quantification of the PLA assay signal between hRme-6 and EGFR in EGF stimulated HeLa cells

Figure 5.21 PLA assay tested the in vivo interaction between hRme-6 and CIP4, TfnR, EGFR in HeLa cells, overexpressing hRme-6.

Figure 5.22 PLA assay tested the in vivo interaction between hRme-6 and nup98.

List of tables

Table 2.1 Primary antibodies used in this project

Table 2.2 Secondary antibodies used in this project

Table 4.1 proteins found in the two bands around 480 KD and 720 KD

Table 5.1 Protocol for double-labeling SILAC experiments

Table 5.2 potential candidate selected from Mass Spectrometry data in experiment 1 and experiment 2

Table 5.3 Triple labeling SILAC cell treatment

Table 5.4 potential candidates sensitive to EGF stimulation selected from Mass Spectrometry

Table 5.5 potential candidates sensitive to CK2 inhibitor selected from Mass Spectrometry data

List of abbreviations

Å	Angstrom (1×10^{-10} metres)
AP	adaptor protein
ATP	adenosine triphosphate
ATPase	adenosine triphosphatase
BSA	bovine serum albumin
CCV	clathrin-coated vesicle
<i>C.elegans</i>	<i>Caenorhabditis elegans</i>
CIP4	Cdc42-interacting protein 4
DMEM	Dulbecco's minimum essential medium
DTT	dithiothreitol
ECL	enhanced chemiluminescence
<i>E.coli</i>	<i>Escherichia coli</i>
EDTA	ethylenediaminetetraacetic acid
EE	early endosome
EEA1	early endosome antigen 1
EGF	Epidermal growth factor
EGFR	Epidermal growth factor receptor
EM	electron microscopy
GAP	guanosine triphosphatase activating protein
GEF	guanine nucleotide exchange factor

GTP	guanosine 5'-[γ -thio] triphosphate
GPCR	G protein-coupled receptors
HEPES	<i>N</i> -2-hydroxyethylpiperazine- <i>N'</i> 2-ethanesulphonic acid
HBS	Hanks buffered salts
HRP	horseradish peroxidase
IgG	immunoglobulin G
IPTG	isopropyl- β -D-thiogalactopyranoside
IQGAP1	IQ Motif Containing GTPase Activating Protein 1
LB	Luria-Bertani
mol	moles
PBS	phosphate-buffered saline
PCR	polymerase chain reaction
PMSF	Phenylmethanesulfonyl fluoride
PH	pleckstrin homology
SDS	sodium dodecyl sulphate
SDS-PAGE	sodium dodecyl sulphate polyacrylamide gel electrophoresis
SNX9	Sorting Nexin 9
SNX24	Sorting Nexin 24
TBS	tris-buffered saline
PVDF	polyvinylidene difluoride
CK2	Casein kinase 2

Akt

Protein kinase B

Acknowledgements

I would like to deeply thank my supervisor Liz Smythe for her outstanding guidance and support, her patience, trust and confidence in my capabilities and enthusiastic support during my study.

This thesis would also have not been possible without funding from the Centre for Membrane Interactions and Dynamics, University of Sheffield.

I am grateful to my advisors, Andrew Peden and Kathryn Ayscough, for their critical thinking and valuable feedback.

For providing me with insight and technical experience, I would like to thank all the past and present members of the Smythe lab for their invaluable advice and work discussions. I particularly thank Dr Filipe Ferreira, not only for his work in hRme-6, but for taking time to teach me so many of the skills I now possess. I thank Dr David Turton for his help in the experiment techniques. I thank Dr Richard Beniston and Dr Mark Collins for the support in mass spectrometry. I would also like to thank Dr Svet Tsokov, Chris Hill, Professor Per Bullough for the assistance in working in Electron Microscopy and Dr Darren Robinson in the Light Microscope Facility for their generosity and expertise.

Finally, it is a pleasure to thank my parents for their great understanding and encouragement on my work. I am eternally grateful to Jun for his unconditional support and love.

衷心的感谢一直支持我的导师伊丽莎白·史密斯，衷心感谢她对我的谆谆教诲和悉心关怀，精髓的学术造诣，严谨勤奋的治学风格，都让我永志不忘，深刻影响着日后的工作和生活。衷心感谢学院其他老师给予我的帮助。衷心感谢各位同门师兄弟。衷心感谢一直给予我支持的爸爸妈妈。感谢与我相茹以沫的王骏

对我的支持。

Summary

There is increasing understanding that endocytosis and signalling are linked to each other. Signalling receptors are particularly interesting as cargoes which are precisely regulated through the process of endocytosis. However it is still not clear that how the overlap between endocytosis and signalling occurs mechanistically.

Rme-6, a Rab5 GEF, is a potential candidate that is involved in the endocytosis of transferrin and EGFR and also the signalling pathway of Ang1-Tie2. The objective of this thesis was to investigate the structure/function relationship of hRme-6 to understand how it integrates trafficking and signalling processes.

Initially I confirmed the RasGAP activity of RasGAP domain of hRme-6 and the Rab5GEF activity of Flag-hRme-6 purified from insect cells. I then explored the function of hRme-6 in an Ang1-Tie2 model in HUVECs and an EGF-EGFR model in HeLa cells. I demonstrated that hRme-6 specifically interacted with phosphorylated p42/44 in Ang1 stimulated HUVECs and that overexpression of hRme-6 in EGF stimulated HeLa cells also changed the signalling output.

In a second approach, I investigated the structure of hRme-6, showing by a variety of approaches that recombinant hRme-6 exists as two different multimeric conformations while endogenous hRme-6 in HeLa cells mainly exists as one higher molecular weight species. The higher multimer of Flag-hRme-6 was then separated through gel filtration and the structure of hRme-6 was reconstructed through negative staining combined with Imagic-5 software. Using this approach, the surface structure of hRme-6 was revealed.

Thirdly I explored the function of hRme-6 through investigating the interaction partners of hRme-6 through SILAC experiments based on EGF stimulated HeLa cells. I successfully found several interaction partners of hRme-6, including SNX9, SNX24, IQGAP1 and CIP4. These potential candidates all showed direct interactions with

hRme-6 in vitro. CIP4 and IQGAP1 also showed in vivo interactions with hRme-6 while the interaction between IQGAP1 and hRme-6 was differentially regulated by cargo uptake.

My data provided important insight into the structure and binding partners of hRme-6.

1. Introduction

1.1 General introduction

Endocytosis was originally defined as a simple, fundamental process that delivers nutrients or other molecules that cannot pass through the plasma membrane into the cell. However, the role of endocytosis extends well beyond this. It involves almost all aspects of the relationships of the cell with the extracellular environment as well as intracellular communication, including integration of information—and movement of material within the cell. It is a pathway often used by pathogens for cellular entry [1].

Endocytosis is linked to all aspects of cell life through the organisation of cellular signalling, which provides real-time information to cells about the nature of their environment. Plasma membrane receptors deliver the extracellular message to the interior of the cells and the signal cascades, activating the corresponding physiological response. The balance between trafficking and signalling must therefore be tightly controlled through the endocytic compartments in order to achieve the appropriate cellular response [2].

1.2 Pathways of endocytosis

The functions of endocytosis are achieved by the diversity of pathways, which allows internalisation and different mechanisms of cargo sorting inside cells.

According to the size of the initial membrane invagination, endocytosis can be classified into six groups (Figure 1.1). Large invaginations of membrane into phagosomes and macropinosomes is referred to as phagocytosis and macropinocytosis. Phagocytosis mainly refers to large particles (>500 nm), including pathogens and apoptotic cells[3], while macropinocytosis (0.2-10 μm) relates to

non-selective fluid uptake including solute molecules, nutrients and antigens which initialises from surface membrane ruffles[4]. These two processes are guided by actin filament remodeling but not dynamin filament remodeling. Conversely, small invaginations (<200 nm) relate to micropinocytosis, which can be further divided into clathrin-mediated endocytosis (CME) and clathrin-independent endocytosis (CIE)[2].

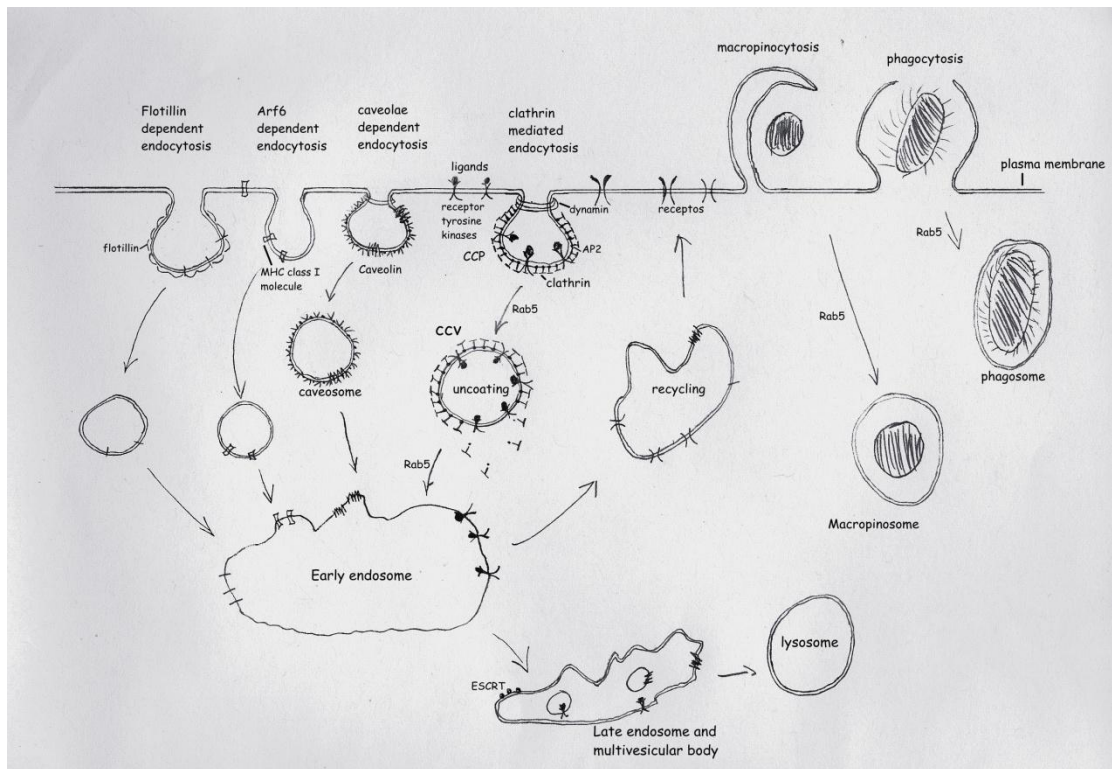


Figure 1.1 Multiple Endocytic trafficking pathways. Many different mechanisms are available for cargoes to enter the cell by. There is evidence for at least seven pathways, including phagocytosis, macropinocytosis, clathrin-mediated endocytosis, caveolae-, ADP-ribosylation factor 6(Arf6)-, flotillin-dependent endocytosis and fast endophilin-mediated endocytosis (not shown).

Clathrin-mediated endocytosis is the canonical and best-described endocytic route. It involves the internalisation of cargo by endocytic vesicles coated with the protein clathrin [2, 5]. Clathrin functions by its triskelion-shaped conformation polymerising around the cytoplasmic face of membrane and vesicles [6, 7]. During the formation of

clathrin-coated vesicles, several stages can be defined.

The initiation of clathrin-mediated endocytosis starts with the assembly of the coated pits which are specialised sites in the plasma membrane where clathrin polymerises[8]. Clathrin is unable to bind directly to membranes and so the adaptor protein 2 (AP2) forms a bridge between clathrin and cargo. Clathrin-coated pits begin to form when one clathrin and two AP2 molecules bind to an area of the plasma membrane enriched in phosphatidylinositol-4, 5-bis phosphate (PIP₂)[9]. Phosphatidylinositol-4-kinase (PI4K) and phosphatidylinositol-4-phosphate-5-kinase (PI4P5K) catalyse the formation of PIP₂ from phosphoinositide [10, 11]. Pit formation proceeds by adding clathrin triskelions, adaptors and receptors to the edge of the pits. The binding of clathrin and cargo also leads to the activation of AP2, which is autoinhibited when the level of PIP₂ or cargo is low [12, 13]. Cargo molecules are recruited to coated the pits through the interaction of specific targeting sequences in their cytoplasmic tails with adaptor proteins [14, 15] and they in turn stabilise the forming clathrin-coat nucleation complexes [16, 17].

With the accumulation of adaptor proteins on the lipid layer, more clathrin triskelia are recruited to the pit. The propagation of the clathrin lattice, combined with the internal stress leads to increased curvature and invagination of the membrane [18, 19]. As the clathrin-coated pits grow, the concentration of cargo increases in the pits. During this process, the α -adapitin subunit of the AP2 complex mediates recruitment of accessory proteins which include other adaptor proteins, regulatory proteins such as kinases and curvature sensing proteins, like the Bin/amphiphysin/Rvs (Bar) domain-containing proteins, such as sorting nexin 9 (SNX9) and amphiphysin-1. Phosphatidylinositol-3, 4-bisphosphate (PI (3, 4) P₂) is also catalysed by phosphatidylinositol-3-kinase C2 α (PI (3) K C2 α) and this allows the selective recruitment of SNX9 [20]. SNX9 and amphiphysin-1 can stabilise the membrane curvature, bind both clathrin and AP2, and recruit dynamin to the neck of the budding vesicle [21-24].

The final step in clathrin-coated pit formation is to pinch off the budding pit. Lots of proteins, like myosin and WASP, all have been discovered to play important roles in the invagination and stabilisation of clathrin-coated pits [25-27]. The major role in pit maturation is played by dynamin. Dynamin exists as a tetramer[28] and further self assembly into higher oligomers on the necks of invaginated pits[29, 30]. The self-assembled dynamin oligomers create force, compressing the membrane tubule and finally leading to scission [31]. SNX9 was also discovered to stimulate dynamin's GTPase activity and induce dynamin self-assembly[32].

Following scission, the PIP₂ level is decreased due to the 5' lipid phosphatases [33]. After scission, phosphatidylinositol 3-phosphate (PI (3) P) then becomes the dominant phosphoinositide in early endosomes which is generated by class III PI3K Vps34 complex II and class II PI3Ks [34-39].

Soon after the budding, the clathrin-coated vesicle is quickly uncoated by removing the clathrin cage from the vesicle surface by the heat shock cognate 70 KD proteins (Hsc70) [40]and auxilin2 (cyclin-G-associated kinase, GAK) [41]to enable the fusion of the vesicles with the target membrane and also regulate recycling of coat components[42, 43]. In this process, one auxilin binds to one clathrin triskelion which causes further binding of three Hsc70-ATP molecules. Next, Hsc70-ATP hydrolysis catalysed by auxilin leads to the dissociation of the clathrin triskelion from the vesicle and leaves the free clathrin triskelion bound to Hsc70-ADP [44, 45]. The released vesicles are then transported along cytoskeletal networks to different early endosome populations[46].

Clathrin-coated vesicles then fuse with early endosomes [47-50]. Early endosomes have an acidic internal environment (pH~6) due to H⁺ ATPase pumps in the endosomal membrane[51]. The acidic environments help the release of cargo from receptors or carrier proteins [52]. Cargo proteins are further sorted at early endosomes to be recycled back to the cell surface, or delivered to the multivesicular body (MVB) pathway and lysosomes for degradation[53]. Delivery of material to the MVB requires

the activity of the endosomal sorting complexes required for transport (ESCRT) proteins (Figure 1.1).

Signalling receptors, for example most receptor tyrosine kinases (RTKs) and many G protein-coupled receptors (GPCRs), are internalised by clathrin-mediated endocytosis. During this process, ligand binding increases the recruitment of receptor to clathrin-coated pits through adaptors, such as AP-2 and β -arrestins. Clathrin then polymerises, which drives invagination of the pits which are then released to the cytoplasm through the function of the large molecular weight GTPase, dynamin[54]. However, receptor-mediated endocytosis can also be constitutive. In the constitutive process, receptors are constantly internalised, sorted in the endosome and then recycled back to the cell surface[55].

Compared to CME, CIE is not sensitive to clathrin depletion but is often sensitive to cholesterol depletion. There are several routes of clathrin-independent endocytosis which have been identified, including caveolae-, ADP-ribosylation factor 6(Arf6)-, and flotillin-dependent endocytosis, and fast endophilin-mediated endocytosis (FEME).

Caveolae are flask-shaped invaginations of the plasma membrane first found in endothelial cells [56-58]. Later caveolae were found in many cell types and are especially abundant in smooth muscle, fibroblasts and adipocytes. Caveolae-dependent endocytosis could be affected by overexpression of dynamin or disrupting actin assembly[59]. The abundance of caveolae in cells experiencing mechanical stress led to the finding that caveolae act as membrane stores that can be mobilised when cells need to increase the surface area of the plasma membrane [60, 61].

Arf6 is a small molecular weight GTPase that is found at the plasma membrane and at endosomal compartments. Arf6 forms vesicular and tubular structures to mediate the internalisation of CD59, CD55, and MHC class I proteins, and GLUT1[62]. Like other GTPases, Arf6 cycles between its active GTP-bound and inactive GDP-bound

conformations to regulate ligand internalisation and endosomal recycling. Arf6 in its GTP conformation is required for ligand internalisation and recycling. It was also found that Arf6-GTP is associated with clathrin-coated pits at the plasma membrane via a requirement for the adaptor protein AP2 [63]. Arf6 could further recruit JNK-interacting protein 3 and 4 (JIP3 and JIP4) after clathrin uncoating to regulate a fast recycling pathway. After internalisation, membrane-associated Arf6 is recycled back to the cell surface.

Flotillin-dependent endocytosis is involved in the uptake of GPI-anchored proteins: cholera toxin B subunit, cationic molecules and polyplexes, proteoglycans and proteoglycan bound ligands. Flotillin-dependent endocytosis is achieved by the ubiquitous and conserved flotillin proteins, flotillin-1 and flotillin-2 [64]. Flotillin-1 and flotillin-2 bind to each other, form higher order oligomers in the plasma membrane and define specific microdomains. The microdomains created by flotillins are detergent-resistant and can directly bud into the cell [65, 66]. However, Flotillins are also found to form higher order oligomers to recruit transmembrane proteins, like dopamine transporters, into flotillin rafts for pre-endocytic clustering. Cargo then can be internalised without direct involvement of flotillins [67].

Fast endophilin-mediated endocytosis triggers the invagination of the membrane into tubular structures. Then endophilin, dynamin and actin regulate the tubule to form vesicles [68, 69]. This pathway is involved in the uptake of several GPCRs such as α 2a- and β 1-adrenergic, RTKs such as EGFR and HGFR, and the interleukin-2 receptor. It mainly happens at the leading edges of the cell, and also involves the formation of PI (3, 4) P₂ from PI (3, 4, 5) P₃ by SH2 containing inositol 5-phosphatase 1 (SHIP1) and SH2 containing inositol 5-phosphatase 2 (SHIP2).

After internalisation, by either clathrin-mediated endocytosis or clathrin-independent endocytosis, internalised cargoes are routed to early endosomes, and then different cargoes are sorted to different fates: transported to the Golgi, recycled back to the plasma membrane or degraded in the lysosome.

During these processes, the small GTPase, Rab superfamily, plays important roles in the different sorting fates of cargoes.

1.3 Rab proteins

Though the different pathways of endocytosis each are regulated by their own specific factors, they all involve Rab GTPases which are recruited and involved in the process of endocytosis[70].

Rab proteins belong to the Ras superfamily of small GTPases. Like other small GTPases, they function as molecular switches. Rabs cycle between an inactive (GDP-bound) and an active (GTP-bound) state, regulated by GTPase-activating proteins (GAPs) that promote GTP hydrolysis and guanine nucleotide exchange factors (GEFs) that promote exchange of GDP for GTP(Figure 1.2)[71].

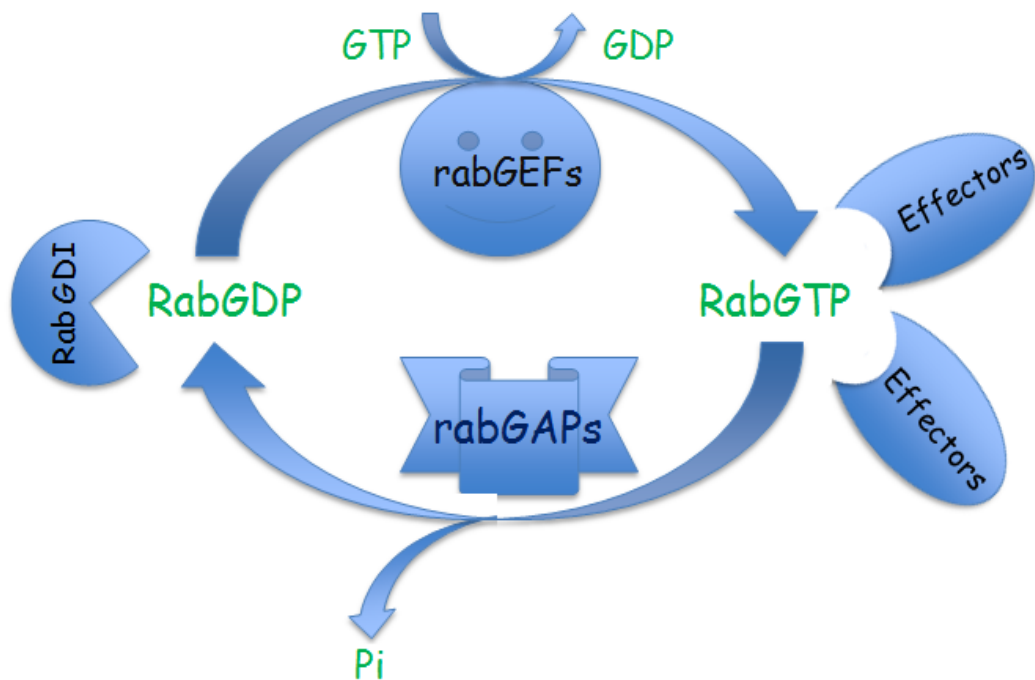


Figure 1.2 Rabs switch and its circuitry. RabGEFs catalyse the exchange of GTP for GDP-bound Rab. The active Rab is recognised by multiple effectors and is converted back to a GDP-bound form by a RabGAP (GTPase activating protein). The GDP-bound Rab is kept soluble by Rab GDP dissociation inhibitor (GDI) [72, 73].

Rab GTPase cycles through a soluble cytoplasmic pool and a membrane-associated pool. Rab proteins in their GDP conformation stay in the cytoplasm through association with Rab GDP dissociation inhibitor (GDI). RabGDI with the help of GDI-displacement factor[74] and Rab GEFs [75] serve to target the Rab-GDP to specific intracellular membranes. The membrane bound Rab-GDP is then converted to Rab-GTP by Rab GEFs. The activated Rab proteins can then interact with specific effector molecules. Over 80 different Rab effectors have been found, including sorting adaptors, tethering factors, kinases, phosphatases and motors, to regulate the trafficking process[76-78]. Conversely, Rab GAPs are thought to control the lifetime of the activated state of Rabs.

Due to the diverse range of Rab effectors and the distinct membrane localisation of different Rab proteins, Rab GTPases control specific membrane trafficking processes, including cargo binding during vesicle formation, driving interaction between motor proteins with membranes, regulating vesicle fusion and vesicle transport[79]. For example, Rab5, the first mammalian Rab protein identified, plays important roles in early endocytic pathways including endosome fusion, vesicle targeting, uncoating and signalling, which will be further described in the next section. Rab7 functions following those of Rab5, mainly in late endosomes and lysosomes. As a late endosome marker, it affects early-to-late endosome and late endosome-to-Golgi transport and also lysosome biogenesis [80-82]. Recent studies found that the roles of Rab7 also involved selective sorting of distinct cargoes at early endosomes [83, 84]. Rab4 and Rab11 are localised to recycling endosomes, which regulate the return of cargo to the cell surface with Rab4 regulating a fast recycling pathway and Rab 11 a slower one. Rab4 dependent cargo includes recycling integrins, receptor tyrosine kinases and also GPCRs.

As endocytosis impacts diverse cellular functions, Rab GTPases act not only as regulators of trafficking, but also directly or indirectly affect cell signalling, migration, cell division, cell polarity and even disease.

1.4 Rab5

The small GTPase, Rab5 is a 25 KD protein that is located at early endosomes and the plasma membrane [85].

Rab5 was originally found to target plasma-membrane-derived vesicles to endosomes and to be in charge of fusion between endosomes [47, 48]. It modulates the half-life of CCVs on the plasma membrane and is directly involved in the fusion of uncoated vesicles with early endosomes (EE) and the fusion between EE[48]. In BHK and HeLa cells the expression of Rab5^{Q79L} (constitutively active form) leads to a dramatic cell morphology change with the appearance of unusually large early endosomes. Expression of Rab5^{Q79L} also increases the internalisation of transferrin and decreases recycling. Cytosol prepared from cells overexpressing Rab5^{Q79L} greatly increase endosome fusion in vitro. However, overexpression of the dominant negative mutant, Rab5^{S34N}, leads to the formation of very small endocytic vesicles and inhibits transferrin endocytosis. Rab5^{S34N} also inhibits fusion between early endosomes in vitro[86]. These studies further suggested that the control of Rab5 activity is the rate-limiting step for early endocytosis. Later it was found that Rab5 also mediates the formation of clathrin-coated pits in the plasma membrane[87].

Rab5 achieves its functions by binding to many different interacting proteins. For example, the Rab5 effector Rabaptin-5 interacts with Rab5-GTP and is also essential for endosome fusion[88]. Rabex-5, a Rab5 GEF, forms a tight complex with Rabaptin-5 to stabilise Rab5 in its GTP conformation[89] and is also required for endosome fusion[90]. EEA1 is another Rab5 effector that functions in the endosome docking and

fusion process. It is a long coiled-coil molecule that is thought to tether endocytic vesicles to the endosomal membrane. EEA1 also binds to phosphatidylinositol-3-phosphate (PI3P) [91, 92], which is specifically on the early endosome. PI (3) Ks regulate the recruitment of EEA1 to early endosome membranes, which then leads to the binding of EEA1 to activated Rab5 and directs the transport of CCV to EE.

The function of Rab5 extends far beyond control of endosomal fusion. The identification of over 20 proteins that bind specifically to Rab5-GTP suggested that Rab5 has a wider regulatory role than previously imagined[93]. Later Rab5 was confirmed as a key regulator of the early endocytic pathway. Rab5 not only controls vesicle formation, and endosomal fusion but also controls phosphoinositide synthesis, affects protein sorting within endosomes, regulates motility of early endosomes and affects signalling intensity.

Regarding the phosphoinositide synthesis, Rab5 was found to interact with two PI 3-kinases (Vps3 and PI3K β) and also interacts with PI5- and PI4-phosphatases (PI5-Pase, PI4-Pase). The interaction of PI5-Pase and PI4-Pase with Rab5 could stimulate their activities and the siRNA of the two phosphatases inhibited Tfn uptake in HeLa cells [94].

Rab5 is involved in endosome protein sorting through the Rab5 effector Rabenosyn-5 by regulation of membrane tethering/fusion in early endosomes[95]. However Rabenosyn-5 not only interacts with Rab5 but also Rab4, which regulates rapid recycling. Overexpression of Rabenosyn-5 in A431 cells increase the co-localisation between Rab5 and Rab4, and in these cells there is faster recycling of Tfn from early endosomes to the cell surface [96]. It is suggested that Rabenosyn-5 works as a dual Rab effector to regulate protein sorting and recycling.

Rab5 also regulates the interaction between endosomes and microtubules. Rab5-positive endosomes move on microtubules in vivo and an in vitro assay found

that Rab5 directed early endosome movement toward the minus ends of microtubules through the involvement of PI (3) K kinase hVPS34[49]. Another Rab5 effector HTT-associated protein 40 (HAP40) mediates the recruitment of Huntingtin (HTT) onto early endosomes. Overexpression of HAP40 in HeLa cells significantly inhibited early endosomal motility through transferring the early endosomes from microtubules to the actin network [97].

During insulin stimulation, glucose transporter isoform 4 (GLUT4) is translocated from intracellular membrane compartments to the cell surface by an increase of GLUT4 exocytosis and inhibition of endocytosis. In 3T3-L1 cells, Rab5 was constantly associated with the motor protein dynein. The decrease of GLUT4 endocytosis was achieved by the inhibition of Rab5 activation and dissociation of dynein from microtubules by microinjection of anti-Rab5 or anti-dynein antibody [98].

The relationship between Rab5 and signalling control came originally from the finding that Rab5a was strongly phosphorylated by ERK1[99]. Overexpression of Rab5^{S34N} in NR6 cells greatly reduced EGF induced cell growth and activation of the Raf-MEK-p42/44 pathway while overexpression of Rab5^{WT} or Rab5^{Q79L} enhanced the activation of Raf-MEK-p42/44[100].

The relationship between Rab5 and signalling was further confirmed by studies on the Rab5 effector adaptor protein, phosphotyrosine interacting with PH domain and leucine zipper 1 (APPL1) and adaptor protein, phosphotyrosine interacting with PH domain and leucine zipper 2 APPL2[101]. APPL1 and APPL2 are primarily located in the cell cytoplasm and on endosomes underneath the plasma membrane with little proximity to the nucleus. APPL1 and APPL2 specifically bind Rab5-GTP. Following serum starvation, APPL1 wholly remains in the cytoplasm. However, EGF stimulation leads to the translocation of APPL1 from the cytoplasm to the nucleus accompanied by Rab5 GTP hydrolysis. The nuclear translocation of APPL1 leads to cell proliferation through the interaction between APPL and metastasis associated protein MTA2, RbAp46 (components of nucleosome remodeling) and histone deacetylase

(NuRD/MeCP1 complex). The function of APPL1 was confirmed in zebrafish development[102]. It was found that APPL1 regulates Akt activity and is required for cell survival as the depletion of APPL1 in fish strongly diminishes Akt activity and induces apoptosis. Remarkably, the function of APPL1 is based on its endosomal localisation.

Rab5 in its GTP form recruits many factors to promote the early endocytic process. However it is essential that Rab5 cycles back to its GDP conformation as overexpression of constitutively active Rab5^{Q79L} leads to giant endosomes. RN-tre was found as a Rab5 GAP protein, the overexpression of which inhibited both EGFR and Tfn endocytosis [103, 104]. However the specificity of RN-Tre for Rab5 was subsequently challenged and it was suggested that it is actually a GAP for Rab41, with RabGAP-5 fulfilling the role of GAP for Rab5 on the endocytic pathway (Haas et al., Nat Cell Biol 2005).

The function of Rab5 was also confirmed by an animal model. Depletion of all Rab5 isoforms in mouse liver severely damaged the endocytic system. Loss of Rab5 leads to a significant decrease in the numbers of early endosomes, late endosomes and lysosomes. It also blocks the endocytosis of low density lipoprotein and damages the delivery of apical protein to bile canaliculi, which implies a function for Rab5 in cargo sorting in polarised cells [105].

Although Rab5 contributes to endocytosis in the plasma membrane, few Rab5-interacting proteins were found to localise at the plasma membrane[106]. The *C.elegans* Rme-6 is a novel Rab5 GEF localised to the plasma membrane, which acts on clathrin-coated vesicles, and which has been identified as a likely candidate to integrate endocytic trafficking and signalling pathways.

1.5 Endocytosis and signalling

Cell signalling and endocytosis membrane trafficking were traditionally viewed as two different processes. Although there are still some controversies, there is increasing evidence that endocytosis and signalling are linked to each other. For example, evidence from EGF-stimulated NR6 cells found that stimulation induced rapid and transient activation of Rab5a[107]. EGF also leads to the translocation of EEA1 from cytoplasm to the endosomal membrane. In turn, Rab5a expression also activates EGFR endocytosis.

Signalling receptors are particularly interesting endocytic cargoes that are precisely regulated through the process of endocytosis and hence provide clear evidence that endocytosis and signalling affect each other.

1.5.1 Endocytosis regulates Signalling

One early piece of evidence that directly showed trafficking affected signal transduction came from studies using the dynamin mutant^{K44A} which cannot bind to GTP[108]. In EGF-stimulated HeLa cells, EGFR endocytosis was inhibited and it was not subject to normal ligand-induced degradation routes in cells overexpressing dynamin^{K44A} compared to the cells overexpressing dynamin^{wt}. The reduced endocytosis of EGFR also led to enhanced EGF-dependent cell proliferation, which suggested that receptor-mediated endocytosis plays important roles in the attenuation of EGFR signalling. The reduced endocytosis of EGFR also led to varied EGF-dependent tyrosine phosphorylation level, including decreased P13K, p42/44 activity and increased SHC and phosphoinositide phospholipase C- γ (PLC- γ) activity.

It is now clear that endocytosis is one of the primary ways to remove and degrade signalling receptors and their ligands from the cell surface[109]. The internalisation of

activated RTKs and GPCRs following delivery to lysosomes greatly decreases the amount of receptors on the cell surface and also within the cells [110, 111]. NR6 cells expressing the internalisation -defective EGFR showed enhanced ability to exhibit normal growth-factor responses at significantly lower ligand concentrations than the cells expressing WT receptors[112].

Recent studies have increasingly indicated that endocytosis is crucial for the regulation of intracellular signalling by controlling the number of active receptors in the plasma membrane and the activation of receptor or downstream effectors when plasma membrane receptors are stimulated by the extracellular ligand [113-117].

After receptors bind their ligands, their cytoplasmic domain can be post-translationally modified, for example by phosphorylation or ubiquitination. This allows the recruitment of adaptor proteins for signalling or internalisation [118]. In yeast, the GPCR, Ste2, was quickly ubiquitinated following stimulation. The internalisation was severely inhibited in mutant yeast that lack ubiquitin-conjugating enzymes. The β -catenin-mediated Wnt signalling pathway has a crucial role during animal development and tumor progression. Low-density lipoprotein receptor-related protein 6 (LRP6), a single pass transmembrane Wnt receptor, is rapidly phosphorylated by Wnt3a, which leads to binding to the axin complex and stabilization of β -catenin[119]. Inhibition of Wnt3a-dependent phosphorylation of LRP6 by Dickkopf1 (Dkk1) induced the internalised LRP6 to recycle back to the cell surface and respond to Wnt3a signalling again to extend the signalling.

Different internalisation routes can also regulate the signalling output. In the internalisation of EGFR and transforming growth factor beta receptors (TGF- β R)[120, 121], clathrin-mediated internalisation leads to the receptor being delivered to recycling endosomes thus prolonging the signalling but clathrin-independent internalisation directs the receptor to lysosomes, leading to signalling attenuation.

After internalisation, the receptors and ligands arrive at endosomes. Endosomes

can provide key signalling platforms, thus further nuancing the signalling output. There are already numerous studies describing sustained signalling in endosomes from both RTKs and GPCRs. During EGF stimulation, endosomes containing Rab5 and EGFR recruit the Rab5 effectors APPL1 and APPL2, which leads to the activation of Akt to regulate cell survival[101, 102, 122]. Internalised TGF- β R interacts with the FYVE domain-containing adaptor SARA (SMAD anchor for receptor activation) in early endosomes, the interaction of which leads to the phosphorylation of SMAD family member 2 (SMAD2). SMAD2 then forms a complex with SMAD4 and translocates to the nucleus to regulate gene transcription [123-125].

GPCR signalling plays important roles in regulating various physiological functions in cellular processes. It has been shown that the adaptor protein, β -arrestin, dissociates from the β 2 adrenergic receptor (β 2AR) at the plasma membrane, which then recycles and resensitises rapidly. By contrast, β -arrestin internalises together with the vasopressin V2 receptor (V2R) into endosomes, and recycles and resensitises very slowly. The binding between β -arrestin with the internalised receptor further recruits raf-1 and activates ERK, which is required for the activation of ERK 1/2[126, 127]. These are good examples of how endocytosis can regulate both the type of signalling output and its magnitude.

After delivery to the endosome, the receptors may be further sorted to be recycled in case the cell needs to maintain ligand stimulation, or be degraded causing desensitisation. Mutation of the EGFR ubiquitination sites does not affect the internalisation of EGFR but blocks EGFR in early endosomes, thus preventing delivery to lysosomes. This slow degradation EGFR mutant delays the dephosphorylation of MEK[128]. Similarly, increasing EGFR recycling following siRNA of the endosomal sorting complexes is required for transport I (ESCRT I) component tumor susceptibility gene 101 (Tsg 101) causes sustained EGF-activated MAPK pathway [129].

As signalling molecules traverse the endocytic pathway, they encounter different endocytic compartments harboring distinct signalling modules, linked to specific

signalling pathways. The rate of movement of signalling molecules along the endocytic pathway is crucial for the regulation of intracellular signalling pathway. The balance between the endocytosis and signalling must be achieved.

1.5.2 Signalling regulates endocytosis

Numerous studies showed that endocytosis regulates signalling pathway and conversely, signalling also regulates endocytosis.

Activated signalling molecules can directly affect the endocytic machinery. Activation of p38 kinase by stress or cytotoxic drugs causes the activation of GDI (GDP dissociation inhibitor) which increases the Rab5 cycle, resulting in accelerated endocytosis of the fluid phase marker, horseradish peroxidase [130]. Subsequent studies showed that activated P38 further enhanced the internalisation of EGFR that is not associated with ligand[131]. A genome-wide RNAi screen combined with cell proliferation and apoptosis assays in HeLa cells analysed the function of human kinases in clathrin- and caveolae/raft-mediated endocytosis and revealed that actually many kinases could regulate the endocytic process[132]. Several kinases were also found to regulate endocytosis through the activation of P38.

Knockdown of AP2 severely inhibited transferrin receptor endocytosis in HeLa cells but stimulation of EGF still induced coated pit formation that contained EGF, EGFR, clathrin and Grb2[133]. Pit formation required EGFR kinase activity and Grb2. The activation of EGFR also slowed early-to-late endosomal transport[134].

There are many signalling proteins that are involved in the process of endocytosis. Some of them even play a dual function in both signalling and endocytosis, such as β -arrestins, Grb2, P38 and APPL1 and APPL2[101, 102, 126, 130, 131, 135-137]. Studies have shown that the overlap between the process of endocytosis and signalling plays important roles in the regulation of cell proliferation, motility, survival and cell differentiation[138, 139]. However, it is still not clear how the overlap

between endocytosis and signalling occurs mechanically. As such, further investigation into the link between endocytosis and signalling is crucial.

1.6 Ras

Ras is a prototypical member of the Ras superfamily of small GTPases. As a GTPase, Ras also cycles between its GTP conformation and GDP conformation while the activity of Ras is controlled by Ras GEFs and Ras GAPs (Figure 1.2). Ras has been investigated as an oncogene which is important for tumour maintenance and also plays essential roles in controlling multiple signalling pathways [140, 141]. Activated Ras serves as the signalling station responsive to extracellular stimulation, controlling diverse processes including gene expression, cell proliferation, differentiation, cell adhesion and cell survival of which the pathways regulated by Ras, Ras/Raf/MEK/ERK pathway have been most intensively studied[142]. Recent studies showed that the Ras protein is also involved in the process of endocytosis.

Early experiments showed that overexpression of H-Ras in NIT3T3 cells led to increased endocytosis of HRP through PKB/Akt[143]. More evidence about the relationship between Ras and endocytosis came from the Ras-mediated activation of extracellular-stimuli-regulated protein kinase 1/2 (ERK1/2 or p42/44) by EGFR[144]. EGF stimulation leads to the activation of EGFR and auto-phosphorylation of EGFR in the carboxyl terminus, which serves as a docking site to recruit the Grb2 adaptor and its associated protein Son-of-sevenless 1 and 2 (Sos 1/2). Sos 1/2, as a Ras GEF, then quickly leads to the activation of Ras, which then activates the Ras/Raf/MEK/ERK pathway. In the experiments, overexpression of dynamin^{K44A} in HeLa cells blocked EGFR internalisation and also inhibited ERK activation[108]. However, the activation of Ras/Raf/MEK was not affected[145]. Previous studies using transiently or constitutively overexpressed Ras showed that the localisation of Ras was on

intracellular membranes[146]. However, a more recent study, using HRas labeled with the fluorescent protein mVenus, which was expressed at endogenous levels by gene editing, showed that endogenous levels of HRas are actually predominantly localised on the plasma membrane. During EGF stimulation, Ras is quickly activated but activated Ras does not colocalise with EGF or EGFR which are internalised into the endosome. A small amount of active EGFR, still localised at cell surface, ensures that Ras is constantly active and maintains the Ras/Raf/MEK/ERK signal pathway. This study showed that the main purpose of EGFR internalisation was to separate EGFR from Ras at cell surface [147].

Another connection between Ras and endocytosis is RIN1. RIN1 was found as a Ras effector to bind to activated Ras and inhibit its activity [148, 149]. Later inside the Ras binding region of RIN1, a conserved Rab5 GEF domain was found [150, 151]. RIN1 was found to be as a Rab5 GEF in vitro and the Rab5 GEF activity of RIN1 was enhanced by the interaction of Ras-GTP and RIN1. RIN1 is involved in endosome fusion through activation of Rab5. The stimulated endosome fusion by RIN1 could be further enhanced by Ras-GTP. Finally, overexpression of RIN1 in NR6 cells resulted in giant endosomes and increased the internalisation of EGF but did not alter the internalisation of transferrin. The increased internalisation of EGF by RIN1 could be further enhanced by co-expression of Rab5^{wt} and Ras^{wt}. Overexpression of RIN1 could even rescue the inhibited internalisation of EGF in cells expressing Ras^{S17N}. But a RIN1 mutant that lacks Rab5 GEF activity still inhibited the internalisation of EGF, suggesting RIN1 as a Rab5 GEF may specifically regulate certain receptors.

1.7 Ras and Rab5

The relationship between Rab5 and Ras was identified a long time ago even though there was no evidence of a direct interaction between Rab5 and Ras. Ras was known

to regulate endocytosis, especially fluid phase endocytosis [152]. It was found that the increased uptake of HRP in NIH3T3 cells overexpressing Ras was mediated by the Ras downstream effector PKB/Akt[143], but overexpression of dominant negative Rab5^{S34N} blocked the increased endocytosis caused by overexpression of Ras or PKB/Akt. Inhibited endocytosis of HRP in cells expressing kinase-dead PKB/Akt was rescued by transient expression of Rab5^{wt} and even increased by overexpression of Rab5^{Q79L}.

Another relationship between Rab5 and Ras was mediated by Rab5 GEFs, RIN1 and Rabex-5. RIN1 was found to be a Ras effector that interacted with Ras and then inactivates it. It also regulated multiple signalling pathway through binding with 14-3-3, c-ABL and Ras [149, 153]. Later it was found to contain a Rab5 GEF domain. It stimulated the Rab5 guanine nucleotide exchange, regulated Rab5a-dependent endosome fusion and EGF receptor-mediated endocytosis[150]. The functions of RIN1 all could be further enhanced by activated Ras.

Rabex-5 is a well-characterised Rab5 GEF. It also contains a zinc finger at the amino terminus which works as an E3 ubiquitin ligase to specifically promote Ras ubiquitination [154-156]. Overexpression of Rabex-5 increases the location of HRas in endosomes and also promotes the fusion of endosomes. Further investigation showed that the ubiquitination of HRas mediated by Rabex-5 leads to a decrease of Ras-ERK signal. Overexpression of Rin1 also stimulates the ubiquitination of HRas while overexpression of Rab5^{Q79L} obviates the effect of RIN1 [154-156].

Following on from the identification of Rin1, a new Rab5 GEF was found: Rme-6. It not only contains a Rab5 GEF domain but also a potential Ras GAP domain, which will likely further enhance the relationship between Rab5 and Ras and also mediated the endocytic trafficking and signalling pathways.

1.8 Rme-6

Rme-6, also named as Gapex-5, is a multi-domain protein that is composed of a C-terminal Vps9 (Rab5 GEF) domain, which is strongly similar to the catalytic domains found in other Rab5 GEFs, and an N-terminal Ras GAP domain. The mammalian Rme-6 contains a central proline-rich region (Figure 1.3).

In vitro experiments have shown that the Vps9 domain of Rme-6 has GDP release activity for Rab5[157]. The yeast two-hybrid system further confirmed that Rme-6 could interact with Rab5 through its GEF domain[158]. The Ras GAP domain is also a highly conserved domain, implying it is likely to have important functions[159]. Rme-6 is ubiquitously expressed in different organs and species. The human hRme-6 and rat Rme-6 gene showed 90% identity to that of mouse. The Ras GAP, proline-rich region and GEF domains of Rme-6 exhibited 97%, 100%, and 100% identity respectively.



Figure 1.3 hRme-6 structure and comparison with Rabex-5. The mammalian hRme-6 contains an N-terminal Ras GAP, a C-terminal VPS9 domain, and a central proline-rich sequence.

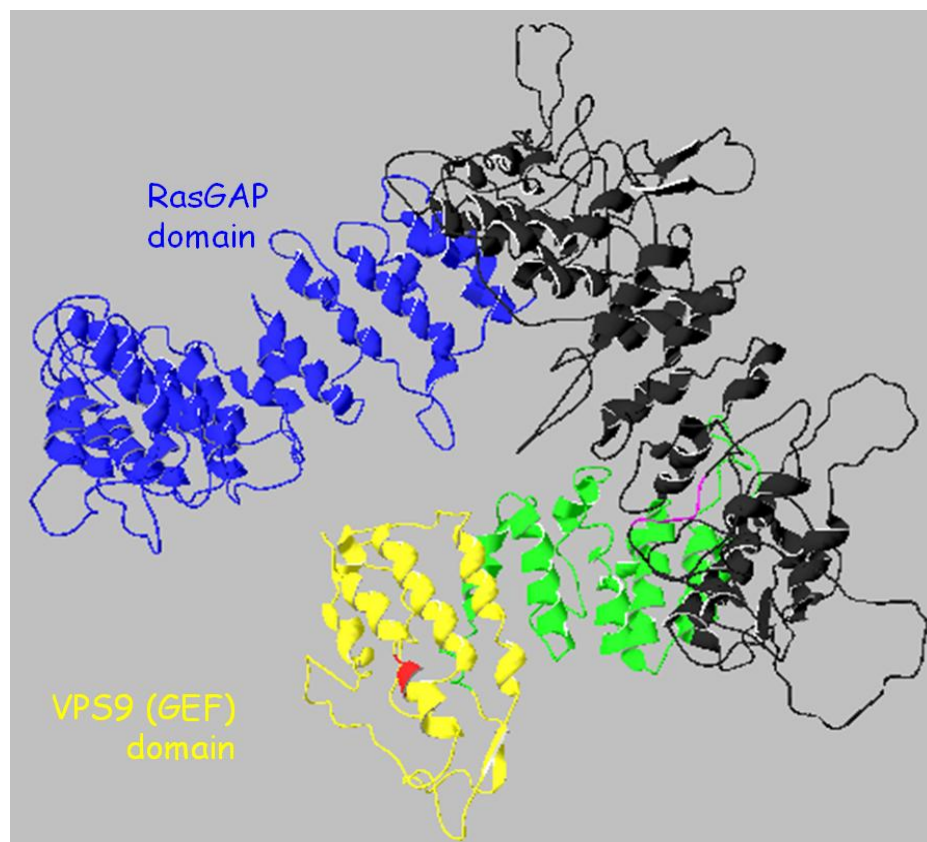


Figure 1.4 Predicted structure of hRme-6. The predicted structure of hRme-6 based on available structures of Rab5 GEF domain of Rabex-5 and Ras GAP domain of p120 by Singh using I-tasser software.

Rme-6 was originally found to mediate both fluid phase and receptor-mediated endocytosis in *C.elegans* via its interaction with Rab5[160]. The Rme-6 mutant

strongly reduced YP170 (a reporter for clathrin-dependent endocytosis) in *C.elegans* uptake in oocytes and showed accumulation of a fluid-phase endocytosis marker in the body cavity. In the Rme-6 mutant coelomocytes, the accumulation of microinjected Texas-Red-labelled BSA was inhibited. In the Rme-6 mutant oocytes, yolk receptor Rme-2 docked very near to the plasma membrane in small vesicles unlike those seen in the wild type. The size of the GFP-Rab-5 positive structures was reduced threefold compared to the wild type. Studies demonstrated that Rme-6 colocalised with mRFP1-CHC-1 and mRFP1- α -adaptin but not with EEA1 or Rab5. Knockdown of CHC-1 but not Rab5 disrupted the localisation of Rme-6 in oocytes, which indicated that Rme-6 colocalised with clathrin-coated pits and that clathrin is required for the localisation of Rab5 to the plasma membrane[160].

1.8.1 hRme-6 and Tfn endocytosis

During clathrin-mediated endocytosis, AP2 adaptor complexes, clathrin and other components including cargoes form clathrin-coated pits. After budding of the pits, the removal of the AP2 adaptor protein complexes is crucial for endocytic progression[161]. The interaction of AP2 with the plasma membrane is mediated by PIP₂ and enhanced by AP2-associated kinase 1(AAK1), which mediates phosphorylation of the μ 2 subunit of AP2[162]. Phosphorylation of the μ 2 subunit increases the interaction of AP2 with cargoes, such as transferrin receptor (TfnR)[163]. Studies showed that clathrin-coated vesicles containing Rab5 and Rab5 participated in the uncoating of AP2 from the clathrin-coated vesicles [157]. siRNA studies indicated that hRme-6, rather than rabex5, was the relevant Rab5 GEF for uncoating. hRme-6 competed with AAK1 for binding to the α -adaptin ear of AP2. Although full-length hRme-6 did not show GEF activity, in the presence of ATP and α -adaptin ear domain hRme-6 showed GEF activity. siRNA of hRme-6 enhanced the levels of phospho- μ 2 while over-expression of hRme-6 decreased the amount of phospho- μ 2. These data

suggested that Rme-6 regulated μ 2 dephosphorylation to further regulate AP2 uncoating [157]. It further confirmed that hRme-6 regulated Rab5 activity and the regulation of hRme-6 on Rab5 was relatively specific.

1.8.2 hRme-6 and EGFR endocytosis

Epidermal growth factor (EGF) stimulation causes EGFR to become rapidly ubiquitinated, internalised and sorted either to be recycled to the plasma membrane or delivered to MVBs or late endosomes for degradation to attenuate signalling [164, 165]. EGF stimulation causes Rab5 activation and in turn Rab5 plays an important role in the early stages of EGFR trafficking[107]. C-Cbl is an ubiquitin E3 ligase, which is recruited to EGFR and initiates the ubiquitination of the activated receptor [166, 167]. During EGF-stimulated EGFR internalisation, down-regulation of hRme-6 by siRNA decreased EGFR degradation impaired EGFR internalisation, ubiquitination and delayed the dephosphorylation of the receptor.

Knockdown of hRme-6 by siRNA also blocked EGFR trafficking from early endosomes to MVBs and late endocytic compartments. This was shown by an increased co-localisation between EGFR and EEA1. Further investigations found that the effect of loss of hRme-6 on EGFR endocytosis was through a reduction in the interaction between c-Cbl and EGFR. Overexpressed hRme-6 could interact with endogenous c-Cbl through the Ras GAP domain of hRme-6. Consistent with these results, over-expression of Rab5a^{S34N} in CHO cells, expressing human EGFR, led to the inhibition of EGFR internalisation and degradation but dramatically lifted the ubiquitination level of EGFR. As depletion of Rab5 isoforms in HeLa cells did not inhibit EGFR ubiquitination, it was suggested that hRme-6 affected EGFR ubiquitination independent of Rab5 activity [159].

1.8.3 Rme-6 and insulin

Insulin stimulation causes the translocation of GLUT4 from intracellular storage vesicles to the cell surface. The underlying mechanism involves recruitment and activation of PI3K forming PIP₃ [168, 169] and phosphorylation of the adaptor protein APS[170], c-Cbl[171] and activation of Rho GTPase TC10[172], which recruits downstream effectors including Cdc4-interacting protein 4 (CIP4)[173].

A yeast two-hybrid screen using CIP4 as bait to explore the role of CIP4 in insulin-stimulated GLUT4 translocation found that Rme-6 was a binding partner for CIP4. The proline-rich region of Rme-6 interacted with CIP4 SH3 domain [174]. Overexpression of Rme-6 in 3T3-L1 adipocytes inhibited the insulin-stimulated GLUT4 translocation while if CIP4 was co-expressed with hRme-6 then, both proteins were translocated from an intracellular compartment to the plasma membrane following stimulation with insulin and rescued the inhibition of Rme-6 in insulin-stimulated GLUT4 translocation. A CIP4 mutant that lacks the Rme-6 interaction domain co-expressed with Rme-6 could not recruit Rme-6 and Rme-6 failed to translocate. However, it was very interesting that Rme-6 lacking the GAP domain also inhibited GLUT4 translocation, which was even stronger than the effect of Rme-6 lacking GEF domain [175].

During this process the GEF domain of Rme-6 was found to be not just a Rab5GEF but also a stronger GEF for Rab31. Overexpression of Rab31 also blocked GLUT4translocation caused by insulin stimulation in adipocytes. Knockdown of Rab31 in adipocytes did not affect GLUT4level or the phosphorylation of Akt or Cbl but enhanced glucose transport during low dose insulin stimulation. These all suggested that insulin stimulation led CIP4/Rme-6 to be translocated to the plasma membrane, which reduced Rab31 activity and then permitted GLUT4to be delivered to the cell surface.

However, the function of Rme-6 in insulin-stimulated 3T3-L1 adipocytes extended

further than these observations. It was shown that insulin stimulation leads to the activation of Rab5 at the plasma membrane[176], likely via CIP4-mediated recruitment of Rme-6 to the plasma membrane and plasma membrane targeted Rme-6-CAAX greatly increased Rab5 activation at the plasma membrane. This all suggested that Rab5 activation by insulin was mediated by Rme-6.

To further explore the mechanism of Rab5 activation, it was surprisingly found that the GAP domain of Rme-6 interacted specifically with the Rho-GTPase TC10. However, the TC10 interaction with the GAP domain of Rme-6 was independent of its nucleotide state. TC10 could activate Rab5 through Rme-6, as the overexpression of active TC10^{Q75L} increased Rab5 activity but co-expression of the Rme-6 mutant lacking the GEF domain blocked the activation of Rab5. siRNA of endogenous Rme-6 also blocked the activation of Rab5 caused by TC10. The activation of Rab5 by TC10 was also regulated by CIP4.

Insulin stimulation not only activates Rab5 but also leads to the formation of PI (3) P at the plasma membrane [37, 176]. Rme-6 and Rab5 regulated the formation of PI (3) P during insulin-stimulated 3T3-L1 adipocytes. However, the effect caused by Rme-6 was independent of its GEF activity to Rab31 but more likely dependent on the activation of Rab5 stimulated by insulin at the plasma membrane. Knockdown of Rme-6 also inhibited the translocation of GLUT4 and glucose uptake stimulated by insulin in adipocytes.

Over all, the function of Rme-6 in adipocytes could be divided into two steps. In cells without insulin stimulation, Rme-6 is mainly found in the cytoplasm and maintains Rab31 in an active state to maintain GLUT4 within the cell. When cells are stimulated with insulin, the CIP4 and Rme-6 complex relocates to the plasma membrane and increases the activity of Rab5 while decreasing the activity of rab31. This causes GLUT4 to be translocated to the plasma membrane and increases insulin-stimulated glucose uptake

1.8.4 hRme-6 and signalling

TEK tyrosine kinase (Tie2) is an endothelial tyrosine kinase receptor for Ang1, both of which are involved in numerous aspects of both normal and pathological angiogenesis[177]. Previous work from our lab showed that in Ang1 stimulated Human Umbilical Vein Endothelial Cells (HUVECs), phosphorylation of Tie2, Akt, p38 and p42/44 MAPK increased. Other data demonstrated that Tie2 internalisation was required for Ang1/Tie2 induced phosphorylation of Akt. Dynamin is a major component and marker of the clathrin-mediated endocytic pathway [178]. Overexpression of dynamin^{K44A} could significantly inhibit Ang1 induced Akt phosphorylation. However, following overexpression of HA-hRme-6 in human umbilical vein endothelial cells, the phosphorylation of Akt MAPK decreased and the phosphorylation of p38 (Figure 1.7) and p42/44 (data not shown) increased.

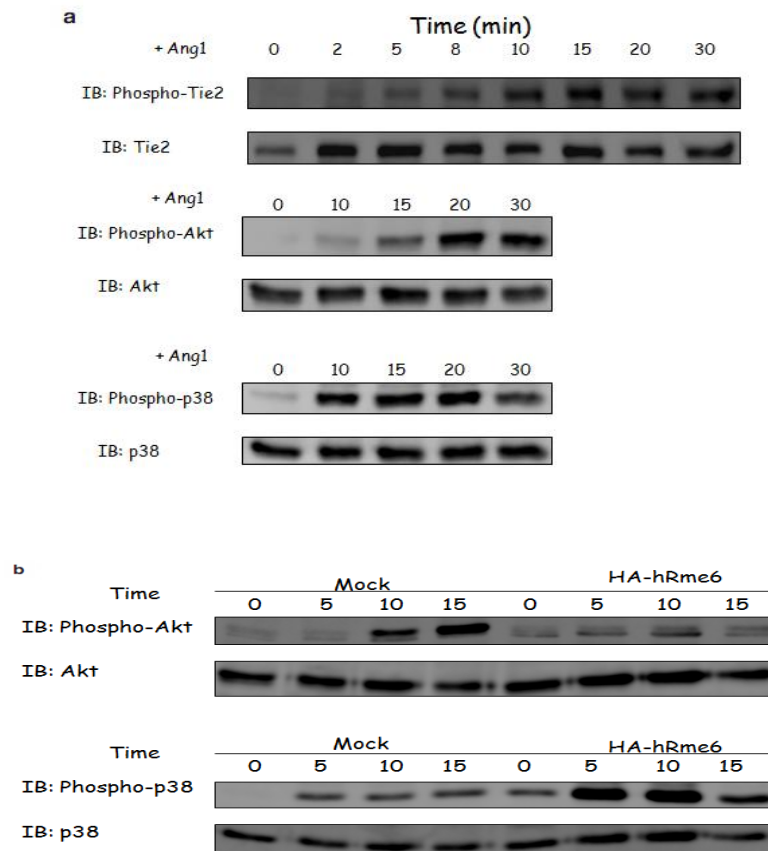


Figure 1.5 hRme-6 regulated p38 and p42/44 signalling. (a) Ang1 activated HUVECs. HUVECs were stimulated with

Ang1 for various minutes. Whole cell lysates were prepared and phosphorylation of Tie2, Akt and p38 were analysed by Western blotting. (b) Levels of hRme-6 affect phosphorylation of Akt and p38. HUVECs were transfected with either mock or HA-hRme-6 construct. Forty-eight hours later, HUVECs were stimulated with Ang1 for various minutes. Whole cell lysates were prepared and phosphorylation of Akt, p38 was analysed. Experiment performed by Emma Maxwell.

1.8.5 hRme-6 and other Rab5 GEFs

Beside Rme-6, there are several Rab5 GEFs that have been reported to regulate the Rab5a guanine nucleotide exchange, including RIN1, Rabex5. The relationship among these different Rab5GEFs is quite interesting.

Rme-6, RIN1 and Rabex-5 were all reported to regulate the process of endocytosis through Rab5 GEF activity. Comparing the structures of these Rab5GEFs, it is interesting to find that they all contain a proline rich region beside the conserved Rab5 GEF domain. However, they appear to regulate endocytic processes in slightly different ways.

Rabex-5 forms a tight complex with the Rab5 effector Rabaptin-5. Rabex5 on its own appears to be conformationally unstable and the Rabex-5 GEF domain is autoinhibited by the Rabex-5 coiled-coil domain[179]. The tight complex formed by Rabex-5 and Rabaptin-5 leads to the conformational change of Rabex-5, activating its GEF activity and leads to a conversion of Rab5-GDP to Rab5-GTP [179]. This complex is also essential for early endosome homotypic fusion [89, 90]. Co-expression of Rabex-5 with EGFR-GFP in NF73 cells sharply increase the degradation of EGF while the siRNA Rabex-5 in HeLa cells do not affect AP2 uncoating, suggesting that it is likely to act more at endosomes than at the cell surface[180].

RIN1 as a Rab5 GEF also regulates endosome fusion[150]. Levels of RIN1 affected EGFR but not Tfn receptor internalisation. Overexpression of RIN1 with Rab5a leads to the formation of giant endosomes, which was similar to the effect of Rabex-5.

However, hRme-6 was found to be involved in the endocytosis process of EGFR, GLUT4 and Tnf receptor [157, 174]. Overexpression of hRme-6 did not lead to apparent endosome enlargement [157].

Similarities exist in the functions of Rabex-5, RIN1 and Rme-6 as they are all related to ubiquitination and Ras during the endocytic process in diverse ways. Rabex-5 contains a zinc finger domain that functions as an E3 ubiquitin ligase. Rabex-5 was reported to interact with the ubiquitinated immunoglobulin superfamily cell adhesion molecule L1 and further regulate the endocytic trafficking of the adhesion molecule L1[181]. Compared to Rabex-5, RIN1 contained a Ras binding domain which allows direct interaction with Ras. Overexpression of RIN1 increases the ubiquitination of HRas and siRNA of RIN1 reduces it. However, there is cross-talk between these two GEFs. The ubiquitination effect mediated by RIN1 is dependent on Rabex-5, again highlighting a link between endocytosis and signalling[153]. By contrast, the Ras GAP domain of hRme-6 may potentially regulate the activity of Ras although it differs in structure from classical Ras GAP domains (see chapter 3). hRme-6 is also involved in the regulation of EGFR through the interaction with E3 ligase, c-Cbl, by the Ras GAP domain of hRme-6.

However, there are also differences in the functions of different Rab5GEFs. For example, in *C.elegans* RNA interference of either the Rabex-5 worm orthologue RABX-5 or Rme-6 had significant effects on YP170-GFP endocytosis by oocytes, but RNAi RABX-5 or RABN-5 (Rabaptin-5 worm orthologue, forming a complex with RABX-5 for function) in the Rme-6 mutant background caused lethality, which is similar to the loss of Rab5 activity. The subcellular localisation of GFP-Rab-5 expressed in Rme-6 mutant or RABX-5 RNAi was also similar. When depleting RABX-5 in Rme-6 mutant, GFP-Rab-5 totally disappeared. These indicated the partial redundancy between Rme-6 and RABX-5-RABN-5 complex during endocytic function.

1.9 The Sorting Nexin 9 and Sortin Nexin 24

Sorting nexin 9 (SNX9) and sorting nexin 24 (SNX24) belong to the sorting nexin family, which has the potential for membrane association through the conserved PX (phox-homology) domain or protein interaction with membrane-associated proteins [182, 183]. The PX domain mostly interacts with PI3P [184], which is enriched in early endosomes. Beside the PX domain, sorting nexins also contain different protein–protein interaction motifs that lead to different subcellular localisation. So far 33 mammalian sorting nexins have been already found. Sorting nexins involved in diverse endocytosis processes, including cargo sorting, endosomal sorting and signalling [185].

SNX9 is one of the best characterized proteins in the sorting nexin family. It contains not only a PX domain, but also a C-terminal BAR domain and an N-terminal Src Homology 3 (SH3) domain[186]. SNX9 is known as an essential protein in clathrin mediated endocytosis through the interaction with AP2, clathrin and dynamin-2[32, 187]. SNX9 is transiently recruited to clathrin-coated pits during late stages of vesicle formation. It recruits dynamin to the neck of the vesicle. The interaction between SNX9 and dynamin is through the interaction between the SH3 domain of SNX9 and the proline rich domain of dynamin. The SH3 domain of SNX9 also interacts with synaptojanin[188], N-WASP[189]. SNX9 is known to affect EGFR degradation through its SH3 domain interaction with non-receptor-activated Cdc42-associated kinase (ACK)[190]. In addition to these observations, SNX9 localizes in actin-rich structures and is involved in fluid phase endocytosis through regulating actin dynamics[191].

Compared to SNX9, the function of SNX24 is poorly understood. SNX24 contains only an N-terminal PX domain[185]. The gene expression level of SNX24 is regulated by estrogen in breast cancer cell lines[192]. It was also shown that siRNA of SNX24 did not directly affect the degradation of EGFR in HeLa cells [193].

1.10 IQ motif containing GTPase activating protein 1 (IQGAP1)

IQGAP1 is known as a scaffolding protein with multiple protein interaction domains. It contains four isoleucine and glutamine (IQ) domains, one calponin homology domain, one Ras GAP-related domain and one WW domain [194-196]. The Ras GAP domain of IQGAP1 is quite similar to the Ras GAP domain of hRme-6. But the Ras GAP domain of IQGAP1 does not have detectable GTPase-activating protein activity. IQGAP1 has been shown to interact with Cdc42, Rac 1, actin, calmodulin, E-cadherin, β -catenin and CLIP-170 [197].

IQGAP1 is involved in both Tf α and EGF endocytosis. SiRNA of IQGAP1 inhibits the endocytosis of Tf α in MIN6 cells [198]. It is known that EGF stimulation can induce phosphorylation of IQGAP1^{Ser1443} [199]. Previous SILAC experiments by Matthias Mann et al show that there is interaction between EGFR and IQGAP1 [200]. IQGAP1 affects tyrosine phosphorylation of EGFR during EGF stimulation. IQGAP1 later is found to work as a MAPK Scaffold to bind to EGFR and B-Raf, MEK, and p42/44 to regulate the signalling activity in response to EGF stimulation. Knockdown or overexpression of IQGAP1 could decrease EGF-stimulated activation of MEK and p42/44. EGF stimulation promotes the interaction of IQGAP1 with MEK1, but decreases the binding of IQGAP1 with MEK2. However, the interaction between p42/44 and IQGAP1 is independent of EGF [199, 201].

1.11 The key unanswered questions about hRme-6

There is still no clear evidence showing that the Ras GAP domain of hRme-6 has Ras GAP activity as there is a lack of the conserved arginine in its Ras GAP domain. Previous studies showed that dominant positive H-Ras^{G12V} delayed EGFR degradation [167]. This implies that the Ras GAPs may exhibit Ras GAP activity or

directly bind to Ras protein to regulate Ras and Ras downstream signalling pathways, affect the endocytosis of EGFR. However, if the Ras GAP domain displays Ras GAP activity, as activated Ras and Rab5 proteins both can stimulate the process of endocytosis, it implies that the functions of the Ras GAP and Rab5 GEF domains oppose each other. While Rab5 GEF domain activates Rab5 and is predicted to further increase endocytosis, the Ras GAP domain would inhibit Ras activity and then inhibit endocytosis through decreasing Ras signalling. One possible explanation for this paradox could be that the activities of Rme-6 are different when Rme-6 encounters different signals or cargoes.

Moreover, previous work from the Smythe lab showed that when HUVECs were incubated with Ang1 and Cy5-transferrin (Tfn), no more than 10% of Ang1 colocalized with Tfn during the first ten minutes. Only after ten minutes, did the degree of co-localisation of Ang1 with Tfn significantly increase (Ferriera, Maxwell and Smythe, unpublished). As Rme-6 regulates Tfn endocytosis and also shifts the Tie2 signalling intensity in Ang1 stimulated HUVECs, one possibility is that hRme-6 is recruited to subpopulations of endosomes containing different cargoes which cause differences in the way the different activities are activated.

Another question is the relationship between hRme-6 and other Rab5 GEFs. The different Rab5 GEFs all regulate Rab5 and have a connection with Ras. As Rme-6 shows a potential interaction with Ras, it is possible that hRme-6 also could bind to Ras and different Rab5 GEF proteins form a network to regulate the dynamic process of endocytosis and signal transduction. But how Rme-6 formed this network is still unknown.

1.12 Aims and objectives of this work

The objective of this work were to investigate the domain functions of hRme-6 and

the regulation of the activities of hRme-6 to find the role of hRme-6 during integrated endocytosis and signalling process.

In this chapter I highlighted the relationship between endocytosis and signalling and described the major regulators, Rab5 and Ras. I have introduced the key studies in which hRme-6 was shown to relate to the functional regulation of Rab5, Ras and endocytosis and signalling process.

The first stage of my study attempted to confirm the domain activities of hRme-6 and explored the functions of hRme-6 in different cell models. In the second stage of my study, I focused on the structure study of hRme-6 in vivo and tried to reconstruct the structure of hRme-6. The third stage of the research was the investigation of the interaction partners of hRme-6 in EGF stimulated HeLa cells.

I wanted to understand the molecular mechanism of the domain functional regulations of hRme-6 behind integrated endocytosis and signalling process. Using these approaches I hope to gain insight into the relationship between endocytosis and signalling.

2. Materials and methods

2.1 Reagents

General laboratory chemicals were obtained from Sigma-Aldrich Ltd.(The Old Brickyard, New Road, Gillingham, England, SP8 4XT) or VWR International Ltd.(Merck House, Poole, England, BH15 1TD), unless otherwise indicated. Chemicals were AnalaR grade. Ultra Pure Protogel 30% (w/v) acrylamide: 0.8% (w/v) bis-acrylamide stock solution (37.5:1) mix was from Geneflow Ltd. (Fradley Business Centre, Wood End Lane, Fradley, England, WS13 8NF). Enhanced Chemiluminescence (ECL) reagent, Enhanced Chemiluminescence prime (ECL prime) and Enhanced Chemiluminescence select (ECL select) were from Amersham Biosciences UK Ltd. (Pollards Wood, Nightingales Lane, Chalfont St.Giles, England, HP8 4SP). Tissue culture plastic ware was obtained from Greiner Bio-one (Brunel Way, Stroudwater Business Park, Stonehouse, Glos.GL10 3SX). Hyclone foetal calf serum was from Perbio Science UK Ltd. (Century House, High street, Tattenhall, Chester, England, CH3 9RJ). Bio-Rad Protein (Bradford) assay reagent, Mini-protean II protein electrophoresis, Mini Trans-Blot protein blotting, wide min-sub cell agarose gel electrophoresis and gel drying equipment were from Bio-Rad Laboratories Ltd. (Bio-Rad House, Marylands Avenue, Hemel Hempstead, England, HP2 3TD). Schleicher & Schuell Protran Nitrocellulose transfer membrane was from Inverclyde Biologicals (2 Teal Court, Strathclyde Business Park, Bellshill, Scotland, ML4 3NN). Whatman 3MM paper was from Fisher Scientific UK Ltd. (Bishop Meadow Road, Loughborough, England, LE11 5RG). Complete protease inhibitor cocktail tablets and Fugene 6 transfection reagent were from Roche Diagnostics Ltd. (Bell Lane, Lewes, England, BN7 1LG). Dulbecco's Modified Eagle Medium (DMEM), Penicillin/streptomycin solution, trypsin-EDTA, glutamine, BL21 DE3 pLys bacteria, subcloning efficiency DH5 α chemically competent *E.coli* and LipofectamineTm 2000 transfection reagent were obtained from Invitrogen

Ltd. (3 Fountain Drive, Inchinnan Business Park, Paisley, Scotland, PA4 9RF). Plasmid DNA purification kits and Qiaquick gel extraction kits were from Qiagen (Qiagen House, Fleming Way, Crawley, England, RH10 2AX). Jackson ImmunoResearch HRP conjugated secondary antibodies were obtained from Stratech Scientific Ltd. (Unit 4, Northfield Business Park, Northfield Road, Soham, England, CB7 5UE). Konica AX blue X-ray film was obtained from Hospital Engineering Ltd. (Unit 6, Mercury Way, Manchester, England, M41 7HS). British Biocell International (Golden Gate, Ty Glas Avenue, Ilanishen, Cardiff, CF14 5DX) supplied 5nm colloidal gold. EM grids, uranyl acetate and EM grade paraformaldehyde were from Agar (66A Cambridge Road, Stansted, Essex, CM26 8DA). 5nm Ni-NTA-Nanogold was obtained from Universal Biologicals Ltd. (Passhouse Farmhouse, Papworth St. Agnes, Cambridge, CB23 3QU).

2.2 Antibodies

2.2.1 Primary antibody

Antibody	species	Raised against	supplier	Dilution
anti-Akt	Rabbit affinity purified	mouse Akt	Cell Signalling (prod.code:9272)	WB 1:1000
anti-CIP4	Mouse affinity purified	467-558 aa of human CIP4	Santa Cruz (prod.code:sc-166810)	IF 1:500 WB 1:1000
anti-EGFR	Mouse affinity purified	human EGFR	ThermoFisher (prod.code:MS-400-P1)	IF 1:500
anti-Flag	Mouse affinity purified	Flag Tag	Sigma (prod.code:F3040)	IF 1:500 WB 1:5000
anti-GST	Mouse affinity purified	GST	Sigma (prod.code:G1160)	WB 1:1000
anti-hRme-6	Rabbit affinity purified	700-750 aa of hRme-6	Bethyl Lab (prod.code:A302-116A)	IF 1:1000
anti-hRme-6	Rabbit affinity purified	550-600 aa of hRme-6	Bethyl Lab (prod.code:A302-115A)	WB 1:1000
anti-his	Mouse affinity purified	His Tag	R&D system	WB 1:1000

			(prod.code:MAB050)	
anti-IQGAP1	Goat affinity purified	human IQGAP1	Santa Cruz (prod.code:sc-8737)	IF 1:500
anti-TfnR	Mouse affinity purified	TfnR	B3/25 MAb In house	IF 1:500
anti-p42/44	Rabbit affinity purified	Rat p44 MAPK	Cell Signalling (prod.code:4695)	WB 1:1000
anti-p38	Rabbit affinity purified	human p38 MAPK	Cell Signalling (prod.code:9212)	WB 1:1000
anti-Phospho -p42/44	Rabbit affinity purified	Thr202/Tyr204 of human p44 MAPK	Cell Signalling (prod.code:4370)	WB 1:1000
anti-Phospho -p38	Rabbit affinity purified	Thr180/Tyr182 of human p38 MAPK	Cell Signalling (prod.code:9211)	WB 1:1000
anti-Phospho -Akt	Rabbit affinity purified	Ser473 of mouse Akt	Cell Signalling (prod.code:4058)	WB 1:1000
anti-SNX9	Mouse affinity purified	391-436 aa of human SNX9	Santa Cruz (prod.code:sc-166863)	IF 1:500
Anti-Nup98	Mouse affinity purified	581-880 aa of human Nup98	Santa Cruz (prod.code:sc- 74553)	IF 1:500

Table 2.1 Primary antibodies used in this project. Table detailing the species, source, supplies and working concentrations of the primary antibodies used in this project.

2.2.2 Secondary antibodies

Antibody	species	Raised against	supplier	Dilution
anti-rabbit HRP	Goat affinity purified	Rabbit IgG	Jackson Immunoresearch Labs (Prod.Code: 111-035-144)	1:5,000
anti-mouse HRP	Goat affinity purified	Mouse IgG	Jackson Immunoresearch Labs (Prod.Code: 111-035-003)	1:5,000
anti-mouse alexa fluor 488	Donkey affinity purified	Mouse IgG	Invitrogen (Prod.Code: A21202)	1:1,000

Table 2.2 Secondary antibodies used in this project. Table detailing the species, source, suppliers and working concentrations of the secondary antibodies used in this project.

2.3 Primers used

Subcloning of GST and hRme-6 into pSL1180

F 5' - TCC CCG CGG ATG TCC CCT ATA CTA GGT TA

R 5' -CTT CAA GAC AAG GTC CCC GGG CGC CGG CGT TT

F 5' – TTG CGG CCG CAT ACC CAT ACG ATG TTC CAG AT

R 5' -TTT TGG TAG CTA CTG GCT TTC GTA GTA GTA GTA GTA ACT AGA TCT CG

Subcloning of GST-hRme-6 into pRSET A

F 5' –CGA GCT CAA GAT GGA TCC ACT AGT CCA GTG TGG TG

R 5' –AAT TTT GGT AGC TAC TGG CTT TCA CTC CAT GGG G

Subcloning of GST-hRme-6 into pcDNA3.1-Flag

F 5' –TTG CGG CCG CAG ATG GAT CCA CTA GTC CAG TG

R 5' -TTT TGG TAG CTA CTG GCT TTC ACT AGA TCT CG

Subcloning of Ras GAP domain of hRme-6 into pRSET A

F 5' –CCC TCG AGT ACC CAT ACG ATG TTC CAG ATT

R 5' -TTT TGG TAG CTA CTG GCT TTC ACT CCATGG GG

Subcloning of middle I domain of hRme-6 into pcDNA3.1-Flag

F 5' –TTG CGG CCG CAT ACA ATA CAC CTC AGC TAT C

R 5' –AGG CCG TAT TCA CGT TGG AGA ACT AGA TCT CG

Subcloning of middle II domain of hRme-6 into pcDNA3.1-Flag

F 5' –TTG CGG CCG CAT CTG AGG ATA TTC CCA ATA A

R 5' –TGA GAC GTT CGG TTC GTC GGA CTA GAT CTC G

Subcloning of Rab5 GEF domain of hRme-6 into pcDNA3.1-Flag

F 5' –TTG CGG CCG CAG CCC ACC CGC AGG ATT CAG CT

R 5' -TTT TGG TAG CTA CTG GCT TTC ACT AGA TCT CG

2.4 Common buffers

2.4.1 PBS

1.76 mM KH₂PO₄, pH 7.4, 137 mM NaCl, 2.68 mM KCl, 8.1 mM Na₂HPO₄ (Sambrook et al., 1989). Store at room temperature.

2.4.2 TBS

20 mM Tris, pH 7.4, 137 mM NaCl. A 10X stock was made and stored at room temperature.

2.4.3 KSHM buffer

20 mM Hepes, pH 7.4, 100 mM potassium acetate, 85 mM sucrose, 1 mM MgCl₂.

Buffer was sterile filtered and stored at 4°C for up to one week.

2.4.4 5XSDS gel loading buffer

0.25M Tris, pH6.8, 0.5 M DTT, 10% (w/v) SDS, 0.25% (w/v) bromophenol blue, 50% (w/v) glycerol

2.4.5 SDS electrophoresis running buffer

25 mM Tris, 190 mM glycine, 1% (w/v) SDS. Store at room temperature.

2.4.6 Western blotting transfer buffer

25 mM Tris, 190 mM glycine, 20% (v/v) methanol. Store at room temperature.

2.4.7 TAE

27. mM Tris acetate, 1 mM EDTA, pH 8.0

2.4.8 HBS

27.2 mM HEPES, pH 7.0, 137 mM NaCl, 1.12 mM Na₂HPO₄·7H₂O. Buffer components were mixed, filtered and re-adjusted. Store at -20°C in aliquots.

2.4.9 4xNative PAGE sample buffer

50 mM Bis-Tris, 6 N HCl, 50 mM NaCl, 10% (w/v) Glycerol, 0.001% (w/v) Ponceau S, pH 7.2. Store at -4°C up to half year.

2.4.10 Native PAGE running buffer

50 mM Bis-Tris, 50 mM Tricine, pH 6.8

2.4.11 Native PAGE dark blue Cathode buffer

50 mM Bis-Tris, 50 mM Tricine, pH 6.8, 0.02% Coomassie G-250

2.4.12 Native PAGE light blue Cathode buffer

50 mM Bis-Tris, 50 mM Tricine, pH 6.8, 0.002% Coomassie G-250

2.4.13 Native PAGE Coomassie R-250 stain solution

0.02% (w/v) Coomassie R-250 in 30% (v/v) methanol and 10% (v/v) acetic acid

2.4.14 Ponceau S stain solution

0.1% (w/v) Ponceau S in 5% (v/v) acetic acid

2.4.15 SDS trapping buffer

0.3 M Tris base, 30% (w/v) glycerol, 5% (w/v) SDS, 0.05% (w/v) bromophenol blue,
pH 6.8

2.4.16 10x GAP assay nucleotide loading buffer

500 mM Hepes, pH 6.8, 10 mg/ml BSA, 10 mM DTT

2.4.17 γ -P³² GTP dilution buffer

50 mM Tris-HCl, pH 8.0, 1 mM DTT, 1 mM ATP.

2.4.18 GEF assay preloading buffer

20 mM Tris-HCl, pH 8.0, 62.5 mM NaCl, 10 mM EDTA, 5 mM MgCl₂, 0.36% (w/v) chaps, 0.5 mM DTT, 120 μ M GDP.

2.4.19 GEF assay reaction buffer

40 mM Tris-HCl, pH 8.0, 62.5 mM NaCl, 5 mM EDTA, 15 mM MgCl₂, 0.36% (w/v) chaps, 0.5 mM DTT, 100 μM GTP.

2.4.20 GEF assay stop buffer

20 mM Tris-HCl, pH 8.0, 100 mM NaCl, 20 mM MgCl₂

2.4.21 CK2 assay enzyme buffer

50 mM Tris-HCl, pH 7.5, 10 mM MgCl₂, 0.1 mM EDTA, 2 mM DTT, 0.01% Brij 35

2.4.22 PLA assay wash buffer A

10 mM Tris-HCl, 150 mM NaCl, pH 7.4, 0.05% (v/v) Tween 20. Buffer was filtered through a 0.22 μm filter and stored at 4°C.

2.4.23 PLA assay wash buffer B

0.2 M Tris, 0.1 M NaCl. Buffer was filtered through a 0.22 μm filter and stored at 4°C.

2.5 Molecular biology techniques

2.5.1 Transforming competent bacteria

Competent bacteria were transformed as follows: 50 μl of competent bacteria cells (stored at -80°C) per transformation were thawed slowly on ice before 0.2 μg of plasmid DNA was added. The mixture was then incubated on ice for a further 20

minutes before heat shocking at 42°C for 90 seconds. The bacteria were placed on ice for 2 minutes. 800 µl of LB media without antibiotic was then added before incubating the cells at 37°C for 1 hour with shaking at 150 rpm (allowing the transformed cells to express antibiotic resistance genes). Cells were pelleted by centrifugation at 4,000 rpm for 5 minutes and 600 µl media was discarded. The cells were re-suspended in the remaining 200 µl LB media and spread out on an LB plate supplemented with the appropriate selective antibiotic. The plate was incubated over-night at 37°C and colonies were selected for further processing.

2.5.2 Preparation of glycerol stocks of bacteria for freezing

3 ml of LB containing 100 µg/µl Ampicillin or 50 µg/µl Kanamycin was incubated with a single colony of bacteria over-night with shaking at 37°C. 1.5 ml of bacterial culture was pelleted by centrifugation at 4,000 rpm for 5 minutes. LB media was removed and the pellet resuspended in 400 µl LB media. After the addition of 400 µl 40% (w/v) glycerol, the bacteria were frozen at -80°C.

2.5.3 Isolation and purification of DNA (Mini prep protocol)

Plasmid DNA was isolated and purified from bacteria using QIAprep Miniprep according to the manufacturer's instructions. Bacteria from a single colony were shaken overnight at 37°C in 3 ml LB media containing 100 µg /ml Amphotericin or 50 µg/µl Kanamycin. 1.5 ml of bacteria was pelleted by centrifugation at 12,000 rpm for 1 minute. The bacterial pellet was resuspended in 250 µl buffer P1 (10 mM Tris pH 8.0, 0.5 mM EDTA, 100 µg /ml RNase, pH 9.0). Bacteria were lysed by adding 250 µl buffer P2 (200 mM NaOH, 1% SDS). The mixture was inverted six times and left at room temperature for 1 minute. Then the reaction was neutralized by 350 µl buffer N3 (4.2 M Gu-HCl, 0.9 M potassium acetate, pH 4.8) and centrifuged at 12,000 rpm for 10 minutes to separate plasmid DNA with other materials in the cell. The supernatant containing plasmid DNA was transferred to QIAprep spin column and centrifuged for

60 seconds at 12,000 rpm. The column was then washed by 750 µl buffer PE (10 mM Tris-HCl, 80% ethanol, pH 7.5) and centrifuged for 30 seconds at 12,000 rpm. The plasmid was eluted with 65 µl distilled water and stored at -20°C.

2.5.4 Purification of DNA (Maxi prep protocol)

Plasmid DNA was purified from bacteria using Hipure Plasmid Filter Maxprep kit according to the manufacturer's instructions. Bacteria from a single colony were incubated at 37°C in 250 ml LB media containing 100 µg /ml Ampicillin or 50 µg/µl Kanamycin for 16 hours. Bacteria were pelleted by centrifugation at 4000 rpm for 10 minutes. The pellet was resuspended in 10 ml resuspension buffer R3 (50 mM Tris-HCl, pH 8.0, 10 mM EDTA, 20 mg/mL RNase A). Bacteria were lysed by adding 10 ml lysis buffer L7 (0.2 M NaOH, 1% (w/v) SDS). The mixture was inverted gently six times and left at room temperature for 5 minutes. Then the reaction was neutralized by 10 ml precipitation buffer N3 (3.1 M Potassium acetate, pH 5.5). The precipitated lysate was transfer in to the pre-equilibrated column to allow the plasmids to bind to the column. The column was washed by 50 ml buffer W8 (0.1 M Sodium acetate, pH 5.0, 825 mM NaCl, 80% ethanol). Plasmid was eluted by 15 ml elution buffer E4 (100 mM Tris-HCl, pH 8.5, 1.25 M NaCl). The elution was mixed with 10.5 ml isopropanol and centrifuged at 12,000 rpm for 30 minutes at 4°C. The plasmid pellet was further washed by 5 ml 70% ethanol. After 15 minutes air-drying, 500 µl distilled water was added to the pellet to dissolve the plasmid. The plasmid concentration was measured and the plasmid was then stored at -20°C.

2.5.5 DNA Agarose gel electrophoresis

1% agarose gels were prepared by boiling 0.5 g agarose in 50 ml TAE. 2 µl ethidium bromide (10 mg/ml) or 5 µl SYBR® Safe DNA gel stain were added to the agarose prior to pouring into the gel apparatus. The gel was then allowed to solidify at room temperature for 20 minutes. Gels were run at 120 volts for 40 minutes. Images were

then captured by Bio-Rad Gel Doc EZ System.

2.5.6 Purification of DNA from agarose gels

DNA was purified using a QIAquick gel extraction kit according to the manufacturer's instructions. After electrophoresis, DNA bands were visualised under blue light and cut out of the gel by scalpel. The gel slice was resuspended in three volumes of buffer QG at 50°C for 10 minutes. After the gel dissolved, an equivalent gel volume of isopropanol was added to the sample and mixed. The whole sample was then applied to a QIAquick spin column and centrifuged at 12,000 rpm for 1 minute. The column was then washed by 750 µl buffer PE (10 mM Tris-HCl, 80% ethanol, pH 7.5) and centrifuged for 30 seconds at 12,000 rpm. The plasmid was eluted with 35 µl distilled water and stored at -20°C.

2.5.7 Restriction enzyme digests

1 µg DNA was digested with 10 U restriction enzyme in PCR tube at 37°C for 3 hours. If the sample was going to be used for DNA ligation, the vectors were treated with 1 µl Alkaline Phosphatase for 30 minutes to prevent self ligation after double digestion.

2.5.8 DNA ligation

Ligation mix contained 33% empty vector (~33 ng), 67% insert gene (~64 ng), 400 units of T4 DNA ligase in 1X T4 ligation buffer. Ligation was allowed to proceed for 12 hours at 14°C. The ligation sample was then transformed into competent cells.

2.6 Mammalian cell culture techniques

2.6.1 Culture conditions

HEK293 and HeLa cells were cultured in Dulbecco's Modified Eagle Medium supplemented with 10% heat inactivated fetal bovine serum and 1% penicillin/streptomycin and glucose. Cells were incubated at 37°C in a humidified atmosphere with 5% CO₂ and passaged 1:5 -1:10 every three days.

2.6.2 Mammalian cell transfection strategies

2.6.2.1 Transfection of HEK293 cells

HEK293 cells were transfected by the calcium phosphate method (Sambrook et al). Cells were split to 20% confluence three hours before transfection in 10cm dishes. 10 µg DNA was mixed with 62 µl 2 M CaCl₂ and H₂O to the final volume of 500 µl. This was added drop wise to 500 µl 2x HBS. 15 minutes later, the mixture was dropped to the cells. 48 hours later, the cells were harvested for further use.

2.6.2.2 Transfection of HeLa cells

HeLa cells were transfected by polyfect transfection reagent according to the manufacturer's instruction. 4×10^5 cells were seeded in 6-well plates with 3 ml growth media 20 hours prior to transfection. The cells would be 40% confluent on the day of transfection and the cell media was changed to fresh cell growth media (containing serum and antibiotics) at the beginning of transfection. 1.5 µg of DNA was diluted in cell growth media containing no serum, protein, or antibiotics to the volume of 100 µl. 12 µl polyfect transfection reagent was mixed with the DNA solution. This was then incubated at room temperature for 15 minutes. 15 minutes later, 600 µl cell growth media (containing serum and antibiotics) was added to the reaction tube. The mixer

was immediately added to the cells in the 6-well plate.

2.7 Insect cell culture techniques

2.7.1 Sf21 cell Culture

Sf21 cells were cultured in Sf-900™ II SFM media supplemented with 5% heat inactivated foetal bovine serum and 1% penicillin/streptomycin and glucose. Cells were cultured at 25°C and split 1:5 -1:10 every three days and maintained between 10^5 - 10^6 cells per ml.

2.7.2 Baculovirus infection of Sf21 cells

150 ml Sf21 cells were cultured in 0.5×10^6 density 16 hours before infection. 5 ml of baculovirus (6×10^6 pfu/ml, made by Elizabeth Smythe, Department of Biomedical Science, University of Sheffield) was added to the cell. 72 hours later the cells were harvested for further use. The original viral stock was a generous gift from Professor Katada's lab at the University of Tokyo.

2.8 Protein techniques

2.8.1 Bradford assay

Protein concentration was determined by the Bradford method (Bradford, 1976). 1 ml Bradford dye reagent concentrate was diluted with 4 ml H₂O. 5 µl of the protein sample to be assayed was added to 995 µl diluted dye. The absorbance was measured at 595 nm and compared to known BSA standards.

2.8.2 SDS-polyacrylamide gel electrophoresis

The separating gels were prepared as a 5 ml mix of 1.7 ml acrylamide (30%w/v), 1.3 ml 1.5 M Tris (pH 8.8), 2 ml H₂O, 50 µl 10% SDS, 50 µl ammonium persulphate and 4 µl TEMED. The stacking gels were prepared as a 3 ml mix of 2.1 ml H₂O, 500 µl acrylamide (30% w/v), 380 µl 1 M Tris (pH 6.8), 30 µl 10% SDS, 30 µl ammonium persulphate and 3 µl TEMED. Before electrophoresis, protein concentrations were measured by the Bradford assay. Samples were equalized for protein and boiled at 100°C for 5 minutes in SDS loading buffer. Polymerized gels were assembled into a Bio-Rad Mini-Protein II apparatus and filled with SDS gel running buffer. The gel was run at 100 volts for 30 minutes until the samples had left the stacking gel and then 120 volts for 1-2 hours to electrophorese through the separating gel. Protein ladders (colorplus prestained protein ladder broad range, New England Biolabs) were run alongside lysates to assess the size of protein bands.

2.8.3 Coomassie blue staining of gels

A 45% (v/v) methanol, 10% (v/v) acetic acid solution was mixed with phast gel blue tables. Gels were stained for 2 hours and de-stained in de-stain buffer (10% v/v methnol, 10% v/v acetic acid) for 4 hours.

2.8.4 Immunoblotting

After electrophoresis, gels were removed from the retaining plate and overlaid with pre-wet nitrocellulose sandwiched by Whatmann 3 MM paper. Transfer was carried out at 400 mA/constant current for 80 minutes at 4°C in Bio-Rad mini protean II apparatus. Once transferred, the membrane was stained with Ponceau S solution to check the transfer quality and blocked with 5% (w/v) milk powder dissolved in TBS for 1 hour at room temperature. Following blocking, the membrane was incubated with primary antibody (see table 1) diluted in blocking buffer, against the target protein,

overnight at 4°C. The membrane was then rinsed in TBS 3 times for 10 minutes and incubated with secondary antibody conjugated to HRP at 1:5000 for 1 hour at room temperature. Following three x 10 minutes washes in TBS, membranes were incubated with ECL select western blotting reagents (GE Healthcare), according to the manufacturer's instructions. Images were then captured by Bio-Rad cameras.

2.8.5 Bis-Tris Native PAGE electrophoresis

Native PAGE™ Novex™ 3-12% Bis-Tris Protein Gels were obtained from Invitrogen and assembled into XCell SureLock® Mini-Cell mini apparatus. Samples were mixed with 4X native PAGE sample buffer. Mixed samples and 5µL of Native Mark™ Unstained Protein Standard (Invitrogen) were loaded into the wells. Samples were then top filled with dark blue Cathode buffer to provide easy visualization of the sample wells. The upper buffer chamber was then filled with 220ml dark blue cathode buffer, so the buffer level did not exceed the level of the wells and the lower buffer chamber was filled with 200ml Native PAGE running buffer. Samples were run at 100 volts for 1 hour. Then the upper buffer chamber was changed to light blue cathode buffer and the sample continued run at 150 voltages for 4-5 hours.

2.8.6 Coomassie staining of native PAGE

After native PAGE electrophoresis, the gel was quickly placed in fix solution (40% methanol, 10% acetic acid), microwaved on high power for 45 seconds and incubated in fix solution for 15 minutes at room temperature. The gel was then stained in 100 ml Coomassie R-250 Stain solution for 2 hours at room temperature. The gel was finally de-stained in 8% acetic acid solution.

2.8.7 Native PAGE western blot

The polyvinylidene difluoride (PVDF) membrane was pre-wetted in methanol for 15

seconds. The membrane was briefly rinsed in distilled water and then placed in 1X transfer buffer. After native PAGE electrophoresis, gels were removed from the retaining plate and overlaid with pre-activated PVDF membrane sandwiched by Whatmann 3 MM paper. Transfer was carried out at 25mA/constant current overnight at room temperature. After transfer, the membrane was incubated in 20 ml of 8% acetic acid for 15 minutes to fix the proteins. The membrane then could be used for immunoblotting.

2.9 Protein purification

2.9.1 Purification of GST fusion proteins

pGEX plasmids encoding GST fusion proteins were transformed into BL21 DE3 cell strain. A single colony from the transformed bacteria plate was cultured in 5 ml LB media containing 100µg/ml ampicillin at 37°C with shaking overnight. 5ml of the overnight media was transferred to 500ml LB media containing 100 µg/ml ampicillin. After 3 hours shaking at 37°C, when the OD of bacteria at 600 nm reached 0.6~0.7, IPTG was added to final concentration of 250 µM to induce the target protein expression. The bacteria were incubated with shaking at 37°C for another 4 hours before harvesting. For GST-GAP and GST-GEF fusion protein, the induction temperature was 25°C. For GST-hRme6 and GST-IQGAP1, fusion protein, the induction temperature was 20°C. Bacteria were harvested by centrifugation at 4,000 rpm for 10 minutes in a JLA10.5 rotor.

The bacterial pellet was then resuspended in 25 ml cold TBST (TBS containing 1% Triton X-100 (w/v), complete protease inhibitor cocktail (Roche) and 1 mM PMSF). Bacteria were further broken by sonication with 10x10 second bursts with 20 seconds interval on ice. Samples were then centrifuged for 30 minutes at 12,000 rpm in a

Beckman JA 25.50 rotor to separate the insoluble material from the lysate. At the same time, 1 ml of glutathione agarose slurry was pre-washed twice with 50 ml cold TBS. The bacterial supernatant was isolated and incubated with glutathione agarose beads at 4°C for 1 hour on a rotating wheel. After incubation, the beads were washed three times with 50 ml cold TBS. Fusion protein was eluted from the beads by fresh made elution buffer (10 mM glutathione in TBS, pH 7.4). The purified GST fusion protein was aliquoted and stored at -80°C. The concentration of the protein was measured by Bradford method. 30 µl of beads and 30 µl eluted protein were prepared for SDS-PAGE to check the purity of the protein.

2.9.2 Purification of GST-Rab5 protein

pGEX-6p-1 plasmids encoding GST-Rab5 protein were transformed into BL21 (DE3) cell line. Bacteria were grown according to the method described above for GST fusion proteins. The harvested bacterial pellet was resuspended in 25 ml cold buffer A (50 mM Tris, pH 7.5, 50 mM NaCl, 5 mM MgCl₂, 50 µM GDP) with 1% Trion X-100(w/v)containing complete protease inhibitor cocktail and 1 mM PMSF. Bacteria were further broken by sonication with 10x10 second burst with 20 seconds interval on ice. Samples were then centrifuged for 30 minutes at 12,000 rpm in a Beckman JA 25.50 rotor to separate the insoluble material from the lysate. 1 ml of 50 % glutathione beads slurry was washed three times with 50 ml buffer A with 1% Trion X-100 and 100 µM GDP. The supernatant was then incubated with the beads at 4°C for 1 hour on a rotating wheel. After incubation, the beads were washed three times with buffer A containing 1% Trion X-100 and twice more with just buffer A. The protein was then eluted from the beads by freshly made elution buffer (10 mM glutathione in buffer A, pH was checked to ensure that it was >8.0)

2.9.3 Purification of his-SNX9 and his-SNX24 proteins from bacteria

Bacteria were grown as described above for GST-fusion proteins. After sonication

and centrifugation, the supernatant was incubated with Ni-NTA resin at 4°C for 1 hour on a rotating wheel. The beads were washed three times with 50ml cold TBS containing 20 mM imidazole. The protein was eluted from the beads by TBS containing 250 mM imidazole (pH 7.4). The purified protein was aliquoted and stored at -80°C. The concentration of the protein was measured by Bradford method.

2.9.4 Purification of Flag-hRme-6 from insect cells and HEK293 cells

Sf21 cells overexpressing Flag-hRme-6 were centrifuged and the pellet from 150 ml of cells was lysed in 20 ml lysis buffer (20 mM Hepes (pH 7.4), 150 mM KCl, 1 mM MgCl₂, 1% Triton X-100 (w/v), containing complete protease inhibitor cocktail and 1 mM PMSF) for 15 minutes on ice and centrifuged at 12,000 rpm for 30 minutes at 4°C. At the same time, 0.5 ml Flag M2 affinity gel slurry was pre-washed twice using 50 ml cold TBS. The insect cell supernatant was incubated with Flag M2 affinity gel at 4°C for 2 hours on a rotating wheel. The beads were then washed three times with 100 ml cold TBS. Flag-hRme-6 was eluted from the beads by 1.5 ml TBS containing 50 ng/ml Flag peptide. The purified protein was aliquoted and stored at -80°C. The concentration of the protein was measured by Bradford method.

pcDNA3.1-Flag-hRme-6 or pcDNA3.1-Flag-hRme-6-his plasmid was transfected into HEK293 cells by calcium phosphate[202]. 3x10⁶ HEK293 cells overexpressing Flag-hRme-6 were lysed in 5 ml lysis buffer (20 mM Hepes (pH 7.4), 150 mM KCl, 1 mM MgCl₂, 1 mM CaCl₂ containing 1% NP-40 (w/v) containing complete protease inhibitor cocktail and 1 mM PMSF) for 15 minutes on ice. Cells were then centrifuged at 12,000 rpm for 30 minutes at 4°C. The Flag-hRme-6 was then purified as described above from insect cells.

2.10 Immunoprecipitation

40 μ l 50% protein G agarose beads slurry was washed twice with 1.5 ml PBS to remove the ethanol. The beads were then incubated with 2 μ g antibody for the target protein for 1 hour at 4°C. Unbound antibody was removed by three washes in TBS.

After cell stimulation, the cell culture dish was placed on ice and washed twice with cold PBS. Pre-chilled cell lysis buffer (1 ml per 10^7 cells/100 mm dish/150 cm² flask; 0.5 ml per 5×10^6 cells/60 mm dish/75 cm² flask) was added to the dish. Cells were then scraped off the dish using a cold plastic cell scraper and the cell lysate was gently transferred into a pre-cooled microfuge tube. The cell lysate was then kept on ice for 10 minutes and centrifuged at 12,000 rpm for 30 minutes. After centrifugation, the supernatant was transferred to a fresh tube and kept on ice. The protein concentration of the lysate was measured by Bradford assay. 700 μ g of cell lysis was mixed with the beads preloaded with antibody and incubated at 4°C under rotary agitation overnight.

After incubation, the tube was centrifuged for 5 minutes at 500 *g*. The supernatant was removed and the beads were washed in lysis buffer three times (each time the beads were incubated with lysis buffer 5 minutes following centrifugation at 4°C and the supernatant was discarded). Finally, the last supernatant was removed and 20 μ l of 2x loading buffer was added to the beads. The sample was boiled at 100°C for 5 minutes to denature the proteins and separate them from the protein G beads. The sample was centrifuged and the supernatant was loaded to the SDS PAGE. After SDS-polyacrylamide gel electrophoresis, the sample was analyzed by Immunoblotting.

2.11 In-vitro Ras GTPase stimulating assays (GAP assay)

Recombinant human hRas was preloaded with γ -P³² GTP in a reaction containing

100 μl GST-Ras (34 ng/ μl) protein, 100 μl $\gamma\text{-P}^{32}$ GTP (4 pmol $\gamma\text{-P}^{32}$ GTP) (6000 Ci/mmol; PerkinElmer Life Sciences) in 50 mM Hepes, pH 6.8, 1 mg/ml BSA, 1 mM DTT at 30°C for 30 minutes. The amount of bound $\gamma\text{-P}^{32}$ -GTP was determined by filtration of 1 μl of the pre-loaded GST-Ras onto a nitrocellulose filter and Cherenkov counting. During Ras preloading, 19 μl of the GAP sample to be assayed was mixed with 11 μl of reaction buffer (5 μl of 10x GAP assay nucleotide loading buffer, 5 μl of 10 mM GTP, 1 μl of 250 mM MgCl_2) on ice. The reaction was started by adding 20 μl of the pre-loaded GST-Ras to the 30 μl GAP/buffer combination, mixing, and placing at 30°C with gentle shaking. As there were high amount of nonradioactive GTP in the reaction buffer, GST-Ras cannot bind radioactive GTP again after hydrolysis, so the GAP activity was measured by the single round turnover of the released γ -phosphate into the reaction. At individual time points, 10 μl of the reaction sample was taken and mixed with 790 μl ice-cold 5% (w/v) activated charcoal in 50 mM NaH_2PO_4 to stop the reaction. The charcoal was pelleted, and the amount of released P^{32} in 400 μl of the supernatant was determined by Cherenkov counting. The percentage of released $\gamma\text{-P}^{32}$ was then calculated and expressed as the amount of nonradioactive GTP been catalysed [203].

2.12 In-vitro GEF assay

400 μl GST-Rab5 proteins immobilized on glutathione agarose beads were washed once with fresh GEF assay pre-loading buffer and incubated in this buffer for 20 minutes at 30°C with constant shaking to load GDP. The beads coupled with GST-Rab5 protein were then washed twice with reaction buffer and mixed with 100 pmol $\alpha\text{-P}^{32}$ GTP (6000 Ci/mmol; PerkinElmer Life Sciences) to the volume of 600 μl . Equal volumes of beads were added to various conditions and incubated at 30°C with constant shaking. A 50 μl reaction contained 30 μl preloaded GST-Rab5, 20 μl other additions including 4 pmol $\alpha\text{-P}^{32}$ GTP and 5 mmol cold GTP. The reaction was stopped by add 950 μl ice-cold stop buffer to the 50 μl reaction. The beads were then washed

twice with cold stop buffer at 2,000 rpm for 5 mins. The beads were then counted. The amount of nucleotide exchange was reflected by the amount of GTP bounded to GST-Rab5 on beads[157].

2.13 Gel filtration

SuperdexTM-200 gel filtration (GE Healthcare) column was equilibrated with cold KSHM buffer. Superose 6 HR 10/30 gel filtration column (GE Healthcare) was equilibrated with the control buffer (20 mM HEPES (pH 7.4), 100 mM KCl, 1 mM EDTA, 1 mM EGTA, 2 mM MgCl₂, 10% glycerol, and 0.5 mM DTT). Protein samples were centrifuged at 12,000 ×rpm for 10 minutes at 4°C before being injected into the column. 100-500 µg of the protein supernatant was loaded onto the column which was run at a flow rate 0.15 ml/min. Every 0.15 ml sample was collected as a fraction. 25 µl aliquot of each fraction was subjected to SDS PAGE and checked by immunoblotting.

2.14 Electron Microscopy

2.14.1 Electron Microscopy hardware

All negative samples were sectioned using a Reichert-Jung Ultracut E microtome. Samples were examined at 100kv using the Philips CM100 transmission electron microscope which were recored by Gatan Multiscan 794, 1K X1K charge-couple device camera, and at an accelerating voltage of 80Kv using FEI Tecnai transmission electron microscope which were recorded using a Gatan Orius 1000 digital camera and Digital Micrograph software.

2.14.2 Negative staining

2.14.2.1 Preparing uranyl formate

0.75% uranyl formate was prepared and stored in the fridge. 4.5 ml boiling water was added to 0.0375 g of uranyl formate. This was protected from the light and stirred for 5 minutes. 5 M NaOH (~8 μ l) was added until a slight change of the colour happened. The solution was stirred for another 5 minutes, filled to 5 ml and then filtered through a 0.2 μ m filter.

2.14.2.2 Glow discharging of carbon-coated grids

Glow discharge of grids was sectioned using a Reichert-Jung Ultracut E microtome. Glow discharge of grids was carried out on a parafilm coated microscope slide. Time for glow discharging varied but was typically 15 seconds for fresh grids, 25-30 seconds for one-week to one-month old grids and 30-60 seconds for grids older than one month. Times could be prolonged up to 120 seconds depending on the specimen.

2.14.2.3 Negative staining

Staining of the sample was carried out on a piece of parafilm on double sticky tape on a safe tray. Two drops of distilled water and two drops of 0.75% uranyl formate were placed on the parafilm. 5 μ l of protein sample was dropped on to a freshly glow-discharged grid, left for 60 seconds and quenched by clean filter paper. The grid was then washed shortly over two drops of water and one drop of uranyl formate with blotting between each drop. The grid was then incubated in the final drop of uranyl formate for 20 seconds, blotted with filter paper and dried with the pump. The grids were then kept at room temperature for future use.

2.15 Fluorescence Microscopy

2.15.1 Coverslip preparation

Coverslips were sterilized immediately before the experiment. This was achieved by microwaving the glass coverslips for three minutes at 900W in the Petri dish.

2.15.2 Preparation of paraformaldehyde

4% (v/v) paraformaldehyde (PFA) was prepared. 8 g paraformaldehyde was added to 100 ml milliQ water. The mixture was stirred and heated to 60°C in the fume hood. NaOH was added drop-wise until the solid was completely dissolved. The solution was then cooled down to room temperature and mixed with 100 ml 2XPBS, and the pH readjusted. The final solution was then aliquoted and stored at -20°C.

2.15.3 Immunofluorescence protocol

HeLa cells were grown on coverslips placed in 35-mm tissue culture dish the day before the experiment. Cells were seeded to achieve a maximum confluency of 60% the following day. On the next day the growth medium was removed and HeLa cells were incubated in media without serum for 24 hours before stimulation. After starvation HeLa cells were then stimulated with EGF for 2, 5, 10, 20 or 30 minutes or left untreated. Plates were then washed twice with PBS and fixed by 1 ml of 4% PFA for 20 minutes on ice. The plates were washed twice with 50 mM NH₄Cl in PBS to quench the PFA fixative. Cells were then permeabilized with 0.2% Triton X-100 in PBS for 3 minutes. To minimize nonspecific binding of the antibody, the coverslips were incubated with blocking buffer (0.2% fish skin gelatin in PBS) for 30 minutes. Cells were then incubated with primary antibodies diluted in blocking buffer at room temperature for 60 minutes or overnight at 4°C as below. 30 µl diluted primary antibody was dropped on clean parafilm for each coverslip. The coverslips were

carefully taken from the plates and inverted onto the 30 μ l drop. After incubation, the coverslips were returned to the plates and unbound primary antibodies were removed by washing three times for 5 minutes with PBS. The fluorescence secondary antibody staining was performed as above for 30 minutes in the dark. After antibody incubation, the coverslips were put back to the plates and washed twice with PBS. To visualize nuclei, the coverslips were then incubated with DAPI at 1 μ g/ml followed by three more washes with PBS and three times with milliQ water to remove any residual salt. A drop of pro-long mounting reagent was added to the glass and the coverslips were inverted onto it. The coverslips were left overnight in the dark to allow the mounting media to permeate the fixed cells. Slides were then stored at -20°C before further imaging.

2.16 Proximity ligation assays

After fixation and permeabilisation and incubation with primary antibody as described above for the immunofluorescence protocol, the coverslips were washed three times for 5 minutes each with wash Buffer A from the kit to remove unbound antibody. Secondary proximity probes are donkey anti-mouse, donkey anti-rabbit or donkey anti-goat affinity purified antibodies conjugated with aldehyde-modified oligonucleotides to generate mouse MINUS, rabbit PLUS probes, goat MINUS. The secondary antibodies were diluted 1:5 in blocking buffer and staining was performed as above for 60 minutes at 37°C in a humidified chamber. Unbound proximity probes were removed by washing twice for 5 minutes in wash buffer A. Then the hybridization/ligation mixture (10 mM Tris acetate at pH 7.4, 10 mM magnesium acetate, 50 mM potassium acetate, 250 mM NaCl, 0.25 μ g/ μ l BSA, 0.05% Tween-20, 1 mM ATP, 0.05 unit/ μ l T4 DNA ligase) was prepared. The coverslips were incubated in the ligation mixture for 30 minutes at 37°C in a humidified chamber. Residual ligation

mixture was removed by washing twice for 2 minutes in wash buffer A. Then the amplification was performed in amplification buffer (33 mM Tris acetate at pH 7.9, 10 mM magnesium acetate, 66 mM potassium acetate, 0.25µg/µLBSA, 0.1% Tween-20, 1 mM DTT, 250µM dNTP, 0.05 unit/µl DNA polymerase) for 100 minutes at 37°C in a humidified chamber. Residual amplification mixture was removed by washing twice for 10 minutes in wash buffer B and 1 minute in 0.01x wash buffer B. The coverslips were dried in the dark and mounted on microscope slides with Duolink in Situ mounting medium with DAPI. Slides were then stored at -20°C for further imaging.

2.17 Mass spectrometry

All the samples were preceded by in gel digestion as described below.

2.17.1 Gel fragment preparation and destaining

After immunoprecipitation of the target protein, the sample was electrophoresed in NuPAGE™ Novex™ 4-12% Bis-Tris Protein Gels (Life Technology). The gel was stained in InstantBlue (Expedeon) for 15 minutes in a clean petri dish and de-stained by washing 3 times for 5 minutes each with 40 ml Milli-Q water. The sample lane was then carefully cut into 1 mm piece within a fume hood by a fresh clean scalpel. The gel pieces were transferred into a clean siliconized eppendorf tube and dehydrated twice for 30 minutes with 200 µl 200 mM NH₄HCO₃ / 50% Acetonitrile. The pieces were then dried down in a vacuum concentrator for 15 minutes which caused the gel pieces to shrink and become white.

2.17.2 Reduction and Alkylation

The gel pieces were then rehydrated in 200 µl freshly prepared reduction buffer (10 mM Dithiothreitol in 50 mM NH₄HCO₃) for 1 hour at 56°C. The gel pieces were then cooled down to room temperature and the reduction buffer was discarded. 200µl

freshly prepared alkylation buffer (55 mM iodoacetamide in 50 mM NH_4HCO_3) was added to the gel pieces and incubated at room temperature for 30 minutes in the dark. After the incubation, the alkylation buffer was discarded and the gel pieces were washed twice by 15 minutes in 50 mM NH_4HCO_3 . Then 200 μl of 50 mM NH_4HCO_3 / 50% Acetonitrile were added to dehydrate gel pieces at 56°C for 30 minutes. The pieces were then dried down in a vacuum concentrator for 15 minutes.

2.17.3 Trypsin Digestion

Gel pieces were then rehydrated for 5 minutes at room temperature in 20 μl digestion solution containing 400 ng Trypsin (Promega Sequence Grade Modified) in 40 mM NH_4HCO_3 / 9% Acetonitrile. The rehydrated gel pieces were overlaid with 50 μl of 40 mM NH_4HCO_3 / 9% Acetonitrile to keep the gel immersed throughout the digestion. The gel pieces were then incubated at 37°C overnight.

2.17.4 Peptide recovery and solid phase extraction

After Trypsin digestion, the gel pieces were centrifuged at 13,000 rpm for 10 seconds. The solution was then transferred to a fresh siliconized eppendorf tube. The gel pieces were then further extracted twice by incubated with 20 μl 100% Acetonitrile at 37 °C for 15 minutes, followed by 50 μl 5% Trifluoroacetic acid at 37°C for 15 minutes. The gel pieces were finally extracted by 50 μl 50% Acetonitrile/5% Trifluoroacetic acid at 37°C for 30 minutes. All the extracted solutions were collected to the siliconized eppendorf tube and dried completely in a vacuum centrifuge for 3 hours. The peptides were then re-suspended in 20 μl of Millipore water / 0.1% TFA by incubating for 5 minutes at room temperature with intermittent vortexing. Sample pool was created by mixing of 10 μl of each digested sample. The sample pool would be re-dried and re-suspended to the final volume around 20 μl . The sample was then transferred into a sample vial and loaded into autosampler tray of Dionex 3000 system by Richard Beniston / Mark Collins (BiOMiCs Facility, University of Sheffield).

Remaining individual samples were stored at -20°C.

3. Chapter 3 Exploration of the functional domains of hRme-6

3.1 Introduction

hRme-6 is a multi-domain protein which is involved in clathrin mediated endocytosis. It is composed of a C-terminal GEF or Vps9 domain, and an N-terminal potential Ras GAP domain. In vitro experiments have shown that the GEF domain of hRme-6 has GDP release activity for Rab5 [204]. The yeast two-hybrid system confirmed that Rme-6 had a strong interaction with Rab5-GDP [158, 160]. The Ras GAP domain is a highly conserved domain from *C. elegans* to human, implying that it may have important functions. However, it is still not clear how the activities of the two domains of hRme-6 are regulated and whether the activity of one is dependent on the other. Previous studies failed to identify genetic or physical interactions between Rme-6 and LET-60, the canonical *C. elegans* Ras [204]. Previous studies from our lab showed that hRme-6 recruited Rab5 to clathrin-coated vesicles via interactions with the AP2 adaptor complex. SiRNA of hRme-6 but not Rabex5 caused a delay in AP2 uncoating during Tfn endocytosis in HeLa cells, suggesting a role of hRme-6 at the very early stages of endocytosis. Work from the Stahl group indicated that hRme-6 also played important roles in EGFR phosphorylation, ubiquitination and degradation in HeLa cells [205]. The function of hRme-6 in EGFR endocytosis was independent of its GEF ability to activate Rab5 but through the interaction between its Ras GAP domain with the ubiquitin ligase, c-Cbl. These data implied that there might be the different functions of the Rab5 GEF domain and Ras GAP domain of hRme-6 depending on which cargoes were being internalized. The underlying cause of the different functions is not yet known. Characterization of the domain activities should provide further insight into how the two domains of hRme-6 affect its functions.

Previous work from our lab showed that in Ang1 stimulated HUVEC cells, the ligand Ang1 promotes internalisation of the receptor tyrosine kinase, Tie2, and

phosphorylation of Akt and p38 MAPK. However, over-expression of hRme-6 decreased the phosphorylation of Akt and increased the phosphorylation of p38 MAPK. This work suggested a role for hRme-6 during signal transduction of Tie2. However, whether the role of hRme-6 in Tie2 signal transduction was also applicable for other signalling cargoes and how hRme-6 was involved in signal transduction was unknown.

My aim in this section was to investigate the activities of the Rab5 GEF and Ras GAP domains of hRme-6 and explore their roles during Tie2 and EGFR signal transduction. The objective was to get the outline of the domain activities and use the information to build the model system to investigate the biochemical basis for hRme-6-mediated segregation of signalling as hRme-6 appears to be required for transferrin internalisation while its overexpression appears to inhibit Tie2 uptake.

3.2 Investigating the GAP domain of hRme-6 Ras GAP activity

Although there was already some research that focused on the Rab5 GEF domain and Ras GAP domain of hRme-6 and its activities, there is still no clear evidence showing that the Ras GAP domain of hRme-6 has Ras GAP activity. I started to investigate the activity of Ras GAP domain of hRme-6 in vitro.

The GAP domain of hRme-6 and Ras protein were expressed in *E.coli* BL21 (DE3) as described in Materials and Methods. The expression level of GST-hRme-6-GAP domain and GST-Ras were relatively high in *E.coli* BL21 (DE3). But most of the fusion proteins stayed in the pellet after sonication (Figure 3.1). Although the concentrations of the purified GST-hRme-6-GAP domain and GST-Ras were not high, they were greatly enriched following purification on GSH agarose and were thus suitable for testing in a GAP assay.

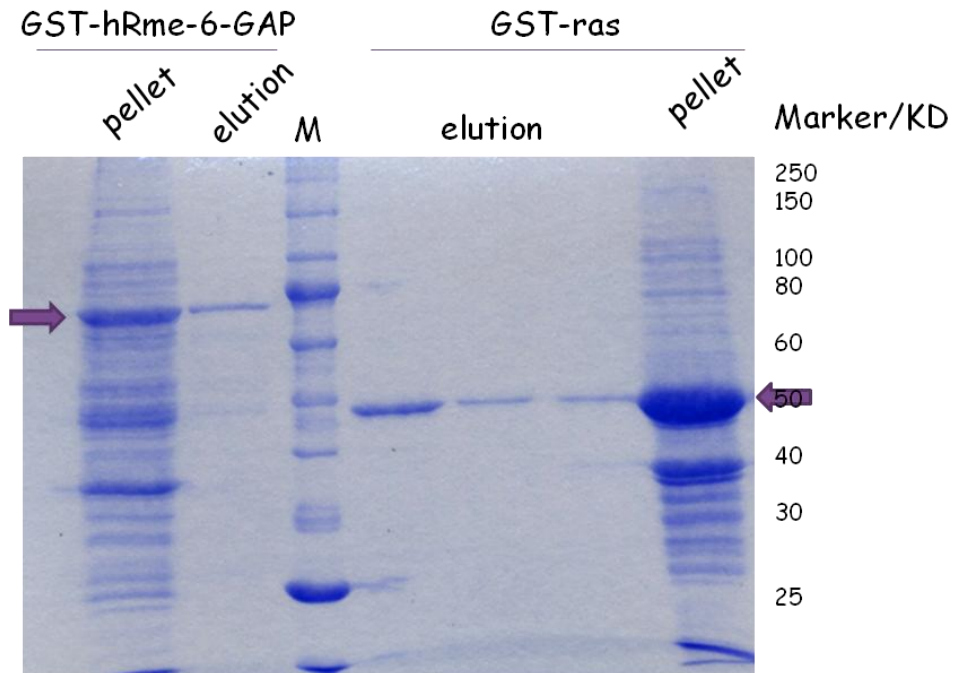


Figure 3.1 Purification of GST-hRme-6-GAP domain and GST-Ras from *E.coli*. pGEX-6p-1-hRme-6-GAP and pGEX-6p-1-Ras plasmids were transfected into BL21 (DE3) competent cells. Bacterial cell lysates were prepared as described in material and methods and incubated with GSH agarose beads at 4°C for 1 hour. The beads were washed three times with cold TBS containing 1% Triton X-100. GST proteins were further eluted by 15 mM GSH. Eluted GST proteins were analyzed by SDS-PAGE and stained with coomassie blue. The positions of the purified proteins are indicated by the arrows.

The Ras GTPase stimulating assays were set up to test the Ras GAP activity of GST-hRme-6-GAP domain. As it is shown in figure 3.2, the GST-GAP domain of hRme-6 displayed Ras GAP activity in vitro. In 30 minutes, 6.4 pmol of the GST-GAP domain of hRme-6 catalysed 0.43 nmol Ras-GTP to Ras-GDP. It was equal to that 2.26 mol of Ras-GDP was produced per 1 mol GAP per minute. The published data showed that the typical activity of Ras GAP protein p120 was around 10 mol/min. Compared to the p120 Ras GAP, the GST- Ras GAP damain of hRme-6 exhibited lower activity. However subsequent studies from our lab have revealed that full length Rme-6 can be activated to demonstrate RasGAP activity comparable to that of p120rasGAP. Further purification of GST protein would help the test and clarify the activity of Ras GAP

domain of hRme-6.

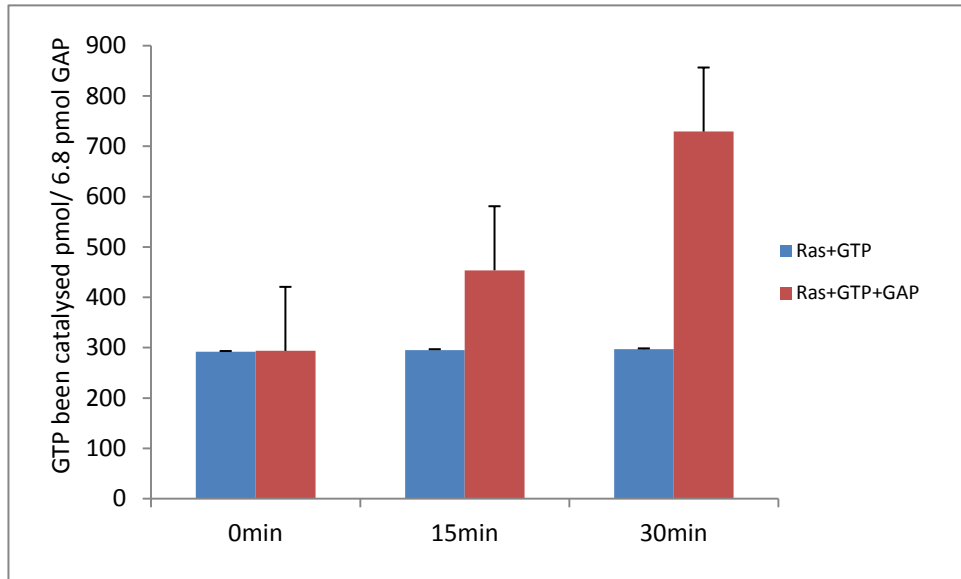


Figure 3.2 Ras GAP domain of hRme-6 exhibits GAP activity. A GAP assay was carried out as described in Materials and methods. Reaction mixes contained GST-GAP protein, GST-Ras pre-loaded with γ -P³²-GTP. The reactions were incubated at 30 °C and stopped at the indicated time points. The amount of released ³²Pi was determined by Cherenkov counting and changed to GTP been catalysed in each assay. Results are the mean \pm SD of two experiments each performed in duplicate.

3.3 Investigating hRme-6 Rab5 GEF activity

Full length Flag-hRme-6 was purified from the lysates of Sf21 cells that infected with baculovirus expression Flag-tagged hRme-6 (Figure 3.3A) and GST-Rab5 was purified from *E.coli* BL32 (DE3) (Figure 3.3B) as described in Materials and Methods.

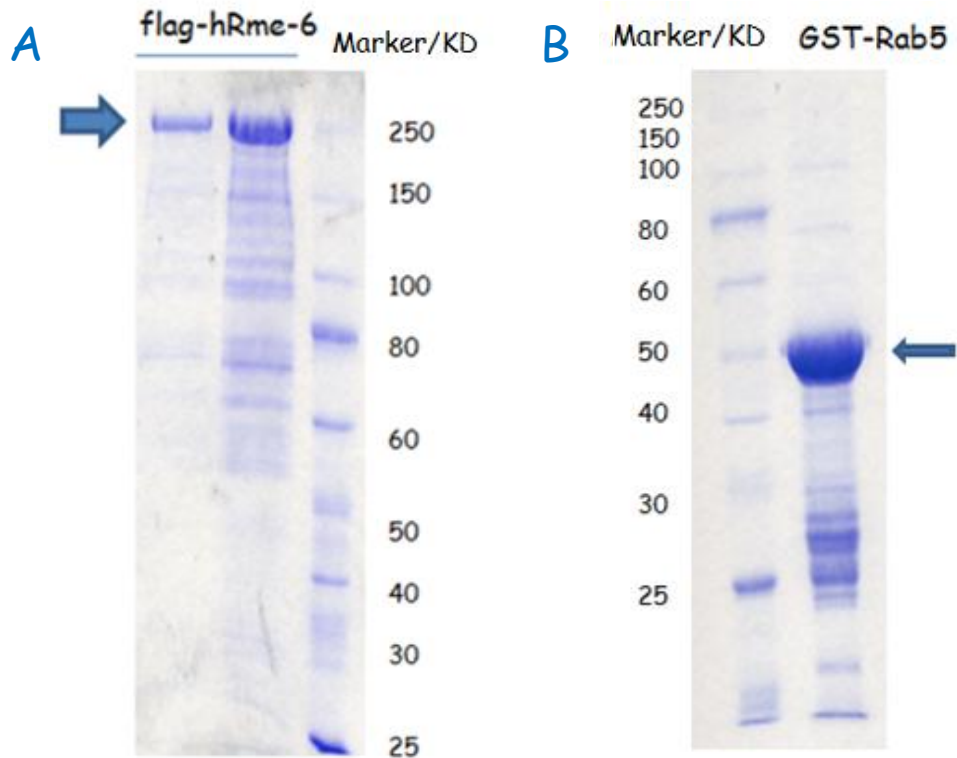


Figure 3.3 purified Flag-hRme-6 from insect cells and GST-Rab5 from *E.coli*. A, Flag-hRme-6 was immunoprecipitated using M2 anti-Flag beads from Sf21 cells overexpressing Flag-hRme-6. After elution from the beads by Flag peptide, 15 μ l purified Flag hRme-6 was loaded on 10% SDS-PAGE gel and stained with coomassie blue. The arrow shows the purified protein. B, GST-Rab5 was purified using glutathione agarose beads and eluted by 15 mM GSH. Eluted GST-Rab5 were analyzed by SDS-PAGE and stained with coomassie blue. The arrow showed the purified protein location.

Previous work from our lab had shown that hRme-6, purified from HEK293 cells, has GDP release activity for Rab5 in vitro only in presence of ATP and AP2 [206]. Using purified Flag-hRme-6 from insect cells and GST-Rab5 from *E.coli* BL32 (DE3) strains, the GEF assay was set up. As it is shown in Figure 3.4, Flag-hRme-6 also exhibited strong Rab5 GEF activity in presence of ATP and AP2. There is no GEF activity of hRme-6 on Rab5 with either ATP or AP2 single (data not shown as it just tested once). In 30 minutes time, the increase in GEF activity of hRme-6 alone was nearly the same as the increase of intrinsic activity of Rab5. However, in presence of

ATP and AP2, the Rab5 GEF activity of hRme-6 increased significantly compared to incubations missing one or the other of these components. After 30 minutes, the activity of hRme-6 slowed down relatively and the background increased.

It is known that Rme-6 physically interacts with endogenous α -adaptin (AP2) [204]. Our labs previous data also showed that HA-hRme-6 purified from HEK293 cells also exhibited strong Rab5 GEF activity only in presence of ATP and AP2 [206], although the C-terminal Rab5 GEF domain alone also showed specific GEF activity against Rab5. It was also shown that hRme-6^{F1487A}, which could not bind to AP2, did not exhibit GEF activity in presence of ATP and AP2. This implied that the autoinhibition of the GEF activity of full-length hRme-6 may be based on a conformational change. Purified Flag-hRme-6 from insect cells showed the same characteristics as that from HEK293 cells, which suggested that the recombinant protein had the same conformation and activity as the protein purified from HEK293 cells. However the amount of HA-hRme-6 that could be purified from HEK293 cells was quite low whereas the amount of Flag-hRme-6 purified from insect cells was relatively large. Moreover the Rab5 GEF assay suggested that the purified Flag-hRme-6 from insect cells showed similar Rab5 GEF activity to the HA-hRme-6 purified from HEK293 cells and thus could be used for further analysis.

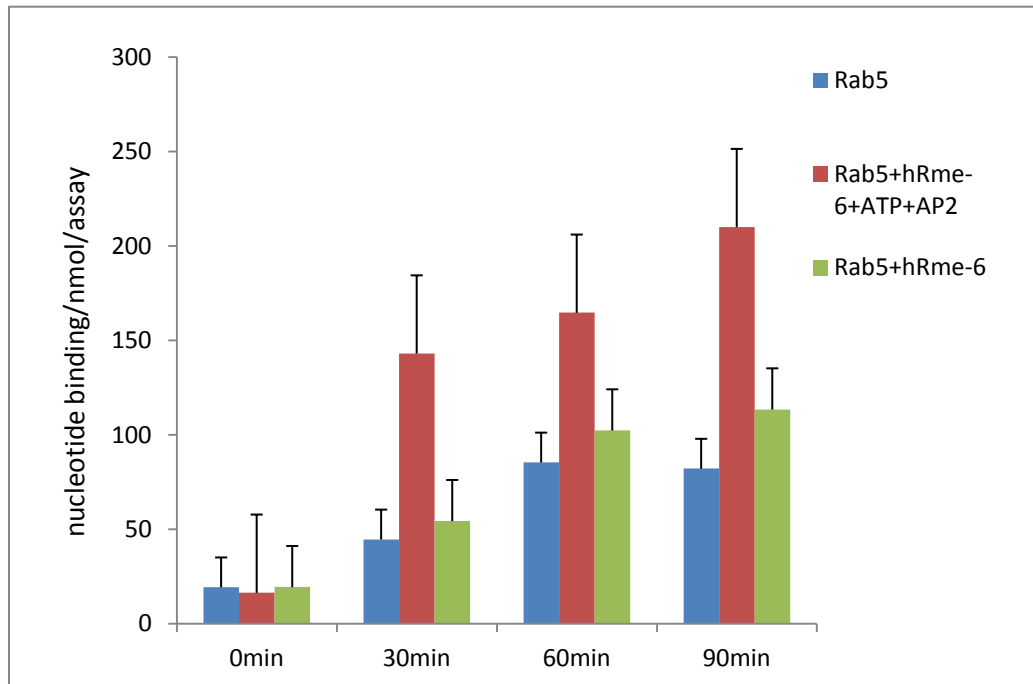


Figure 3.4 hRme-6 exhibited GEF activity. GST-Rab5 beads were preloaded with 120 μ M GDP and added to exchange reactions containing α -p³² labeled GTP in the presence or absence of 2 μ M purified Flag-hRme-6, 1 mM ATP and 2 μ M GST α -adaplin. At the indicated time points, Rab5 beads were taken from the reactions, washed and subjected to Cherenkov counting. The amount of GTP that bound to Rab5 in each assay was presented as a function of time. Results are the means \pm SD of at least two experiments performed in duplicate.

3.4 hRme-6 may interact with phosphorylated p42/44

As mentioned above, Tie2 is an endothelial tyrosine kinase receptor for Ang1. Previous data from our lab suggested that hRme-6 modulates signalling by the Tie2 receptor tyrosine kinase in endothelial cells. Ang1 is the ligand for Tie2 and both MAPK and Akt are activated following binding of Ang1 to Tie2. Overexpression of hRme-6 increased MAPK signalling while decreasing Akt signalling.

To further investigate the role of hRme-6 in the regulation of Tie2 signal transduction, purified Flag-hRme-6 from insect cells (Figure 3.3A) that

immunoprecipitated by M2 Flag beads, was used as a bait to pull down interacting partners using lysates from Ang1 stimulated HUVECs cells. As shown in Figure 3.5A, hRme-6 could bind to phosphorylated p42/44 MAPK. The interaction appeared to occur following 5 minutes of Ang1 stimulation and peaked at 10 minutes and started to decrease at 30 minutes. There was only a small but not significant interaction between Flag-hRme-6 and phosphorylated Akt and p38 (Figure 3.5B). It is worth noting that the appearance of phosphorylated p42/44 is time- and Ang1-dependent. Therefore this experiment has been quantified with the amount of phospho-p42/44 and phosphor-Akt being estimated from the corresponding inputs at each time point (Figure 3.2B).

A further control that could strengthen this experiment would be to confirm that Flag beads incubated with lysates from non-transfected cells do not capture phosph-p42/44.

The fact that Flag-hRme-6 may bind to phosphorylated p42/44 MAPK suggested that hRme-6 may directly involve in the signal transduction process in Ang1 stimulated HUVECs. However, the assay was based on an in vitro experiment and the role of hRme-6 in signalling transduction would require more direct evidence. But it does support the idea that Rme-6 might act as a signalling platform for Tie2 signalling.

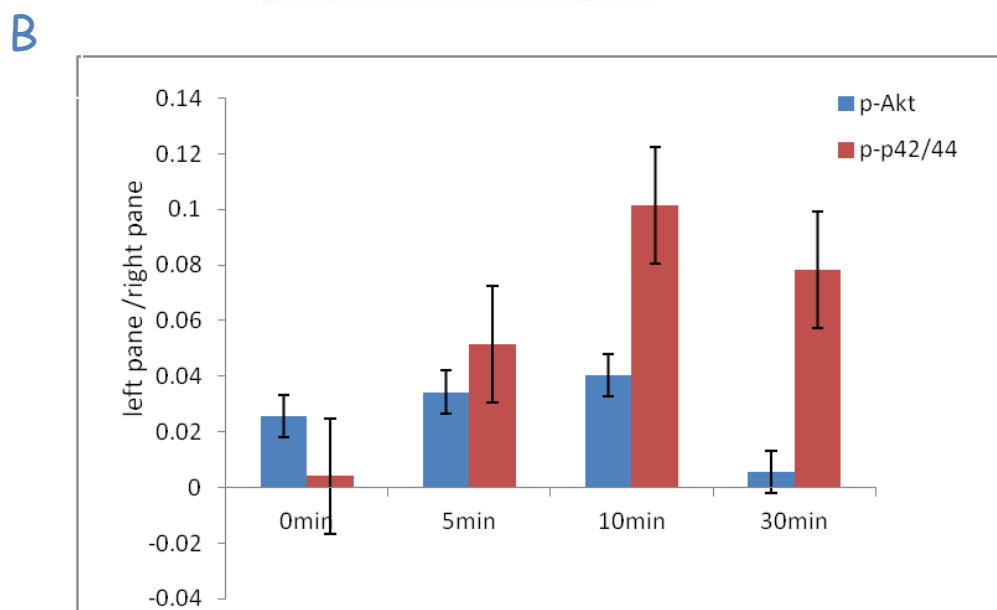
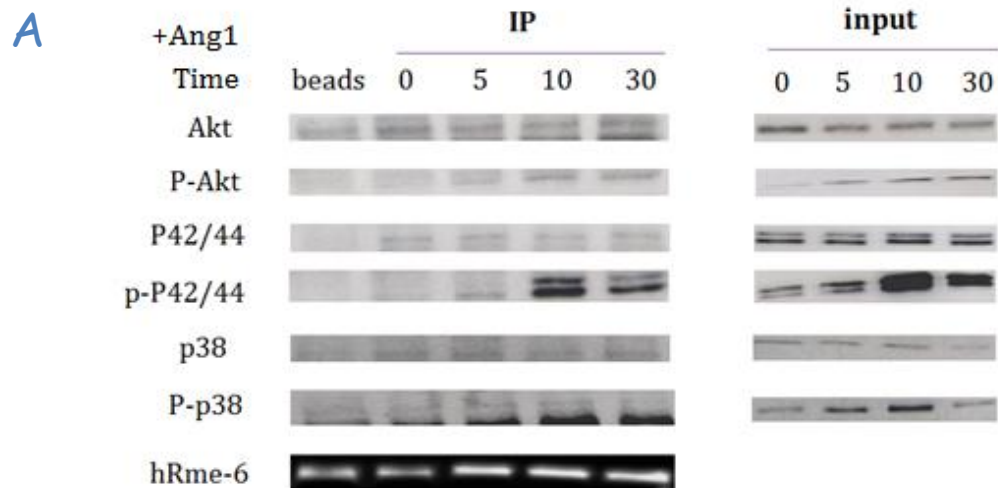


Figure 3.5 hRme-6 binds phosphorylated p42/44 MAPK. A, Flag hRme-6 was immunoprecipitated from Sf21 cells as shown in Figure 3.3A. Flag-hRme-6 purified from insect cells conjugated to the beads was incubated with HUVEC cell lysates prepared from cells which had been stimulated with Ang1 for the indicated time points (the cell lysis was prepared by Dr Filipe Ferreira). The Flag beads were analyzed by SDS-PAGE followed by immunoblotting with the relevant antibodies. Input indicated 10% of cells lysates used for flag-hRme-6 M2 beads incubation. B, Quantification of the interaction signals. The amount of phospho-p42/44 and phospho-Akt bound to beads is expressed as a proportion of the input at the indicated times. Results are the means \pm SD of two experiments.

3.5 Overexpression Flag-hRme-6 in HeLa cells affects EGF signalling

Previous data from our lab showed that overexpression of HA-hRme-6 changed the phosphorylation level of Akt, P38 and p42/44 MAPK in Ang1 stimulated HUVECs cells. However, whether hRme-6 functioned in a similar way in other cell types and other signalling models was still unknown. The Stahl group found the hRme-6 is involved the phosphorylation, ubiquitination and degradation of EGFR in HeLa cells[159]. This function of hRme-6 relied on the interaction between the Ras GAP domain and ubiquitin E3 ligase c-Cbl. So we decided that overexpression of hRme-6 in HeLa cells would be a good model to test the function of hRme-6 in signalling transduction.

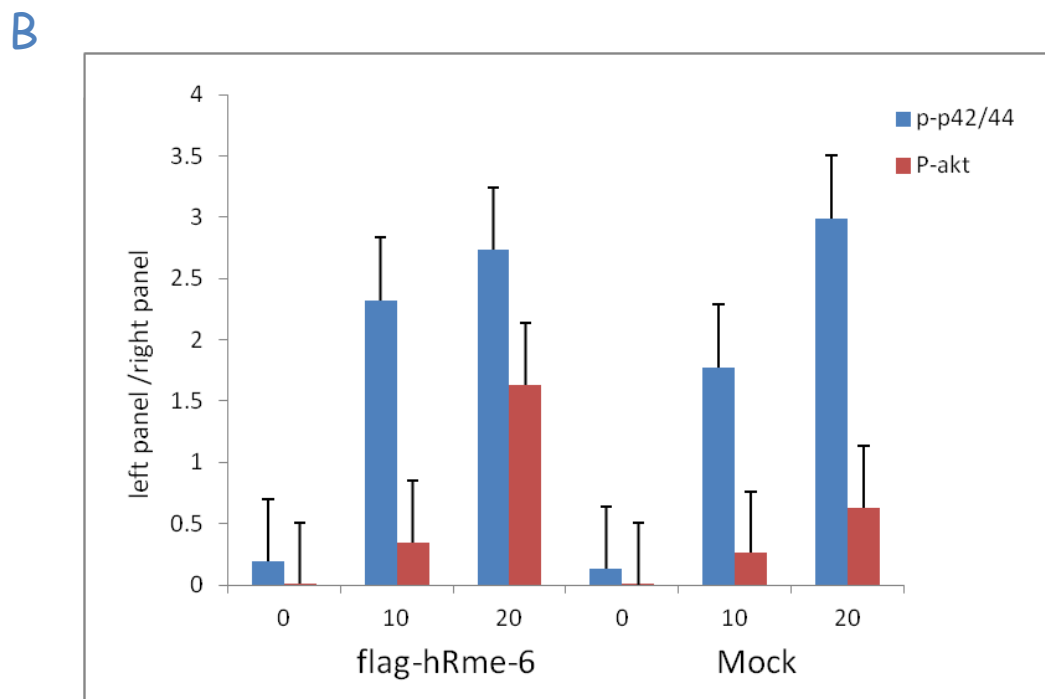
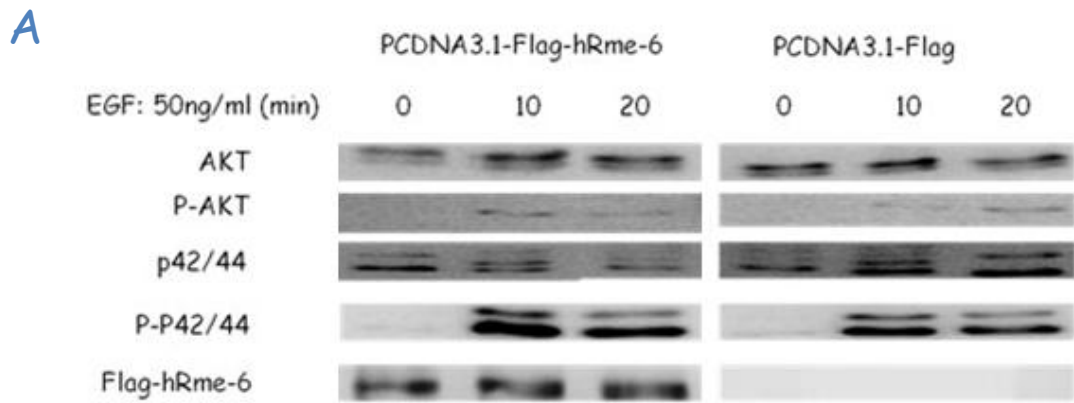


Figure 3.6 Levels of Rme-6 affect phosphorylation of Akt and p42/44. (A) HeLa cells were transfected with either mock or Flag-hRme-6 construct. Forty-eight hours later, HeLa cells were stimulated with EGF for various minutes. Whole cell lysates were prepared and the levels of Akt, p42/44, pAkt, p-p42/44 and hRme-6 were analysed by Western blotting. (B) Quantification of the signal density of the phosphorylated Akt and p42/44 MAPK versus total Akt and p42/44 at the indicated time points. Results are the means \pm SD of two experiments.

As shown above, overexpression of Flag-hRme-6 in HeLa cells increased the level of phosphorylation of Akt at 10 minutes compared with mock transfected cells while

there was no significant change in the level of phosphorylation p42/44. These data were different from the overexpression of hRme-6 in Ang1 stimulated HUVECs. This is likely due to different cells lines and different ligand stimulations. However, it still confirmed that in EGF stimulated HeLa cells, Flag-hRme-6 is involved in the control of signal strength.

3.6 CK2 but not non-phosphorylated p42/44 can phosphorylate hRme-6

Casein kinase 2 (CK2) is the main kinase responsible for the phosphorylation of clathrin-coated vesicles associated proteins. It is activated once clathrin uncoating occurs [207]. Ji et.al found that during EGF stimulation, p42/44 MAPK which was activated by EGFR signalling directly bound to CK2 via the p42 docking groove, phosphorylated CK2 and subsequently enhanced CK2 activity[208]. Previous data from our lab showed that CK2 phosphorylates hRme-6 in vitro (Singh and Smythe, unpublished data). As my previous work found that the hRme-6 could specifically bind phosphorylated p42/44 MAPK in Ang1 stimulated HUVECs cells, it suggested the hypothesis that p42/44 MAPK might be involved in the phosphorylation of hRme-6 through CK2. To address this question, an in vitro kinase assay using purified Flag-hRme-6 from insect cells (Figure 3.3A) was carried out using either CK2 or p42/44 MAPK or both.

As shown in Figure 3.7, CK2 did cause significant phosphorylation of Flag-hRme-6 while p42/44 MAPK only caused a low level of phosphorylation of hRme-6. CK2 and p42/44 MAPK together led to a slightly increased phosphorylation level of Flag-hRme-6 although this is likely an additive rather than a synergistic effect. This data confirmed our previous data that CK2 could phosphorylate hRme-6 in vitro.

Although Flag-hRme-6 specifically bound phosphorylated p42/44 MAPK in Ang1 stimulated HUVECs cells, purified Flag-hRme-6 was a poor substrate for p42/44 MAPK in vitro. Thus it is unclear whether the function(s) of hRme-6 could be regulated by phosphorylated p42/44.

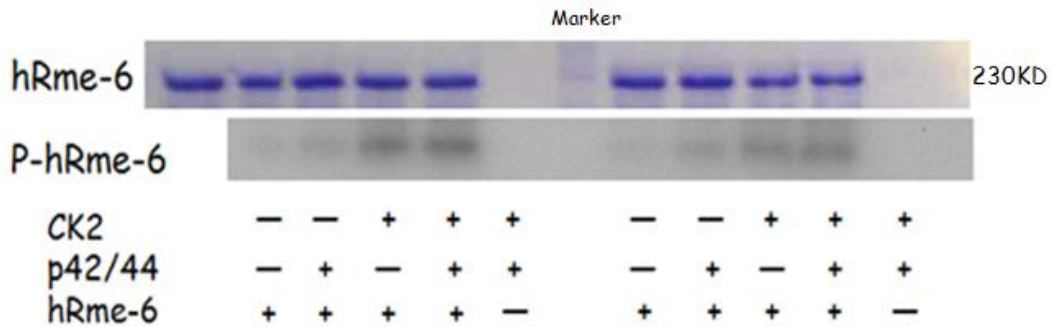


Figure 3.7 CK2 but not p42/44 MAPK phosphorylates hRme-6. Flag-hRme-6 purified from insect cells was incubated with ³²P-ATP in presence of CK2 or p42/44 MAPK in 30°C for 30 minutes. Samples of two independent experiments were then loaded in 10% SDS-PAGE. The gel was dried and autoradiography was used to visualise the phosphorylation level of hRme-6. M, marker.

3.7 In HeLa cells treated with a CK2 inhibitor, phosphorylation of p42/44 increases while the phosphorylation of Akt decreases during EGF stimulation

My previous data showed that hRme-6 is involved in regulating signal transduction. Overexpression of hRme-6 shifted the signalling output in Ang1 stimulated HUVEC cells and EGF stimulated HeLa cell. An in vitro assay found that hRme-6 directly bound to p42/44 MAPK and CK2 phosphorylated hRme-6. It seems that CK2 and phosphorylated hRme-6 may play important roles in modulating signalling strength changes caused by overexpression of hRme-6. Pharmacological inhibition of CK2

activity could thus be a good way to investigate the function of hRme-6. I decided to test this by using the CK2 inhibitor tetrabromocinnamic acid (TBCA), which is a cell-permeable, ATP-competitive inhibitor. TBCA was used to pre-treat HeLa cells for 10 minutes before EGF stimulation to investigate the role of hRme-6.

As shown in Figure 3.8, following EGF stimulation p42/44 and Akt MAPK were both activated and phosphorylated in HeLa cells. But after CK2 inhibitor treatment, EGF stimulation caused the phosphorylation of p42/44 MAPK increasing. An Akt loading control is missing in Figure 3.8. However, it was demonstrated in subsequent experiments that the phosphorylation of Akt is modulated in the presence of a CK2 inhibitor (E.Smythe, personal communication, University of Sheffield).

This was very similar to the effects of overexpression of hRme-6 in Ang1 stimulated HUVEC cells. However, overexpression of hRme-6 in Ang1 stimulated HUVEC cells more potently inhibited the phosphorylation of Akt compared to CK2 inhibition treatment in EGF stimulated HeLa cells. In addition, overexpression of hRme-6 in Ang1 stimulated HUVEC cells strongly activated p38 but had virtually no effect on p38 activation in EGF stimulated HeLa cells. These data were different from the overexpression of hRme-6 in EGF stimulated HeLa cells which led to the phosphorylation of Akt increase but no effect in the phosphorylation level of p42/44.

The data suggested that CK2 inhibition acts in the opposite way to the effect of overexpression of hRme-6 at least in some contexts. CK2 inhibition might decrease the phosphorylation of hRme-6 and the decreased phosphorylation of hRme-6 caused the subsequent change in the signal.

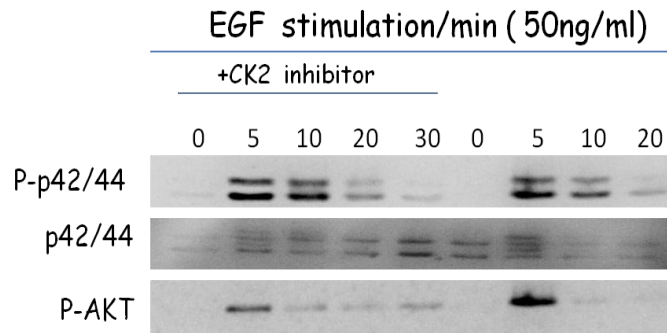


Figure 3.8 CK2 inhibitor altered signalling in EGF stimulated HeLa cells. HeLa cell was grown in 60 mm dish to a confluency of 60-70%. After 24 hours serum starvation, HeLa cell was stimulated by 50 ng/ml EGF or incubated with CK2 inhibitor TBCA for 10 minutes before 50 ng/ml EGF stimulation. At the indicated time points, cells were lysed and cell lysates was analyzed by immunoblotting.

3.8 Discussion

Rme-6 was found to mediate both fluid phase and receptor-mediated endocytosis in *C.elegans* via its interaction with Rab5 [204]. These studies demonstrated that Rme-6 colocalized with mRFP1-CHC-1 and mRFP1- α -adaptin but not with EEA1 or Rab5. Rme-6 also affected EGFR internalisation in HeLa cells and the trafficking of GLUT4 vesicles in adipocytes [174]. Together these studies showed that the function of hRme-6 relied not only on the Rab5 GEF domain but also on the Ras GAP domain. My initial aim in this section of work was to test the Ras GAP and Rab5 GEF activities of hRme-6 and further explore the functions of hRme-6.

3.8.1 Analysis of the activities of hRme-6

My early attempts demonstrated that the Ras GAP domain of hRme-6 alone may just show little GAP activity in vitro compared to the canonical p120 Ras GAP [209]. The low activity of the Ras GAP domain might be due to the lack of the conserved

arginine finger in the structure of hRme-6 as the arginine finger could help change the conformation of Ras-GTP to expose the GTP as a better substrate for the reaction. Previous work from Barbieri had shown that the Ras GAP domain of hRme-6 exhibited Ras GAP activity [158]. However I was unable to compare the specific activity of my preparations with their published data because they presented the activity as the percentage of saturated Ras GAP activity.

An alternative explanation for the weak activity is that the Ras GAP activity of hRme-6 needs certain interaction partners to activate its GAP function. As the Rab5 GEF domain of hRme-6 mainly exhibited Rab5 GEF activity in the presence of AP2 and ATP [157], the Ras GAP domain might also need some interaction partners to show the Ras GAP activity. Indeed preliminary data from our lab suggests that full length hRme-6 is also auto-inhibited for Ras GAP activity and that IQGAP1 (see chapter 5) can relieve this auto-inhibition (E.Smythe, unpublished data).

To get more information about the structure/function relationships of hRme-6, Flag-hRme-6 was then purified from Sf21 insect cells. Using this system, it was possible to purify high amounts of Flag-hRme-6 which was tested in a Rab5 GEF assay. My data confirmed that Flag-hRme-6 exhibited strong Rab5 GEF activity only in presence of AP2 and ATP, as had been shown for HA-hRme-6 purified from HEK293 cells. Because it was possible to purify a significant amount of Flag-hRme-6 from insect cells, it made it possible to analyze the structure and characteristic functions of hRme-6.

3.8.2 Identification of the function of hRme-6 in signal transduction

Previous data from our lab found that the overexpression of hRme-6 altered signalling strength by Akt, p38 and p42/44 MAPK in Ang1 stimulated HUVEC cells. It seemed that hRme-6 was not only involved in the process of endocytosis by direct interaction with the important endocytic regulators, AP2 and Rab5, but may also play important roles in the control of signal strength. One possibility was that hRme-6

could directly regulate the signalling molecules to control the signal strength. To test this hypothesis, purified hRme-6 from insect cells was incubated with Ang1 stimulated HUVEC cells lysate. I observed that hRme-6 could bind to phosphorylated p42/44 MAPK but not other signalling molecules. The Akt and p42/44 MAPK both act as molecular switches responsible for a variety of mitogenic, metastatic and other tumor promoting cellular activities. This specific binding implied that the outcome of p42/44 MAPK may be modified by binding to hRme-6. Previously work from Annette Schenck et al found that APPL1 modulated Akt activity and specifically recruited GSK-3 β but not TSC2 to Appl1 endosomes upon stimulation [102]. It suggested that APPL1 defined a small subpopulation of endosomes and regulated its signalling specificity. It is possible that Rme-6 also sets up a signalling domain specific for p42/44 signalling in HUVECs.

We do not understand why overexpression of hRme-6 inhibited Akt activation in Ang1 stimulated HUVECs but activated Akt in EGF stimulated HeLa cells. It is possible that overexpression of hRme-6 inhibited the process of clathrin mediated endocytosis which, in turn, caused changes in the signalling and the endocytic pathways of Tie2 and EGFR. Work from our lab showed that siRNA of hRme-6 was inhibitory for transferrin internalisation. Stahl group found that siRNA of hRme-6 inhibited the internalisation and degradation of EGFR in HeLa cells and overexpression of hRme-6 enhanced EGFR degradation in HEK293 cells, suggesting that the function of hRme-6 may be limited in certain cell types, without compensation from other Rab5 GEFs. It has been shown that Akt phosphorylation could facilitate the degradation of EGFR [210]. Overexpression of hRme-6 enhanced the degradation of EGFR which may be due to the enhanced Akt activation.

3.8.3 Phosphorylation of hRme-6 by CK2

One of the aims of this chapter was to clarify the activities of the different domains of Rme-6, in particular the Ras GAP domain. Previously our lab had shown that

hRme-6 was phosphorylated by CK2 (Singh and Smythe, unpublished). Protein phosphorylation not only has the potential to affect signal transduction but also could affect protein structure. Moreover CK2 is not only in charge of the phosphorylation of hRme-6 but also the main kinase responsible for the phosphorylation of CCV associated proteins. Evidence suggests that it is activated following CCV scission which is temporally the time when Rme-6 is thought to act. Since inhibition of CK2 led to effects similar to that of overexpression hRme-6, at least in some cell types, and hRme-6 could selectively bind to activated p42/44, I tested whether there is a direct crosstalk between p42/44 and CK2 as that has been shown in other systems [211], leading perhaps to enhanced phosphorylation of Rme-6. However there was no evidence that Rme-6 was a substrate for p42/44 or that there was direct cross-talk between CK2 and p42/44.

Due to the lack of phosphorylated p42/44, the relationship between hRme-6 and phosphorylated p42/44 is still unclear. It is possible that the active form p42/44 may incharge of the phosphorylation of hRme-6. However, the purified Flag hRme-6 might already been partly phosorylated so that the phosphorylation of hRme-6 was not strongly dependent on p42/44 MAPK or phsophorylated p42/44 but mainly on CK2 in vitro.

4. Chapter 4 Structural studies on hRme-6

4.1 Introduction

A key question concerning hRme-6 is how its structure relates to function during the internalisation of different cargoes. Previous data from our lab had implied a role for the GEF domain in the uptake of the housekeeping cargo, transferrin [157]. This contrasted with the uptake of the epidermal growth factor receptor (EGFR) where the Ras GAP domain of Rme-6 appeared to be the key [159]. The data I presented in the previous chapter showed that hRme-6 could regulate the endocytosis and signalling of both EGFR in HeLa cells and Ang1 in HUVECs. The Ras GAP domain and Rab5 GEF domain are connected by a large linker region including a proline rich domain which could allow considerable conformational changes within the protein. Together these observations led us to propose a hypothesis that different cargoes may have differential requirements for the Rab5 GEF and Ras GAP activities of hRme-6, as shown below (Figure 4.1). The different requirements for different cargos may lead to changes in the structure of hRme-6 as outlined below.

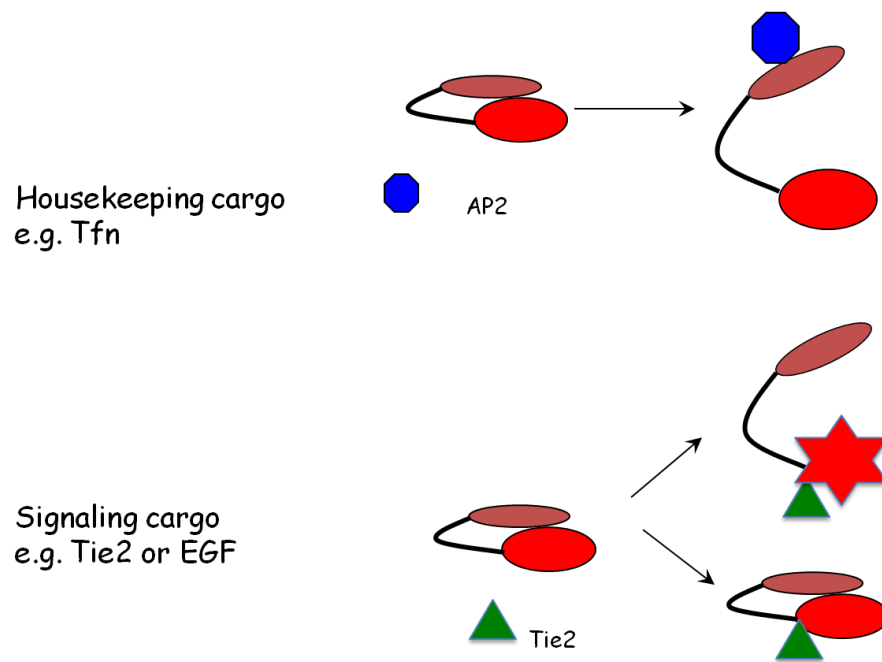


Figure 4.1 Hypothesis I for the structure/function relationship of hRme-6: Hypothesis for changes in the monomeric structure of hRme-6 in response to different cargo. Incubation of housekeeping cargo like Tfn may lead to the release of the autoinhibited conformation of hRme-6 and activation of GEF domain while stimulation of signalling cargo like Tie2 or EGF may lead to different conformations of hRme-6, affecting the activity of the Ras GAP domain.

However, this hypothesis was based on a monomeric structure of hRme-6. There also could be another hypothesis to fit the diverse functions of hRme-6 as shown in Figure 4.2. Different cargo could cause changes in an oligomeric structure of hRme-6 resulting in activation of different activities of hRme-6. Alternatively the structure of hRme-6 could reflect a combination of the two models above. Therefore it was important to investigate the structure of hRme-6. It was also anticipated that this might provide insight into the relationship between endocytosis and signalling.

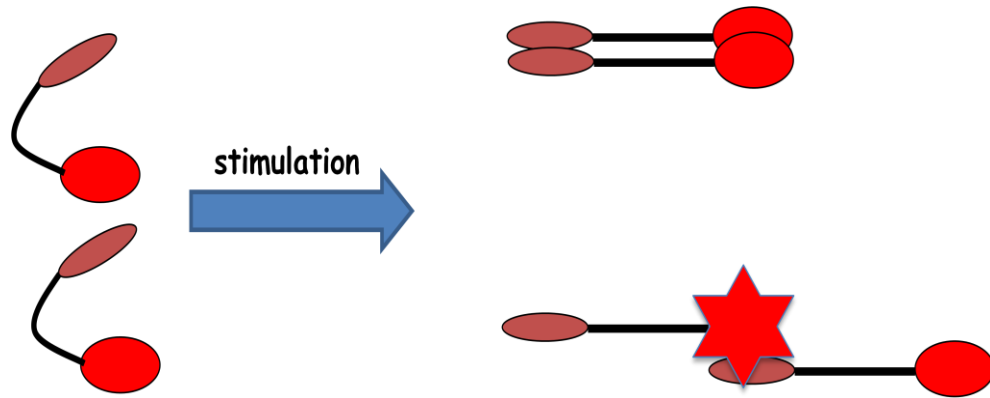


Figure 4.2 Hypothesis II for the structure/function relationship of hRme-6. Hypothesis for a multimeric structure of hRme-6 Incubation of cells with different cargos may lead to different conformations of hRme-6.

When this work started, there was very little known about the structure of hRme-6. The conserved Ras GAP domain and Rab5 GEF domain from other proteins provided some information about the structure of these domains. However, these two domains constitute only about 50% of the entire protein. Besides these, a proline rich region had been identified (residues 876 to 885) and shown to bind the SH3 domain containing protein, endophilin (Singh and Smythe, unpublished). Furthermore, there was no information about the conformation of hRme-6.

The primary aim of this section was to investigate the structure of hRme-6 in order to allow a better understanding for the structure/function relationships of hRme-6.

4.2 hRme-6 exists in an SDS resistant form

The predicted molecular weight of hRme-6 based on its sequence is approximately 166KD. However on SDS-PAGE, hRme-6 from a variety of sources, insect, mammalian and bacterial, appears as a band of approximately 230 KD (Figure 3.3A). Its identity was confirmed by immunoblotting (Figure 3.5A). In order to understand whether

hRme-6 adopts different conformations or oligomers and the nature of the kinetic stability of these structures, a time-dependent SDS trapping assay was used to analyze the equilibrium of hRme-6. SDS-resistant proteins refer to those proteins that would not be denatured by SDS without heating. Previous studies had shown a correlation between kinetic stability and resistance of a protein to SDS [212] .

Purified hRme-6 from insect cells was incubated with SDS trapping buffer at 70°C for different time points and subjected to SDS PAGE. As shown in Figure 4.3 A, hRme-6 migrated at 230 KD when the sample of hRme-6 was boiled at 100 °C in normal SDS PAGE loading buffer. However, when purified hRme-6 protein was incubated in SDS trapping buffer (1% SDS) at 70°C, three bands appeared on the gel, one band of 230 KD and another two bands at higher molecular weights. It was unclear as to whether the top band had even entered the resolving gel from the stacking gel. There was no difference between the time treatments. This experiment suggested that purified hRme-6 protein is an SDS resistant protein, which requires boiling at 100°C in order to generate the 230 KD form. The higher bands also suggested that purified hRme-6 might exist in higher molecular weight conformations. It was also very interesting that all other lower molecular weight protein bands present in normal SDS PAGE disappeared in SDS trapping assay buffer (compare Figure 4.3 A with Figure 4.3 B). It seems that SDS treatment without boiling led to a stronger interaction or aggregation of hRme-6, or it may be just SDS treatment could not denature the structure of hRme-6. Boiling of the sample in SDS buffer resulted in the breakdown of hRme-6 complex.

Over all, it indicated that hRme-6 would not be denatured by SDS without boiling and that hRme-6 exists in SDS resistant forms. It also suggested that the structure of hRme-6 oligomers was likely to be very tight.

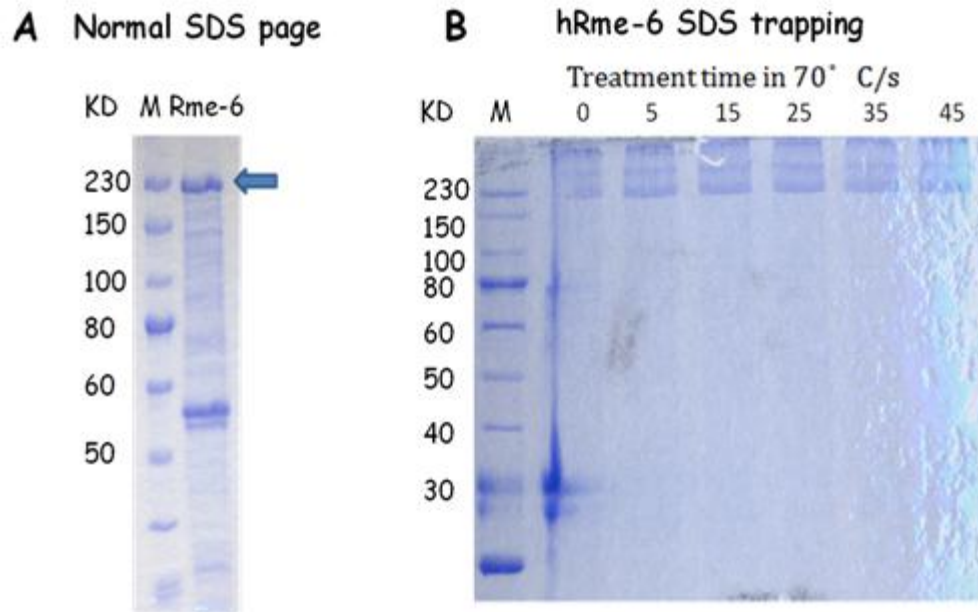


Figure 4.3 hRme-6 exists in SDS resistant forms. A, 4µg purified hRme-6 was boiled in SDS buffer in 100°C for 5 minutes. Samples were loaded in SDS page. B, Aliquots of 4 µg purified hRme-6 were incubated with 5XSDS trapping buffer at 70°C at different times. Samples were then directly loaded on SDS page.

4.3 hRme-6 can assemble into oligomeric structures in cells

The previous results suggested that hRme-6 exists in multimeric forms. To address this more rigorously I tested if oligomers could be detected in cells. hRme-6 was cloned into both pcDNA3.1-Flag and pcDNA3.1-HA plasmids to create hRme-6 with two different tags. HeLa cells were then co-transfected with the same amount of pcDNA3.1-Flag-hRme-6 and pcDNA3.1-HA-hRme-6 plasmids. hRme-6 was then immunoprecipitated from HeLa cell lysates expressing both Flag-hRme-6 and HA-hRme-6, using either anti-HA antibody or anti-Flag antibodies

As shown in Figure 4.4, anti-HA antibodies successfully immunoprecipitated HA-hRme-6. In the anti-HA immunoprecipitation, it detected Flag-hRme-6. However, although the anti-Flag antibody also immunoprecipitated significant amounts of

Flag-hRme-6, there was no HA-hRme-6 detected in the sample (in the lane of IP: anti-Flag).

One possible explanation may be due to the fact that the FLAG antibody is much less efficient at immunoprecipitation compared to the anti-HA antibody. As shown in Figure 4.4, the HA antibody captured ~50% of HA-hRme-6 from the whole cell lysate while the anti-Flag antibody only captured 2-4% of total Flag-hRme-6 in the whole cell lysate. It is possible that the small amount of HA-hRme-6 co-immunoprecipitated in the anti-FLAG immunoprecipitation was too low to be detected by the anti-HA antibody on Western blots.

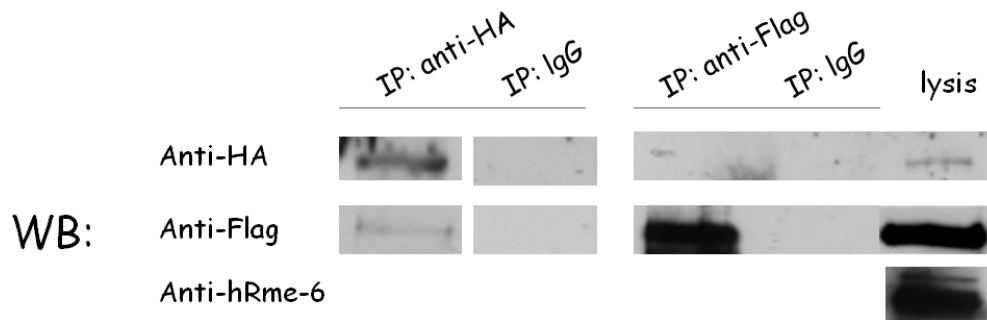


Figure 4.4 hRme-6 forms multimers in cells. HeLa cells were co-transfected with the same amount pcDNA3.1-Flag-hRme-6 and pcDNA3.1-HA-hRme-6 plasmids. hRme-6 was then immunoprecipitated from HeLa cell lysates by anti-HA or anti-Flag antibody. The immunoprecipitates were then analyzed by immunoblotting with anti-HA antibody or anti-Flag antibody respectively. Lysis indicated 2% of total cell lysates used for immunoprecipitation. Results were one of two repeat experiments.

4.4 Gel filtration shows that hRme-6 exists in multimeric forms

As my previous experiment showed that HA-hRme-6 could interact with Flag-hRme-6, it provided one line of evidence that hRme-6 may exist in multimeric

forms. To further analyze the conformation of hRme-6, purified Flag-hRme-6 from insect cells was injected onto a SuperdexTM-200 gel filtration column. Fractions from the column were analyzed by immunoblotting using anti-hRme-6 antibodies. As shown in Figure 4.5, hRme-6 eluted from elution volume 10.05 ml to 14.7 ml and was observed to elute as two peaks, Peak 1 (elution volume: 10.05 to 11.25 ml) and Peak 2 (elution volume: 13.35 to 14.7 ml). To get a better estimate of the molecular weight of hRme-6, purified clathrin heavy chain trimer (CHC) and normal rabbit IgG were also injected into the column with purified hRme-6. As shown in Figure 4.5, the first peak of hRme-6 co-eluted with clathrin heavy chain from elution volume 10.05-11.25 ml, implying that this conformation of hRme-6 has the same molecular weight as clathrin heavy chain trimer (molecular weight ~ 630 KD). The second peak of hRme-6 eluted at a volume that corresponded to a larger molecular weight than normal rabbit IgG (molecular weight at 150 KD).

The calculated molecular weight of hRme-6 by amino acid is 166 KD. But the size of purified hRme-6 protein from insect cells or mammalian cells on SDS-PAGE was around 230 KD (Figure 4.3A). By gel filtration, purified hRme-6 migrated at the same fraction as CHC. It indicated that purified hRme-6 from insect cells exists in a multimeric form. However, it was still unclear about the accurate molecular weight of the multimeric form of hRme-6 and the conformations of hRme-6 in vivo.

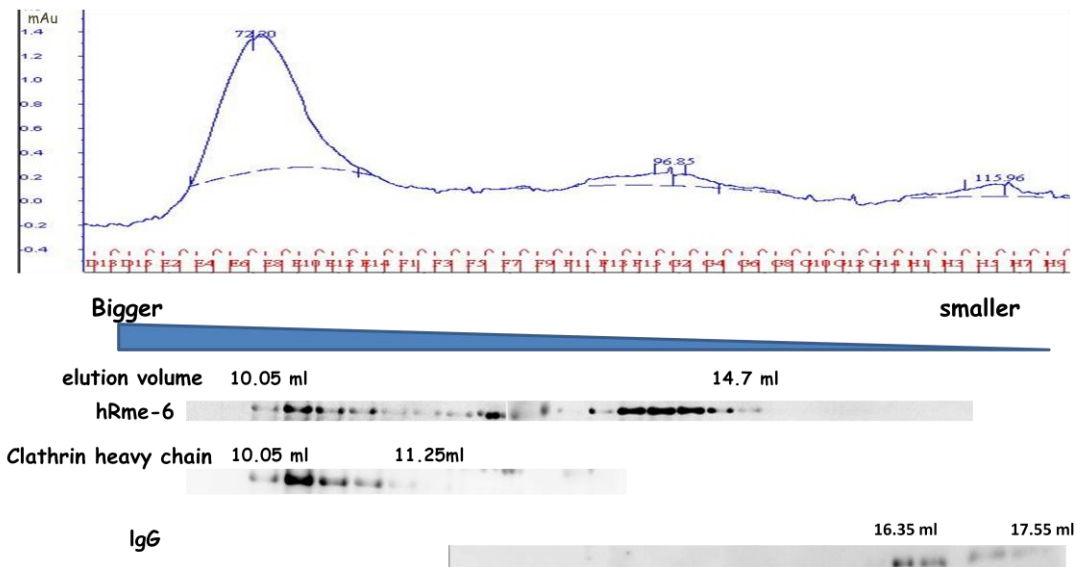


Figure 4.5 hRme-6 exists in multimeric forms. 20 μ g purified Flag-hRme-6 from insect cells, 8 μ g clathrin heavy chain (trimer formation) and 8 μ g normal rabbit IgG were injected into SuperdexTM-200 gel filtration column. Aliquots of 20 μ l column fractions were analyzed by immunoblotting. Results are repeated at least twice.

In previous experiment, purified hRme-6 from insect cells was used and multimeric conformations of hRme-6 were found. However, there was a possibility that the multimeric forms of hRme-6 were due to the aggregation of hRme-6 but not the native conformation of hRme-6. To check the conformation of hRme-6 *in vivo*, HeLa cells were transfected with pcDNA3.1-HA-hRme-6. Cell lysates were injected into the SuperdexTM-200 gel filtration column and the eluted fractions were analyzed by immunoblotting. As shown in Figure 4.6, HA-hRme-6 eluted from elution volume 10.2 ml to 15.6 ml. In order to estimate the molecular weight of HA-tagged hRme-6, CHC and IgG were injected together with the HeLa cell lysates at the same time and also tested by immunoblotting. The results indicated that clathrin heavy chain trimer conformation eluted slightly earlier than hRme-6 from the column. But hRme-6 did not colocalize with IgG. This experiment further confirmed the existence of hRme-6 multimeric forms not only in the purified protein but also *in vivo*.

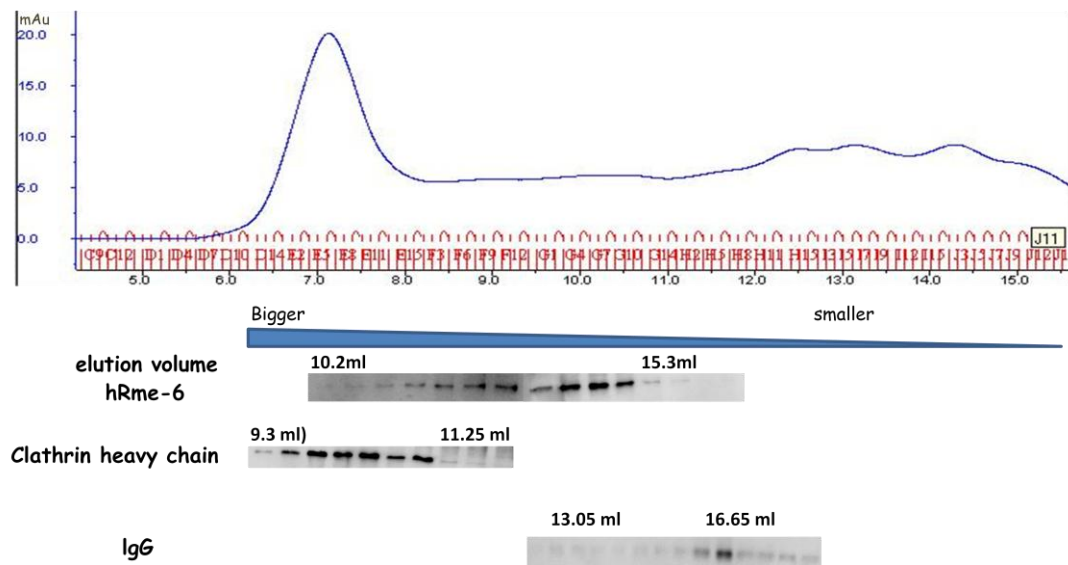


Figure 4.6 Overexpressed HA-tagged hRme-6 exists as a higher order oligomer. 1200 μ g of lysate prepared from HeLa cells overexpressing HA-hRme-6, 12 μ g clathrin heavy chain (trimer conformation) and 8 μ g normal rabbit IgG were injected into SuperdexTM-200 gel filtration column. Aliquots Of 20 μ l of each column fractions were analyzed by immunoblotting. Results are repeated at least twice.

My previous experiment in Figure 4.5 showed that gel filtration successfully separated purified hRme-6 from insect cells into two peaks. The SDS trapping assay showed that hRme-6 existed in SDS resistant forms. The samples from the gel filtration were further tested to see if the SDS-trapping assay could detect any differences between the different peaks of hRme-6 separated by gel filtration. Fractions from elution volume 10.2 ml, 12 ml and 14.1 ml were analyzed. As shown in Figure 4.7, the different fractions showed different behavior following SDS treatment. There were mainly two bands detected in all the fractions, indicating that in the previous experiment, the top band (Figure 4.3) was very likely to be samples stacked in the bottom of the stacking gel and unable to enter the resolving gel. Samples from elution volume 10.2 ml and 12 ml only showed bands higher than 230 KD and the sample at volume 10.2 ml was more SDS-resistant. Samples from elution volume 14.1 ml existed mainly at 230 KD. It further confirmed that there were different

conformations of hRme-6 in the purified sample and the two conformations of hRme-6 exhibited different SDS resistance.

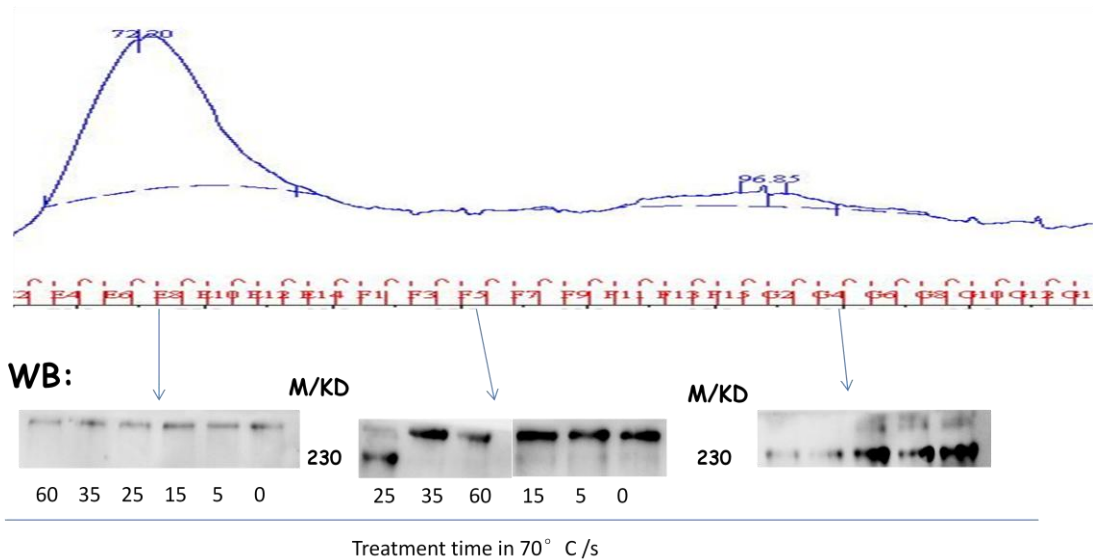


Figure 4.7 Different conformations of hRme-6 show different SDS resistance. 20 µg purified Flag-hRme-6 from insect cells was injected into Superdex™-200 gel filtration column. Aliquots of 20 µl hRme-6 from gel filtration fraction at 10.8 ml, 12 ml, 14.1 ml were incubated with 5XSDS trapping buffer at 70°C for the indicated times. Samples were loaded in SDS PAGE and analyzed by immunoblotting. Results were repeated twice.

4.5 Native gels reveal two higher molecular weight conformations of hRme-6

My previous experiment showed that purified hRme-6 existed in multimeric forms. However, the precise molecular mass and multimeric conformations of hRme-6 was still not clear. To address these questions, native PAGE was used as it could show high-resolution analysis of native proteins, protein complexes for molecular mass estimations and assessment of purity. Purified Flag-hRme-6 from insect cells was subjected to native gel electrophoresis. As shown in Figure 4.8, most of the purified Flag-hRme-6 migrated as two species around 720 KD and 480 KD. Flag-hRme-6

purified from insect cells (Figure 4.3A) migrated as a 230 KD species on SDS-PAGE. But the results from the native gel implied that hRme-6 is unlikely to exist in a monomeric conformation in native conditions. It also matched with previous data from gel filtration and SDS trapping assay that purified hRme-6 from insect cells exists in higher order conformations.

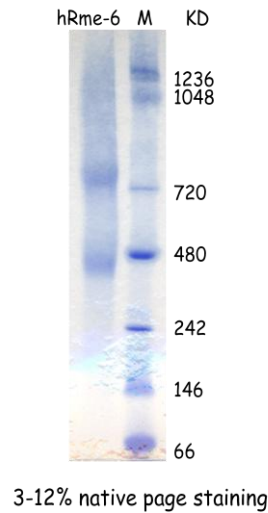


Figure 4.8 hRme-6 exists in multimeric forms. Purified Flag hRme-6 from insect cells was mixed with native PAGE loading buffer and loaded on a 3-12% native PAGE and stained with commassie blue.

4.6 Native gels confirmed that hRme-6 exists in multimers in HeLa cells

Although native gels showed that purified Flag hRme-6 existed in multimeric forms, there were some possibilities that these conformations of hRme-6 were due to the aggregation of purified proteins or that multimeric forms may alter in vivo. Further investigation of the native conformation of endogenous hRme-6 in cells was required. In addition I wanted to check whether cargoes would affect the multimeric structure of hRme-6. So lysates from HeLa cells treated plus or minus EGF, were subjected to

native gel electrophoresis. As shown in Figure 4.9, after stimulation with 50 ng/ml EGF at different time points, HeLa cells were immediately lysed, loaded on native PAGE and followed by immunoblotting using antibodies specific for hRme-6 to check the conformations of endogenous hRme-6. Endogenous hRme-6 showed clearly one band at 720 KD in native PAGE but not two bands found in purified hRme-6 from insect cells. This result suggested that the 480 KD band observed in purified hRme-6 from insect cells may not be a true physiological conformation of hRme-6. It may be due to the degradation of hRme-6 or just the dissociation of the multimer of hRme-6.

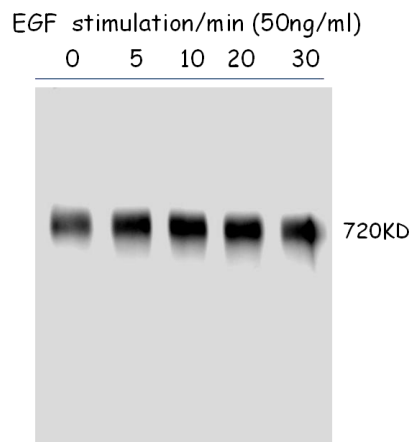


Figure 4.9 Endogenous hRme-6 exists in a higher molecular weight conformation in HeLa cells independently of EGF stimulation. HeLa cells were serum starved for 24 hours and then were stimulated by 50 ng/ml EGF at different time points. Cells were lysed and subjected to native PAGE followed by immunoblotting using antibodies specific for hRme-6.

Evidence in support of the former option was that when lysates from HeLa cells were first frozen before being subjected to Native PAGE, a band around 480 KD appeared on the gel (Figure 4.10). It was similar to that in purified Flag-hRme-6 from insect cells. The lower band of endogenous hRme-6 was not due to EGF stimulation and there was no significant change between the two conformations of hRme-6 during EGF stimulation. Interestingly, there was also no species of hRme-6 lower than 480 KD, which also implied that endogenous hRme-6 did not exist in a monomeric

conformation.

Overall, these experiments further confirmed that the endogenous hRme-6 exists mainly in multimeric forms around 720 KD.

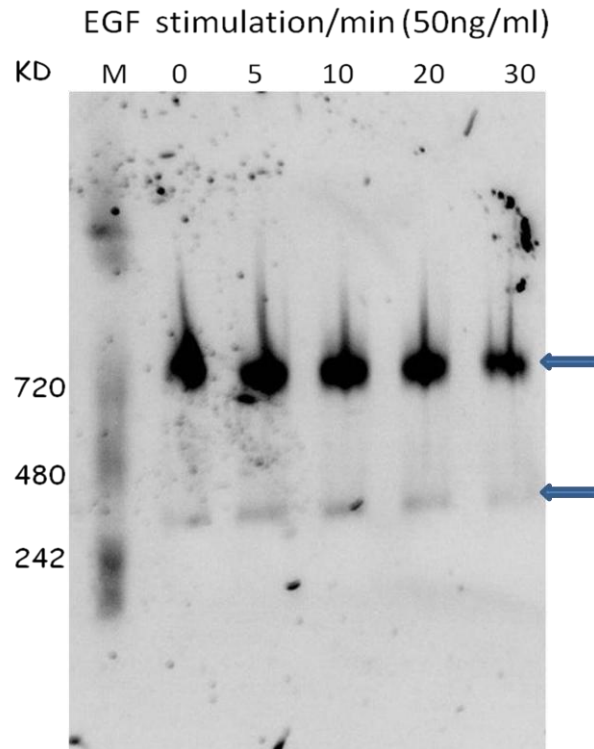


Figure 4.10 Endogenous hRme-6 appears as a lower molecular weight conformation following freezing of HeLa cell lysates. HeLa cells were serum starved for 24 hours and then were stimulated by 50 ng/ml EGF at different time points. Cells were lysed and the lysates were frozen at -80 °C overnight and then subjected to native PAGE followed by immunoblotting using antibodies specific for hRme-6.

4.7 Mass spectrometry analysis of hRme-6 multimers

As endogenous hRme-6 appeared as only one band at 720 KD on native PAGE but two bands in frozen samples while the purified Flag-hRme-6 from insect cells also showed two species around 480 KD and 720 KD, it was possible that the 480 KD band in purified Flag-hRme-6 from insect cells might be a degraded form of hRme-6. To test

this hypothesis, purified Flag-hRme-6 from insect cells was loaded on the 3-12% Bis-Tris native PAGE. The two bands around 480 KD and 720 KD were cut separately from native PAGE followed by reduction, alkylation and trypsin digestion. The peptides from the two species were then injected into autosampler tray of Dionex 3000 system and analyzed by Dr Richard Beniston (BiOMiCs, University of Sheffield). The data is shown in table 4.1 and appendix 1.

proteins found in 720 kD band				
Accession	Description	Coverage	MW [kDa]	calc. pI
Q14C86	GTPase-activating protein and VPS9 domain-containing protein 1	62.04	164.9	5.22
P29844	Heat shock 70 kDa protein cognate 3	14.79	72.2	5.36
P11147	Heat shock 70 kDa protein cognate 4	12.29	71.1	5.52
P06603	Tubulin alpha-1 chain	42.00	49.9	5.14
Q24560	Tubulin beta-1 chain	32.21	50.1	4.86
P61858	Tubulin beta-2 chain	16.14	49.8	4.83
Q05825	ATP synthase subunit beta, mitochondrial	27.52	54.1	5.27
O97125	Heat shock protein 68	9.45	69.7	5.83
P29843	Heat shock 70 kDa protein cognate 1	10.30	70.6	5.49
Q26365	ADP,ATP carrier protein	20.83	34.2	9.80
P02572	Actin-42A	12.77	41.8	5.48
P0CG69	Polyubiquitin	40.63	85.7	7.66
P35381	ATP synthase subunit alpha, mitochondrial	7.79	59.4	9.01
P29845	Heat shock 70 kDa protein cognate 5	3.50	74.0	6.35
proteins found in 480 kD band				
Accession	Description	Coverage	MW [kDa]	calc. pI
Q14C86	GTPase-activating protein and VPS9 domain-containing protein 1	68.67	164.9	5.22
P11147	Heat shock 70 kDa protein cognate 4	13.06	71.1	5.52
P29844	Heat shock 70 kDa protein cognate 3	8.23	72.2	5.36
P06603	Tubulin alpha-1 chain OS	29.78	49.9	5.14
O97125	Heat shock protein 68 OS	7.72	69.7	5.83
P61858	Tubulin beta-2 chain OS	7.62	49.8	4.83
P29845	Heat shock 70 kDa protein cognate 5	3.50	74.0	6.35
Q24560	Tubulin beta-1 chain	19.24	50.1	4.86
Q05825	ATP synthase subunit beta, mitochondrial	8.32	54.1	5.27
P0CG69	Polyubiquitin	40.63	85.7	7.66

Table 4.1 Mass spectrometry analysis of the protein composition of the 480 and 720 KD forms of hRme-6.

Purified Flag hRme-6 from insect cells was subjected to Native PAGE. The two bands of Flag-hRme-6 were excised separately from the gel. The proteins within each of the bands were then identified by in gel digestion coupled to mass spectrometry. The MS data was further analyzed by MaxQuant compared with the database of Homo sapiens and *Drosophila melanogaster*.

In both bands, the major peptides found all belonged to hRme-6. There was no significant difference or loss of specific peptides between the peptides found in the two bands. The peptides of the two bands found in MS covered 60% (720 KD) and 66% (480 KD) of the whole range of the hRme-6 protein sequence from the N-terminus to the C-terminus. This suggested that the 480 KD conformation of hRme-6 was not a degradation form but more likely, a disassembled form from the bigger conformation. Apart from hRme-6, there were also some other proteins present in small amounts in both bands: 13 other proteins in 720 KD band and 9 other proteins in 480 KD. These included Actin, Tubulin and some mitochondrial proteins which are likely to be contamination proteins from the purification process or sample preparation steps. Heat shock 70 KD protein was the main protein present in both conformations. A likely role for this chaperone is to ensure correct folding of hRme-6. However, both hRme-6 (Semerdjieva et al) and HSC70 have been implicated in clathrin-coated vesicle uncoating [40, 43, 44]. So we cannot rule out the possibility that they are associated because of common roles in the removal of the clathrin coat. Interestingly, there were also some polyubiquitin but not any ubiquitin-related enzymes in both conformations of Flag-hRme-6. It indicated that Flag-hRme-6 purified from insect cells may be ubiquitinated. However, most of the contaminants were present in very small amounts which indicated that hRme-6 isolated from insect cells was quite pure. Overall, these data indicated that the 480 KD band of hRme-6 purified from insect cell was not a degradation form and the purity of hRme-6 purified from insect cell was quite high.

4.8 Sec-malls experiment estimate the molecular weight of hRme-6 monomers

Although the purified Flag-hRme-6 from insect cells contained two conformations of ~720 KD and ~480 KD, the accurate molecular weights of them were still unknown. To help explore the size of the hRme-6 monomers, I attempted to use Size Exclusion Chromatography–Multi-Angle Laser Light Scattering (sec-malls). Purified Flag-hRme-6 from insect cells was analyzed by the Molecular Interactions Lab at Department of Biology, University of York. The results were as shown (Figure 4.11 and appendix 2).

There were clearly two UV peaks formed when the hRme-6 sample eluted from the Superdex S200 column. The first peak (from 15.51 min to 17.24 min, which is equal to elution volume 7.75 ml to 8.62 ml) showed a significant refractive index (RI). But this peak seems to represent the bigger aggregated form of Flag-hRme-6 as the matched molecular weight of this peak was 10 MKD, which was never found in the running of Flag-hRme-6 in SuperdexTM-200 gel filtration column. It is possible that the separation range was too small in SuperdexTM-200 column so these giant oligomers were not detected.

The second peak (from 17.25 min to 24.02 min, which equals to elution volume 8.625 ml to 12.01 ml) was the main peak of Flag-hRme-6. The average molecular weight of this peak was 330 KD. However, it was also notable that in the beginning of the second peak, the matched molecular weight was above 1000 KD while the low molecular weight towards the end of the second peak was 250 KD. As the purified sample contained different conformations, the column failed to separate the different conformations of Flag-hRme-6 as shown in Figure 4.6. There was just one big peak cross the column. So the calculated average molecular weight based on the mixture was 330 KD

The overall picture from this assay suggested that the monomer size of

Flag-hRme-6 may be around 250 KD. However it was impossible to draw any firm conclusions from these experiments.

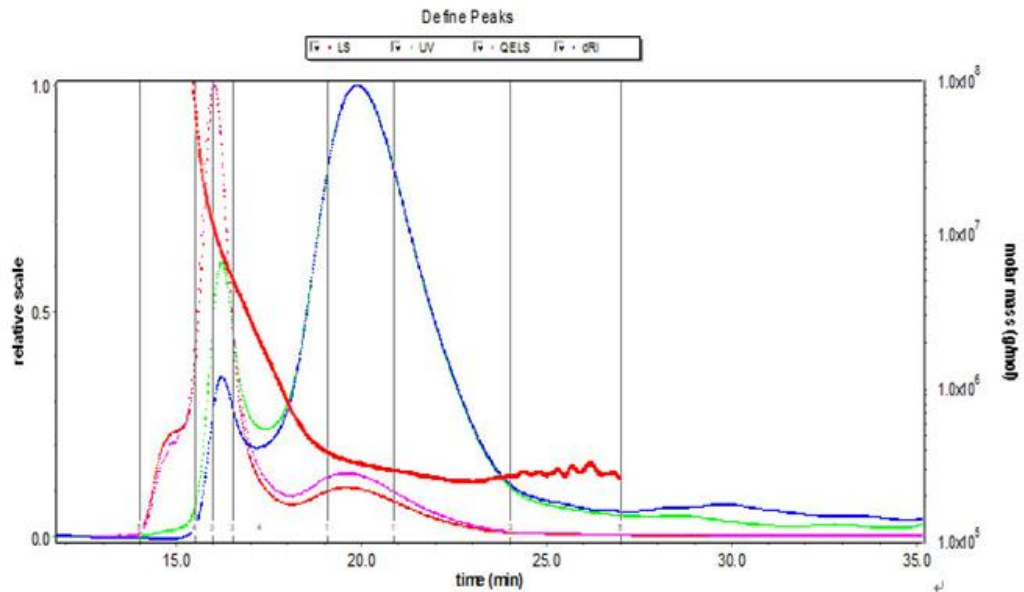


Figure 4.11 hRme-6 elution profile and peak positions in sec malls experiment. Flag-hRme-6 was injected into Superdex S200 column linked to a Shimadzu HPLC system (SPD-20A UV detector, LC20-AD isocratic pump system, DGU-20A3 degasser and SIL-20A autosampler, which was connected with a Wyatt HELEOS-II multi-angle light scattering detector and a Wyatt rEX refractive index detector). The elution profile shows UV (280 nm) in green, refractive index (RI) in blue, light scattering (LS) in red and quasi-elastic light scattering (QELS) in magenta. The thick red trace showed the MW analysis across the whole of the eluted material (right hand Y axes).

4.9 Gel filtration separates the 720 and 480 KD conformations of Flag-hRme-6 purified from insect cells

As purified Flag-hRme-6 from insect cells contained two different conformations while endogenous hRme-6 in HeLa cells mainly showed the higher species, we wanted to understand how the different conformations of Flag-hRme-6 identified on gel filtration linked to the species observed in native gels. As shown in Figure 4.12,

purified Flag-hRme-6 was gel filtered in Superdex™200. The chromatogram showed the absorbance at 280 nm and Flag-hRme-6 eluted in three peaks as before. The fractions from the three peaks were then further analyzed by SDS-PAGE and also by Native PAGE. SDS-PAGE revealed that the purity of all the fractions from three peaks was quite high. In each fraction the main protein was hRme-6 (Figure 4.12B). When the same fractions were subjected to Native PAGE, samples from the first peak did not show any bands between 720 KD and 12 KD. It might be because the first peak was some kind of aggregation of the protein, which was not easy to get into the native PAGE. The amount in this peak was also much less so it was difficult to detect by native PAGE. Later it was found that the molecular weight of this peak was above 1000 KD. Samples from the second peak only contained one conformation of ~720 KD while the fractions from the third peak had species that migrated both at ~720 KD and 480 KD.

Overall, the fraction from the second peak of gel filtration contained the same conformation as the endogenous hRme-6, which implied that the separation of hRme-6 was successful and the fractions from the second peak could be used for further analysis.

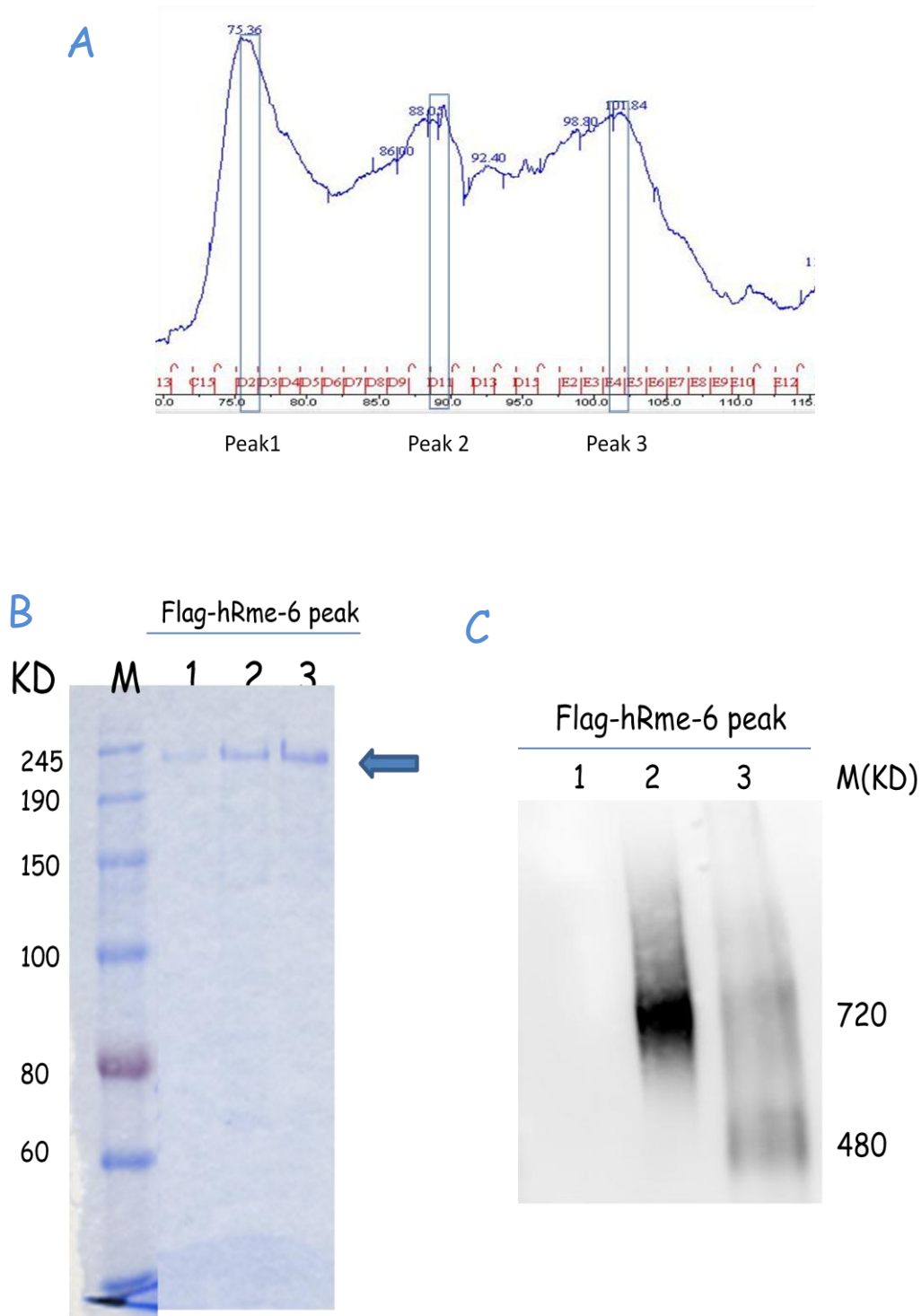


Figure 4.12 Gel filtration separates different conformations of hRme-6. A, 80 μ g purified-Flag hRme-6 was injected into a SuperdexTM-200 gel filtration column. The chromatogram shows the absorbance at 280 nm. B, Aliquots (20 μ l) of the indicated column fractions from peaks 1-3 (A) were analyzed by 10% SDS-PAGE. The arrow indicates full-length hRme-6. C, Aliquots (20 μ l) of the indicated column fractions from peaks 1-3 (A) were subjected to native PAGE and further analyzed by immunoblotting using antibodies specific for hRme-6.

4.10 Negative staining reveals the basic shape of hRme-6

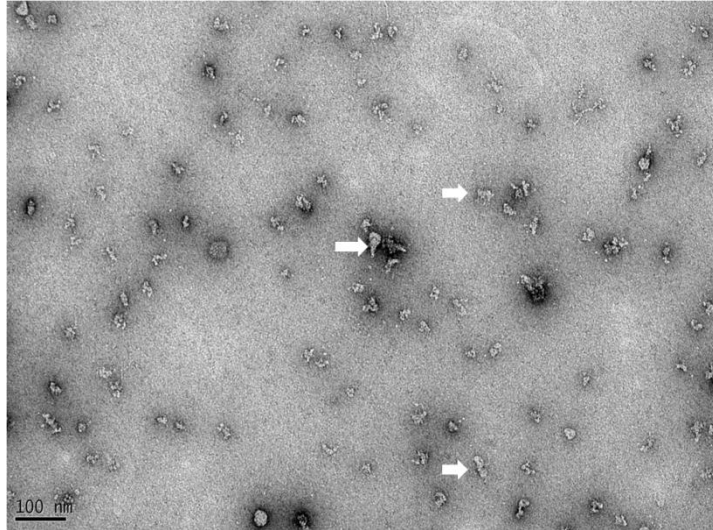
Having demonstrated that endogenous hRme-6 exists as a high molecular weight multimer, we wanted to gain more information about the structure of hRme-6. Previous studies implied that the functions of hRme-6 were highly dependent on its activities and the activities of hRme-6 might be modulated by different cargoes. Therefore understanding the structure of hRme-6 should help us to understand the structure/function relationship of hRme-6.

Although high amounts of Flag-hRme-6 could be purified from insect cells, it existed in two conformations. Gel filtration allowed successful isolation of the different conformations of hRme-6, but the amount of the 720kD conformation was not much. Although it was possible to achieve concentrations of Flag-hRme-6 of 1.3 mg/ml from insect cells, after gel filtration the concentration of Flag-hRme-6 dropped to only 0.08 mg/ml in Peak 2 from the gel filtration column. Another factor which prevented the possibility of preparing samples with high concentrations was the aggregation of hRme-6. This often occurred when attempts were made to concentrate samples after gel filtration. Additionally I had also shown that hRme-6 purified from insect cell existed in two conformations and hence the dynamic equilibrium could affect visualization of the structure of Flag-hRme-6. All those reasons made it hard to get highly concentrated hRme-6 in a single conformation. The large size of hRme-6 in its monomeric form also made it difficult to get the structure of hRme-6 through protein crystallization. However, as I could get the single high molecular conformation of Flag-hRme-6, an alternative approach was to use single particle electron microscopy (EM), including both negatively stained and cryo-microscopy (cryo-EM) of unstained samples in combination with image analysis, to get some information of the structure of hRme-6. This approach also required considerably less protein.

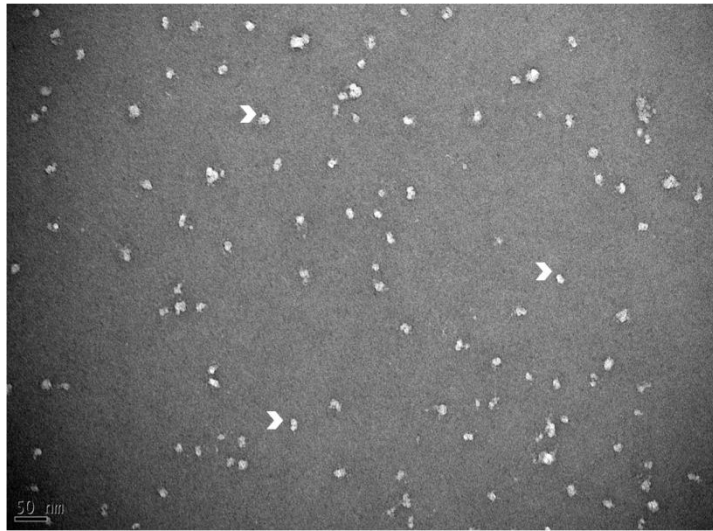
Samples of each of the fractions from gel filtration (shown in Figure 4.12) were loaded on carbon coated grids, stained by uranyl formate solution and viewed by

transmission electron microscopy. As displayed in Figure 4.13, all three samples clearly showed single particles. Samples in the first peak were large aggregations and the sizes of the particles were quite random (Figure 4.13A) in accordance with the behavior of this peak in native- and SDS-PAGE. Samples from the second peak, which contained only the 720 KD conformation of Flag-hRme-6, were stained much more uniformly. Some surface information of hRme-6 was shown. Samples from the third peak, as shown by native PAGE, were mixed with both large particles, similar to those from Peak 2, and also smaller particles.

A



B



C

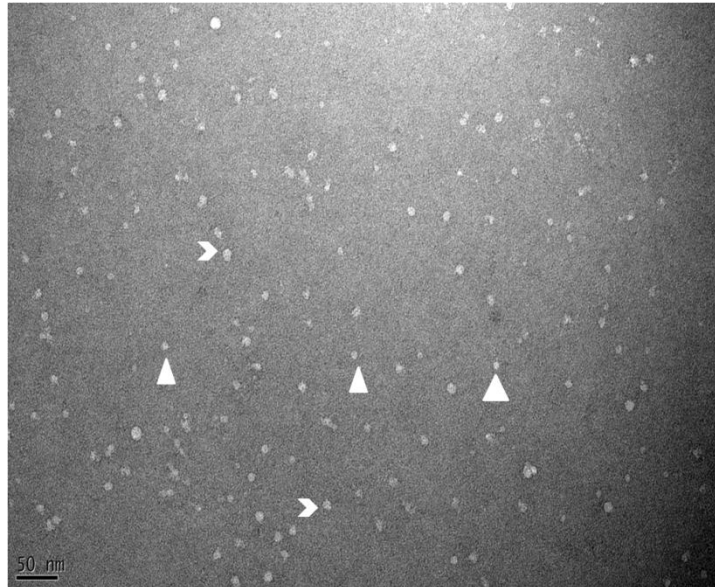


Figure 4.13 Negative staining of different conformations of hRme-6. Negative staining was performed on carbon-coated, 600-mesh copper grids that were glow-discharged prior to staining and viewing by electron microscopy. A: fraction from Peak 1 staining of hRme-6. B: fraction from Peak 2 staining of hRme-6. C: fraction from Peak 3. Arrows indicate the protein aggregation present in peak 1, arrowheads indicate the large protein particles present in both Peaks 2 and 3 and triangles indicate the smaller particles only evident in Peak 3 in the staining of hRme-6.

4.11 Single particle reconstruction of the structure of hRme-6

After obtained the images of hRme-6 from the second peak by EM negative staining, Imagic-5 software was used for further data analysis in collaboration with Dr. Svetomir Tzokov (Department of Molecular Biology and Biotechnology, University of Sheffield). All the particles with the same magnification obtained from EM images were picked out (totally 1,900 single particles) and boxed into one initial file (named as bxd1, Figure 4.14A) to start the data process.

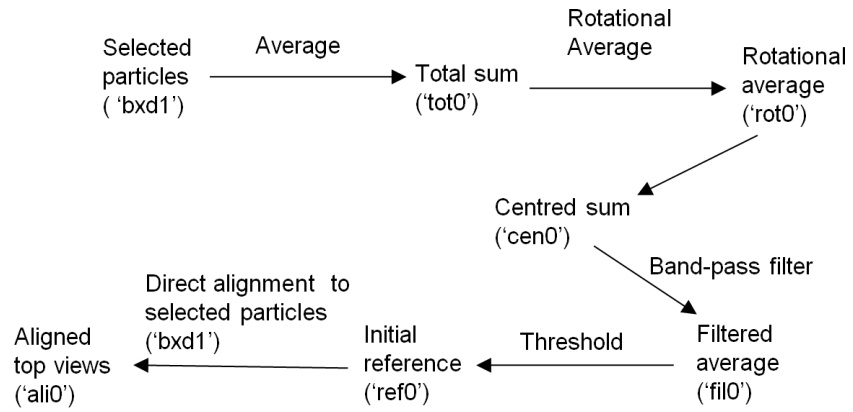
As shown below, the particles were first processed by direct alignment. The process started from the initial alignment (Figure 4.14A, initial alignment). Briefly, the particles

were averaged and a total sum view of all the particles (named as tot0, Figure 4.14A) was generated. The averaged view 'tot0' was then rotated, centered, band pass filtered and thresholded to center the particle, and remove noisy spatial frequencies. After these processes, the initial reference, named as ref0 (Figure 4.14A), was generated, which also contained all information of these processes. Ref0 was used to align with initial individual particles. Specifically, individual particles were processed according to the ref0.

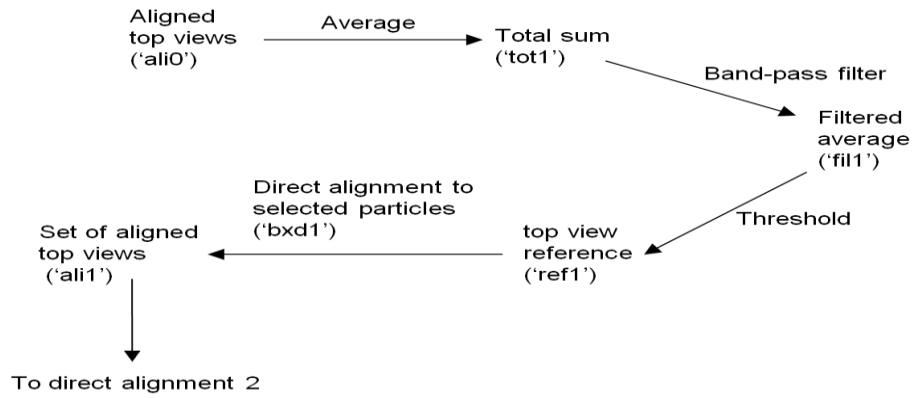
After the initial alignment, the aligned particles (named as ali0, Figure 4.14A) were then re-averaged and re-generated a new sum view ((named as tot1, Figure 4.14A). The sum view tot1 was then band pass filtered, thresholded and generated the second alignment reference (named as ref1, Figure 4.14A) to align with all particles showed in Figure 4.14A, direct alignment 1. The same step of direct alignment 1 was repeated four times to further remove all noisy spatial frequencies and get clear structure information of hRme-6. However, the protein blobs did not exhibit a regular distribution after these calculations (Figure 4.14 C).

A

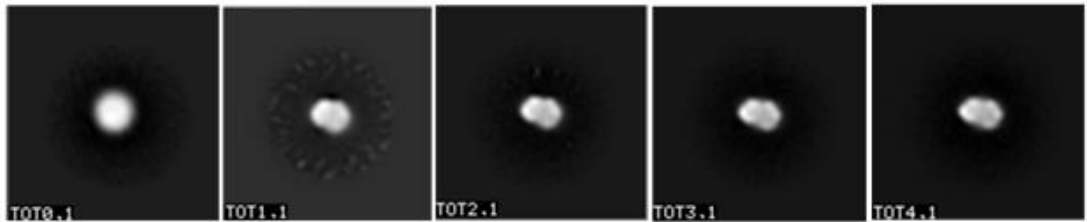
Initial alignment



Direct Alignment 1



B



C

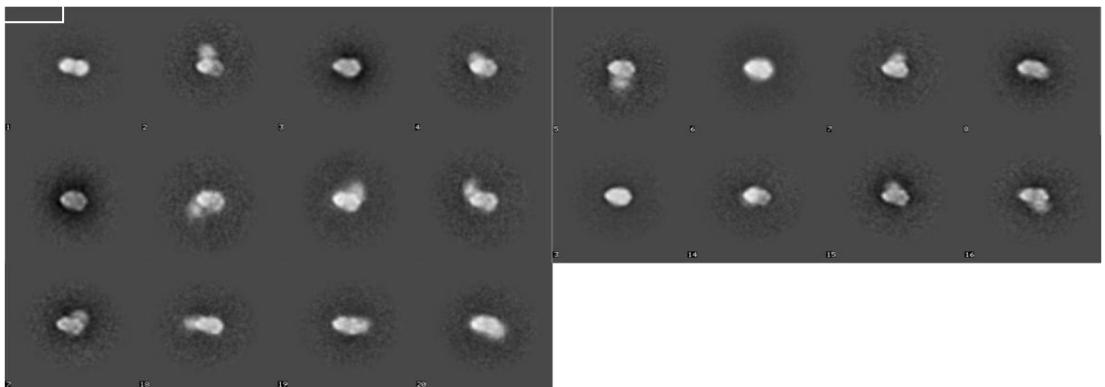


Figure 4.14 Direct alignments of all the particles. A. Initial alignment and direct alignment 1 process. Initially, all particles were boxed into one file named as bxd1. It was then averaged to generate a total sum view of all the particles named as tot0. The total sum tot0 was then rotated, centered, band pass filtered, thresholded and initial reference (ref0) was generated. Then all particles were processed according to the initial reference information. The aligned particles were then processed in direct alignment 1 through averaging, band pass filtering, thresholding and generating the second reference (ref1). The particles were re-aligned according to ref1. The file names at each step were indicated at the quotation mark. B. total sum views of hRme-6 particles during five steps of alignment. C. According to the reference generated from sum4, the top views of hRme-6 particles were classified to 20 groups.

As there is still lack clear information of the structure of hRme-6, alignment by classification was also then performed, which is a method that obtains classes by aligning the particles to references generated from the data set itself by multivariate statistical analysis (MSA).

Brifely, after the final direct alignment, all particles were classified into 20 groups. All groups were band pass filterd, thresholded and generated references accrodngly. Multi-reference alignment (MRA) was first performed against all particles using these references. After MRA, the aligned particles were re-divided in to new groups according to symmetry and particle numbers in MRA reference groups. The new groups of particles were then summed up, band pass filtered, thresholded to re-generated multi-references for the next MRA distrubtion. There were totally five multi-reference alignments that were carried out. And the final selected top views were used to reconstruct the structure of hRme-6 are shown in Figure 4.15. The final reconstructed structure of hRme-6 was shown in Figure 4.16.

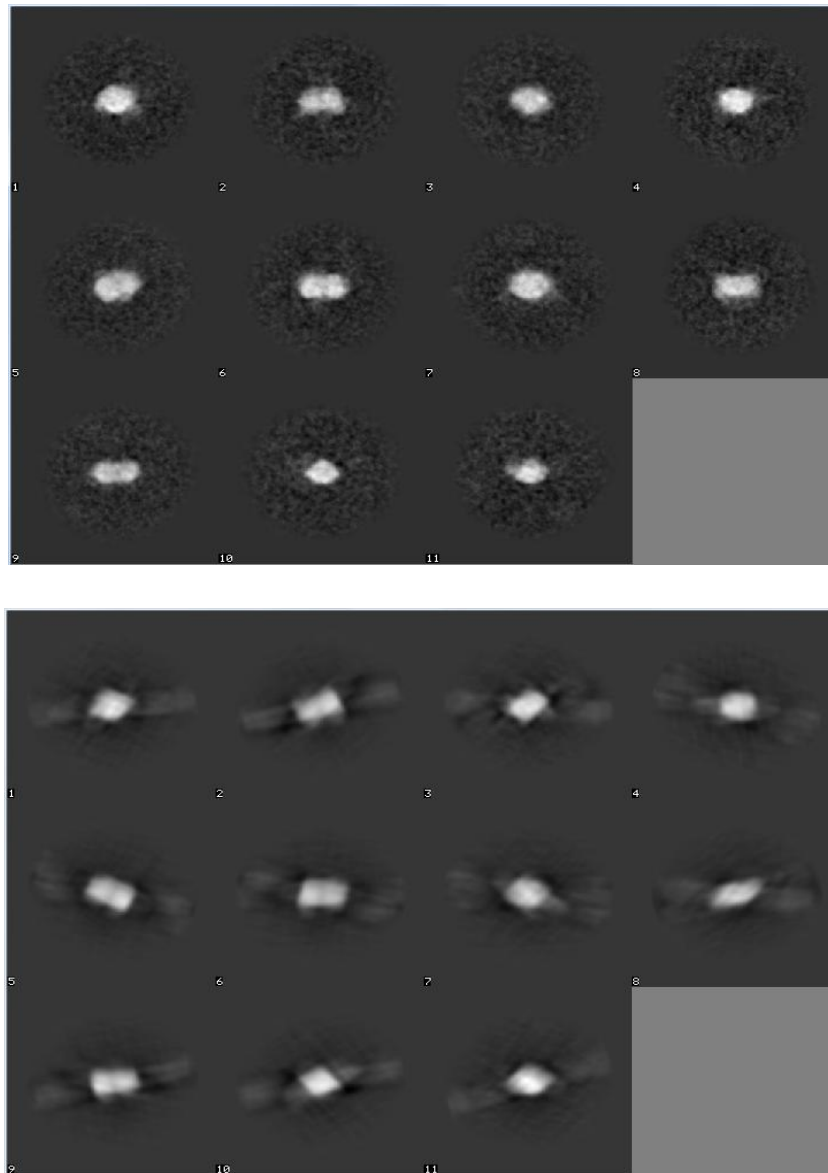


Figure 4.15 A selection of the final top view images used to reconstruct the structure of hRme-6. A, the selected top views after the fifth multi-reference alignments. B, the corresponding Euler angles of each view.

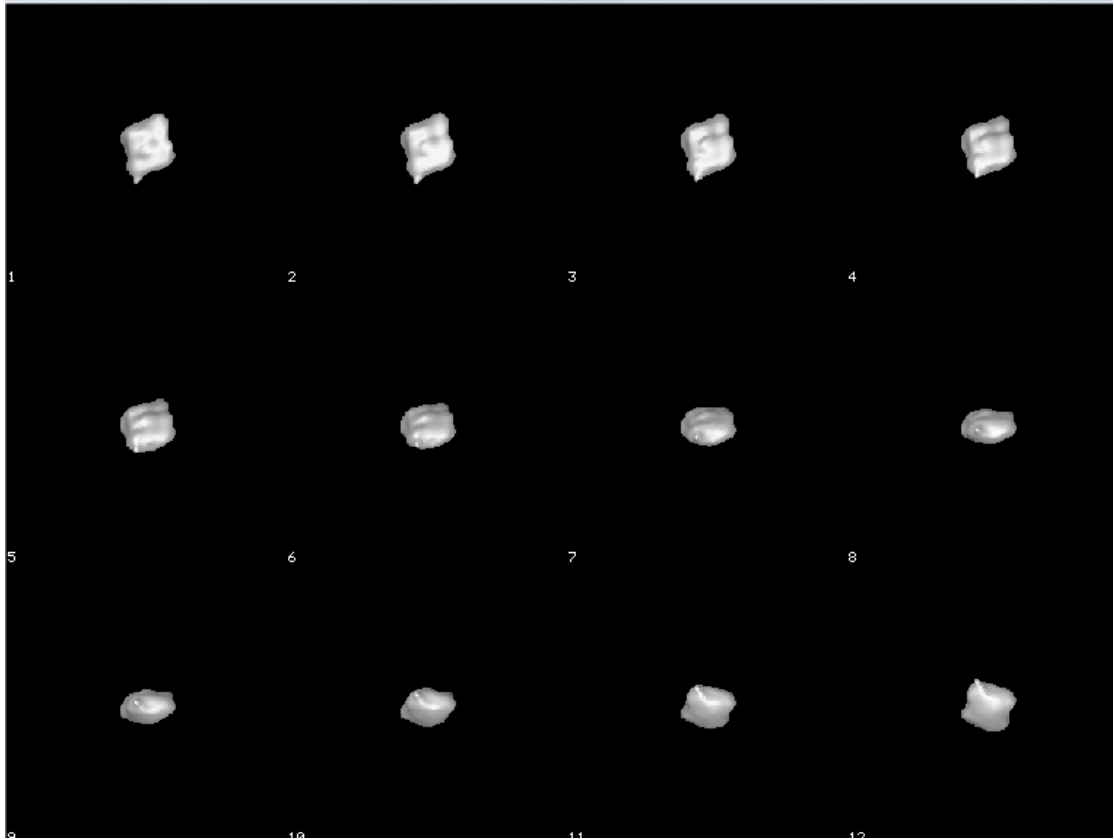


Figure 4.16 A reconstruction of hRme-6. The final reconstructed structure of hRme-6 viewed in different angles.

4.12 Nanogold labeling of His-hRme-6

As the structural information for hRme-6 still needed improvement, we planned to establish conditions for cryo-EM. As a first step, I developed conditions for nanogold labeling to help identify hRme-6 particles in cryo-EM. In addition, although the negative staining analysis had provided some surface information of hRme-6, there was still no clear information about monomer numbers in the higher multimeric conformation of hRme-6 (720KD). An alternative way to get the information about the multimer information was to use nanogold labeling. As purified hRme-6 from insect cells contained only Flag tagged protein and contained equal amount of the two conformations, I decided to investigate whether the amount of the 720 KD species

could be boosted by using a mammalian expression system. hRme-6 was cloned into pcDNA3.1-Flag plasmids with or without a 6XHis tag at the C-terminus. pcDNA3.1-Flag-hRme-6-his and pcDNA3.1-Flag-hRme-6 plasmids were transfected into HEK293 cells. Flag-hRme-6-his and Flag-hRme-6 were immunoprecipitated by Flag M2 affinity gel. As Figure 4.17A showed, Flag-hRme-6-his and Flag-hRme-6 were successfully purified from HEK cells. Purified protein was also checked by native PAGE (Figure 4.17B). The purified Flag-hRme-6-his from HEK293 cells contained both the 720 KD and 480 KD conformations of hRme-6. But the 720 KD species constituted approximately 90% of the total protein.

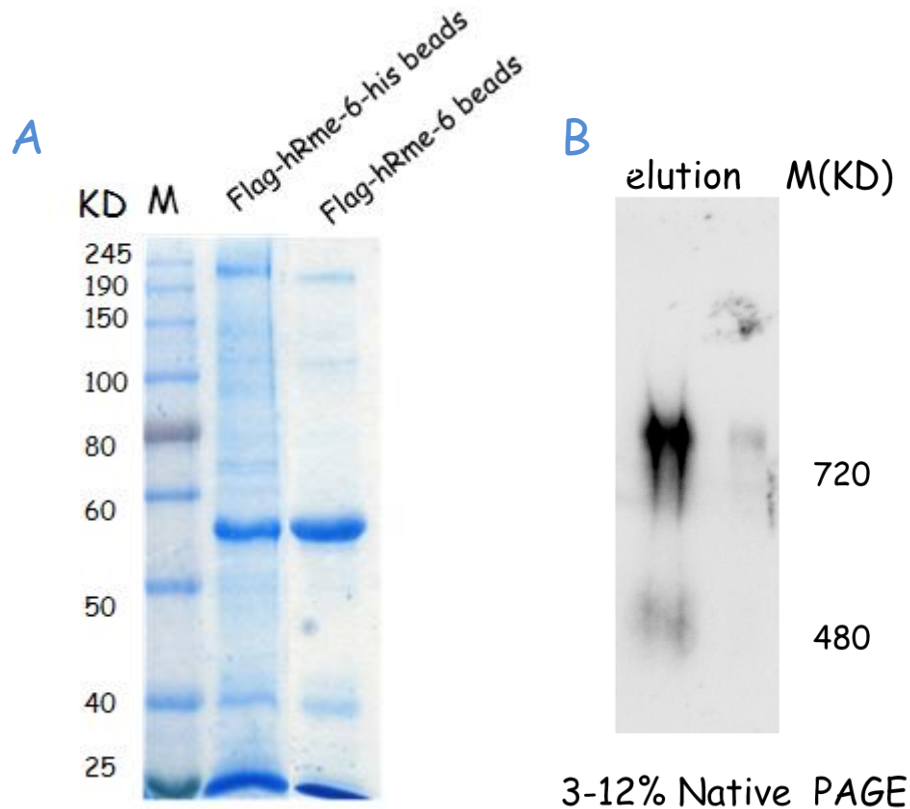
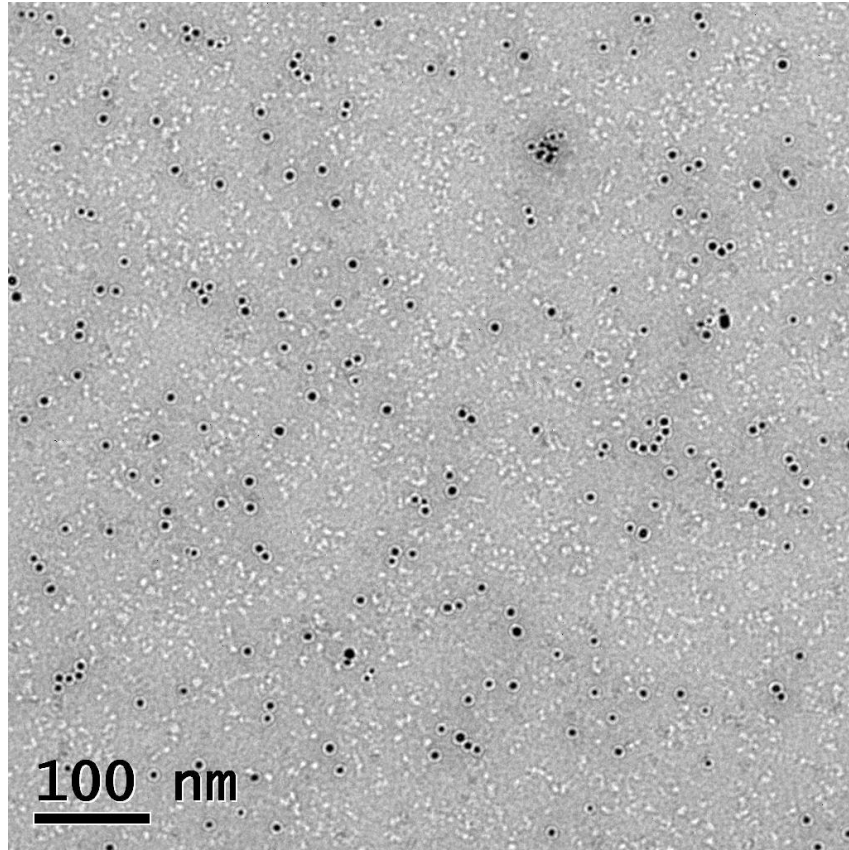


Figure 4.17 Purified Flag-hRme-6 and Flag-hRme-6-his from HEK cells. A, Flag-hRme-6 and Flag-hRme-6-His were immunoprecipitated by M2 anti-Flag beads from HEK293 cells that overexpressed Flag-hRme-6 and Flag-hRme-6-his. A. purified protein was loaded on 10% SDS-PAGE gel and stained with coomassie blue. B, Purified Flag-hRme-6-his from HEK cells were mixed with native PAGE loading buffer and loaded on a 3-12% native PAGE. The PAGE was further analyzed by immunoblotting using antibodies specific for hRme-6.

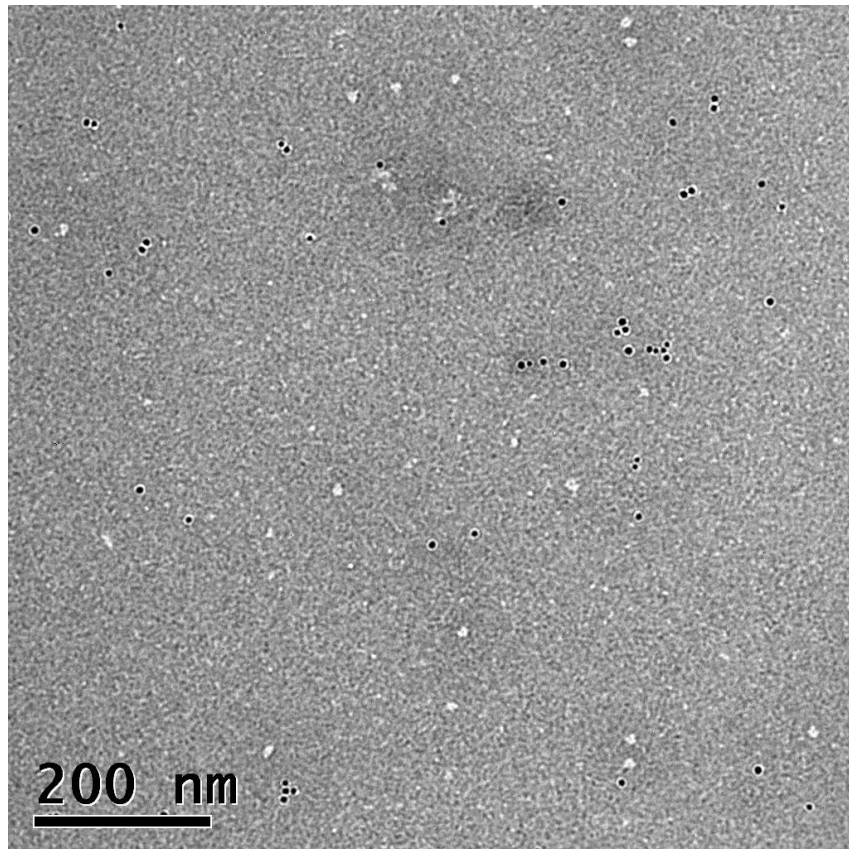
To analyse the constitution of the multimeric form of hRme-6, purified Flag-hRme-6-His, Flag-hRme-6 and BSA, were incubated with 5 nm Ni-NTA-Nanogold, followed by negative staining. As shown (Figure 4.18), there was clear co-localisation between the purified Flag-hRme-6-his and nanogold. BSA and Flag-hRme-6 did not show co-localisation with 5 nm Ni-NTA-Nanogold. It indicated that the labeling of naogold was specific. The purified Flag-hRme-6-His particles bound to at least one nanogold while the majority colocalized with two nanogold. Some particles even bound with three or four nanogold.

The purified Flag-hRme-6-His protein preparation still contained lower molecular weight conformations of hRme-6. Due to time limitations, purified proteins were not gel filtered to separate the different conformations, so the nanogold labeling was expected to label a mixture of structures. The nanogold labeling indicates that the C terminus of hRme-6 is exposed to the outside and not buried inside the multimer. From this we can conclude that the multimer constitution of hRme-6 would be at least a dimer as we cannot rule out the possibility that the C-terminus of hRme-6 was hidden inside the structure. It also could be because of the steric block that the nanogold could not bind to the particles effectively. Over all, the purification of hRme-6 from HEK293 cells was successful. The nanogold labeling of Flag-hRme-6-his was specific and effective. This thus lays the foundation for future cryo-EM studies of hRme-6.

A



B



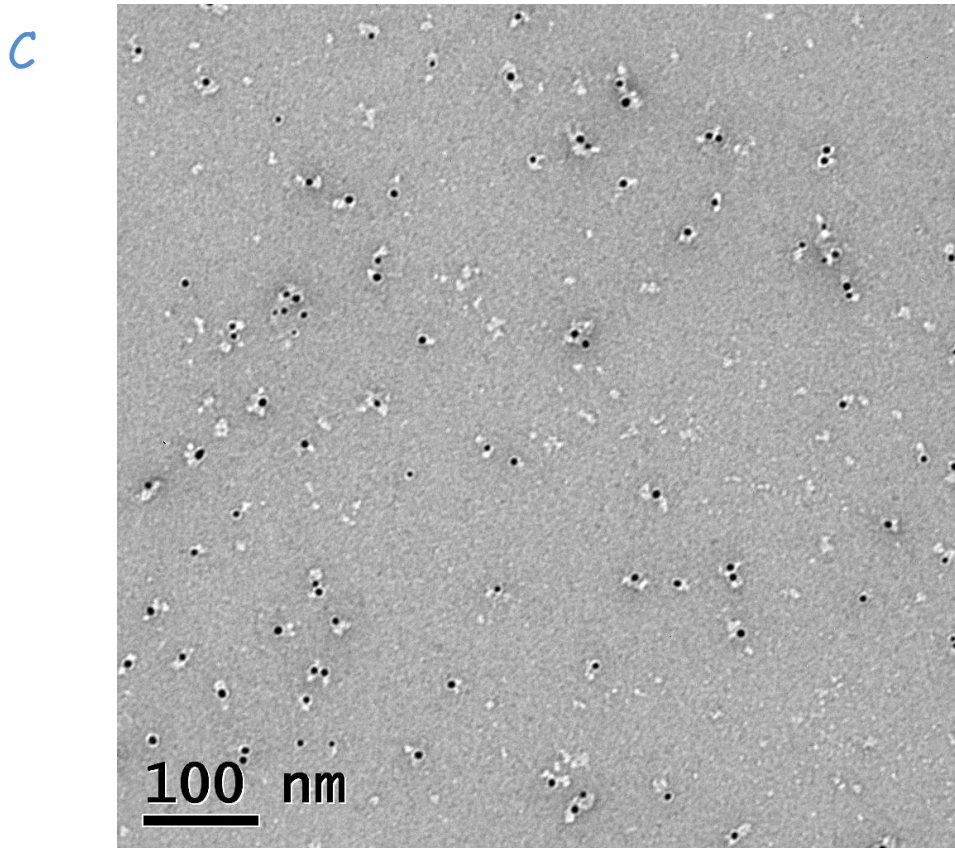


Figure 4.18 Ni-NTA-Nanogold labeling of hRme-6. Negative staining was performed on carbon-coated, 600-mesh copper grids that were glow-discharged prior to staining. 10 μ l of the samples (around 0.12 μ g) in 16 mM imidazole were mixed with 1 μ l 0.5 μ M 5 nm Ni-NTA-Nanogold on ice for 10 minutes. 5 μ l of the mixture was loaded on grids. The sample was adsorbed for 60s, washed with 32 mM imidazole, stained with freshly filtered 0.75 % uranyl acetate, dried, and then viewed in the electron microscope at 100 kV. A, nanogold labeled BSA. B, nanogold labeled Flag-hRme-6. C, nanogold labeled Flag-hRme-6-his.

4.13 Domain interaction test

Although the reconstructed structure of Flag-hRme-6 revealed some surface information about hRme-6, how the different domains of hRme-6 interacted with each other to form the multimers was still unknown. To investigate the potential interaction among different domains of hRme-6, a construct encoding the Rab5 GEF

domain with a Flag tag was engineered. HEK293 cells were co-transfected with this plasmid and pCDNA3.1-HA-hRme-6 plasmids. HA-hRme-6 and Flag-GEF was then immunoprecipitated from HEK293 cell lysates using either an anti-HA or anti-Flag antibody.

As is demonstrated on Figure 4.19, HA-hRme-6 can be detected in the sample immunoprecipitated with anti-Flag antibody. Conversely, in the HA-hRme-6 immunoprecipitate, Flag-GEF was detected. Although this suggests that the full-length protein can interact with the GEF domain, the experiment would need to be strengthened by carrying out incubations with a control IgG. This would provide more conclusive evidence that the GEF domain can interact with the full length hRme-6.

Overall, this experiment just gave a brief hint that GEF domain of hRme-6 may interact with full-length HA-hRme-6.

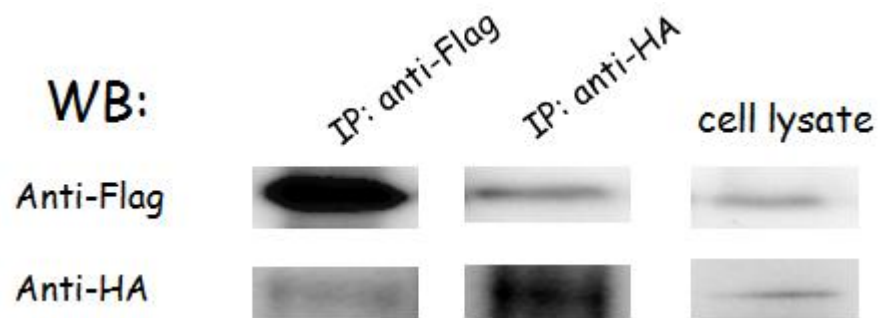


Figure 4.19 The GEF domain of hRme-6 can interact with full length HA-hRme-6. HEK293 cells were co-transfected with the same amount of pCDNA3.1-HA-hRme-6 plasmids and pCDNA3.1-Flag-GEF plasmids. HA-hRme-6 and Flag-GEF was then immunoprecipitated from HEK293 cell lysates by either an anti-HA antibody or anti-Flag antibody. The immunoprecipitated samples were then analyzed by immunoblotting with anti-HA antibody or anti-Flag antibody. Lysis indicated 2% of total cell lysates used for immunoprecipitation.

4.14 CK2 inhibition changes the conformation of hRme-6 in EGF stimulated HeLa cells

My previous experiments showed that CK2 inhibitor treatment altered EGF signalling. To further explore the relationship between the signal changes with the structure of hRme-6, lysates from CK2 inhibitor treated HeLa cells followed by different times of EGF stimulation were gel filtered in a SuperdexTM-200 column. Fractions were analyzed by immunoblotting. Figure 4.20 showed that in HeLa cells, treated with a CK2 inhibitor, hRme-6 appeared as two peaks (peak1: 7.65 ml to 8.85 ml; peak 2: 9.15 ml to 10.5 ml). However after 10min EGF stimulation, Peak 1 of hRme-6 shifted and hRme-6 eluted mainly in Peak 2. This experiment showed that CK2 inhibitor changed the conformations of hRme-6 in EGF stimulated HeLa cells and suggested that there may be a dynamic equilibrium between the two conformations in vivo.

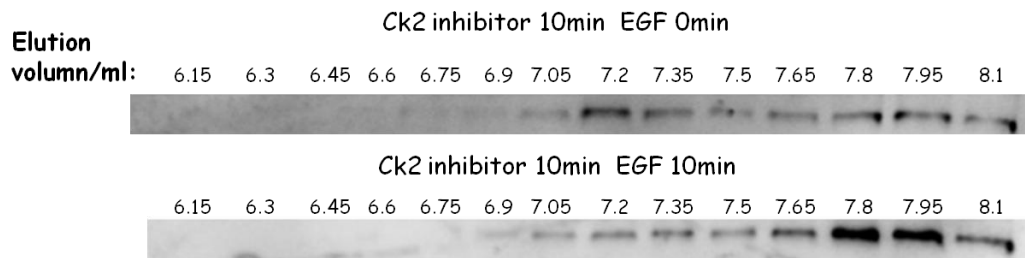


Figure 4.20 Inhibiting CK2 changes the conformation of hRme-6 in EGF stimulated HeLa cells. Following 24 hours serum starvation, HeLa cells were stimulated by 50 ng/ml EGF plus or minus a 10 minute pre-incubation with the CK2 inhibitor, TBCA. At the indicated time points, cells were lysed and cell lysates was injected into SuperdexTM-200 gel filtration column. Fractions were analyzed by immunoblotting specifically to hRme-6.

4.15 Discussion

hRme-6 is a multidomain protein with a Ras GAP and a Rab5 GEF domain. One of the main aims of my project was to understand how these different domains of the protein might be regulated. Previous studies had implicated the activity of the Rab5 GEF domain in transferrin endocytosis[157] while other studies showed that EGFR internalisation was more dependent on the Ras GAP domain [159]. The experiments described in this chapter aimed to understand the structure of hRme-6 in order to understand more fully its diverse functions.

4.15.1 hRme-6 forms multimers in vitro and in vivo

There were early hints that hRme-6 might adopt an oligomeric structure: the protein migrated as a species of 230 KD on SDS-PAGE instead of the predicted 166 KD. Then in SDS trapping assay, purified hRme-6 from insect cells showed clear signs of SDS resistance and there were higher molecular bands of hRme-6 in the SDS trapping buffer treated protein sample.

The first experiments to understand the conformation of hRme-6 showed that overexpressed HA-hRme-6 in HeLa cells could co-immunoprecipitate overexpressed Flag-hRme-6. Other evidence supporting a higher order structure was the gel filtration data which showed that purified hRme-6 from insect cells or hRme-6 overexpressed in HeLa cells eluted in multiple peaks. The largest of the peak was the same, or slightly larger than, the molecular weight of a CHC trimer (~630kD). Furthermore hRme-6, purified from insect cells, subjected to native PAGE further confirmed that hRme-6 forms multimers of ~ 720 KD and 480 KD. Endogenous hRme-6 in HeLa cell lysates mostly migrated at a molecular weight around 720 KD. Overall all the data showed clear evidence that hRme-6 forms high molecular weight multimers in vitro and in

vivo.

These data provided strong evidence that hRme-6 existed as a multimer in vivo and in vitro. This indicated that hypothesis I about the function/structure relationship (Figure 4.1) was likely to be incorrect. Neither was our second hypothesis that hRme-6 might assemble into a multimeric conformation supported by our experimental findings: endogenous hRme-6 mainly existed as the larger 720 KD conformation with little at 480 KD and EGF stimulation did not lead to a conformation change of hRme-6. However, it might be expected that the diverse functions of hRme-6 might require a structural basis. It is still possible that the activities of hRme-6 differ depending on cargo and that there are alterations in the structure which are not reflected in changes in the conformation. An alternative possibility is that hRme-6 may form a big platform to interact with different proteins depending on the uptake of specific cargo.

Evidence in support of the former option was that during CK2 inhibitor treatment combined with EGF stimulation the conformation of hRme-6 shifted (Figure 4.20). As my previous work showed that CK2 could phosphorylate hRme-6, CK2 inhibitor treatment may inhibit phosphorylation of hRme-6. But the conformation of hRme-6 after CK2 inhibitor treatment warrants further exploration. It is possible that changes in hRme-6 conformation coupled to changes in different binding partners contribute to differential functions of hRme-6 in cargo uptake. The interaction partners of hRme-6 have been further explored in next chapter.

4.15.2 Determination of the size of hRme-6 monomers

An important question which I tried to address was the size of the monomeric form of hRme-6. The calculated molecular weight of hRme-6 by amino acid sequence is 166 KD. However, hRme-6 purified from insect cells or HEK293 cells both migrated at 230 KD in normal SDS PAGE. Even the purified hRme-6 from *E.coli* (data not shown) also

migrated at 230 KD in normal SDS PAGE. The sec malls results suggested that the lowest molecular weight of hRme-6 was around 250 KD, which also seemed to support the idea that monomer size of hRme-6 was 230 KD. However, if the oligomer size of hRme-6 is 230 KD, it is unclear about the reason that leads the shift of the size from 166 KD to 230 KD. In normal SDS PAGE, the sample should be totally boiled and the multimeric conformations should be disassembled and it would be expected that the size would represent the monomeric conformation. It appears that there was some unknown robust conformation or modification to hRme-6 which led to the molecular weight shift. There may be several different possible modifications, like ubiquitination or glycosylation, which could cause such a shift in the monomer molecular weight.

Another possibility was that there could be a strong binding partner that did not dissociate, even following treatment of the sample at high temperature and high concentrations of SDS. However, again this seemed unlikely given that the mass spectrometry analysis of the 480 KD and 720 KD forms after native PAGE did not reveal the presence of any major interacting partner.

In immunoblotting assays, there was sometimes a band detected by anti-hRme-6 antibodies around 190 KD, which was still higher than 166 KD. It was possible that this band could be a protein degradation product from the native higher molecular weight form as this band was often observed in frozen but not fresh samples. The commercial antibody for hRme-6 was targeted to the sequence from 550 aa to 650 aa of the protein. This region is just in the middle of the structure of hRme-6, which also made it impossible to gain additional information as to whether the lower form was a degradation product.

Based on these approaches we were still unable to determine accurately why Rme-6 migrates enormously on SDS-PAGE.

4.15.3 Rme-6 exists in several multimeric forms

One question that I addressed was about the exact subunit composition of the multimeric conformation of hRme-6. In gel filtration column, purified hRme-6 from insect cells co-eluted with CHC, which has a molecular weight around 630 KD. However in native PAGE, hRme-6 migrated higher than 720 KD. The difference between gel filtration and native PAGE may be due to poor resolution within the higher molecular weight ranges as the separation range of SuperdexTM-200 column is from 5 KD to 500 KD. It maybe cannot separate the bigger size particles properly, which caused the CHC trimer conformation and hRme-6 of 720 KD conformation overlapped.

Another question which I tried to address was how many monomers formed the high molecular multimer of hRme-6. As I could not determine a precise monomer molecular weight, the number assembling to form the multimer is also controversial. In native PAGE, the molecular weight is dependent on the native structure as well as the molecular weight. If hRme-6 was modified as suggested above, this might also affect its migration on native PAGE. If the calculation of monomer of hRme-6 was 166 KD, the conformation of nature hRme-6 around 720 KD would be a tetramer or pentamer. However if the calculation was based on 230 KD, the conformation hRme-6 would be more like a trimer.

As the sec malls data did not provide a clear answer to the molecular weight of the protein, I also tried the nanogold labeling to get an estimate of the number of subunits present in the multimeric conformation. As you could see from Figure 4.18, there was a mixture of conformations in the sample with labeling from one nanogold particle to four nanogold particles per particle of hRme-6. As the structure of the multimer was unknown, the nanogold bound to the protein should be equal to or lower than the number of monomers as some of the His tag may be hidden inside the particles. It is also possible that there were steric blocks which inhibited the effective

labeling of nanogold to the protein. Although the information obtained is not conclusive, it should be possible to perform further separation of the different conformations of hRme-6 by gel filtration, to further improve the label specificity and to expose the hints of the multimer conformation. The nanogold labeling also could guide identification of the orientation of hRme-6 subunits during cryo-EM.

Another way that could be used to calculate the number of the monomers in multimeric forms of hRme-6 is by crosslinking. Crosslinking could potentially stabilize dimeric, trimeric, pentameric or tetrameric forms of hRme-6. The size change of hRme-6 after crosslinking could be compared with the native conformations of hRme-6. However, as the mechanism of crosslinking requires the formation of covalent bonds between two proteins by using bifunctional reagents [213], we would have to make an assumption as to the monomeric molecular weight of hRme-6. And another thing was that the electrophoretic mobility of hRme-6 following SDS-PAGE is already relatively big and crosslinking would increase this even further making it difficult to distinguish the band in normal SDS-PAGE gels. Moreover, as the mechanism of crosslinking is different from that of native PAGE, samples after crosslinking may also exhibit different sizes compared to native PAGE results. This might facilitate determination of subunit composition.

In addition to the 720 KD conformation, hRme-6 purified from insect cells showed an additional species of approximately 480 KD. Similarly hRme-6 in HeLa lysates which was frozen and then thawed also showed two conformations at 720 KD and 480 KD. It seemed to match the two species from insect cells. In some preparations as the length of time of storage at -80°C increased, the proportion of the 480 KD conformation increased. Flag-hRme-6 purified from HEK293 cells also contained two species similar to those from insect cells, but the 480 KD conformation was much less compared to that from insect cells. This contrasted with endogenous hRme-6 in HeLa cell lysates which were assayed immediately following lysis and only contained the 720 KD conformation. The underlying cause for the conformation of 480 KD is unclear.

As the 480 KD conformation increased with storage and time, it was initially suspected to be a protein degradation product. However, data from mass spectrometry of the two different conformations of hRme-6 suggested that the 480KD conformation was more likely to be a dissociation form from the larger conformation. In addition my previous data (Figure 4.20) showed that in CK2 inhibitor treated HeLa cells, the conformation of hRme-6 shifted from 720kD to 480kD, and again these two conformations of hRme-6 just matched the two bands found in purified hRme-6 protein from HEK cells and insect cells. This suggests that the two conformations may both represent functional intermediates although it is interesting that the lower molecular weight form is only seen when cells are treated with a pharmacological reagent. One way to test this idea would be to run the sample from the corresponding fractions in native page to check the size of hRme-6. It is possible that the shifting between the different conformations helps to control the protein activities and the functions of hRme-6. This could be tested by looking for differences in the interaction partners of hRme-6, which is further explored in next chapter. An alternative possibility is that the different conformations of hRme-6 may show differences in Ras GAP, Rab5 GEF activities and even the binding ability to phosphorylated P42/44 or other signalling molecules.

One way to test the dynamic equilibrium between the 720 and 480 KD species would be to re-run the different peaks of hRme-6 after gel filtration again in the same gel filtration column. However, due to the limited amount of sample volume that could be injected into gel filtration column and the low protein concentration of hRme-6 which was difficult to concentrate, this was not technically feasible as reinjection of the sample resulted in too much dilution a making the protein difficult to detect.

Together these results indicate that Rme-6 exists as a higher order multimer in vitro and in vivo.

4.15.4 Towards an EM reconstruction of hRme-6

Although relatively high amounts of hRme-6 could be purified from insect cells, and subsequent gel filtration allowed for significant enrichment of the protein, there was a corresponding sharp loss in yield. When the purified protein was held at high concentration, it also led to aggregation of the protein. Additionally the relatively large size of the individual monomers, independent of the multimeric state, would make X-ray crystallography of the whole protein a challenge. However, as the structure of Rab5 GEF domains of Rabex5 [214] and Ras GAP domains of p120 [215] has been crystallized, 50% information about the structure of hRme-6 was known due to the similarities of the Ras GAP domain of hRme-6 to p120 and Rab5 GEF domain of hRme-6 to Rabex-5. My studies using negative staining resulted in clear images of the particles to allow reconstruction of the structure of the protein. The known crystal structures of the Rab5 GEF domain and Ras GAP domain will help to check the reconstructed structure.

From the reconstructed structure of the 720 KD conformation of hRme-6, some surface information of hRme-6 was revealed. The shape of hRme-6 appeared to be irregular and the structure was also asymmetrical. The whole structure was like an irregular tetrahedral. The length was longer than width while the thickness was less than the width. The two sides of the structure were also different. One side was smoother while the other one contained several bulges.

However, there was no clear information about the domain structure and monomer constitution displayed from the reconstructed structure. The structure I got was just an initial surface view of the structure of hRme-6. Due to the irregular and asymmetrical structure, it is impossible to identify the structure of the monomer or distinguish the distribution of the monomers. Although we already had some structural information of the Ras GAP domain and Rab5 GEF domain of hRme-6 from other conserved Ras GAPs and Rab5 GEFs, the asymmetrical structure of hRme-6

made it difficult to distinguish the location of the two domains of hRme-6 in the reconstructed structure. The average image resolution was around 40 Å, which also made it impossible to get more information about the peptide distribution.

There were several reasons that contributed to the lack of clarity in understanding the shape of hRme-6 from the reconstructed structure. The samples used for negative staining were from insect cells where two kinds of conformation existed in the sample. Although gel filtration could separate the different conformations, there were still other contaminating proteins present in the sample (Figure 4.12B). Although these contaminants were present in low abundance, they still are likely to have disturbed the image data. However, as the negative staining is more sensitive with big particles that are larger than 500 KD, small molecular weight proteins would not affect so much the images.

Since there were two kinds of conformations of hRme-6 in dynamic equilibrium in purified hRme-6, the separated single conformation might also quickly form a new dynamic equilibrium. Although native PAGE immunoblotting showed that there was only one conformation in the second peak, there may be still a certain amount of the 480 KD conformation. As the separation range of gel filtration column we used was 5 KD to 500 KD, the separation was not perfect. During the sample preparation the new protein equilibrium may form again. As a result the negatively stained samples I prepared were likely to be a mixture. Although negatively staining particles from Peak 2 were much more uniform compared to those from Peaks 1 and 3, the particles sizes of the second peak still drifted a lot. There were some particles the sizes of which were indeed bigger than others as well as some of which were quite similar to the particles in the images from Peak 3. Basically during negative staining the particles could be fixed in all orientations, so the reconstruction process can shift and combine all the orientations together to form the final structure. However, the possibility that there were other conformations of hRme-6 made it difficult to distinguish the particles because the smaller particles may be at different angles of the protein or

small conformations of hRme-6. So during the reconstruction process, all the particles were picked. It is properly that the final reconstructed structure is a mixed structure of the two conformations of hRme-6. It makes the structure difficult to interpret.

There are several ways to improve the negative staining. As my previous mass spectrometry data found that the 720 KD conformation was quite pure, a sample eluted from the 720kD band on native gels would be one way to avoid contamination with other proteins. Alternatively the eluted sample from the gel could be gel filtered to further improve the purity of the sample. Another way would be to improve the gel filtration conditions, as the separation range of the gel filtration column used in the experiment was relatively narrow. A Superose 6 10/300 with a separation range of 5 KD to 5,000 KD, might more fully separate the two different conformations of hRme-6. So further purifying the samples of hRme-6 could greatly improve the uniform of the particles and make the reconstruction more reliable.

One more method was to analyze the protein structure by cryo-EM. Although negative staining could show the surface structure of hRme-6 and improved method will make the surface structure more clear, the image resolution of the reconstructed structure from negative staining will be still above 10 Å and the detail about the protein structure will be limited. However, cryo-EM, where the sample is studied at cryogenic temperatures, could arrive at near atomic resolution. As the images are taken under the nature condition, it also does not affect much of the protein structure [216-218]. So cryo-EM will further help investigate the structure of hRme-6. My early experiment already tried several conditions and got some basic images of hRme-6 which can be used to build on in future cryo-EM studies. Cyro-EM will further help investigate the structure of mutant forms hRme-6, especially phosphorylation mutations and mutations in the proline rich region, which will greatly help understand the structure of hRme-6.

4.15.5 The domain interaction test

My previous works showed that hRme-6 formed a high molecular multimer in vivo. But I did not get a clear image about the structure of hRme-6 from negative staining and the reconstructed structure. hRme-6 were divided into four main domains, including Ras GAP, middle 1, middle II and Rab5 GEF domains. So one way to investigate the structure of hRme-6 was to find how the multimer of hRme-6 was formed and which domains of hRme-6 could interact with itself. As shown in Figure 4.19, there was some early evidence that the GEF domain of hRme-6 may interact with full length hRme-6. Due to the time limit, other domains of hRme-6 were not tested for interactions. But this will be a useful approach which will synergize with structural studies.

4.15.6 Benefits of a multimeric structure

The multimeric structure of hRme-6 could allow the functions of hRme-6 to be regulated in multiple ways and also increase the number of its functions.

During purification of the Rab5 GEF and Ras GAP domains, most of the sample stayed in the protein pellet. Only a small amount of soluble protein was purified. It implied that the Rab5 GEF and Ras GAP domains might be hydrophobic and buried inside the structure of hRme-6. The multimeric structure will make it possible for the Rab5 GEF and Ras GAP domains to hide inside the structure.

On the other hand, the multimeric form of hRme-6 made it possible to interact with different proteins at the same time. The big structure of hRme-6 may function as a platform to integrate different information and regulate the related activities of interaction partners. The different multimer conformation also may make it possible to regulate the functions of hRme-6 through the change of conformations of hRme-6,

which could lead the different functions of hRme-6 interaction partners.

5. Chapter 5 Identification of interacting partners of hRme-6

5.1 Introduction

Previous data in this thesis and within the Smythe lab had shown that hRme-6 played important roles not only in the trafficking of Tfn and EGFR, but also in signalling intensity regulation. The structural studies about hRme-6 demonstrated that hRme-6 exists as a higher order multimer, which raised the possibility that hRme-6 could interact with many proteins. Identification of the interaction partners of hRme-6 could give insight to explore the functions of hRme-6 during endocytosis and signalling intensity control.

At the start of this work, hRme-6 was known to interact with AP2 [157], Rab5 [160], c-cbl [159] and clathrin (Sato et al) and my previous work found that hRme-6 could interact with phosphorylated p42/44. None of the interaction partners of hRme-6, apart from p42/44, were directly related to signalling control.

My studies and work from other labs showed that during EGF stimulated HeLa cells, hRme-6 affected the internalisation and signalling of EGFR. This made the model of EGF stimulated-HeLa cells a good candidate to study the multi-functions of hRme-6. Previous work (this thesis and Singh and Smythe, unpublished) found that CK2 could phosphorylate hRme-6. During EGF stimulation, inhibiting CK2 with the inhibitor, TBCA, altered the signalling profile of targets, downstream of EGFR, and also shifted the conformation of hRme-6 in HeLa cells (Figure 3.8 and 4.20). These data implied that the function of hRme-6 was partly dependent on the phosphorylation of hRme-6, which mediated by CK2. I therefore decided to combine CK2 inhibitor treatment with EGF stimulation in HeLa cells as a model to investigate the interaction partners of hRme-6.

The experimental approach that I decided to use was Stable Isotope Labeling with

Amino Acids in Cell culture (SILAC) which is a straightforward approach for in vivo mass spectrometry (MS)-based proteomics. As SILAC experiments can directly show quantitative protein changes under different stimulation conditions, it would provide not just the interaction partners of hRme-6 but also how they changed during different stimulations.

5.2 SILAC experiments to identify proteins that interact with hRme-6

In the initial experiments, double-labeling SILAC experiments were set up. One contained the light labeling (R0K0) and the other one contained heavy labeling (R10K10). When cells are growing in the SILAC media, they incorporate the different isotopic arginine and lysine residues into all of their proteins. HeLa cells have a doubling time of 20 hours. So in two weeks time, the cell population increased 2^{18} times and it was predicted that nearly all of the proteins in the cells would incorporate the corresponding label. To verify this, the cell lysates were load on SDS PAGE. Individual bands from the gels were excised, reduced, alkylated and digested by trypsin. The digested peptides were then injected into autosampler tray of Dionex 3000 system and analyzed by Richard Beniston (BiOMICs, University of Sheffield). The lysates all showed efficient labeling and there was no cross labeling contamination (appendix 3).

SILAC experiments were then set up according to the protocol shown in table 5.1. After stimulation, no detergent was added but the cells were permeabilised by freeze/thraw. The cell lysates were then incubated with anti-hRme-6 antibody. After immunoprecipitation, the samples from each of the immunoprecipitations were mixed, subjected to SDS PAGE and individual bands from the gels were excised,

reduced, alkylated and digested by trypsin as described in the Materials and Methods. The digested peptides were then injected into autosampler tray of Dionex 3000 system and analyzed by Richard Beniston (BiOMICS, University of Sheffield).

The data were shown in table 5.2 and appendix 4. As experiments 3 and 4 were actually control experiments to test the background created by the CK2 inhibitor treatment, the data were not included in table 5.2.

However, as shown in table 5.2, these initial experiments did not find any known interaction partners of hRme-6, like AP2, Rab5, c-Cbl and TC10. There were still some interesting candidates in the list, including transferrin receptor protein 1, Ras-related protein Rab-11A and Ras GTPase-activating-like protein IQGAP1. Later Triton X-100 was used in the lysis buffer, but there was still no improvement in identifying either known or potential interaction partners of hRme-6 (appendix 5).

	Experiment 1		Experiment 2		Experiment 3		Experiment 4	
	ROK0	R10K10	ROK0	R10K10	ROK0	R10K10	ROK0	R10K10
TBCA	—	—	+	+	—	+	—	+
EGF	—	+	—	+	—	—	+	+

Table 5.1 Protocol for double-labeling SILAC experiments. Cell populations grown in either light or heavy medium as indicated were grown in dishes. Cells were serum starved for 24 hours and then treated with 50 ng/ml EGF for 10 minutes in the presence or absence of CK2 inhibitor TBCA.

Experiment 1		
Gene name	H/L	protein intensity
Ubiquitin-like modifier-activating enzyme 1	3.907	5.327E6
L-lactate dehydrogenase A chain	3.002	7.811E7
Plastin-3	2.455	4.912E6
Alpha-crystallin B chain	2.405	2.291E6
Transferrin receptor protein 1	0.494	1.450E7
Germinal-center associated nuclear protein	0.488	2.382E6
Nucleolar pre-ribosomal-associated protein 1	0.485	2.803E6
Protein RRP5 homolog	0.457	3.503E6
N-acetyltransferase 10	0.454	2.484E6
Small subunit processome component 20 homolog	0.453	1.770E6
Nucleolar protein 6	0.452	5.458E6
Disks large homolog 5	0.438	6.820E6
Desmoplakin	0.423	1.076E6
E3 ubiquitin-protein ligase TRIP12	0.394	6.929E5
Dolichol-phosphate mannosyltransferase subunit 1	0.332	1.745E6
Kinesin-like protein KIF14	0.318	1.732E6
Keratin, type II cytoskeletal 2 epidermal	0.252	1.702E8
Dermcidin	0.139	7.372E6
Keratin, type II cytoskeletal 6C	0.074	7.285E7
Keratin, type I cytoskeletal 10	0.054	2.070E8
Keratin, type I cytoskeletal 9	0.048	1.705E8
Keratin, type II cytoskeletal 1	0.041	3.347E8
Serum albumin	0.031	2.193E9
Experiment 2		
Gene name	H/L	protein intensity
Transketolase	1.653E8	0.498
L-lactate dehydrogenase B chain	6.093E7	0.429
Peroxiredoxin-2	2.640E7	0.426
Ubiquitin-like modifier-activating enzyme 1	3.464E6	0.411
Carbamoyl-phosphate synthase [ammonia], mitochondrial	1.442E7	0.400
Hornerin	2.698E8	0.320
L-lactate dehydrogenase A chain	1.224E8	0.283
Protein-glutamine gamma-glutamyltransferase 5	7.025E6	0.254
Keratin, type I cytoskeletal 17	1.095E9	0.174
Keratin, type II cytoskeletal 1	1.895E10	0.105
Catalase	4.131E7	0.095
Keratin, type II cytoskeletal 5	2.272E9	0.068
Keratin, type II cytoskeletal 6A	2.272E9	0.054

Keratin, type II cytoskeletal 2 epidermal	2.699E9	0.035
Keratin, type I cytoskeletal 10	1.445E9	0.034

Table 5.2 Candidate hRme-6 interactors identified by mass spectrometry in experiment 1 and experiment 2. The protein hits were selected based on a H/L ratio which was higher than 2 or lower than 0.5.

The weak signals and failure to identify known interaction partners of hRme-6 may be due to the absence of detergent or using the wrong detergent in the lysis buffer. So other optimization trials included lysis in the presence of 1% Triton X-100, 0.5% NP 40 or 0.2 M salt in 20 mM Hepes buffer were performed.

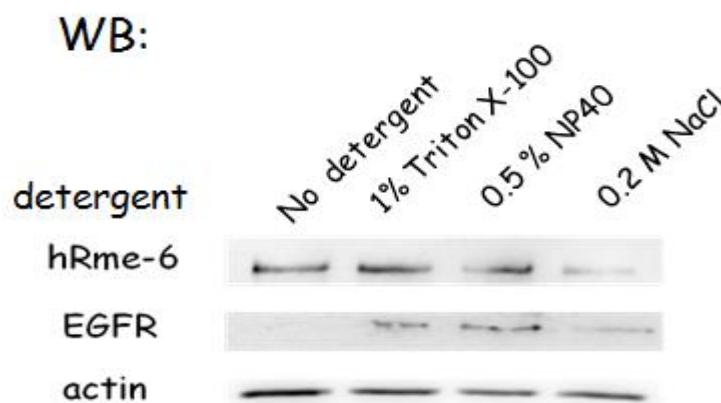


Figure 5.1 Different cell lysis buffers lead to different protein extraction efficiency. HeLa cells were serum starved for 24 hr and then stimulated with 50 ng/ml EGF for 10 minutes. The cells lysates were prepared in 20 mM Hepes buffer, pH 7.4 containing different detergents, including no detergent but freeze/ thaw, 1% Triton X-100, 0.5% NP 40 or 0.2M salt. Cell lysis was then analyzed by immunoblotting with antibodies to hRme-6, actin and EGFR.

As shown, when Triton X-100 and NP 40 were used in the lysis buffer, it was possible to clearly detect hRme-6 in the cell lysate. Lysis in the presence of high salt showed a relatively weak extraction of hRme-6 from the cells, perhaps because of aggregation and precipitation of hRme-6. However, since hRme-6 is a cytosolic protein which is recruited to endosomal membranes in order to activate Rab5, I wanted to be sure that the lysis conditions gave a good extraction of membrane proteins. To check

this, I used the extraction of EGFR as a positive control to assess which lysis conditions gave the best extraction. I found that the presence of NP40 gave the best extraction of EGFR.

To further improve the accuracy of the experiment, triple labeling SILAC experiments were set up. As shown in Figure 5.2, HeLa cells were cultured in light isotope labeling media (R0K0), medium isotope labeling media (R6K4) and heavy isotope labeling media (R10K8) accordingly. HeLa cells from the different labeling conditions were then treated as shown in table 5.3. The light labeled cells were used as the control groups, in which two dishes of cells were treated with 50 ng/ml of EGF for 5 minutes, with or without TBCA. The medium labeling cells were treated with both EGF and CK2 inhibitor while the heavy labeling cells were just treated with EGF for 5 minutes.

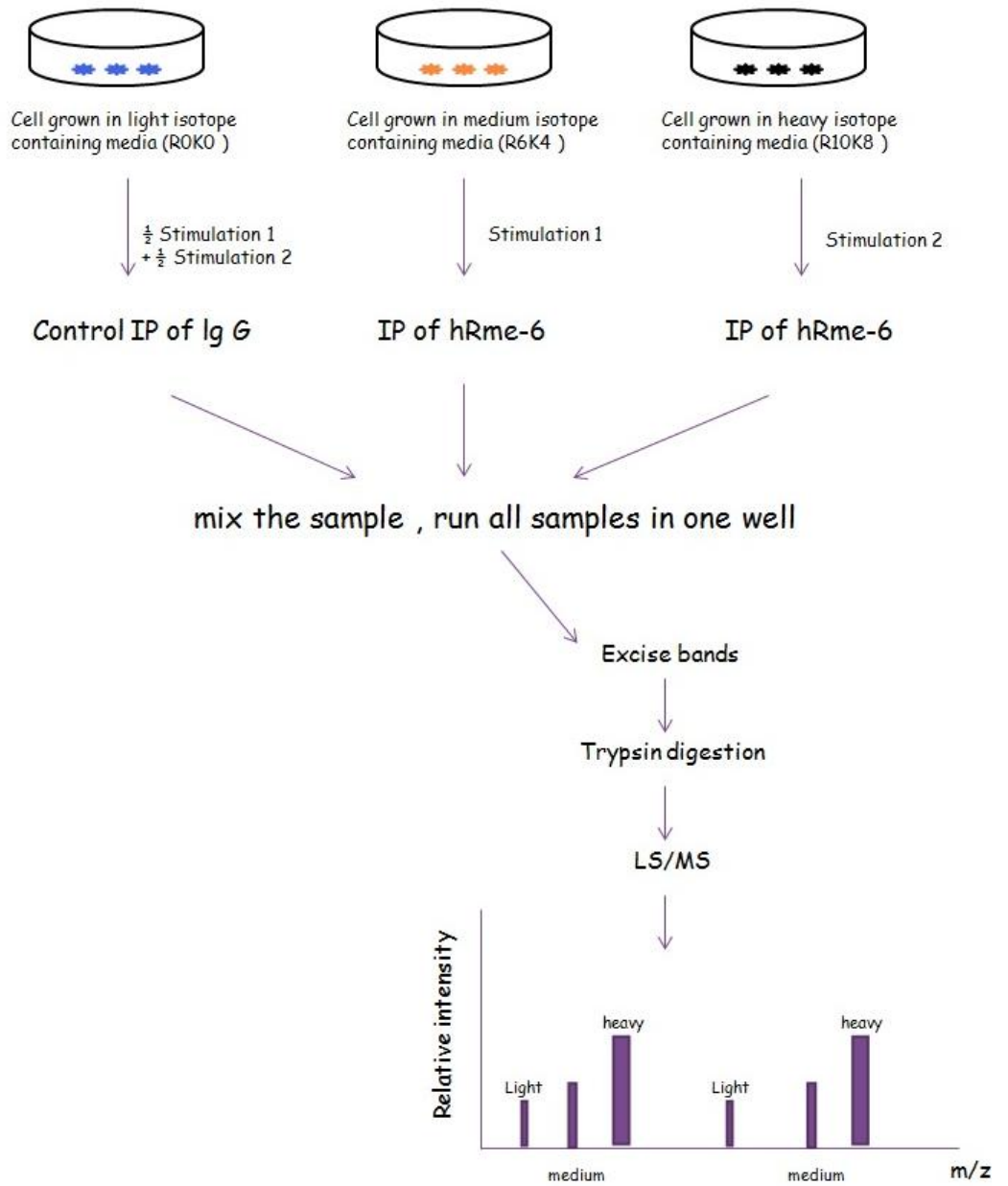
	R0K0	R0K0	R6K4	R10K8
TBCA	—	+	+	—
EGF	+	+	+	+

Table 5.3 Triple labeling SILAC cell treatment. Three cell populations with different labeling were grown in four dishes. Cells without labeling were treated with 50 ng/ml EGF or pretreated with CK2 inhibitor. Cells with medium labeling were treated both CK2 inhibitor TBCA (40 μ M) and 50 ng/ml EGF while the cells with heavy labeling were just stimulated by 50 ng/ml EGF.

After the different treatments, cells were lysated in presence of NP40 and processed as shown in Figure 5.2. After immunoprecipitation, different samples were mixed and run in SDS-PAGE. The gel staining is shown in Figure 5.2B. Individual bands from the gels were excised, reduced, alkylated and digested by trypsin as described in the Materials and Methods. The digested peptides were then injected into

autosampler tray of Dionex 3000 system and analyzed by Richard Beniston and Mark Collions (BioMICs, University of Sheffield). Data was shown in Figure 5.3, appendix 6.

A



B

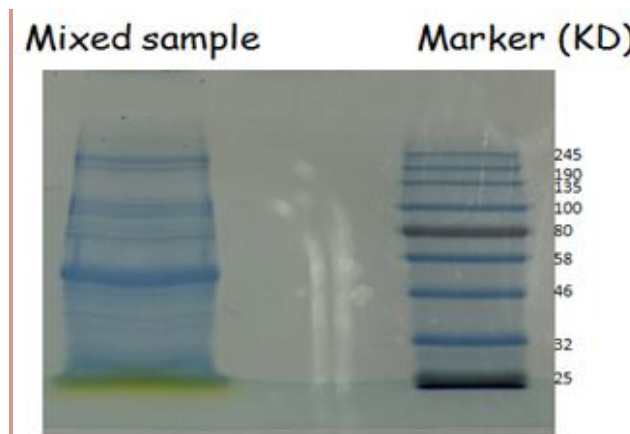


Figure 5.2 Triple labeling SILAC experiment protocol. A, three cell populations are labeled separately with light amino acids, medium (L-ARGININE-13C6 HYDROCHLORIDE, L-LYSINE-4, 4, 5, 5-D4 HYDROCHLORIDE), or heavy amino acids (L-ARGININE-13C6, 15N4 HYDROCHLORIDE, L-LYSINE-13C6, 15N2 HYDROCHLORIDE). Lysates were either incubated with anti-hRme-6 or anti-IgG antibodies and samples were then combined and analyzed together by LC-MS/MS. In the MS spectra, each peptide appears as a triplet with distinct mass differences. The ratios between the samples are calculated directly by comparing the differences in the intensities of the peaks. B, after immunoprecipitation, different samples were mixed and run through 4-15% gradient SDS-PAGE at 130 KV for 15-20 minutes. The gel was then stained by instant blue.

5.3 Mass Spectrometry data further analysis

Appendix 6 showed the results of the mass spectrometry of the triple SILAC labeled samples. Figure 5.3 below showed the ratio of the protein groups compared between heavy and light, medium and light respectively.

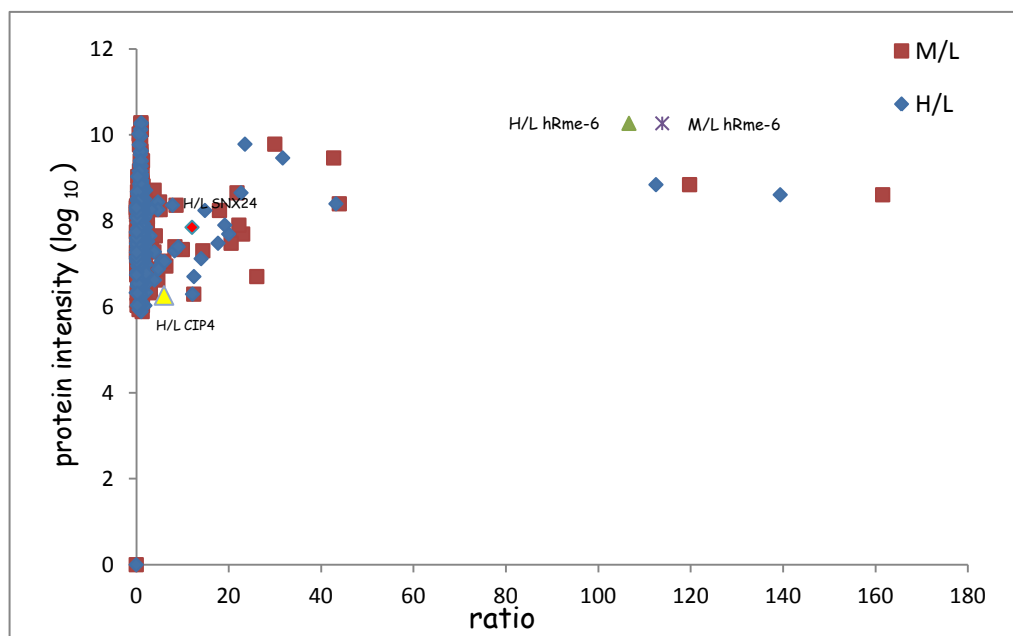


Figure 5.3 Protein ratio distributions in M/L and H/L. The protein ratio was calculated by comparing the protein intensities of the matched light labeling peptides (L) with that of medium labeling (M) and heavy labeling (H)

respectively. The green triangle shows the ratio of hRme-6 comparing medium labeling peptides with light labeling peptides (M/L). The blue stars showed the ratio of hRme-6 comparing heavy labeling peptides with light labeling peptides (H/L). The yellow triangle showed the H/L ratio of CIP4 and the red diamond showed the ratio H/L of SNX24. The Y axis shows the logarithm of total protein intensity.

It was reassuring that high amounts of hRme-6 were found in the immunoprecipitates from medium (M) and heavy (L) labeled cell lysates but not in the light (L) lysates (the ratio M/L and H/L was 93.752 and 168.7 respectively). It suggested that the immunoprecipitation of hRme-6 was successful and the antibody for hRme-6 used in immunoprecipitation was specific. The protein intensity of the proteins found in Mass Spectrometry spread from 10^8 to 10^{10} , which suggested that the proteins found were reliable. To analyze the data, the ratio was defined to be significant if the ratio of the comparison was higher than 2 or lower than 0.5. Table 5.4 showed the protein hits which were sensitive to EGF in the presence or absence of CK2 inhibitor TBCA.

Protein names	Ratio M/L	Ratio H/L	Protein Intensity
Opsin-5	161.6	139.42	4.05E+08
Large proline-rich protein BAG6	119.8	112.52	6.95E+08
GTPase-activating protein and VPS9 domain-containing protein 1	113.88	106.68	1.86E+10
Sjogren syndrome/scleroderma autoantigen 1	43.968	43.242	2.5E+08
Microtubule-associated protein 1B;MAP1B heavy chain;MAP1 light chain LC1	42.75	31.718	2.91E+09
Cell cycle and apoptosis regulator protein 2	30	23.546	6.09E+09
Protein IWS1 homolog	26.103	12.492	5059200
Formin-like protein 1	23.049	20.025	49326000
WD repeat-containing protein 91	21.826	22.695	4.49E+08
Chromosome alignment-maintaining phosphoprotein 1	22.23	19.174	79385000
Protein Hook homolog 3	20.55	17.714	30128000
MKL/myocardin-like protein 2	18.03	14.878	1.75E+08
Caspase recruitment domain-containing protein 10	14.424	8.2974	20127000
Sorting nexin-24	13.014	12.087	70702000
Kaptin	12.457	12.186	1970600
Vimentin	9.9947	0.82889	21501000
WD repeat-containing protein 81	8.6322	7.8747	2.31E+08
Casein kinase I isoform delta;Casein kinase I isoform epsilon	8.3858	9.1038	24948000
Golgi to ER traffic protein 4 homolog	6.4193	5.0839	8878900
Serine/threonine-protein phosphatase PGAM5, mitochondrial	6.0125	5.4263	11461000
Protein kinase C delta-binding protein	5.7332	6.1264	11347000
Polymerase I and transcript release factor	5.0568	4.6991	2.75E+08
Enscosin	5.1877	4.7168	1.83E+08
14-3-3 protein epsilon	4.6799	3.9545	4202600
Eukaryotic translation initiation factor 3 subunit G	3.3471	2.4983	33105000
Eukaryotic translation initiation factor 3 subunit A	4.4038	3.1338	1.84E+08
Cdc42-interacting protein 4	4.304	6.0231	1838800
Protein AHNAK2	4.428	4.8068	7535000
Eukaryotic translation initiation factor 3 subunit F	3.8807	2.0589	5.16E+08
Eukaryotic translation initiation factor 3 subunit E	4.1363	2.9957	44763000
Eukaryotic translation initiation factor 4 gamma 1	3.8373	3.9398	18951000
Folate receptor alpha	3.0608	1.081	2124900
Protein PRRC2A	2.9079	1.3407	4453400
Heat shock protein HSP 90-beta;Heat shock protein HSP 90-alpha	2.4243	2.0459	71098000
Ras GTPase-activating protein-binding protein 1	2.4053	1.9283	55490000
Splicing factor 3B subunit 2	2.4275	1.8226	1.22E+08
14-3-3 protein gamma;14-3-3 protein gamma, N-terminally	2.4264	1.5604	6984700

processed			
KH domain-containing, RNA-binding, signal transduction-associated protein 1	2.2221	1.8512	2.44E+08
40S ribosomal protein S23	2.0208	1.8877	10013000
40S ribosomal protein S7	1.7059	2.0991	17445000
WD repeat-containing protein 74	1.7955	2.0678	2166800
Thioredoxin domain-containing protein 5	1.6088	2.0826	3370600
Splicing factor 1	0.79234	0.24126	13622000
AT-rich interactive domain-containing protein 1B	0.58853	0.44673	23419000
SWI/SNF-related matrix-associated actin-dependent regulator of chromatin subfamily D member 2	0.48098	0.2669	20733000
Splicing factor, proline- and glutamine-rich	0.49311	0.42382	3.42E+08
Ataxin-2-like protein	0.46694	0.41153	64951000
Papilin	0.47542	0.7436	1090200
SWI/SNF-related matrix-associated actin-dependent regulator of chromatin subfamily E member 1	0.4751	0.15018	35928000
Actin-like protein 6A	0.4508	0.34757	2.09E+08
SWI/SNF complex subunit SMARCC1	0.42836	0.35315	4.18E+08
	0.43158	0.3416	93521000
Probable E3 ubiquitin-protein ligase TRIM8	0.38469	0.55391	2399600
SWI/SNF-related matrix-associated actin-dependent regulator of chromatin subfamily D member 3	0.42096	0.35742	2990700
Procollagen-lysine,2-oxoglutarate 5-dioxygenase 1	0.36582	0.79711	1.29E+08
SWI/SNF-related matrix-associated actin-dependent regulator of chromatin subfamily D member 1	0.34622	0.31983	29717000
Zinc finger protein ubi-d4	0.37705	0.31967	39428000
AT-rich interactive domain-containing protein 1A	0.35243	0.2945	2.95E+08
Non-POU domain-containing octamer-binding protein	0.34508	0.38179	28852000
UPF0568 protein C14orf166	0.33596	0.27097	3.22E+08
Importin subunit alpha-5;Importin subunit alpha-5, N-terminally processed	0.34576	0.33344	9045700
Zinc finger CCCH-type antiviral protein 1-like	0.31897	0.27916	3480800
tRNA-splicing ligase RtcB homolog	0.33799	0.30934	1.07E+09
Zinc finger protein 281	0.33274	0.33379	6062900
Histone H1x	0.32187	0.37562	11593000
Complement C4-B;Complement C4 beta chain;Complement C4-B alpha chain;C4a anaphylatoxin;C4b-B;C4d-B;Complement C4 gamma chain;Complement C4-A;Complement C4 beta chain;Complement C4-A alpha chain;C4a anaphylatoxin;C4b-A;C4d-A;Complement C4 gamma chain	0.3228	0.080224	30854000
Serpin H1	0.33373	0.29562	66530000
SWI/SNF complex subunit SMARCC2	0.31387	0.27519	1.32E+08

Protein FAM98A	0.29419	0.25591	4.77E+08
Transcription activator BRG1	0.32642	0.42075	2.83E+08
Probable ATP-dependent RNA helicase DDX6	0.27552	0.29756	11533000
ATP-dependent RNA helicase DDX1	0.29419	0.33207	1.76E+08
Forkhead box protein C2	0.28056	2.1426	5992300
Ubiquitin-associated protein 2-like	0.28523	0.31064	1.76E+08
Desmocollin-1	0.2529	0.92236	1098300
Histone H4	0.21806	0.078712	1.73E+08
Probable ubiquitin carboxyl-terminal hydrolase FAF-X	0.22288	0.23526	1087000
Src substrate cortactin	0.19709	0.26742	25496000
ELM2 and SANT domain-containing protein 1	0.19583	0.25019	2068100
Calcium homeostasis endoplasmic reticulum protein	0.18111	0.43542	15743000
Ig kappa chain V-I region AU;Ig kappa chain V-I region WAT;Ig kappa chain V-I region WEA;Ig kappa chain V-I region Rei;Ig kappa chain V-I region Hau;Ig kappa chain V-I region Gal;Ig kappa chain V-I region AG	0.16845	0.051261	8925300
Transcriptional-regulating factor 1	0.17162	0.18689	12996000
Protein transport protein Sec31A	0.1462	0.18052	22473000
Splicing factor 1	0.13741	0.14124	1.17E+08
U2 snRNP-associated SURP motif-containing protein	0.13577	0.13634	6449800
Histone H3;Histone H3.3C;Histone H3.2;Histone H3.1t;Histone H3.3;Histone H3.1	0.12787	0.074214	11150000
ATP synthase subunit beta;ATP synthase subunit beta, mitochondrial	0.12138	0.15793	53129000
Pre-B-cell leukemia transcription factor 1	0.11436	0.060734	11634000
Sodium/potassium-transporting ATPase subunit alpha-3;Sodium/potassium-transporting ATPase subunit alpha-1	0.10117	0.086882	5528100
Paraspeckle component 1	0.090109	0.062993	29000000
YLP motif-containing protein 1	0.089836	0.05622	14598000
Ubiquitin-associated protein 2	0.079064	0.079346	1.79E+08
Endoplasmic reticulum resident protein 44	0.079624	0.077892	40366000
Ataxin-2	0.054502	0.063463	2.24E+08
Uncharacterized protein C17orf53	0.045783	0.046903	18599000
Serine/threonine-protein kinase greatwall	0.03171	0.22644	55368000
Ig gamma-1 chain C region;Ig gamma-2 chain C region;Ig gamma-4 chain C region;Ig gamma-3 chain C region	0.019022	0.020796	1.59E+08
Protocadherin gamma-C3	0.012336	0.005991	2.02E+08

Table 5.4 Potential candidate hRme-6 interactors sensitive to EGF stimulation identified from Mass Spectrometry following triple label mass spectrometry experiments. The protein hits were selected if the ratio of M/L or H/L was higher than 2 or lower than 0.5.

The data were also analyzed by comparing the protein intensities of the matched medium labeling peptides with heavy labeling peptides. These data would suggest that the protein hits interacted with hRme-6 but were also sensitive to the treatment with CK2 inhibitor TBCA during EGF stimulation. Figure 5.4 shows the distribution of protein ratio between medium labeling peptides with heavy labeling peptides. Here, the ratio was defined to be significant if the ratio was higher than 1.5 or lower than 0.5. Table 5.5 shows the protein hits which were sensitive to the CK2 inhibitor TBCA during EGF stimulation.

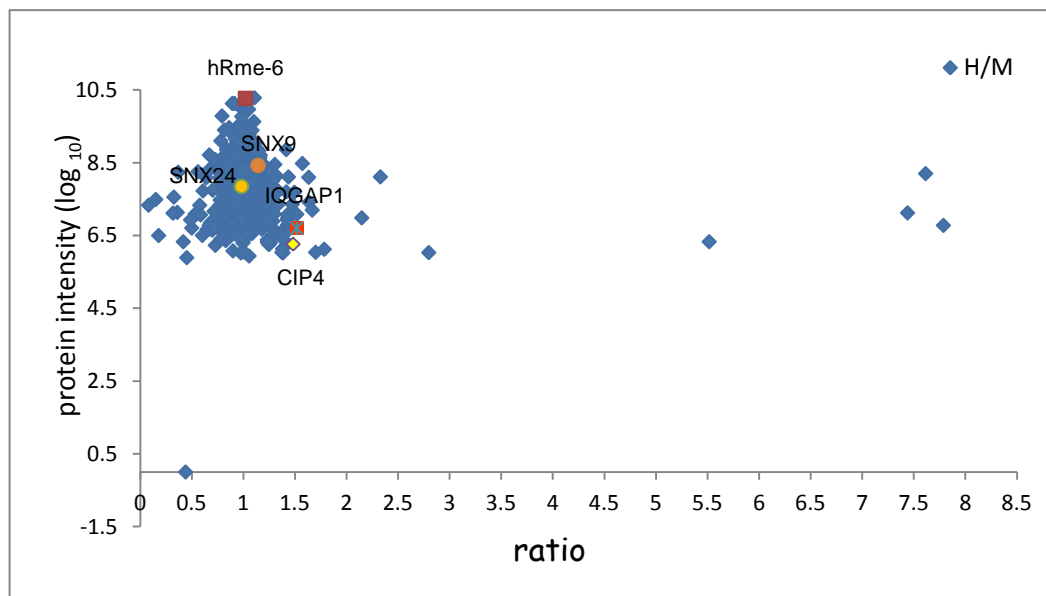


Figure 5.4 Protein ratio distribution of H/M following triple label SILAC experiment. The protein ratio was calculated by comparing the protein intensities of the matched medium labeling (M) peptides with heavy labeling (H) peptides. The red square indicates the ratio of hRme-6 comparing heavy labeling peptides with medium labeling peptides (H/M). The yellow diamond shows the H/M ratio of CIP4, the yellow circle shows the H/M ratio of SNX24, the brown circle shows the H/M ratio of SNX9 and the red star shows the H/M ratio of IQGAP1. The Y axis shows the logarithm of total protein intensity.

Protein names	Ratio H/M	Intensity
Forkhead box protein C2	7.7889	5992300
Serine/threonine-protein kinase greatwall	7.6159	55368000
Eukaryotic translation initiation factor 3 subunit K	5.5179	2128200
Sulfide:quinone oxidoreductase, mitochondrial	2.799	1070200
Procollagen-lysine,2-oxoglutarate 5-dioxygenase 1	2.3302	1.29E+08
Malectin	2.1494	9639800
Calcium homeostasis endoplasmic reticulum protein	1.6694	15743000
Small nuclear ribonucleoprotein-associated protein N;Small nuclear ribonucleoprotein-associated proteins B and B	1.6388	25993000
Putative elongation factor 1-alpha-like 3;Elongation factor 1-alpha 1;Elongation factor 1-alpha;Elongation factor 1-alpha 2	1.5739	3.01E+08
Protein IWS1 homolog	0.50108	5059200
Mitochondrial ribonuclease P protein 1	0.48988	8460600
Protein LSM14 homolog A	0.45298	775950
Protocadherin gamma-C3	0.44128	2.02E+08
Folate receptor alpha	0.41931	2124900
Histone H4	0.36977	1.73E+08
Splicing factor 1	0.36089	13622000
SWI/SNF-related matrix-associated actin-dependent regulator of chromatin subfamily E member 1	0.32791	35928000
Keratin, type I cytoskeletal 18	0.18021	3152700
Vimentin	0.082688	21501000

Table 5.5 Potential candidate interactors of hRme-6 that are sensitive to CK2 inhibition selected from mass spectrometry data. The protein hits were defined as the ratio of which was higher than 1.5 or lower than 0.5.

As shown in table 5.4 and table 5.5, the proteins that showed significant ratios, beside hRme-6, were mainly cytoskeletal as well as lots of proteins from the nucleus, ribosome or related to nucleus and ribosome in all three immunoprecipitations. There were not many proteins related to endocytosis or signal transduction on the list. Most of the known interaction partners of hRme-6, like AP2, Rab5, c-Cbl, were not identified by mass spectrometry. From the list of top hits I identified four candidates that were related to signalling or endocytosis: Cdc42 interacting protein (CIP4), Sorting nexin 9 (SNX9), sorting nexin 24 (SNX24) and IQGAP1. CIP4 is a previously identified binding partner of hRme6 and was found to interact with hRme-6 during

insulin stimulation (Lodhi et al). My data showed that CIP4 also interacted with hRme-6 in EGF stimulated HeLa cells. CK2 inhibitor treatment caused the interaction between hRme-6 and CIP4 decrease. The identification of CIP4 also indicated that the SILAC method to find the interaction partners of hRme-6 was effective. The sorting nexins are involved in trafficking and SNX9 is known to regulate the late stages of CCV budding. IQGAP1 acts as a scaffold in many signalling pathways including EGFR signalling [199, 201]. Additionally SNX24 and IQGAP1 had been identified as interaction partners for Rme-6 in the BioGrid database (<http://thebiogrid.org/117568/summary/homo-sapiens/gapvd1.html>) by immunoprecipitation of a tagged hRme-6 from in HEK293 cells.

There were also some other potential interaction proteins of hRme-6 in the list, like 14-3-3 proteins, Sec16A, Galectin-1, Opsin-5, Large proline-rich protein BAG6. But due to the time limit and their more defined roles in endocytosis or signalling, I mainly focused on the relationship of hRme-6 with CIP4, SNX24, SNX9 and IQGAP1.

5.4 Verification of mass spectrometry ‘hits’ by in vitro binding assays

In order to verify these ‘hits’ and to investigate the relationships of the candidates with hRme-6, I set up in vitro binding assays. Plasmids that contained the cDNA for the potential interaction partners were purchased from Addgene. The plasmids were transfected into *E.coli* BL21 (DE3) competent cell strain for protein expression. The corresponding proteins were purified and direct interaction tests between Flag-hRme-6 purified from HEK293 cells and selected candidates were investigated.

5.4.1 Interaction test between hRme-6 and SNX24

Flag-hRme-6 was purified from HEK293 cells, overexpressing Flag-hRme-6, by Flag M2 affinity gel (Figure 4.17A). SNX24 protein was expressed in *E.coli* BL21 (DE3) as described in Materials and Methods. The fusion protein was purified by Ni-NTA agarose beads. As shown below, the concentrations of the purified His-SNX24 were very high and the purity was suitable for an interaction test.

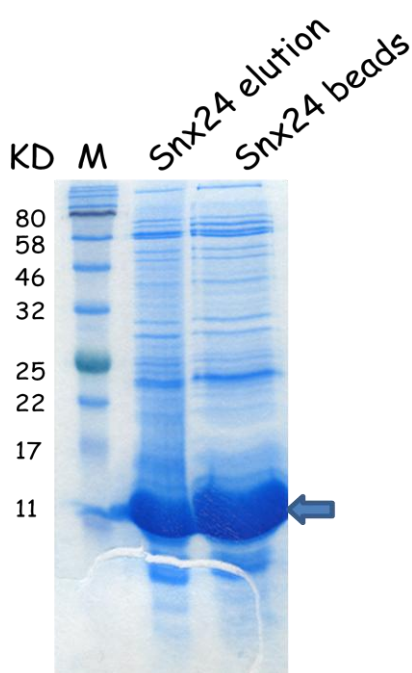
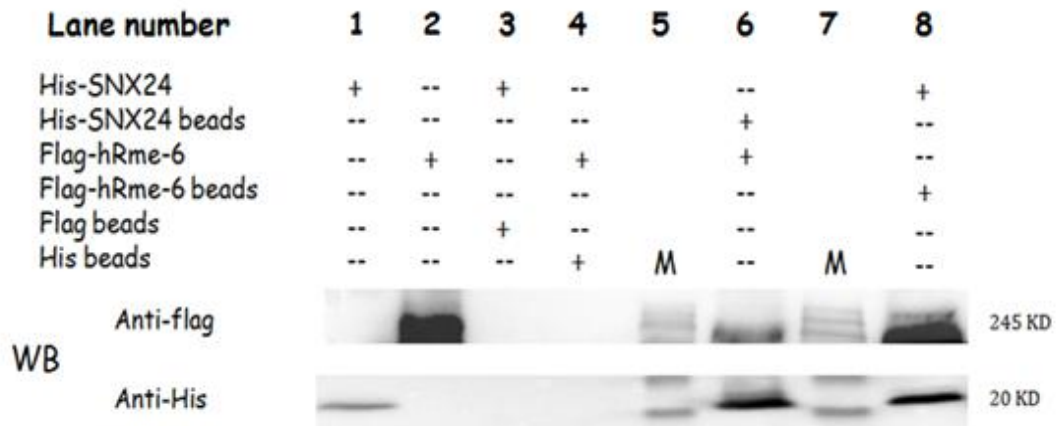


Figure 5.5 Purification of His- SNX24 from *E.coli*. pNIC28-Bsa4s-SNX24A-c003 plasmids were transfected into BL21 (DE3) competent cell strain. Bacterial cell lysates were prepared as described in material and methods and incubated with Ni-NTA agarose beads at 4°C for 1 hour. The beads were washed three times with cold TBS containing 25 mM imidazole. His-SNX24 was eluted by 250 mM imidazole. Eluted proteins were analyzed by SDS-PAGE and stained with coomassie blue. The arrow shows the purified His-SNX24.

His-SNX24 conjugated to Ni-NTA agarose beads was incubated with Flag-hRme-6 that was purified from HEK293 cells. Conversely, Flag-hRme-6 conjugated to Flag M2 affinity beads was incubated with His-SNX24 purified from bacteria. The beads from each experiment were then tested by both anti-hRme-6 antibody and anti-His antibody. As shown below, Flag-hRme-6 conjugated to Flag M2 affinity gel bound a significant amount of His-SNX24, indicating a good interaction. At the same time a weak band of 230 KD corresponding to hRme-6 was detected on His-SNX24 conjugated Ni-NTA agarose beads. However, there was a much stronger band around 150 KD at the same lane, which also was present in the Flag-hRme-6 lane. This lower molecular weight species was occasionally observed following SDS-PAGE of hRme-6. It is possible that His-SNX24 binds better to a disassembled form of Rme-6 but further experiments would be required to verify this.

A



B



Figure 5.6 His-SNX24 and Flag-hRme-6 interact directly in vitro. A, Flag-hRme-6 purified from HEK293 cells was isolated on Flag beads and incubated with His-SNX24 (lane 6). SNX24 conjugated to Ni-NTA agarose beads was incubated with Flag-hRme-6 that was purified from HEK293 cells (lane 8). At the same time Flag M2 beads were also incubated with His-SNX24 (lane 3) and His beads without protein were also incubated with Flag-hRme-6 (lane 4) as control experiments. The beads were then washed with cold TBS and analyzed by immunoblotting. M, marker. B, over-exposure of lane 5-8. The arrow showed the size of hRme-6. M, marker. Results are representative of one of three experiments. Note the blots were cropped to probe for anti-flag antibody in the same blot .

5.4.2 Interaction test between hRme-6 and SNX9

Flag-hRme-6 was purified from HEK293 cells, overexpressing Flag-hRme-6, by Flag

M2 affinity gel as Figure 4.17A. SNX9 protein was expressed in *E.coli* BL21 (DE3) as described in Materials and Methods. The fusion protein was purified by Ni-NTA agarose beads. As shown below, the concentrations of the purified His-SNX9 were very high and the purity was suitable for an interaction test.

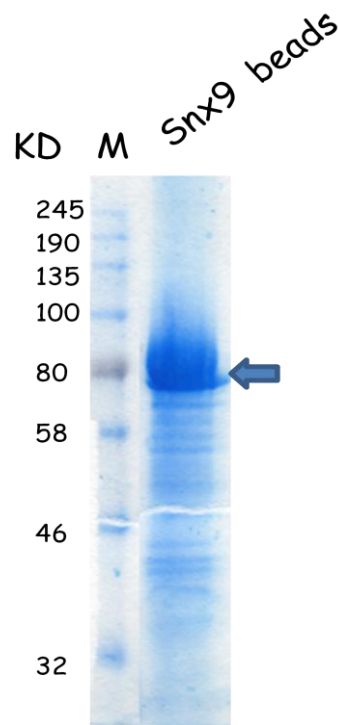


Figure 5.7 Purification of His- SNX9 from *E.coli*. 6XHis-SNX9 pET15b plasmids were transfected into BL21 (DE3) competent cell. Bacterial cell lysates were prepared as described in material and methods and incubated with Ni-NTA agarose beads at 4°C for 1 hour. The beads were washed three times with cold TBS containing 25 mM imidazole. His tag proteins were further eluted by 250 mM imidazole. Eluted proteins were analyzed by SDS-PAGE and stained with coomassie blue. The arrow showed the location of SNX9.

His-SNX9 conjugated to Ni-NTA agarose beads was incubated with Flag-hRme-6 that was purified from HEK293 cells. Conversely, Flag-hRme-6 conjugated to Flag M2 affinity gel was incubated with His-SNX24 purified from bacteria. The beads from each experiment were then immunoblotted with both anti-hRme-6 antibody and anti-His

antibody. As shown below, Flag-hRme-6 conjugated to Flag M2 affinity gel bound a significant amount of His-SNX9. A clear band of 230 KD corresponding to hRme-6 was detected in His-SNX9 conjugated to Ni-NTA agarose beads. This assay indicated a good, direct interaction between the two proteins in vitro.

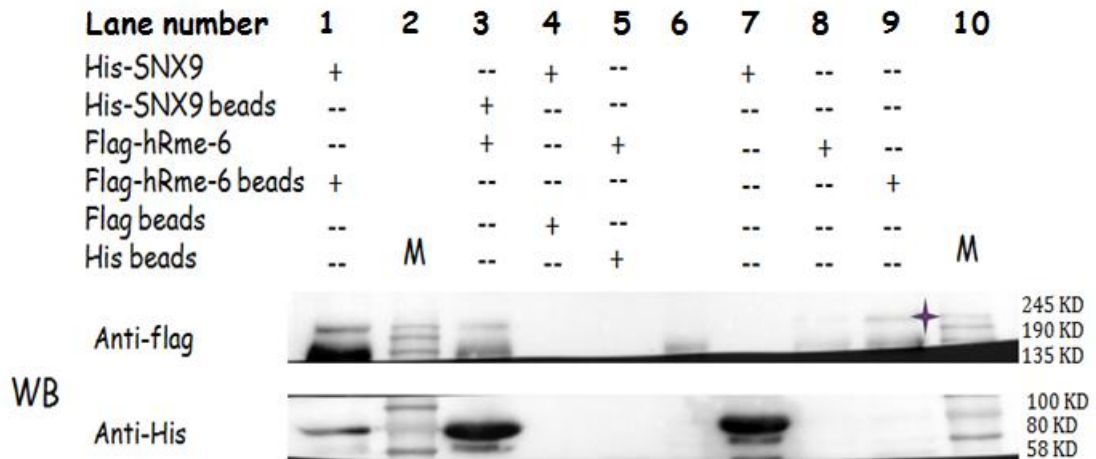


Figure 5.8 His-SNX9 and Flag-hRme-6 directly interact in vitro. Flag-hRme-6 purified from HEK293 cells was isolated on Flag beads and incubated with His-SNX9 (lane 1). SNX9 conjugated to Ni-NTA agarose beads was incubated with Flag-hRme-6 purified from HEK293 cells (lane 3). At the same time Flag M2 beads were also incubated with His-SNX9 (lane 4) and His beads without protein were also incubated with Flag-hRme-6 (lane 5) as control experiments. The beads were then washed with cold TBS and analyzed by immunoblotting. The asterisk showed the band of hRme-6. M, marker. Results are representative of one of three experiments.

5.4.3 Interaction test between hRme-6 and IQGAP1

Flag-hRme-6 was purified from HEK293 cells, overexpressing Flag-hRme-6, by Flag M2 affinity gel (Figure 4.17A). GST and GST-IQGAP1 protein were expressed in *E.coli* BL21 (DE3) as described in Materials and Methods. The fusion proteins were purified by GST agarose beads. As shown below, the purified GST protein was very clean. However, the purified GST-IQGAP1 on GSH beads contained many other contaminating proteins. The eluted protein also contained the same contaminants. However there was still clearly detectable GST-IQGAP1 associated with the beads and in the elution sample. So the interaction test between hRme-6 and IQGAP1 was still

set up.

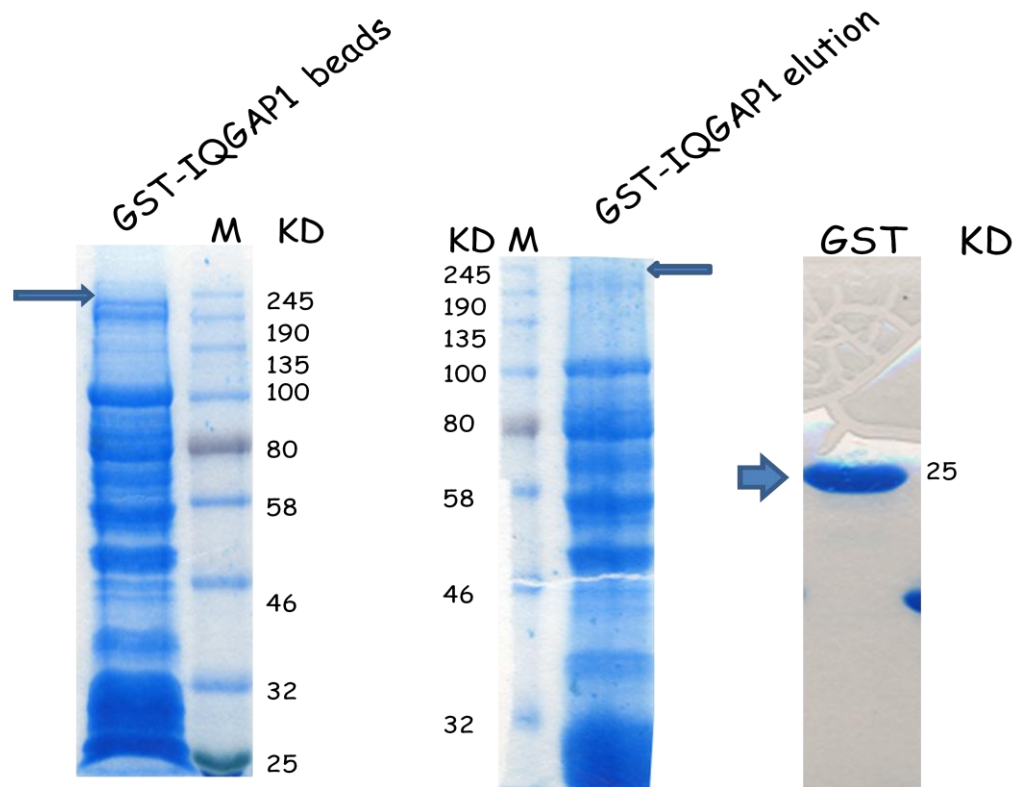


Figure 5.9 Purification of GST and GST-IQGAP1 from *E. coli*. pGEX-GST and pGEX-2T-IQGAP1 plasmids were transfected into BL21 (DE3) competent cell strain. Bacterial cell lysates were prepared as described in material and methods and incubated with GST agarose beads at 4°C for 1 hour. The beads were washed three times and further eluted by 10 mM Glutathione. Eluted proteins were analyzed by SDS-PAGE and stained with coomassie blue. The arrow shows the location of the purified GST and GST-IQGAP1.

GST and GST-IQGAP1 conjugated to GST agarose beads were incubated with purified Flag-hRme-6 and the beads were then subjected to Western blotting. Figure 5.10 indicates that only beads with GST-IQGAP1 could capture Flag-Rme-6 (Lanes 3 and 4). In the converse experiment, Flag-hRme-6 conjugated to Flag M2 affinity gel was incubated with soluble GST or GST-IQGAP1. The beads from each experiment were then tested by Western blot using anti-GST antibodies. Beads with Flag-Rme-6 captured GST-IQGAP1 although they also captured a small amount of GST as well (Lanes 1 and 2) which calls into question the specificity of the interaction with

GST-IQGAP1. A further caveat of this experiment is that the preparation of GST-IQGAP1 contained many bands that cross-reacted with anti-GST antibodies. These may have been degradation products or premature translation products arising from bacterial expression of such a large protein (~150kDa). Future confirmation of this in vitro experiment would require incubation of GST and GST-IQGAP1 with FLAG beads without Rme-6 and also the expression of IQGAP1 in a system that yielded a more homogenous preparation of protein.

Over all, this experiment suggested that hRme-6 and IQGAP1 may interact with each other, however, the high numbers of contaminants in the sample and lack of controls make it difficult to draw a confirm conclusion from this experiment.

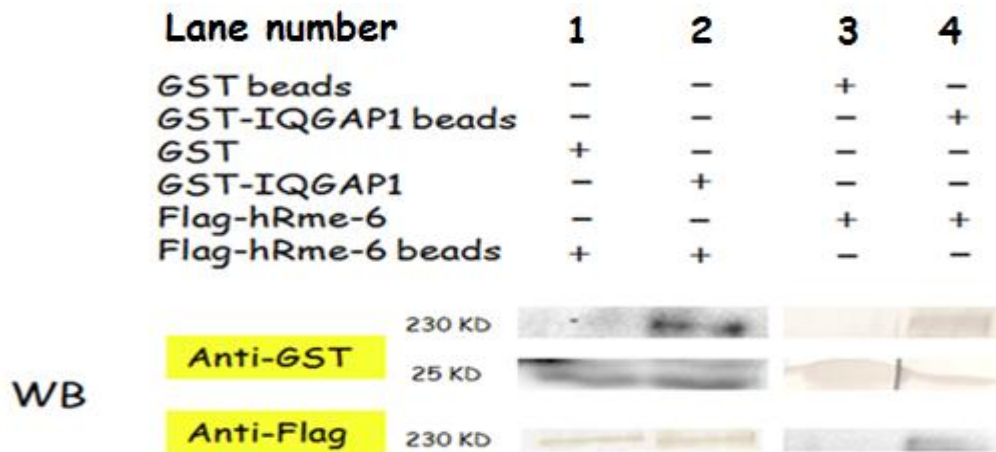


Figure 5.10 GST-IQGAP1 and Flag-hRme-6 interact in vitro. Flag-hRme-6 purified from HEK293 cells was isolated on Flag beads and incubated with GST-IQGAP1 (lane 2) and GST (lane 1). GST and GST-IQGAP1 conjugated to GST agarose beads were incubated with Flag-hRme-6 respectively. The beads were then washed with cold TBS and analyzed by immunoblotting. The bands of Flag-hRme-6 beads and GST beads and GST-IQGAP1 beads directly scanned from the membrane without exposure. Results are representative of two experiments.

5.5 Validation of the mass spectrometry ‘hits’ in cells

My previous experiments tested the interactions between hRme-6 and SNX24, SNX9 and IQGAP1 using purified proteins in vitro. The four candidates that were identified by the SILAC experiments were based on EGF stimulated HeLa cells. CIP4 and SNX24 were even both sensitive to EGF stimulation. I wanted to test the interactions in cells and particularly following EGF stimulation.

As the first step I wanted to see whether hRme-6 or any of its interacting partners could be co-localized on membranes of the endo-lysosomal system following EGF stimulation by immunofluorescence. To test the co-localisation of hRme-6 with other candidates, mcherry-CIP4 and mcherry-SNX9 plasmids were transfected into HeLa cells. The co-localisation of endogenous hRme-6 with SNX9, CIP4 was examined by confocal microscopy. As shown in Figure 5.11, cells that were transfected with mCherryCIP4 and mCherry SNX9 showed diffuse cytoplasmic labeling as the same of hRme-6. Following EGF stimulation there was no obvious recruitment of these proteins to the membranes. It is possible that if a small population was recruited to membranes that it was masked by the high levels of cytoplasmic staining.

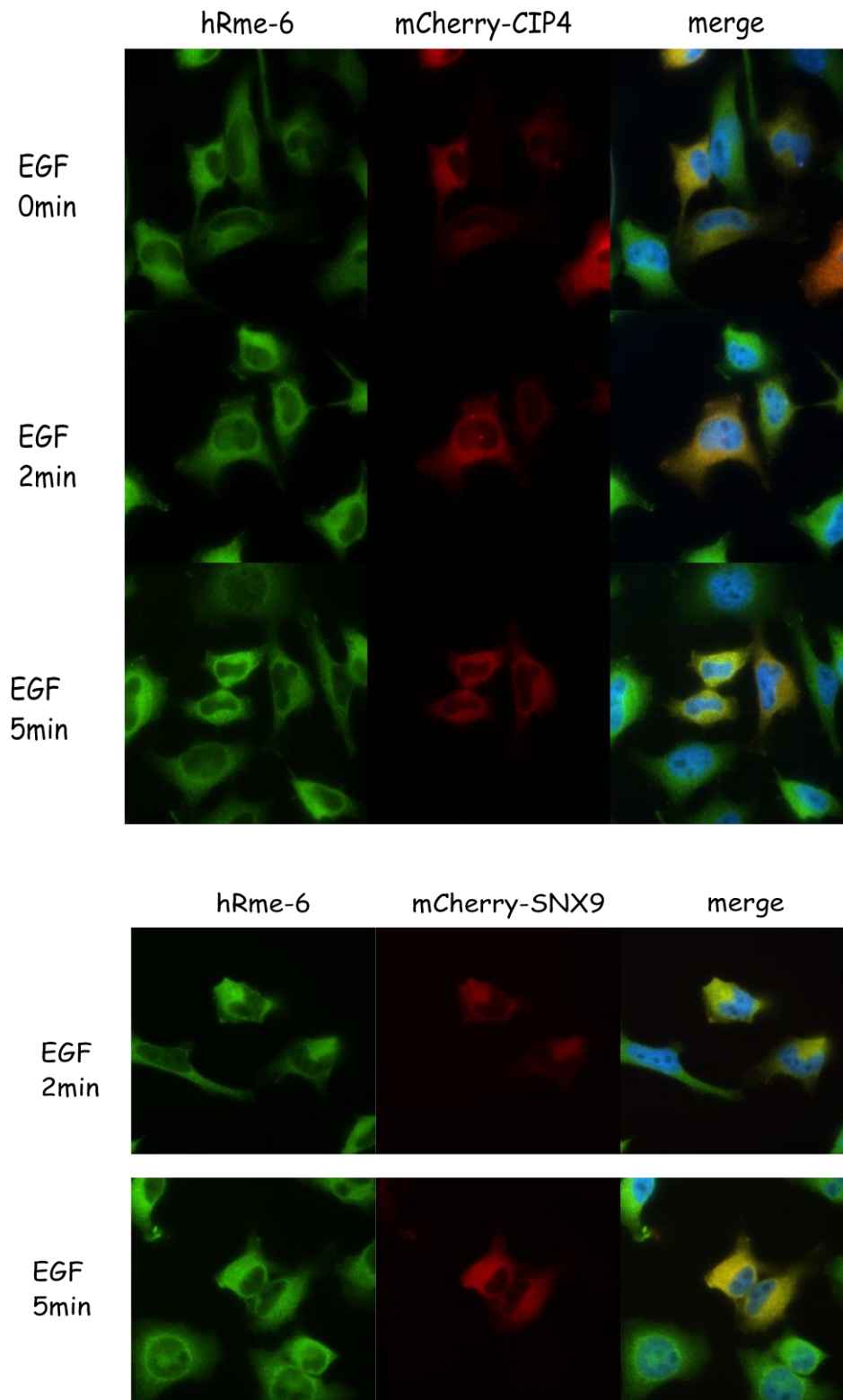


Figure 5.11 Immunofluorescence shows that SNX9, CIP4 and hRme-6 were largely cytoplasmic following overexpression. HeLa cells were transfected with mCherry-CIP4 or mCherry-SNX9 as indicated. Cells were serum starved for 24 hr and then stimulated with 50 ng/ml EGF at different time points. The cells were then fixed with 4%

paraformaldehyde, permeabilized with 0.2% Triton X-100, and stained with anti-hRme-6, followed by Alexa Fluor 488 conjugated secondary antibody and analyzed by confocal microscopy. Results were repeated three times.

5.6 Proximity ligation assay to validate hRme-6 interactions in cells.

Proximity ligation assay (PLA assay) is a powerful technology to detect single protein events such as protein protein interactions and modifications in tissue and cell samples. It can directly detect endogenous protein interactions within a 40 nm range. Our hypothesis was that Rme-6 might interact with different proteins depending on the cargo that was being internalised. To test the interactions of hRme-6 with the different candidates, the internalisation of transferrin and EGF in HeLa cells was used as a model.

To establish the PLA assay, it was important to carry out controls for specificity. One set of controls is set up based on one of the primary antibodies or secondary antibodies used in subsequent experiments. As shown in Figure 5.12, this resulted in little or no signal for all of the antibodies tested.

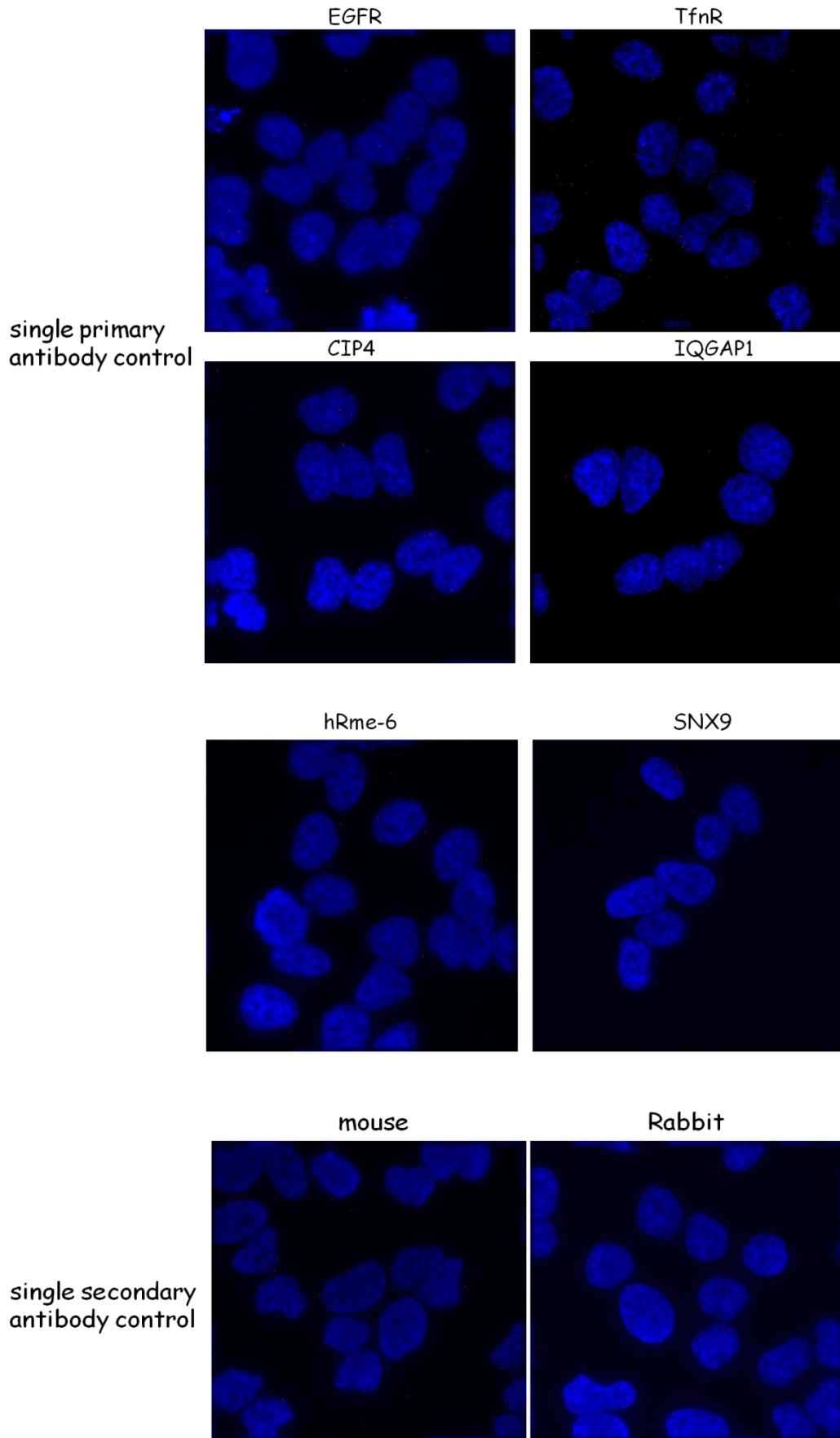


Figure 5.12 PLA assay primary antibody control test. HeLa cells were serum starved for 24 hours and then stimulated with 50 ng/ml EGF for 5 minutes. The cells were then fixed with 4% paraformaldehyde, permeabilized with 0.2% Triton X-100, and stained with only one primary antibody or one secondary antibody as indicated above, followed by Duolink® In Situ Red Starter Kit and analyzed by confocal microscopy. Results were repeated three times.

5.6.1 PLA assay between hRme-6 and SNX9

HeLa cells were seeded on coverslip for 20 hours and then serum starved for 24 hr. The cells were then incubated with 50 ng/ml EGF or 15 µg/ml Tfn. The cells were fixed, processed using Duolink® In Situ Red Starter Kit Mouse/Rabbit according to the manufacturer's instructions. The endogenous hRme-6 and SNX9 interaction was revealed. As shown below, the signal between SNX9 and hRme-6 from PLA assay was very weak during both EGF and Tfn incubation. The signal was nearly the same as the background and did not change during the different cargo stimulations. This contrasted with the strong in vitro interaction between these two proteins. It may be that EGF stimulation or Tfn incubation are not the best cargoes with which to analyze the interaction between SNX9 and hRme-6. The weak interaction was more in line with the SILAC data which also suggested a weak interaction between the two proteins.

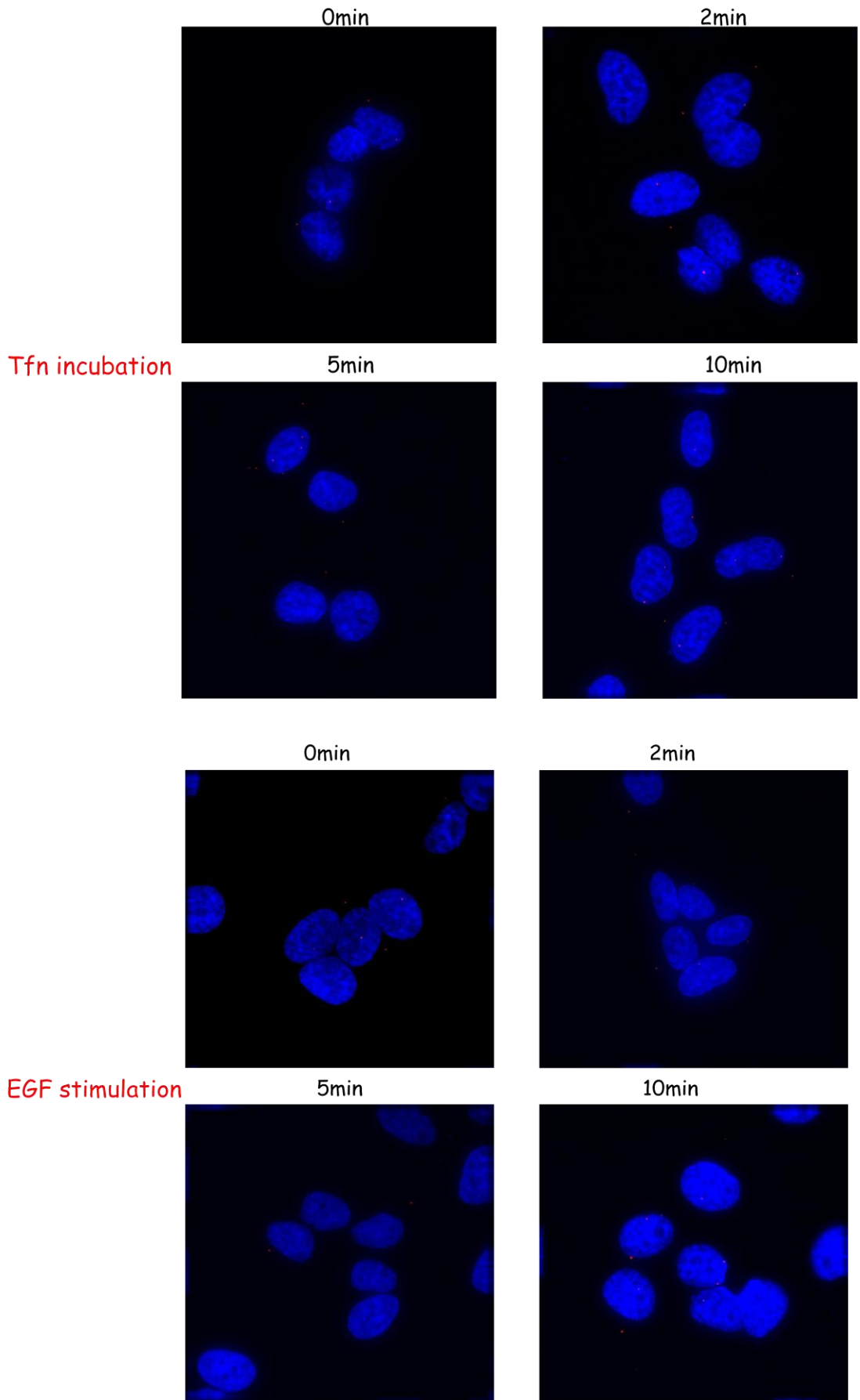


Figure 5.13 PLA assay to test an in vivo interaction between hRme-6 and SNX9. HeLa cells were serum starved for 24 hours and then incubated with 15 µg/ml Tfn or stimulated with 50 ng/ml EGF at different time points. The cells were then fixed with 4% paraformaldehyde, permeabilized with 0.2% Triton X-100, and stained with anti-hRme-6 and anti-snx9 antibody, followed by Duolink® In Situ Red Starter Kit and analyzed by confocal microscopy. Results were repeated three times.

5.6.2 PLA assay between hRme-6 and CIP4

To test the interaction between hRme-6 and CIP4, a PLA assay was carried out as above. As shown in Figure 5.14, the PLA signal between hRme-6 and CIP4 was very strong. However, the PLA signal in the case of both EGF stimulation and Tfn incubation were unstable, which made it difficult to distinguish a clear trend of the signal.

It is also notable that without cargo stimulation, there were also clear interaction signals. It implied that the interaction between hRme-6 and CIP4 was very robust. Later I found that in purified hRme-6 from HEK293 cells there was CIP4 associated with hRme-6 constantly (data not shown).

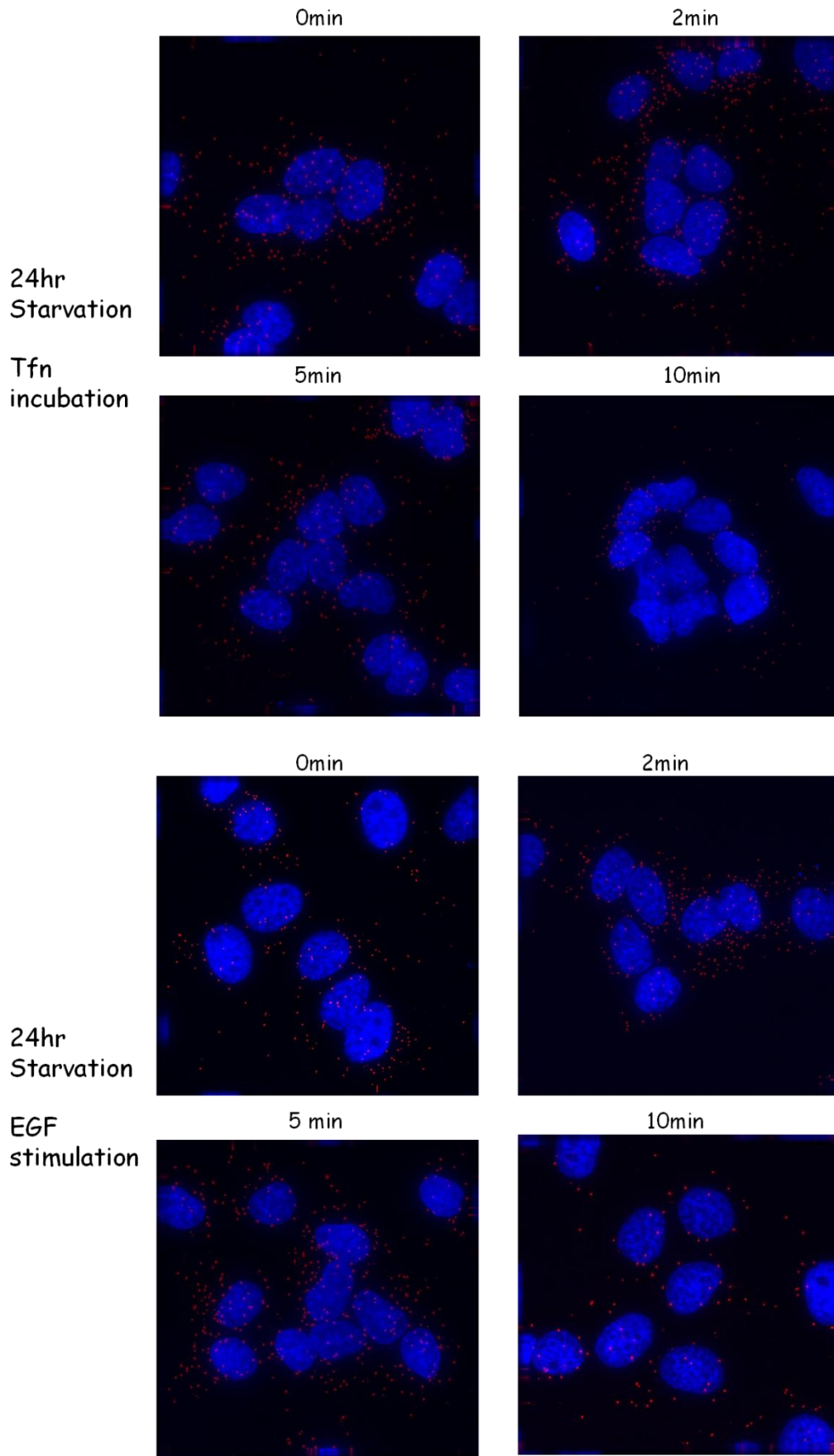


Figure 5.14 PLA assay tested the *in vivo* interaction between hRme-6 and CIP4 in Tfn incubation and EGF stimulation. HeLa cells were serum starved for 24 hours and then incubated with 15 µg/ml Tfn or stimulated with 50 ng/ml EGF at different time points. The cells were then fixed with 4% paraformaldehyde, permeabilized with 0.2% Triton X-100, and stained with anti-hRme-6 and anti-CIP4 antibody, followed by Duolink® In Situ Red Starter Kit and analyzed by confocal microscopy.

5.6.3 PLA assay between hRme-6 and IQGAP1

A PLA assay to test the interaction between endogenous hRme-6 and IQGAP1 was performed as described in the previous section. As shown below, after serum starvation, incubation with either transferrin or EGF resulted in an increased PLA signal. The increase in the presence of transferrin may reflect the longer serum starvation (see section 5.6.4). However, in the presence of EGF there was a transient two-fold increase in the association of IQGAP1 with hRme-6. These results suggested that the interaction between IQGAP1 and hRme-6 was different depending on different cargos.

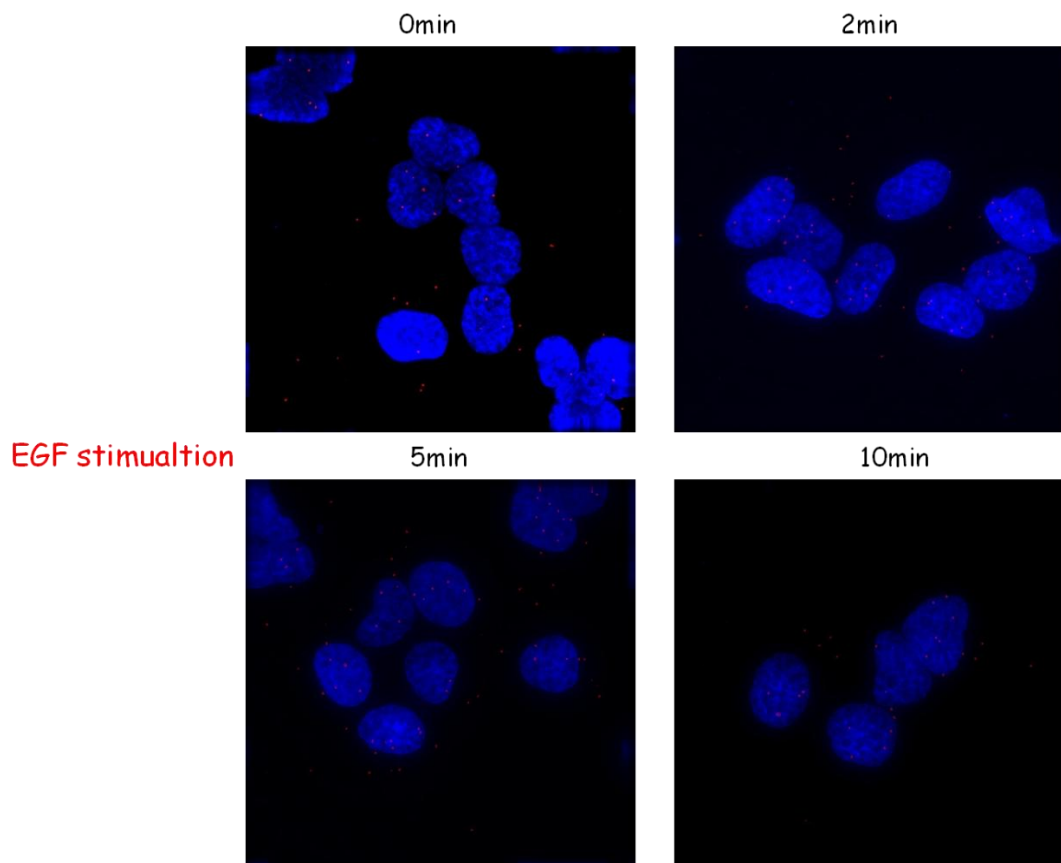
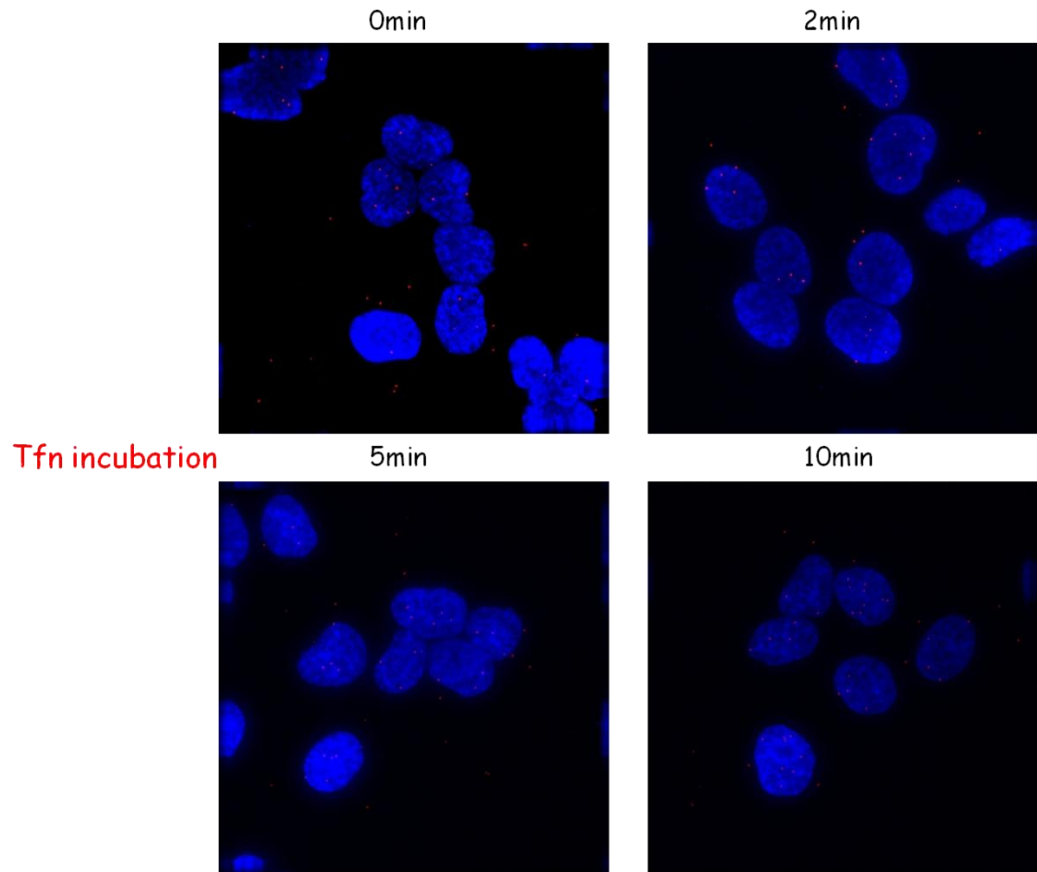


Figure 5.15 PLA assay test of the in vivo interaction between hRme-6 and IQGAP1 following Tfn incubation and EGF stimulation. HeLa cells were serum starved for 24 hours and then incubated with 15 µg/ml Tfn or stimulated with 50 ng/ml EGF at different time points. The cells were then fixed with 4% paraformaldehyde, permeabilized with 0.2% Triton X-100, and stained with anti-hRme-6 and anti-IQGAP1 antibody, followed by Duolink® In Situ Red Starter Kit and analyzed by confocal microscopy.

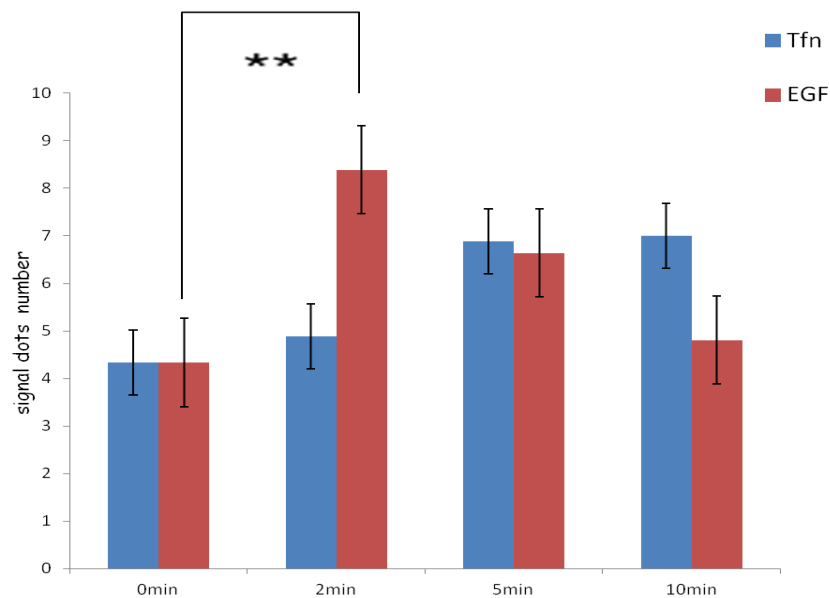


Figure 5.16 Quantification of the PLA assay signal between hRme-6 and IQGAP1 in Tfn incubation and EGF stimulation. Quantification of the interaction dots by Image J in the indicated time point. Results are the means of at least 37 cells. The error bars indicated the Standard Error. Values are significantly different at $P < 0.01$ (**).

5.6.4 PLA assay to test the interaction between cargo receptors and hRme-6.

As PLA assay is based on protein distance and antibody, it can detect protein interactions within 40 nm. It is possible to test the weak interactions between two proteins if the proteins are sufficiently close. The difference in the interactions between hRme-6 and IQGAP1 during Tfn and EGF stimulation led me to explore

whether I could detect interactions of hRme-6 with the cargo receptors. Since hRme-6 was reported to be involved in the internalisation of Tfn and EGFR, I wanted to see whether PLA could be used to determine an interaction between Rme-6 and either TfnR or EGFR.

A Tfn receptor (TfnR) antibody (B3/25) that recognises the ectodomain of the TfnR was used to check the co-localisation between hRme-6 and TfnR. As shown below, there were generally strong interaction signals between hRme-6 and TfnR. It is an indication of the distances over which PLA can generate a signal that there is detectable interaction between an antibody bound to the ectodomain of TfnR and antibody to hRme-6 which would be located on the cytoplasmic face of the vesicle.

But it was very interesting that the interaction between hRme-6 and TfnR was affected by starvation. Figure 5.17 and 5.18 showed that 30 minutes starvation did not change the interaction between hRme-6 and TfnR and the interaction signal was nearly the same during addition of ligand. However, 24 hours starvation significantly changed the mode of the interaction between TfnR and hRme-6. The initial interaction signal was 30% lower compared to that at 30 minutes starvation. The interaction between hRme-6 and TfnR quickly doubled at 2 minutes compared to that at 0 minutes. The interaction signal was approximately the same as that at 30 minutes starvation. However, after 10 minutes the degree of interaction returned to the same as the starting point. This is surprising as TfnR has been shown to be constitutively internalised regardless of the presence of ligand (Watts, 1980). Hence if hRme-6 is involved in transferrin uptake, the results after 30 minute serum starvation are consistent with what we might expect as the association of TfnR with hRme-6 is relatively constant and is unchanged by ligand. The results after 24 hours serum starvation suggest that long times of serum starvation may disrupt normal endocytic trafficking.

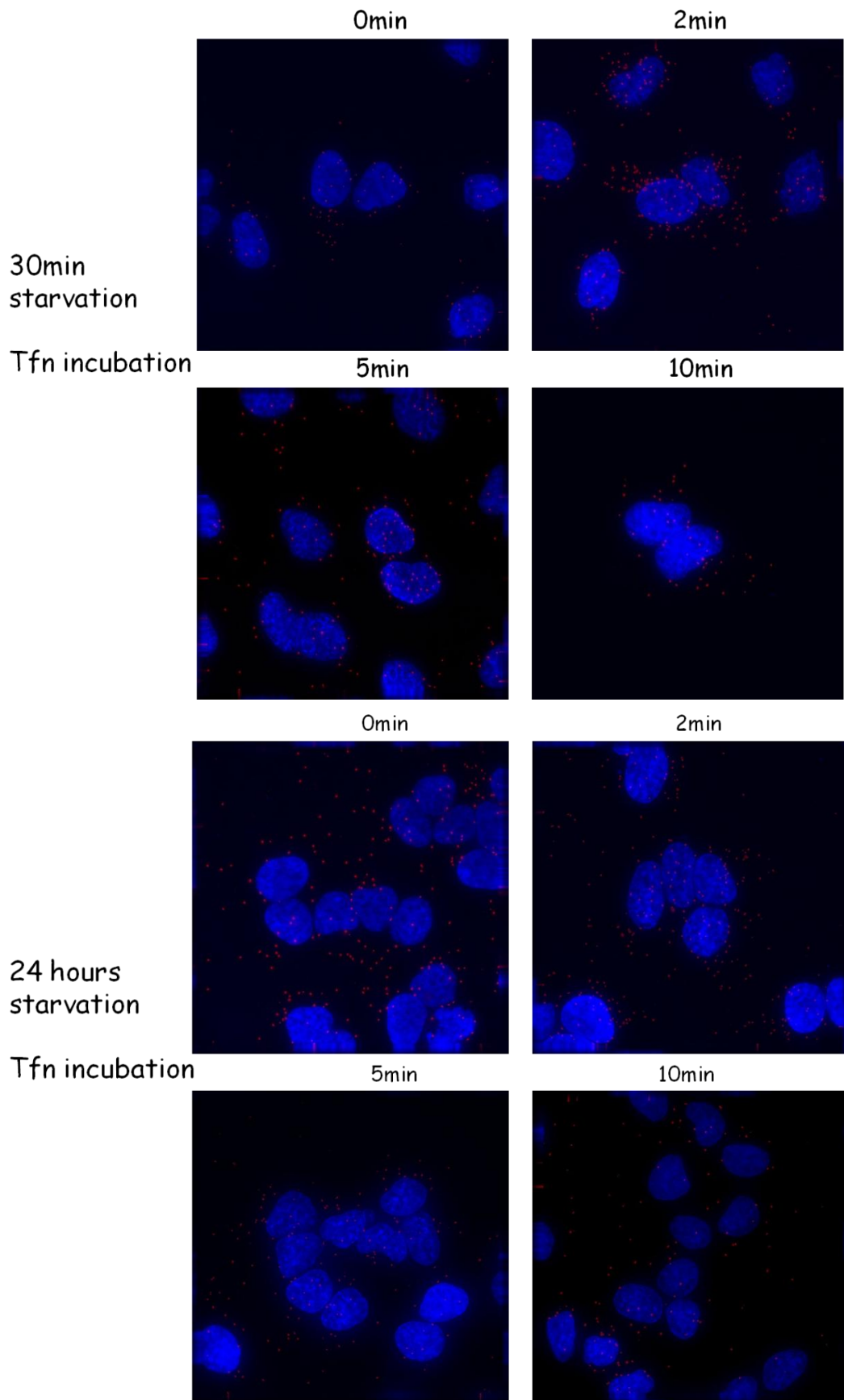


Figure 5.17 PLA assay tested the in vivo interaction between hRme-6 and TfnR following different times of serum starvation during uptake of Tfn. HeLa cells were serum starved for 30 minutes or 24 hours and then incubated with 15 µg/ml Tfn for different time points. The cells were then fixed with 4% paraformaldehyde, permeabilized with 0.2% Triton X-100, and stained with anti-hRme-6 and anti-TfnR antibody, followed by Duolink® In Situ Red Starter Kit and analyzed by confocal microscopy.

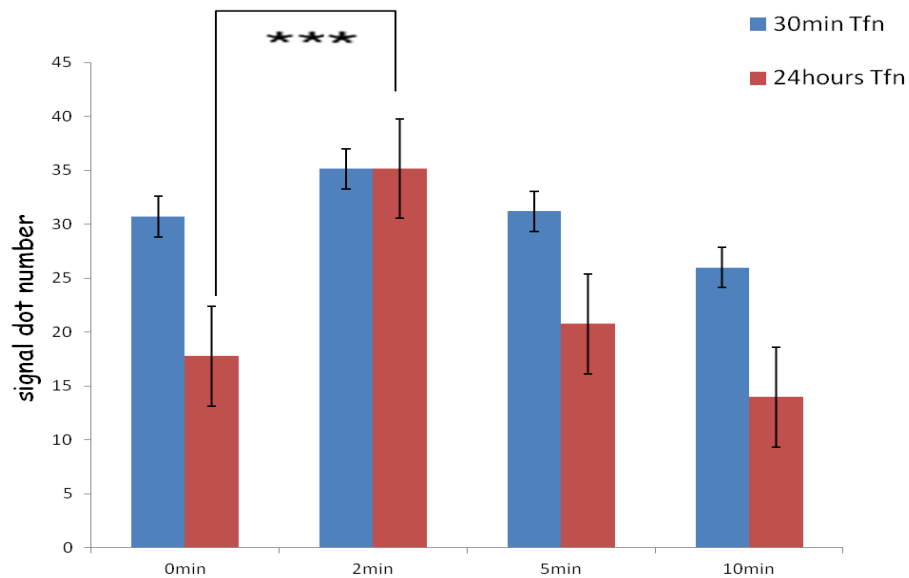


Figure 5.18 Quantification of the PLA assay signal between hRme-6 and TfnR in Tfn incubation. Quantification of the interaction dots by Image J in the indicated time point. Results are the means of at least 34 cells. The error bars indicated the Standard Error. Values are significantly different at $P < 0.01$ (**).

I also measured the interaction between EGFR and hRme-6 (Figure 5.19). Before EGF stimulation, HeLa cells were starved for 24 hours to totally remove the cell surface EGF. The signal dot number between EGFR and hRme-6 was generally less than that between TfnR and hRme-6. There are approximately 1 million of Tfn receptors but only 35,000 EGF receptors per HeLa cells [147, 219]. The lower signal dot number could be because of the different receptor numbers. However, according to the signal measured by PLA, even though there were fewer dots detected between

EGFR and hRme-6, the signal density of EGFR-hRme-6 was actually higher than TfnR-hRme-6. It also could be possible that long time serum starvation changed both TfnR and EGFR sensitivities, which led less hRme-6 interacted with EGFR.

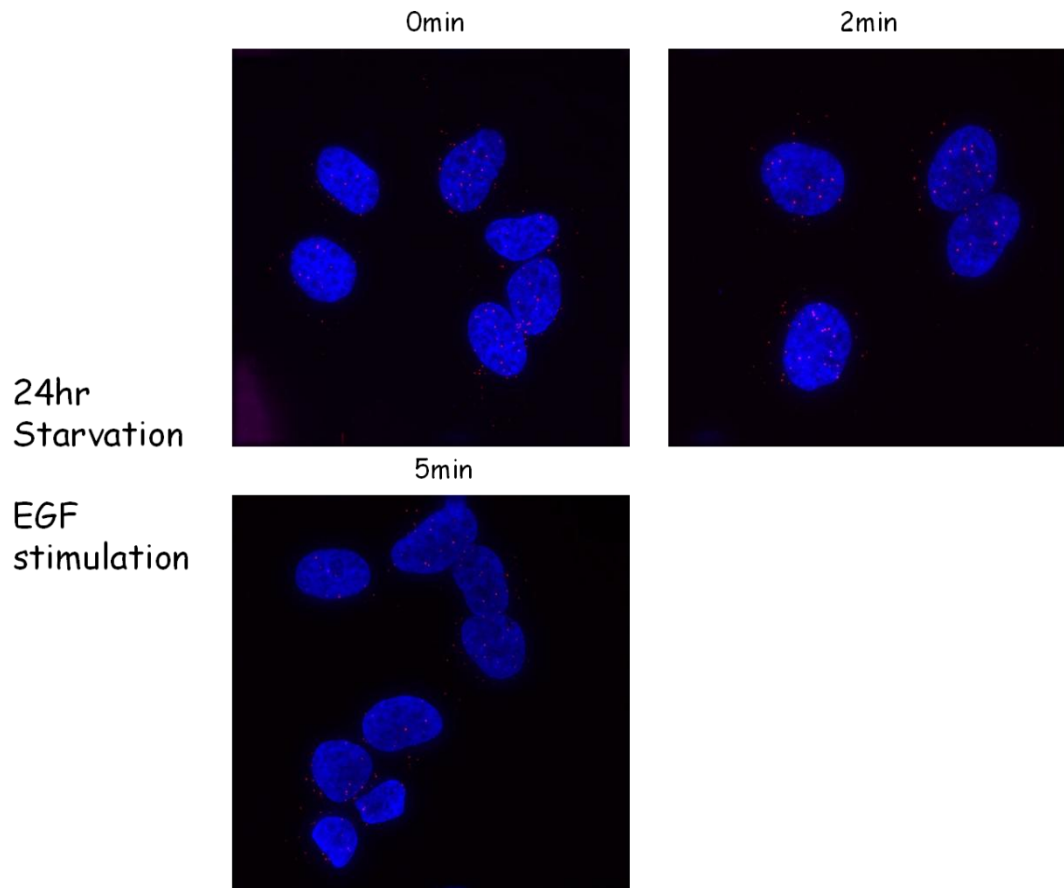


Figure 5.19 PLA assay tested the *in vivo* interaction between hRme-6 and EGFR. HeLa cells were serum starved for 24 hours and then stimulated with 50 ng/ml EGF for different time points. The cells were then fixed with 4% paraformaldehyde, permeabilized with 0.2% Triton X-100, and stained with anti-hRme-6 and anti-EGFR antibody, followed by Duolink® In Situ Red Starter Kit and analyzed by confocal microscopy.

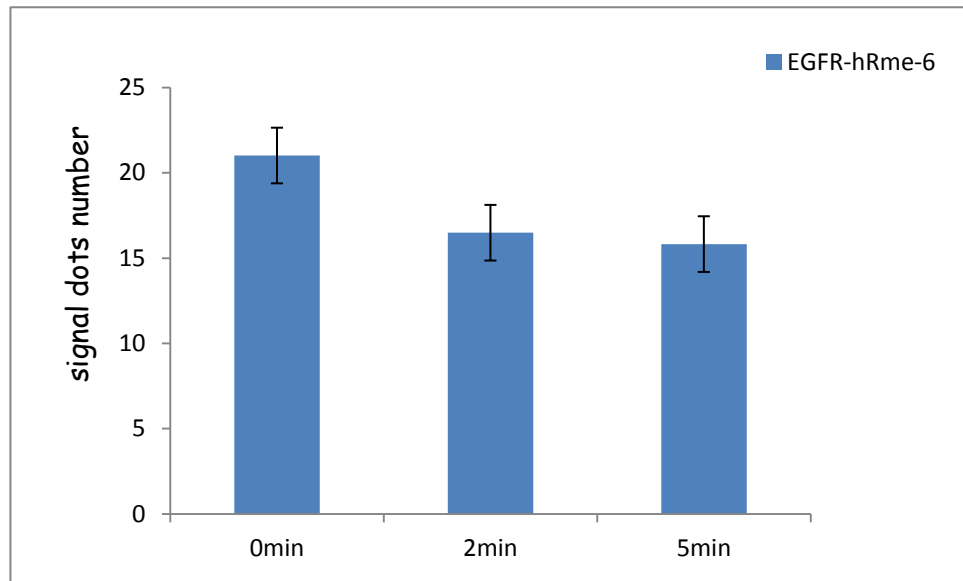


Figure 5.20 Quantification of the PLA assay signal between hRme-6 and EGFR in EGF stimulated HeLa cells. Quantification of the interaction dots by Image J in the indicated time point. Results are the means of at least 29 cells. The error bars indicated the Standard Error. Values are not significantly different at $P > 0.5$.

5.6.5 The interaction between CIP4 and EGFR is enhanced following overexpression of Flag-hRme-6.

As a test for the specificity of the interaction between Rme-6 and its binding partners, HeLa cells overexpressing Flag-hRme-6 were analyzed with anti-CIP4 and anti-EGFR antibodies in the PLA assay. Following the PLA assay, cells were incubated with Alexa Fluor 488 conjugated secondary antibody to highlight the cells overexpressing Flag-hRme-6. As shown below, in cells that overexpress hRme-6, Flag-hRme-6 shows significantly increased interaction with EGFR and CIP4. The strong co-localisation did not change in presence of different time EGF stimulation (data not shown). The conclusions from this experiment could be further strengthened by using siRNA to ablate Rme-6 and demonstrating that the interactions with the cargo and binding partners are no longer evident. And there is slightly lack overexpression of unrelated flag-tagged protein to confirm that the signal specificity between

Flag-hRme-6 and CIP4, EGFR. None-the-less, these data still gave some support for the interaction between endogenous hRme-6 and CIP4 and EGFR.

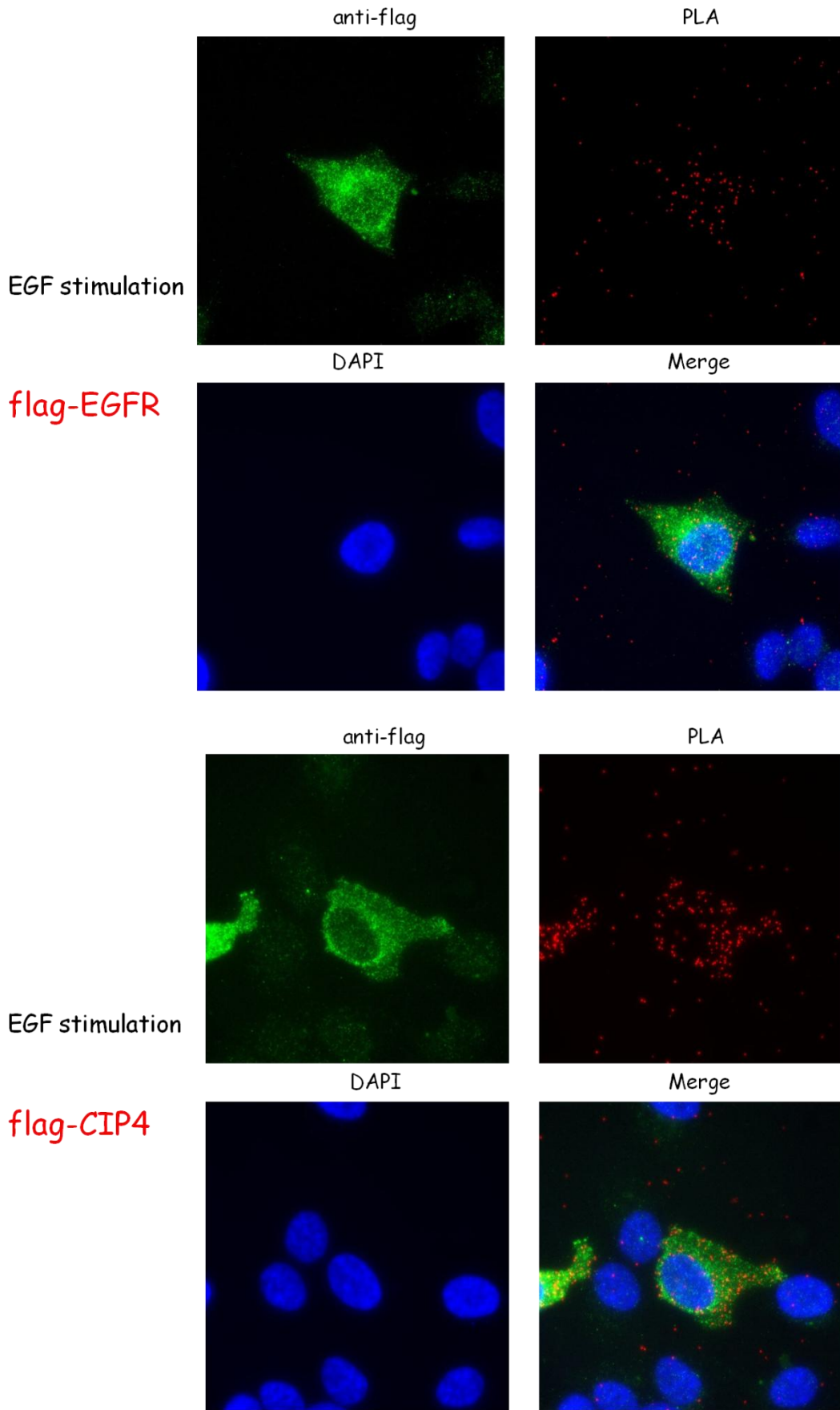


Figure 5.21 PLA assay tested the in vivo interaction between Flag-hRme-6 and CIP4, EGFR in HeLa cells, overexpressing hRme-6. HeLa cells were transfected with Flag-hRme plasmids. After 24 hr, cells were serum starved for 24 hours and then stimulated with 50 ng/ml EGF at different time points. The cells were then fixed with 4% paraformaldehyde, permeabilized with 0.2% Triton X-100, and stained with anti-CIP4/anti-Flag antibody or anti-EGFR/anti-Flag antibody, followed by Duolink® In Situ Red Starter Kit. Samples were then stained with Alexa Fluor 488 conjugated secondary goat anti mouse antibody and analyzed by confocal microscopy.

To further validate the signal specificity of the interactions of Rme-6, another negative control checked the signal between hRme-6 and Nup98 (component of nuclear pore complex) (Figure 5.22). Compared to the signal observed with the interactors of Rme-6 identified by mass spectrometry and in vitro binding, there is fewer dots observed between hRme-6 and Nup98, which further supports that the PLA assay is specific for the interaction between hRme-6 and the interaction partners.

hRme-6/nup98

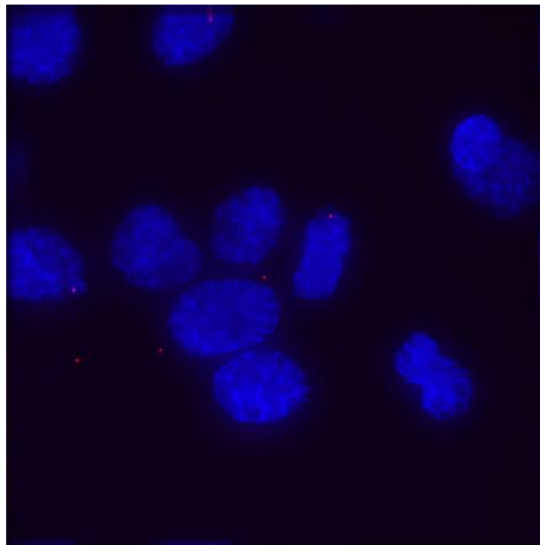


Figure 5.22 PLA assay tested the in vivo interaction between hRme-6 and nup98. HeLa cells were serum starved for 24 hours and then stimulated with 50 ng/ml EGF for 2 minutes. The cells were then fixed with 4% paraformaldehyde, permeabilized with 0.2% Triton X-100, and stained with anti-hRme-6 and anti-Nup98 antibody, followed by Duolink® In Situ Red Starter Kit and analyzed by confocal microscopy.

To summarise these data, PLA assay revealed that there are interactions between

hRme-6 and CIP4, IQGAP1, TfnR and EGFR but not with SNX9. The interaction between hRme-6 and CIP4 was not affected by cargo uptake while the interaction between hRme-6 and IQGAP1 varied during incubation of EGF compared to the incubation of Tfn in HeLa cells.

Over all, PLA assay still showed strong evidence that there are potential interactions between hRme-6 and several candidates.

5.7 Discussion

To understand the functions of hRme-6, my main aim in this chapter was to identify and explore the interaction proteins of hRme-6. SILAC experiments yielded a long list of hRme-6 interaction partners. From this list, four interactions partners were chosen and further explored. In vitro interaction tests and in vivo immunofluorescence experiments confirmed the interactions between hRme-6 and the potential candidates. The PLA further checked the specific interaction between hRme-6 and the candidates in vivo during EGF stimulation and Tfn incubation. One candidate, IQGAP1, was found to exhibit specific increased interaction with hRme-6 during EGF stimulation.

5.7.1 SILAC experiment to find the interaction partners of hRme-6

To find the potential interaction partners of hRme-6 that might be involved in the diverse functions of hRme-6, triple labeling SILAC experiment were set up. As shown in appendix 6, over 500 proteins were found that were specifically immunoprecipitated by an anti-hRme6 antibody that recognises the endogenous hRme-6. Many of the proteins found from the SILAC experiment were actually related

to the nucleus, ribosome and mitochondria. It is perhaps not surprising that ribosomal proteins were identified since the antibody may have immunoprecipitated newly translated hRme-6. But the high proportion of nuclear and mitochondrial proteins was unexpected. One possible reason that led to this result may be because the hRme-6 antibody used for immunoprecipitation was a polyclonal antibody, which may have bound many non-specific proteins. One method to solve this problem could be pre-saturate the antibody by BSA to decrease the non specific binding. Another way is to remove contaminating membranes by centrifugation. But since we were interested in both the membrane and cytosolic pool of Rme-6, we wanted to avoid this step.

Another thing that greatly affected the result was the cell lysis method. Many lysis methods were tried during optimization of the SILAC experiment. I found that only NP40 was effective at releasing membrane components. This is the same condition used in a previous paper that explored the interactome of the EGFR using a SILAC experiment [200]. The known functions of hRme-6 during endocytosis are mainly in the early stages of endocytosis, which involves receptor internalisation and vesicle uncoating. I have shown that hRme-6 was found to function as a high molecular weight complex which is SDS resistant. It is possible that the inclusion of some strong detergent might increase the number of interacting proteins found in the immunoprecipitate of hRme-6.

In the triple labeling SILAC experiments the cells were stimulated for 5 minutes with EGF and this experiment was repeated twice. A third replicate would be required to get a statistically significant analysis of the interactome. However, the hits we chose were robust and appeared in several experiments under different conditions. Another thing found in SILAC experiments was the differences between different EGF stimulation time. An early SILAC experiment that examined the interacting partners of hRme-6 used 10 minutes for EGF stimulation. Most of the selected candidates, including SNX24, SNX9, CIP4 and IQGAP1 were found under these conditions

(appendix 4). However, the ratio of these candidates following 5 minutes and 10 minutes EGF stimulation was slightly different. In particular, SNX24 showed significant interaction with hRme-6 at 5 minutes but little interaction at 10 minutes EGF stimulation. It suggested that the flux of EGF through the endocytic pathway affects the interactions of hRme-6 with its binding partners.

In the proteins found from mass spectrometry, beside CIP4, other known hRme-6 interaction partners, like AP2, Rab5, c-cbl, TC10, p42/44, were not found. It is possible that the binding of the antibody to hRme-6 is blocked when hRme-6 is in complex with some of these binding partners.

Alternatively the interaction between hRme-6 and some of endocytosis interaction partners may be relatively weak and/or transient. The condition used in my assay would not select for these interactions. An alternative mass spectrometry approach such as BioID might be more suitable for detecting such interactions, as BioID was based on the proximity to find all the potential nearby biotinylated interaction proteins by co-expression of a bacterial biotin ligase [220]. So BioID would show more interacting proteins in living cells and may reveal some weak interaction partners that could not be found through classical immunoprecipitation.

After analyzing the list of candidate hits, only four potential candidates were selected to test further due to limited time. But there should be still more candidates sitting in the list that may also affect the functions of hRme-6. It is nearly impossible to check all the hits one by one. One way to solve this problem would be to use an RNAi screen combined with the SILAC experiment. After SILAC experiment, the RNAi screen would highlight all the strong candidates directly that affect the EGF internalisation.

5.7.2 The interaction between hRme-6 and SNX24

From SILAC experiment, in vitro binding experiment and the online data bases SNX24 was selected as a strong interaction partner. Due to the lack of good antibody for SNX24, the in vivo PLA assay was not carried out. In my SILAC experiment, the ratio of SNX24 changed a lot compared to the control groups during both experiments. It suggested that the binding of SNX24 to hRme-6 was specifically modulated in EGF stimulated HeLa cells. How SNX24 involved in the function of hRme-6 during EGF stimulation need further exploration.

5.7.3 The interaction between hRme-6 and SNX9

A second selected candidate SNX9 was selected to test by both in vitro and in vivo experiment. SNX9 and hRme-6 were both reported to interact and colocalize with AP2. SNX9 interacted with β 2 domain and α -adaptin while hRme-6 interacted with α -adaptin. However, while these two proteins interacted very well in an in vitro assay, the interactions in the SILAC experiments and PLA assay were relatively weak.

There may be several reasons for these differences. The PLA assay is based on the recognition of the primary antibody to the protein, the weak signal may be because the SNX9 antibody did not bind to the antigen properly. Another reason could be that SNX9 forms a tight complex with clathrin, AP2 and dynamin 2 so that in the SILAC experiment the anti-hRme-6 antibody was unable to capture them. In my SILAC experiment assay, neither clathrin, AP2 nor dynamin 2 were found. It is possible that in the SILAC experiment the immunoprecipitation of hRme-6 captured only SNX9 that was freely available in the cytoplasm but not that in complex with AP2, clathrin and dynamin.

However, there is another explanation about these phenotypes. It is that the

interaction between SNX9 and hRme-6 is very transient. SNX9 was colocalized with EGFR at very early time points (10 s~2 minutes) [221]. It may be that SNX9 functions at an earlier time point than hRme-6. Live cell imaging shows a recruitment of SNX9 to clathrin coated pits just at the point of scission which would be earlier than the expected recruitment of hRme-6 during uncoating [222]. This may also be the reason that there was not a strong signal between SNX9 and hRme-6 in the PLA assay. The strong in vitro protein interaction may suggest that there is a hand over process between SNX9 and hRme-6.

Another question about SNX9 concerned the domain of SNX9 that interacted with hRme-6. SNX9 and SNX24 both belong to the sorting nexin family. SNX24 is likely to interact with hRme-6 through its PX domain. SNX9 was reported to interact with ACK2 proline-rich domain via its SH3 domain [190]. hRme-6 also contains a proline rich motif. But the interaction domains between hRme-6 and SNX9 are still unknown. If SNX9 and SNX24 both interact with hRme-6 through PX domain, they may interact with the same region with hRme-6. There may be a competition among the interaction of hRme-6, SNX24 and SNX9.

It is notable that SNX9 and hRme-6 both mediate fluid phase endocytosis (macropinocytosis). The Rme-6 mutant showed accumulation of a fluid-phase endocytosis marker in the body cavity in *C.elegans* while Alexa-568-labeled dextran accumulation [160] and horseradish peroxidase (HRP) uptake were all reduced in SNX9-depleted cells [191]. It is possible that the strong interaction of hRme-6 and SNX9 in vitro reflects a real interaction which is not required during EGF stimulation but is more related to the process of macropinocytosis.

5.7.4 The interaction between hRme-6 and CIP4

The interaction between hRme-6 and CIP4 was first found in 3T3-L1 adipocytes to

regulated GLUT4 translocation by insulin stimulation. Although CIP4 was not required in the early stage of clathrin mediated endocytosis of EGFR, CIP4 colocalized with EGFR and Rab5 in early endosome. CIP4 promotes lysosomal targeting and degradation of EGFR [223]. My SILAC experiment suggested hRme-6 interacted with CIP4 during EGF stimulation as well and furthermore the interaction between CIP4 and hRme-6 decreased during CK2 inhibitor treatment.

Due to the interaction between hRme-6 and CIP4 already tested in vitro, it was not tested in my vitro experiment. However, later I found that purified Flag-hRme-6 from HEK293 cells contained CIP4. It also matched with the PLA assay that without stimulation there was already interaction between CIP4 and hRme-6. Overexpression Flag-hRme-6 data further confirmed the interaction.

But the quantifications of PLA signal during Tfn incubation and EGF stimulation were not stable, it failed to show whether the interaction between hRme-6 and CIP4 changed in presence of different cargoes. How CIP4 involved in the function of hRme-6 during EGF stimulation need further exploration.

5.7.5 The interaction between hRme-6 and IQGAP1

The interaction between IQGAP1 and hRme-6 was very exciting. Actually previous studies using SILAC to analyze EGF signalling related proteins had already found that IQGAP1 was recruited to activate Grb2-EGFR complex and directly involved in signalling[224]. My SILAC data suggested that IQGAP1 was a robust interaction partner with hRme-6. Furthermore the SILAC experiment suggested that the interaction between IQGAP1 and hRme-6 decreased during CK2 inhibitor treatment. In vitro experiments, due to the purified IQGAP1 and Flag-hRme-6 were not so pure and lacks of proper controls, there is not clear conclusion for the interaction between Flag-hRme-6 and IQGAP1. It is just an early hint that there may be interaction

between Flag-hRme-6 and IQGAP1. However, the PLA assay revealed that the interaction between hRme-6 and IQGAP1 increased during EGF stimulation but not in Tfn incubation in HeLa cells. This specific change suggested that the interaction between hRme-6 and IQGAP1 may be different depending on which cargo was internalized. It also matched with the original hypothesis that the function of hRme-6 was different during different cargo stimulation. It is possible that the different interaction model between IQGAP1 and hRme-6 leads to different downstream reactions in the cell.

My previous experiments found that overexpression of hRme-6 or treating cells with a CK2 inhibitor both caused a change in the signal intensity of p42/44 and Akt. But how hRme-6 is involved in these processes was unknown. However, IQGAP1 was a strong interaction candidate that is directly involved in the signalling control via hRme-6.

The signal intensity change of Akt caused by hRme-6 overexpression happened mainly at 10 minutes EGF stimulation (Figure 3.6). But the PLA assay found that IQGAP1 and hRme-6 showed peak interaction at very early time point (2 minutes). At 5 minutes stimulation time, the interaction between IQGAP1 and hRme-6 had already started to decrease. It is possible that the interaction between hRme-6 and IQGAP1 regulates the EGFR signal intensity. It also explained the interaction of hRme-6 and IQGAP1 during Tfn incubation as the interaction mainly started at 5 minutes ligand incubation, at which hRme-6 mediates vesicle uncoating. During Tfn incubation because there is no requirement for signal control, this may also delay the interaction between hRme-6 and IQGAP1.

However, there is another reason which may cause the interaction between IQGAP1 and hRme-6 to be more sensitive during EGF stimulation. My experiments showed that serum starvation greatly affected the receptor reaction to the ligand. During Tfn incubation the interaction between TfnR and hRme-6 increased but did not significantly change between EGFR and hRme-6 during EGF stimulation. It appears

that starvation changed the interaction model between hRme-6 and receptors. TfnR recruited more hRme-6 during ligand incubation while EGFR released certain hRme-6.

Another notable thing was that IQGAP1 and hRme-6 both contain a Ras GAP domain. The two Ras GAP domains even show sequence similarity. But the Ras GAP domain of IQGAP1 lacks GAP activity towards Ras but instead interacts with Rac and Cdc42 [225]. The Ras GAP domain of hRme-6 exhibited some low Ras GAP activity. However, the full length hRme-6 did not show significant Ras GAP activity. Interestingly the full length hRme-6 showed Ras GAP activity in presence of IQGAP1 (E.Smythe preliminary experiments). If it is true, it suggests that the interaction between hRme-6 and IQGAP1 would exhibit Ras GAP activity in vivo as well. It is known that EGF stimulation leads the EGFR to activate the tyrosine kinase activity of the cytoplasmic domain and EGFR becomes phosphorylated. Phosphorylation of EGFR leded the docking of GRB2 and GRB2 guanine nucleotide exchange factor SOS and SOS became activated. Activated SOS then promoted the removal of GDP from Ras and activated Ras. Activated Ras then activates RAF kinase. Then RAF kinase phosphorylates and activates MEK. MEK then further activates MAPK, like p42/44. If the interaction between IQGAP1 and hRme-6 led to the Ras GAP activity of hRme-6 being activated, which would in turn inactive Ras and cause the downstream signal to change and diversify the signal intensity. However, combined with the relationship between IQGAP1 and signalling, the interaction between hRme-6 and IQGAP1 could fine-tune the signal.

5.7.6 The interaction between hRme-6 and receptors

As the PLA assay was based on the distance between proteins but not necessarily direct protein interactions, it also can be used to test the interactions between receptors and associated proteins. My previous study found that the co-localisation between hRme-6 and IQGAP1 showed a dramatic change during EGF stimulation. So

the interaction of hRme-6 and different receptors was tested to check if the change between hRme-6 and IQGAP1 was accompanied by the changes between hRme-6 and receptors. As shown in Figure 5.17 and Figure 5.19, the interactions between hRme-6 and EGFR and TfnR were tested successfully. There were generally stronger interaction between hRme-6 and TfnR than that between hRme-6 and EGFR. Interestingly, the interaction between hRme-6 and TfnR sharply increased after 2 minutes of Tfn incubation in 24 hours serum starvated HeLa cells.

The PLA assay signals between hRme-6, EGFR and TfnR were more likely close proximity but not a direct protein interaction, as neither TfnR nor EGFR were identified in the mass spec screens. Nor has Rme-6 been identified in other screens for interactomes of receptors. So the PLA assay signal suggested that hRme-6 was recruited to the vicinity of the receptors.

In the PLA assay, an interaction between hRme-6 and TfnR was detected independent of ligand stimulation. As TfnR is a housekeeping cargo, the endocytosis of TfnR constantly happens in cells and it is known that hRme-6 participates in uncoating of TfnR containing vesicles, it was not surprising that there was always co-localisation signal between hRme-6 and TfnR. But it is surprising to find that actually the interaction signal between hRme-6 and TfnR was changed by the long time serum starvation. After 24 hours serum starvation, the interaction signal decreased nearly 30% compared to that in 30 minutes starvation. During Tfn incubation, there was a transient peak of the interaction between hRme-6 and TfnR, which suggested that hRme-6 was disassociated with the Tfn receptor after 24 hours serum starvation and ligand stimulation recruited hRme-6 to the receptor again. It was shown that in HeLa cells starvation suppressed mTORC1 activity and promoted perinuclear clustering of lysosomes [226]. But it is still unknown why long time starvation led to the separation of hRme-6 with TfnR.

My previous experiment found that short term starvation was not sufficient to cause complete inhibition of phosphorylation of p42/44, p38 and Akt phosphorylation

following EGF stimulation (data not shown). So 24 hours serum starvation was used before EGF stimulation. Unlike TfnR, co-localisation between hRme-6 and EGFR slightly decreased during ligand stimulation. It suggested that after EGF stimulation, some hRme-6 may actually be released from endosomal membranes. But it is very interesting that IQGAP1 and hRme-6 showed high interaction at 2 minutes EGF stimulation. IQGAP1 is known to interact with EGFR. It is still not clear how the interaction between IQGAP1 and hRme-6 changed during EGF stimulation. The different interactions of hRme-6 during EGF and Tfn incubation also indicated that the functions of hRme-6 during the different cargoes appear to be different. A recent study found that the internalisation of EGFR was varied by concentration [227, 228]. When the concentration of EGF applied to the cells was lower than 5 ng/ml, the endocytosis of EGFR was clathrin-dependent. However, if the concentration was higher than 5 ng/ml, the internalisation of EGFR was mediated by both clathrin-dependent endocytosis and clathrin-independent endocytosis. In my experiments I used 50 ng/ml EGF. Different endocytic pathways may affect the functions of hRme-6. It also suggest that the function of hRme-6 in endocytosis is not limited to clathrin mediated endocytosis.

It was interesting to find that the interactions between hRme-6 and TfnR, EGFR, CIP4 all greatly increased in over-expression hRme-6 HeLa cells. It suggested that the interactions were limited by the amount of hRme-6 and also further confirmed that specificity of the interactions.

6. Chapter 6 Conclusion and future perspectives

6.1 Discussion

The aim of this study was to investigate the structure/function analysis of hRme-6 in trafficking and signalling. My study focused on three aspects: exploring the domain functions of hRme-6, investigating the structure of hRme-6 and finally identifying the interacting partners of hRme-6.

There are more and more evidence that endocytosis and signalling are deeply connected with each other. Signalling receptors, such as EGFR, pass through the trafficking process to attenuate the signal while the trafficking process potentially regulates the magnitude and specificity of the signalling. The combined effect from trafficking and signalling then leads to diverse impacts on the cellular functions.

The function of hRme-6 was deeply dependent on the structure of hRme-6, which contains a Rab5 GEF domain and also a Ras GAP domain. The Rab5 GEF domain exhibited GEF activity in presence of AP2 and ATP, implying that structural changes regulated the GEF activity. The Ras GAP domain of hRme-6 interacted with c-Cbl to mediate the functions of hRme-6 in EGFR trafficking. Subsequently, Rme-6 was found also involved in the translocation of GLUT4 in insulin stimulation. The function of hRme-6 was mediated by the proline rich region of hRme-6 with SH3 domain of CIP4.

Therefore I want to investigate the structure/function relationship of hRme-6 to take a glance at the in integrated trafficking and signalling process.

In the first instance I confirmed the activity of Ras GAP domain of hRme-6 in vitro. And the Rab5 GEF domain activity was checked using Flag-hRme-6 purified from insect cells. The purified hRme-6 from insect cells did show the same Rab5 GEF activity as that from HEK cells. So the following experiments were mainly based on the purified protein from insect cells.

As Previous data from our lab showed that overexpression of hRme-6 increased MAPK signalling while decreasing Akt signalling in Ang1 stimulated HUVECs (Emma Maxwell and Smythe, unpublished data), I investigated the role of hRme-6 in the regulation of Tie2 signal transduction by using the purified Flag-hRme-6 from insect cells bound to M2 Flag beads as a bait to pull down interacting partners using lysates from Ang1 stimulated HUVECs cells. It is interesting to find that hRme-6 could specifically bind to phosphorylated p42/44, which also showed the hint for the role of hRme-6 during signalling transduction. Further explore the overexpression of hRme-6 in EGF stimulated HeLa cells increased Akt signalling but not show significant effect on MAPK signalling. The different effect may be due to the different cell lines, but it still confirmed the effect of hRme-6 during signalling transduction.

As the Rab5 GEF activity of hRme-6 relied on AP2 and ATP, which implied that function of hRme-6 may be dependent on phosphorylation. hRme-6 previously was found to be phosphorylated by CK2 in vitro (Singh and Smythe, unpublished data). I then checked whether p42/44 could also phosphorylate hRme-6 in vitro. However, there was no significant phosphorylation of hRme-6 caused by p42/44, which indicated that probably the binding of p42/44 may be not in charge of the phosphorylation of hRme-6 in vitro.

I also observed that the inhibition the activity of CK2 led the increases of phosphorylated p42/44 and the decreased of phosphorylated of Akt in EGF stimulated HeLa cells. The inhibition of CK2 seems got the opposite effect compared to overexpression of hRme-6 in EGF stimulated HeLa cells but similar to the effect of hRme-6 in Ang1 stimulated HUVECs. Overall, these effects led the conclusion that hRme-6 not only involved in the signalling pathway of Ang1-Tie2 but also EGF-EGFR processes. But the clear mechanism of the role of hRme-6 in signalling pathway needs further exploration.

On the following aspect of the study, I decided to focus on the structure study of hRme-6. As the Ras GAP domain and Rab5 GEF domain of hRme-6 all showed activities, but the functional domain in Tfn endocytosis was properly Rab5 GEF domain while that in EGFR endocytosis was mainly the Ras GAP domain of hRme-6. The structure of hRme-6 would support the key question of hRme-6 about how the different domains of hRme-6 functioned in different cargo stimulation like Tfn and EGFR.

The early stage assays, including SDS trapping assay, immunoprecipitation HA-hRme-6 with Flag-hRme-6, native PAGE and gel filtration assay, showed clearly and solid data that hRme-6 formed multimers in vitro and in vivo. However, although the mainly size of hRme-6 was around 720 KD, the formation of hRme-6 around 480 KD was confusion as it did not exist in fresh cell lysis sample. Although there is strong doubt that the lower band around 480 KD was a degradation form of hRme-6, mass spectrometry analyze indicated that the small band of hRme-6 was not a degradation form. SEC data suggested that the monomer size of hRme-6 would be around 250 KD, which made the formation of hRme-6 multimer even confusion as there was actually no monomer conformation of hRme-6 found around the size of 250 KD in native conditions. As a new Superose 6 gel filtration column arrived, I would consider running the purified sample again to further check the conformation of hRme-6 if the opportunity arises.

Due to the limit of the character of hRme-6 itself, the further structure analyze was done by negative staining and Single particle Reconstruction. However, there was just a surface structure of hRme-6 revealed from it. It could not show the information about the domain structure and monomer constitution. Following nanogold labeling, the monomer constitution was still unclear. The nanogold labeling also argued that the C-terminal of hRme-6 was not buried inside even the Rab5 GEF activity strongly rely on the ATP and AP2 and the purified Rab5 GEF domain showed limited solubility. Nonetheless, it would be possible to uncovering the detailed structure of hRme-6

using cryo-EM to finally answer these questions. Cryo-EM also will help to reveal the structure of the GEF mutant form hRme-6^{F1487A} which did not show GEF activity in AP2 and ATP.

Despite the study of structure of hRme-6, I found the conformation change of hRme-6 caused by CK2 inhibition combined with EGF stimulation in HeLa cells. This argued that there may be still dynamic equilibrium in the conformation of hRme-6 in vivo and CK2 inhibitor combined with EGF stimulation in HeLa cells could be a good model to investigate it.

The final aspect of my study proposed the investigation of the interaction partners of hRme-6.

Based on the double and triple labeling SILAC experiments, the potential interaction partners of hRme-6 showed up. Four candidates, including SNX9, SNX24, IQGAP1 and CIP4 were selected according to the ratio and frequency existed in the experiments. However, there are still several potential candidates in the list waiting to be further identified. Further RNAi screen of all the proteins found in SILAC experiment may help identify other potential proteins involved in the function of hRme-6. The weak in vivo interaction between SNX9 and hRme-6 suggested that the interaction may be stronger in other unknown situation. However, the interaction between CIP4 and hRme-6 will need further investigation during EGF stimulated HeLa cells.

Then in vitro test found that SNX9, SNX24 and IQGAP1 all showed directly interaction with hRme-6. In vivo PLA assay showed that the interactions between SNX9 and hRme-6 in Tfn and EGF stimulation were generally very weak and the interactions between CIP4 and hRme-6 in both Tfn and EGF stimulation were relatively strong.

It is interesting that the interaction signal between IQGAP1 and hRme-6 specific increased at 2 minutes EGF stimulation compared to other time points or Tfn incubation. It suggested that the interaction between IQGAP1 and hRme-6 may work potentially to regulate EGFR trafficking process. Especially IQGAP1 and full hRme-6 together showed Ras GAP activity in vitro (E Smythe, unpublished data). It implied that the interaction between IQGAP1 and hRme-6 in vivo may activate the Ras GAP activity of hRme-6, which then could affect the signalling output during the EGFR endocytosis from early time point.

It is also interesting that the interaction between TfnR and hRme-6 sharply increased at 2 minutes Tfn incubation in 24 hours serum starved HeLa cells while there is no significant change in 30 minutes serum starvation or EGF stimulation in 24 hours serum starved HeLa cells.

In conclusion, this study showed that hRme-6 formed multimer in vivo. The function of hRme-6 involved with the interaction with CIP4 and IQGAP1.

6.2 Future perspectives

The aim of this study was to investigate the structure/function analysis of hRme-6 in trafficking and signalling. My study focused on three aspects: exploring the domain functions of hRme-6, investigating the structure of hRme-6 and finally identifying the interacting partners of hRme-6. Future experiments could be performed to gain more ideas about the structure of hRme-6 and how hRme-6 function with its interaction partners to regulate trafficking and signalling.

The surface structure of hRme-6 is already revealed. But the detail of the structure of hRme-6 still needs to be elucidated. Further improvement of the purity of Flag-hRme-6 protein by gel filtration should be feasible to perform. The pure protein then could be used for cryo-EM to resolve the structure of hRme-6. The total separation of different conformations of hRme-6 could also be used for the GEF and

GAP activity test.

As I have demonstrated the GEF domain of hRme-6 could interact with full length of hRme-6, more investigation about the interaction domain of hRme-6 will also help the resolve the structure of hRme-6 and answer how the monomer of hRme-6 form multimer in vivo. One more exciting approach would be analyzing the effect of phosphorylation to the structure of hRme-6. Especially hRme-6^{F1487A} and the amino acid that is sensitive to CK2 inhibitor would give insight about the structure change of hRme-6 in vivo.

The SILAC experiment found lots of potential interaction partners of hRme-6, but only four candidates were selected for further validation. Combining mass spectrometry with RNAi screens could facilitate validation of more candidates from the SILAC experiments. In particular, some ER proteins gave some robust signals and it would be of interest to investigate potential roles for hRme-6 in the formation of ER/endosome contacts sites [229].

For the selected four candidates, further questions arise about the functions of hRme-6 with the potential candidates.

The interaction of IQGAP1 and hRme-6 seems specific for EGFR trafficking. To understand how IQGAP1 and hRme-6 are involved in signalling further studies could combine siRNA of IQGAP1 with overexpression of hRme-6 plus EGF stimulation in the presence or absence of CK2 inhibitor to test whether the signal intensity changes, and or conformational changes in hRme-6.

The interaction between hRme-6 and CIP4, SNX24 in Hela cells need be further validated through both PLA assay. From my finding I have demonstrated that hRme-6 interacted with SNX9 directly in vitro. Since SNX9 and hRme-6 both involved in fluid phase endocytosis, testing the interaction of SNX9 and hRme-6 during fluid phase endocytosis would give insight about the function of the interaction between SNX9 and hRme-6.

My findings have given insight the structure of hRme-6 and how it interacted with interaction partners to affect trafficking and signalling of signalling receptors.

7. References

- [1] Sigismund S, Confalonieri S, Ciliberto A, Polo S, Scita G, Di Fiore PP. Endocytosis and signalling: cell logistics shape the eukaryotic cell plan. *Physiological reviews* 2012;92:273-366.
- [2] Doherty GJ, McMahon HT. Mechanisms of endocytosis. *Annual review of biochemistry* 2009;78:857-902.
- [3] Flannagan RS, Jaumouille V, Grinstein S. The cell biology of phagocytosis. *Annual review of pathology* 2012;7:61-98.
- [4] Lim JP, Gleeson PA. Macropinocytosis: an endocytic pathway for internalising large gulps. *Immunology and cell biology* 2011;89:836-43.
- [5] Traub LM. Tickets to ride: selecting cargo for clathrin-regulated internalization. *Nature reviews Molecular cell biology* 2009;10:583-96.
- [6] ter Haar E, Musacchio A, Harrison SC, Kirchhausen T. Atomic structure of clathrin: a beta propeller terminal domain joins an alpha zigzag linker. *Cell* 1998;95:563-73.
- [7] Kirchhausen T. Imaging endocytic clathrin structures in living cells. *Trends in cell biology* 2009;19:596-605.
- [8] Cocucci E, Aguet F, Boulant S, Kirchhausen T. The first five seconds in the life of a clathrin-coated pit. *Cell* 2012;150:495-507.
- [9] Kelly BT, Graham SC, Liska N, Dannhauser PN, Honing S, Ungewickell EJ, et al. Clathrin adaptors. AP2 controls clathrin polymerization with a membrane-activated switch. *Science* 2014;345:459-63.
- [10] Doughman RL, Firestone AJ, Anderson RA. Phosphatidylinositol phosphate kinases put PI4,5P(2) in its place. *The Journal of membrane biology* 2003;194:77-89.
- [11] Antonescu CN, Aguet F, Danuser G, Schmid SL. Phosphatidylinositol-(4,5)-bisphosphate regulates clathrin-coated pit initiation, stabilization, and size. *Molecular biology of the cell* 2011;22:2588-600.

[12] Jackson LP, Kelly BT, McCoy AJ, Gaffry T, James LC, Collins BM, et al. A large-scale conformational change couples membrane recruitment to cargo binding in the AP2 clathrin adaptor complex. *Cell* 2010;141:1220-9.

[13] Antonescu CN, Aguet F, Danuser G, Schmid SL. Phosphatidylinositol-(4,5)-bisphosphate regulates clathrin-coated pit initiation, stabilization, and size. *Molecular biology of the cell* 2011;22:2588-600.

[14] Bonifacino JS, Traub LM. Signals for sorting of transmembrane proteins to endosomes and lysosomes. *Annual review of biochemistry* 2003;72:395-447.

[15] Kirchhausen T. Adaptors for clathrin-mediated traffic. *Annual review of cell and developmental biology* 1999;15:705-32.

[16] Liu AP, Aguet F, Danuser G, Schmid SL. Local clustering of transferrin receptors promotes clathrin-coated pit initiation. *The Journal of cell biology* 2010;191:1381-93.

[17] Lampe M, Pierre F, Al-Sabah S, Krasel C, Merrifield CJ. Dual single-scission event analysis of constitutive transferrin receptor (TfR) endocytosis and ligand-triggered beta2-adrenergic receptor (beta2AR) or Mu-opioid receptor (MOR) endocytosis. *Molecular biology of the cell* 2014;25:3070-80.

[18] den Otter WK, Briels WJ. The generation of curved clathrin coats from flat plaques. *Traffic* 2011;12:1407-16.

[19] Avinoam O, Schorb M, Beese CJ, Briggs JA, Kaksonen M. ENDOCYTOSIS. Endocytic sites mature by continuous bending and remodeling of the clathrin coat. *Science* 2015;348:1369-72.

[20] Posor Y, Eichhorn-Gruenig M, Puchkov D, Schoneberg J, Ullrich A, Lampe A, et al. Spatiotemporal control of endocytosis by phosphatidylinositol-3,4-bisphosphate. *Nature* 2013;499:233-7.

[21] Lundmark R, Carlsson SR. Sorting nexin 9 participates in clathrin-mediated endocytosis through interactions with the core components. *The Journal of biological chemistry* 2003;278:46772-81.

[22] Lundmark R, Carlsson SR. Regulated membrane recruitment of dynamin-2 mediated by sorting nexin 9. *The Journal of biological chemistry* 2004;279:42694-702.

[23] Yoshida Y, Kinuta M, Abe T, Liang S, Araki K, Cremona O, et al. The stimulatory action of amphiphysin on dynamin function is dependent on lipid bilayer curvature. *The EMBO journal* 2004;23:3483-91.

[24] Peter BJ, Kent HM, Mills IG, Vallis Y, Butler PJG, Evans PR, et al. BAR domains as sensors of membrane curvature: The amphiphysin BAR structure. *Science* 2004;303:495-9.

[25] Yasar D, Waterman-Storer CM, Schmid SL. A dynamic actin cytoskeleton functions at multiple stages of clathrin-mediated endocytosis. *Molecular biology of the cell* 2005;16:964-75.

[26] Kaksonen M, Toret CP, Drubin DG. A modular design for the clathrin- and actin-mediated endocytosis machinery. *Cell* 2005;123:305-20.

[27] Merrifield CJ, Perrais D, Zenisek D. Coupling between clathrin-coated-pit invagination, cortactin recruitment, and membrane scission observed in live cells. *Cell* 2005;121:593-606.

[28] Muhlberg AB, Warnock DE, Schmid SL. Domain structure and intramolecular regulation of dynamin GTPase. *The EMBO journal* 1997;16:6676-83.

[29] Hinshaw JE, Schmid SL. Dynamin self-assembles into rings suggesting a mechanism for coated vesicle budding. *Nature* 1995;374:190-2.

[30] Sweitzer SM, Hinshaw JE. Dynamin undergoes a GTP-dependent conformational change causing vesiculation. *Cell* 1998;93:1021-9.

[31] Morlot S, Roux A. Mechanics of Dynamin-Mediated Membrane Fission. *Annu Rev Biophys* 2013;42:629-49.

[32] Soulet F, Yasar D, Leonard M, Schmid SL. SNX9 regulates dynamin assembly and is required for efficient clathrin-mediated endocytosis. *Molecular biology of the cell* 2005;16:2058-67.

[33] Posor Y, Eichhorn-Gruenig M, Puchkov D, Schoneberg J, Ullrich A, Lampe A, et al. Spatiotemporal control of endocytosis by phosphatidylinositol-3,4-bisphosphate. *Nature* 2013;499:233-+.

[34] Jean S, Cox S, Schmidt EJ, Robinson FL, Kiger A. Sbf/MTMR13 coordinates

PI(3)P and Rab21 regulation in endocytic control of cellular remodeling. *Molecular biology of the cell* 2012;23:2723-40.

[35] Franco I, Gulluni F, Campa CC, Costa C, Margaria JP, Ciralo E, et al. PI3K class II alpha controls spatially restricted endosomal PtdIns3P and Rab11 activation to promote primary cilium function. *Developmental cell* 2014;28:647-58.

[36] Devereaux K, Dall'Armi C, Alcazar-Roman A, Ogasawara Y, Zhou X, Wang F, et al. Regulation of Mammalian Autophagy by Class II and III PI 3-Kinases through PI3P Synthesis. *PloS one* 2013;8.

[37] Maffucci T, Brancaccio A, Piccolo E, Stein RC, Falasca M. Insulin induces phosphatidylinositol-3-phosphate formation through TC10 activation. *Embo Journal* 2003;22:4178-89.

[38] Falasca M, Hughes WE, Dominguez V, Sala G, Fostira F, Fang MQ, et al. The role of phosphoinositide 3-kinase C2alpha in insulin signalling. *The Journal of biological chemistry* 2007;282:28226-36.

[39] Backer JM. The regulation and function of Class III PI3Ks: novel roles for Vps34. *The Biochemical journal* 2008;410:1-17.

[40] Chappell TG, Welch WJ, Schlossman DM, Palter KB, Schlesinger MJ, Rothman JE. Uncoating Atpase Is a Member of the 70 Kilodalton Family of Stress Proteins. *Cell* 1986;45:3-13.

[41] Greener T, Zhao XH, Nojima H, Eisenberg E, Greene LE. Role of cyclin G-associated kinase in uncoating clathrin-coated vesicles from non-neuronal cells. *Journal of Biological Chemistry* 2000;275:1365-70.

[42] Umeda A, Meyerholz A, Ungewickell E. Identification of the universal cofactor (auxilin 2) in clathrin coat dissociation. *Eur J Cell Biol* 2000;79:336-42.

[43] Jiang RF, Gao BC, Prasad K, Greene LE, Eisenberg E. Hsc70 chaperones clathrin and primes it to interact with vesicle membranes. *Journal of Biological Chemistry* 2000;275:8439-47.

[44] Barouch W, Prasad K, Greene L, Eisenberg E. Auxilin-induced interaction of the molecular chaperone Hsc70 with clathrin baskets. *Biochemistry* 1997;36:4303-8.

[45] Greene LE, Eisenberg E. Dissociation of Clathrin from Coated Vesicles by the Uncoating Atpase. *Journal of Biological Chemistry* 1990;265:6682-7.

[46] Lakadamyali M, Rust MJ, Zhuang XW. Ligands for clathrin-mediated endocytosis are differentially sorted into distinct populations of early endosomes. *Cell* 2006;124:997-1009.

[47] Gorvel JP, Chavrier P, Zerial M, Gruenberg J. rab5 controls early endosome fusion in vitro. *Cell* 1991;64:915-25.

[48] Bucci C, Parton RG, Mather IH, Stunnenberg H, Simons K, Hoflack B, et al. The Small Gtpase Rab5 Functions as a Regulatory Factor in the Early Endocytic Pathway. *Cell* 1992;70:715-28.

[49] Nielsen E, Severin F, Backer JM, Hyman AA, Zerial M. Rab5 regulates motility of early endosomes on microtubules. *Nat Cell Biol* 1999;1:376-82.

[50] Rubino M, Miaczynska M, Lippe R, Zerial M. Selective membrane recruitment of EEA1 suggests a role in directional transport of clathrin-coated vesicles to early endosomes. *Journal of Biological Chemistry* 2000;275:3745-8.

[51] Rodman JS, Stahl PD, Gluck S. Distribution and Structure of the Vacuolar H⁺ Atpase in Endosomes and Lysosomes from Llc-Pk1 Cells. *Experimental cell research* 1991;192:445-52.

[52] Hu YB, Dammer EB, Ren RJ, Wang G. The endosomal-lysosomal system: from acidification and cargo sorting to neurodegeneration. *Transl Neurodegener* 2015;4.

[53] Huotari J, Helenius A. Endosome maturation. *Embo Journal* 2011;30:3481-500.

[54] Mettlen M, Pucadyil T, Ramachandran R, Schmid SL. Dissecting dynamin's role in clathrin-mediated endocytosis. *Biochemical Society transactions* 2009;37:1022-6.

[55] Watts C. Rapid endocytosis of the transferrin receptor in the absence of bound transferrin. *The Journal of cell biology* 1985;100:633-7.

[56] Palade GE. Fine Structure of Blood Capillaries. *J Appl Phys* 1953;24:1424-.

[57] Hansen CG, Nichols BJ. Exploring the caves: cavins, caveolins and caveolae. *Trends in cell biology* 2010;20:177-86.

[58] Bastiani M, Parton RG. Caveolae at a glance. *Journal of cell science* 2010;123:3831-6.

[59] Pelkmans L, Helenius A. Endocytosis via caveolae. *Traffic* 2002;3:311-20.

[60] Sinha B, Koster D, Ruez R, Gonnord P, Bastiani M, Abankwa D, et al. Cells Respond to Mechanical Stress by Rapid Disassembly of Caveolae. *Cell* 2011;144:402-13.

[61] Lee J, Schmitschonbein GW. Biomechanics of Skeletal-Muscle Capillaries - Hemodynamic Resistance, Endothelial Distensibility, and Pseudopod Formation. *Ann Biomed Eng* 1995;23:226-46.

[62] Schweitzer JK, Sedgwick AE, D'Souza-Schorey C. ARF6-mediated endocytic recycling impacts cell movement, cell division and lipid homeostasis. *Semin Cell Dev Biol* 2011;22:39-47.

[63] Montagnac G, de Forges H, Smythe E, Gueudry C, Romao M, Salamero J, et al. Decoupling of Activation and Effector Binding Underlies ARF6 Priming of Fast Endocytic Recycling. *Curr Biol* 2011;21:574-9.

[64] Meister M, Tikkanen R. Endocytic trafficking of membrane-bound cargo: a flotillin point of view. *Membranes* 2014;4:356-71.

[65] Otto GP, Nichols BJ. The roles of flotillin microdomains - endocytosis and beyond. *Journal of cell science* 2011;124:3933-40.

[66] Glebov OO, Bright NA, Nichols BJ. Flotillin-1 defines a clathrin-independent endocytic pathway in mammalian cells. *Nat Cell Biol* 2006;8:46-54.

[67] Schneider A, Rajendran L, Honsho M, Gralle M, Donnert G, Wouters F, et al. Flotillin-dependent clustering of the amyloid precursor protein regulates its endocytosis and amyloidogenic processing in neurons. *J Neurosci* 2008;28:2874-82.

[68] Renard HF, Simunovic M, Lemiere J, Boucrot E, Garcia-Castillo MD, Arumugam S, et al. Endophilin-A2 functions in membrane scission in clathrin-independent endocytosis. *Nature* 2015;517:493-+.

[69] Boucrot E, Ferreira APA, Almeida-Souza L, Debard S, Vallis Y, Howard G, et al. Endophilin marks and controls a clathrin-independent endocytic pathway. *Nature*

2015;517:460-+.

[70] Hutagalung AH, Novick PJ. Role of Rab GTPases in Membrane Traffic and Cell Physiology. *Physiological reviews* 2011;91:119-49.

[71] Lee MT, Mishra A, Lambright DG. Structural mechanisms for regulation of membrane traffic by rab GTPases. *Traffic* 2009;10:1377-89.

[72] Gavriljuk K, Itzen A, Goody RS, Gerwert K, Koetting C. Membrane extraction of Rab proteins by GDP dissociation inhibitor characterized using attenuated total reflection infrared spectroscopy. *Proceedings of the National Academy of Sciences of the United States of America* 2013;110:13380-5.

[73] Ullrich O, Stenmark H, Alexandrov K, Huber LA, Kaibuchi K, Sasaki T, et al. Rab Gdp Dissociation Inhibitor as a General Regulator for the Membrane Association of Rab Proteins. *Journal of Biological Chemistry* 1993;268:18143-50.

[74] Sivars U, Aivazian D, Pfeffer SR. Yip3 catalyses the dissociation of endosomal Rab-GDI complexes. *Nature* 2003;425:856-9.

[75] Schoebel S, Oesterlin LK, Blankenfeldt W, Goody RS, Itzen A. RabGDI Displacement by DrrA from Legionella Is a Consequence of Its Guanine Nucleotide Exchange Activity. *Mol Cell* 2009;36:1060-72.

[76] Grosshans BL, Ortiz D, Novick P. Rabs and their effectors: Achieving specificity in membrane traffic. *Proceedings of the National Academy of Sciences of the United States of America* 2006;103:11821-7.

[77] Gillingham AK, Sinka R, Torres IL, Lilley KS, Munro S. Toward a Comprehensive Map of the Effectors of Rab GTPases. *Developmental cell* 2014;31:358-73.

[78] Wandinger-Ness A, Zerial M. Rab Proteins and the Compartmentalization of the Endosomal System. *Csh Perspect Biol* 2014;6.

[79] Bhuin T, Roy JK. Rab11 in Disease Progression. *Int J Mol Cell Med* 2015;4:1-8.

[80] Bucci C, Thomsen P, Nicoziani P, McCarthy J, van Deurs B. Rab7: A key to lysosome biogenesis. *Molecular biology of the cell* 2000;11:467-80.

[81] Vitelli R, Santillo M, Lattero D, Chiariello M, Bifulco M, Bruni CB, et al. Role of the small GTPase RAB7 in the late endocytic pathway. *Journal of Biological Chemistry*

1997;272:4391-7.

[82] Vanlandingham PA, Ceresa BP. Rab7 Regulates Late Endocytic Trafficking Downstream of Multivesicular Body Biogenesis and Cargo Sequestration. *Journal of Biological Chemistry* 2009;284:12110-24.

[83] Girard E, Chmiest D, Fournier N, Johannes L, Paul JL, Védie B, et al. Rab7 is functionally required for selective cargo sorting at the early endosome. *Traffic* 2014;15:309-26.

[84] Vonderheit A, Helenius A. Rab7 associates with early endosomes to mediate sorting and transport of semliki forest virus to late endosomes. *Plos Biol* 2005;3:1225-38.

[85] Chavrier P, Parton RG, Hauri HP, Simons K, Zerial M. Localization of Low-Molecular-Weight Gtp Binding-Proteins to Exocytic and Endocytic Compartments. *Cell* 1990;62:317-29.

[86] Stenmark H, Parton RG, Steelemortimer O, Lutcke A, Gruenberg J, Zerial M. Inhibition of Rab5 Gtpase Activity Stimulates Membrane-Fusion in Endocytosis. *Embo Journal* 1994;13:1287-96.

[87] McLauchlan H, Newell J, Morrice N, Osborne A, West M, Smythe E. A novel role for Rab5-GDI in ligand sequestration into clathrin-coated pits. *Curr Biol* 1998;8:34-45.

[88] Stenmark H, Vitale G, Ullrich O, Zerial M. Rabaptin-5 Is a Direct Effector of the Small Gtpase Rab5 in Endocytic Membrane-Fusion. *Cell* 1995;83:423-32.

[89] Lippe R, Miaczynska M, Rybin V, Runge A, Zerial M. Functional synergy between Rab5 effector Rabaptin-5 and exchange factor Rabex-5 when physically associated in a complex. *Molecular biology of the cell* 2001;12:2219-28.

[90] Horiuchi H, Lippe R, McBride HM, Rubino M, Woodman P, Stenmark H, et al. A novel Rab5 GDP/GTP exchange factor complexed to Rabaptin-5 links nucleotide exchange to effector recruitment and function. *Cell* 1997;90:1149-59.

[91] Christoforidis S, Miaczynska M, Ashman K, Wilm M, Zhao L, Yip SC, et al. Phosphatidylinositol-3-OH kinases are Rab5 effectors. *Nat Cell Biol* 1999;1:249-52.

[92] Simonsen A, Lippe R, Christoforidis S, Gaullier JM, Brech A, Callaghan J, et al. EEA1 links PI(3)K function to Rab5 regulation of endosome fusion. *Nature* 1998;394:494-8.

[93] Christoforidis S, McBride HM, Burgoyne RD, Zerial M. The Rab5 effector EEA1 is a core component of endosome docking. *Nature* 1999;397:621-5.

[94] Shin HW, Hayashi M, Christoforidis S, Lacas-Gervais S, Hoepfner S, Wenk MR, et al. An enzymatic cascade of Rab5 effectors regulates phosphoinositide turnover in the endocytic pathway. *Journal of Cell Biology* 2005;170:607-18.

[95] Nielsen E, Christoforidis S, Uttenweiler-Joseph S, Miaczynska M, Dewitte F, Wilm M, et al. Rabenosyn-5, a novel Rab5 effector, is complexed with hVPS45 and recruited to endosomes through a FYVE finger domain. *Journal of Cell Biology* 2000;151:601-12.

[96] De Renzis S, Sonnichsen B, Zerial M. Divalent Rab effectors regulate the sub-compartmental organization and sorting of early endosomes. *Nat Cell Biol* 2002;4:124-33.

[97] Pal A, Severin F, Lommer B, Shevchenko A, Zerial M. Huntingtin-HAP40 complex is a novel Rab5 effector that regulates early endosome motility and is up-regulated in Huntington's disease. *Journal of Cell Biology* 2006;172:605-18.

[98] Huang J, Imamura T, Olefsky JM. Insulin can regulate GLUT4 internalization by signalling to Rab5 and the motor protein dynein. *Proceedings of the National Academy of Sciences of the United States of America* 2001;98:13084-9.

[99] Chiariello M, Bruni CB, Bucci C. The small GTPases Rab5a, Rab5b and Rab5c are differentially phosphorylated in vitro. *FEBS letters* 1999;453:20-4.

[100] Barbieri MA, Fernandez-Pol S, Hunker C, Horazdovsky BH, Stahl PD. Role of Rab5 in EGF receptor-mediated signal transduction. *Eur J Cell Biol* 2004;83:305-14.

[101] Miaczynska M, Christoforidis S, Giner A, Shevchenko A, Uttenweiler-Joseph S, Habermann B, et al. APPL proteins link Rab5 to nuclear signal transduction via an endosomal compartment. *Cell* 2004;116:445-56.

[102] Schenck A, Goto-Silva L, Collinet C, Rhinn M, Giner A, Habermann B, et al.

The endosomal protein Appl1 mediates akt substrate specificity and cell survival in vertebrate development. *Cell* 2008;133:486-97.

[103] Martinu L, Santiago-Walker A, Qi HW, Chou MM. Endocytosis of epidermal growth factor receptor regulated by Grb2-mediated recruitment of the Rab5 GTPase-activating protein RN-tre. *Journal of Biological Chemistry* 2002;277:50996-1002.

[104] Lanzetti L, Rybin V, Malabarba MG, Christoforidis S, Scita G, Zerial M, et al. The Eps8 protein coordinates EGF receptor signalling through Rac and trafficking through Rab5. *Nature* 2000;408:374-7.

[105] Zeigerer A, Gilleron J, Bogorad RL, Marsico G, Nonaka H, Seifert S, et al. Rab5 is necessary for the biogenesis of the endolysosomal system in vivo. *Nature* 2012;485:465-70.

[106] van der Blik AM. A sixth sense for Rab5. *Nat Cell Biol* 2005;7:548-50.

[107] Dinneen JL, Ceresa BP. Expression of dominant negative rab5 in HeLa cells regulates endocytic trafficking distal from the plasma membrane. *Experimental cell research* 2004;294:509-22.

[108] Vieira AV, Lamaze C, Schmid SL. Control of EGF receptor signalling by clathrin-mediated endocytosis. *Science* 1996;274:2086-9.

[109] Sorkin A, von Zastrow M. Signal transduction and endocytosis: Close encounters of many kinds. *Nat Rev Mol Cell Bio* 2002;3:600-14.

[110] Beguinot L, Lyall RM, Willingham MC, Pastan I. Down-Regulation of the Epidermal Growth-Factor Receptor in K562 Cells Is Due to Receptor Internalization and Subsequent Degradation in Lysosomes. *Proc Natl Acad Sci-Biol* 1984;81:2384-8.

[111] Tsao P, von Zastrow M. Downregulation of G protein-coupled receptors. *Current opinion in neurobiology* 2000;10:365-9.

[112] Wells A, Welsh JB, Lazar CS, Wiley HS, Gill GN, Rosenfeld MG. Ligand-Induced Transformation by a Noninternalizing Epidermal Growth-Factor Receptor. *Science* 1990;247:962-4.

[113] Sorkin A, von Zastrow M. Endocytosis and signalling: intertwining molecular

networks. *Nat Rev Mol Cell Bio* 2009;10:609-22.

[114] Scita G, Di Fiore PP. The endocytic matrix. *Nature* 2010;463:464-73.

[115] Fortini ME. Notch Signalling: The Core Pathway and Its Posttranslational Regulation. *Developmental cell* 2009;16:633-47.

[116] Edeling MA, Mishra SK, Keyel PA, Steinhauser AL, Collins BM, Roth R, et al. Molecular switches involving the AP-2 beta2 appendage regulate endocytic cargo selection and clathrin coat assembly. *Developmental cell* 2006;10:329-42.

[117] Gaidarov I, Krupnick JG, Falck JR, Benovic JL, Keen JH. Arrestin function in G protein-coupled receptor endocytosis requires phosphoinositide binding. *Embo Journal* 1999;18:871-81.

[118] Platta HW, Stenmark H. Endocytosis and signalling. *Current opinion in cell biology* 2011;23:393-403.

[119] Sakane H, Yamamoto H, Kikuchi A. LRP6 is internalized by Dkk1 to suppress its phosphorylation in the lipid raft and is recycled for reuse. *Journal of cell science* 2010;123:360-8.

[120] Di Guglielmo GM, Le Roy C, Goodfellow AF, Wrana JL. Distinct endocytic pathways regulate TGF-beta receptor signalling and turnover. *Nat Cell Biol* 2003;5:410-21.

[121] Sigismund S, Argenzio E, Tosoni D, Cavallaro E, Polo S, Di Fiore PP. Clathrin-mediated internalization is essential for sustained EGFR signalling but dispensable for degradation. *Developmental cell* 2008;15:209-19.

[122] Zoncu R, Perera RM, Balkin DM, Pirruccello M, Toomre D, De Camilli P. A phosphoinositide switch controls the maturation and signalling properties of APPL endosomes. *Cell* 2009;136:1110-21.

[123] Tsukazaki T, Chiang TA, Davison AF, Attisano L, Wrana JL. SARA, a FYVE domain protein that recruits Smad2 to the TGFbeta receptor. *Cell* 1998;95:779-91.

[124] Chen YG, Wang Z, Ma J, Zhang L, Lu Z. Endofin, a FYVE domain protein, interacts with Smad4 and facilitates transforming growth factor-beta signalling. *The Journal of biological chemistry* 2007;282:9688-95.

[125] Hayes S, Chawla A, Corvera S. TGF beta receptor internalization into EEA1-enriched early endosomes: role in signalling to Smad2. *The Journal of cell biology* 2002;158:1239-49.

[126] DeFea KA, Zalevsky J, Thoma MS, Dery O, Mullins RD, Bunnett NW. beta-Arrestin-dependent endocytosis of proteinase-activated receptor 2 is required for intracellular targeting of activated ERK1/2. *Journal of Cell Biology* 2000;148:1267-81.

[127] Oakley RH, Laporte SA, Holt JA, Barak LS, Caron MG. Association of beta-arrestin with G protein-coupled receptors during clathrin-mediated endocytosis dictates the profile of receptor resensitization. *Journal of Biological Chemistry* 1999;274:32248-57.

[128] Huang FT, Kirkpatrick D, Jiang XJ, Gygi S, Sorkin A. Differential regulation of EGF receptor internalization and degradation by multiubiquitination within the kinase domain. *Mol Cell* 2006;21:737-48.

[129] Bache KG, Stuffers S, Malerod L, Slagsvold T, Raiborg C, Lechardeur D, et al. The ESCRT-III subunit hVps24 is required for degradation but not silencing of the epidermal growth factor receptor. *Molecular biology of the cell* 2006;17:2513-23.

[130] Cavalli V, Vilbois F, Corti M, Marcote MJ, Tamura K, Karin M, et al. The stress-induced MAP kinase p38 regulates endocytic trafficking via the GDI : Rab5 complex. *Mol Cell* 2001;7:421-32.

[131] Zwang Y, Yarden Y. p38 MAP kinase mediates stress-induced internalization of EGFR: implications for cancer chemotherapy. *Embo Journal* 2006;25:4195-206.

[132] Pelkmans L, Fava E, Grabner H, Hannus M, Habermann B, Krausz E, et al. Genome-wide analysis of human kinases in clathrin- and caveolae/raft-mediated endocytosis. *Nature* 2005;436:78-86.

[133] Johannessen LE, Pedersen NM, Pedersen KW, Madhus IH, Stang E. Activation of the epidermal growth factor (EGF) receptor induces formation of EGF receptor- and Grb2-containing clathrin-coated pits. *Mol Cell Biol* 2006;26:389-401.

[134] Rink J, Ghigo E, Kalaidzidis Y, Zerial M. Rab conversion as a mechanism of

progression from early to late endosomes. *Cell* 2005;122:735-49.

[135] Rozakisadcock M, Fernley R, Wade J, Pawson T, Bowtell D. The Sh2 and Sh3 Domains of Mammalian Grb2 Couple the Egf Receptor to the Ras Activator Msos1. *Nature* 1993;363:83-5.

[136] Jiang XJ, Huang FT, Marusyk A, Sorkin A. Grb2 regulates internalization of EGF receptors through clathrin-coated pits. *Molecular biology of the cell* 2003;14:858-70.

[137] Varsano T, Dong MQ, Niesman I, Gacula H, Lou X, Ma T, et al. GIPC is recruited by APPL to peripheral TrkA endosomes and regulates TrkA trafficking and signalling. *Mol Cell Biol* 2006;26:8942-52.

[138] Sorkin A, von Zastrow M. Endocytosis and signalling: intertwining molecular networks. *Nature reviews Molecular cell biology* 2009;10:609-22.

[139] Di Fiore PP, von Zastrow M. Endocytosis, signalling, and beyond. *Cold Spring Harb Perspect Biol* 2014;6.

[140] Downward J. Targeting ras signalling pathways in cancer therapy. *Nat Rev Cancer* 2003;3:11-22.

[141] Santarpia L, Lippman SM, El-Naggar AK. Targeting the MAPK-RAS-RAF signalling pathway in cancer therapy. *Expert Opin Ther Tar* 2012;16:103-19.

[142] Wennerberg K, Rossman KL, Der CJ. The Ras superfamily at a glance. *Journal of cell science* 2005;118:843-6.

[143] Barbieri MA, Kohn AD, Roth RA, Stahl PD. Protein kinase B/akt and Rab5 mediate ras activation of endocytosis. *Journal of Biological Chemistry* 1998;273:19367-70.

[144] Pylayeva-Gupta Y, Grabocka E, Bar-Sagi D. RAS oncogenes: weaving a tumorigenic web. *Nat Rev Cancer* 2011;11:761-74.

[145] Kranenburg O, Verlaan I, Moolenaar WH. Dynamin is required for the activation of mitogen-activated protein (MAP) kinase by MAP kinase kinase. *Journal of Biological Chemistry* 1999;274:35301-4.

[146] Jiang XJ, Sorkin A. Coordinated traffic of Grb2 and Ras during epidermal

growth factor receptor endocytosis visualized in living cells. *Molecular biology of the cell* 2002;13:1522-35.

[147] Pinilla-Macua I, Watkins SC, Sorkin A. Endocytosis separates EGF receptors from endogenous fluorescently labeled HRas and diminishes receptor signalling to MAP kinases in endosomes. *Proceedings of the National Academy of Sciences of the United States of America* 2016;113:2122-7.

[148] Han L, Wong D, Dhaka A, Afar D, White M, Xie W, et al. Protein binding and signalling properties of RIN1 suggest a unique effector function. *Proceedings of the National Academy of Sciences of the United States of America* 1997;94:4954-9.

[149] Wang Y, Waldron RT, Dhaka A, Patel A, Riley MM, Rozengurt E, et al. The RAS effector RIN1 directly competes with RAF and is regulated by 14-3-3 proteins. *Mol Cell Biol* 2002;22:916-26.

[150] Tall GG, Barbieri MA, Stahl PD, Horazdovsky BF. Ras-activated endocytosis is mediated by the Rab5 guanine nucleotide exchange activity of RIN1. *Developmental cell* 2001;1:73-82.

[151] Barbieri MA, Tall GG, Horazdovsky BF, Stahl PD. Receptor-mediated endocytosis: EGF/Ras-activated endocytosis is mediated by Rab5 and the Rab5 guanine nucleotide exchange activity of RIN1. *Faseb J* 2001;15:A1162-A.

[152] Barsagi D, Feramisco JR. Induction of Membrane Ruffling and Fluid-Phase Pinocytosis in Quiescent Fibroblasts by Ras Proteins. *Science* 1986;233:1061-8.

[153] Han LM, Wong D, Dhaka A, Afar D, White M, Xie WL, et al. Protein binding and signalling properties of RIN1 suggest a unique effector function. *Proceedings of the National Academy of Sciences of the United States of America* 1997;94:4954-9.

[154] Xu LZ, Lubkov V, Taylor LJ, Bar-Sagi D. Feedback Regulation of Ras Signalling by Rabex-5-Mediated Ubiquitination. *Curr Biol* 2010;20:1372-7.

[155] Tam SY, Tsai M, Snouwaert JN, Kalesnikoff J, Scherrer D, Nakae S, et al. RabGEF1 is a negative regulator of mast cell activation and skin inflammation. *Nat Immunol* 2004;5:844-52.

[156] Mattera R, Tsai YC, Weissman AM, Bonifacino JS. The Rab5 guanine

nucleotide exchange factor Rabex-5 binds ubiquitin (Ub) and functions as a Ub ligase through an atypical Ub-interacting motif and a zinc finger domain. *Journal of Biological Chemistry* 2006;281:6874-83.

[157] Semerdjieva S, Shortt B, Maxwell E, Singh S, Fonarev P, Hansen J, et al. Coordinated regulation of AP2 uncoating from clathrin-coated vesicles by rab5 and hRME-6. *Journal of Cell Biology* 2008;183:499-511.

[158] Hunker CM, Galvis A, Kruk I, Giambini H, Veisaga ML, Barbieri MA. Rab5-activating protein 6, a novel endosomal protein with a role in endocytosis. *Biochemical and biophysical research communications* 2006;340:967-75.

[159] Su X, Kong C, Stahl PD. GAPex-5 mediates ubiquitination, trafficking, and degradation of epidermal growth factor receptor. *Journal of Biological Chemistry* 2007;282:21278-84.

[160] Sato M, Sato K, Fonarev P, Huang CJ, Liou W, Grant BD. *Caenorhabditis elegans* RME-6 is a novel regulator of RAB-5 at the clathrin-coated pit. *Nat Cell Biol* 2005;7:559-U7.

[161] Conner SD, Schmid SL. Regulated portals of entry into the cell. *Nature* 2003;422:37-44.

[162] Stenmark H. Rab GTPases as coordinators of vesicle traffic. *Nat Rev Mol Cell Bio* 2009;10:513-25.

[163] Ricotta D, Conner SD, Schmid SL, von Figura K, Honing S. Phosphorylation of the AP2 mu subunit by AAK1 mediates high affinity binding to membrane protein sorting signals. *Journal of Cell Biology* 2002;156:791-5.

[164] Waterman H, Yarden Y. Molecular mechanisms underlying endocytosis and sorting of ErbB receptor tyrosine kinases. *FEBS letters* 2001;490:142-52.

[165] Joazeiro CAP, Wing SS, Huang HK, Leverson JD, Hunter T, Liu YC. The tyrosine kinase negative regulator c-Cbl as a RING-type, E2-dependent ubiquitin-protein ligase. *Science* 1999;286:309-12.

[166] Ravid T, Heidinger JM, Gee P, Khan EM, Goldkorn T. c-Cbl-mediated ubiquitylation is required for epidermal growth factor receptor exit from the early

endosomes. *Journal of Biological Chemistry* 2004;279:37153-62.

[167] Wu WJ, Tu S, Cerione RA. Activated Cdc42 sequesters c-Cbl and prevents EGF receptor degradation. *Cell* 2003;114:715-25.

[168] Kelly KL, Ruderman NB, Chen KS. Phosphatidylinositol-3-Kinase in Isolated Rat Adipocytes - Activation by Insulin and Subcellular-Distribution. *Journal of Biological Chemistry* 1992;267:3423-8.

[169] Kelly KL, Ruderman NB. Insulin-Stimulated Phosphatidylinositol 3-Kinase - Association with a 185-Kda Tyrosine-Phosphorylated Protein (Irs-1) and Localization in a Low-Density Membrane Vesicle. *Journal of Biological Chemistry* 1993;268:4391-8.

[170] Liu J, Kimura A, Bauman CA, Saltiel AR. APS facilitates c-Cbl tyrosine phosphorylation and GLUT4 translocation in response to insulin in 3T3-L1 adipocytes. *Diabetes* 2002;51:A396-A7.

[171] Liu J, DeYoung SM, Hwang JB, O'Leary EE, Saltiel AR. The roles of Cbl-b and c-Cbl in insulin-stimulated glucose transport. *Journal of Biological Chemistry* 2003;278:36754-62.

[172] Chiang SH, Baumann CA, Kanzaki M, Thurmond DC, Watson RT, Neudauer CL, et al. Insulin-stimulated GLUT4 translocation requires the CAP-dependent activation of TC10. *Nature* 2001;410:944-8.

[173] Chang L, Adams RD, Saltiel AR. The TC10-interacting protein CIP4/2 is required for insulin-stimulated Glut4 translocation in 3T3L1 adipocytes. *Proceedings of the National Academy of Sciences of the United States of America* 2002;99:12835-40.

[174] Lodhi IJ, Chiang SH, Chang L, Vollenweider D, Watson RT, Inoue M, et al. Gapex-5, a Rab31 guanine nucleotide exchange factor that regulates Glut4 trafficking in adipocytes. *Cell Metab* 2007;5:59-72.

[175] Lodhi IJ, Chiang SH, Chang L, Vollenweider D, Watson RT, Inoue M, et al. Gapex-5, a Rab31 guanine nucleotide exchange factor that regulates Glut4 trafficking in adipocytes. *Cell Metab* 2007;5:59-72.

[176] Lodhi IJ, Bridges D, Chiang SH, Zhang YL, Cheng A, Geletka LM, et al. Insulin

stimulates phosphatidylinositol 3-phosphate production via the activation of Rab5. *Molecular biology of the cell* 2008;19:2718-28.

[177] Fukuhara S, Sako K, Noda K, Zhang J, Minami M, Mochizuki N. Angiopoietin-1/Tie2 receptor signalling in vascular quiescence and angiogenesis. *Histology and histopathology* 2010;25:387-96.

[178] McClure SJ, Robinson PJ. Dynamin, endocytosis and intracellular signalling (review). *Mol Membr Biol* 1996;13:189-215.

[179] Zhang Z, Zhang TL, Wang SS, Gong Z, Tang C, Chen JY, et al. Molecular mechanism for Rabex-5 GEF activation by Rabaptin-5. *Elife* 2014;3.

[180] Zhu HP, Liang ZM, Li GP. Rabex-5 Is a Rab22 Effector and Mediates a Rab22-Rab5 Signalling Cascade in Endocytosis. *Molecular biology of the cell* 2009;20:4720-9.

[181] Aikawa Y. Rabex-5 Protein Regulates the Endocytic Trafficking Pathway of Ubiquitinated Neural Cell Adhesion Molecule L1. *Journal of Biological Chemistry* 2012;287:32312-23.

[182] Carlton JG, Cullen PJ. Sorting nexins. *Curr Biol* 2005;15:R819-R20.

[183] Worby CA, Dixon JE. Sorting out the cellular functions of sorting nexins. *Nat Rev Mol Cell Bio* 2002;3:919-31.

[184] Seet LF, Hong WJ. The Phox (PX) domain proteins and membrane traffic. *Bba-Mol Cell Biol L* 2006;1761:878-96.

[185] Cullen PJ. Endosomal sorting and signalling: an emerging role for sorting nexins. *Nat Rev Mol Cell Bio* 2008;9:574-82.

[186] Wang Q, Kaan HYK, Hooda RN, Goh SL, Sondermann H. Structure and Plasticity of Endophilin and Sorting Nexin 9. *Structure* 2008;16:1574-87.

[187] Lundmark R, Carlsson SR. Sorting nexin 9 participates in clathrin-mediated endocytosis through interactions with the core components. *Journal of Biological Chemistry* 2003;278:46772-81.

[188] Ringstad N, Nemoto Y, DeCamilli P. The SH3p4/Sh3p8/SH3p13 protein family: Binding partners for synaptojanin and dynamin via a Grb2-like Src homology 3 domain.

Proceedings of the National Academy of Sciences of the United States of America 1997;94:8569-74.

[189] Shin N, Lee S, Ahn N, Kim SA, Ahn SG, YongPark Z, et al. Sorting nexin 9 interacts with dynamin 1 and N-WASP and coordinates synaptic vesicle endocytosis. *Journal of Biological Chemistry* 2007;282:28939-50.

[190] Lin Q, Lo CG, Cerione RA, Yang W. The Cdc42 target ACK2 interacts with sorting nexin 9 (SH3PX1) to regulate epidermal growth factor receptor degradation. *Journal of Biological Chemistry* 2002;277:10134-8.

[191] Yarar D, Waterman-Storer CM, Schmid SL. SNX9 couples actin assembly to Phosphoinositide signals and is required for membrane remodeling during endocytosis. *Developmental cell* 2007;13:43-56.

[192] Wright PK, May FEB, Darby S, Saif R, Lennard TWJ, Westley BR. Estrogen Regulates Vesicle Trafficking Gene Expression in EFF-3, EFM-19 and MCF-7 Breast Cancer Cells. *Int J Clin Exp Patho* 2009;2:463-75.

[193] Danson C, Brown E, Hemmings OJ, McGough IJ, Yarwood S, Heesom KJ, et al. SNX15 links clathrin endocytosis to the PtdIns3P early endosome independently of the APPL1 endosome. *Journal of cell science* 2013;126:4885-99.

[194] Brown MD, Sacks DB. IQGAP1 in cellular signalling: bridging the GAP. *Trends in cell biology* 2006;16:242-9.

[195] Briggs MW, Sacks DB. IQGAP proteins are integral components of cytoskeletal regulation. *Embo Rep* 2003;4:571-4.

[196] Mateer SC, Wang NN, Bloom GS. IQGAPs: Integrators of the cytoskeleton, cell adhesion machinery, and signalling networks. *Cell Motil Cytoskel* 2003;55:147-55.

[197] Roy M, Li ZG, Sacks DB. IQGAP1 binds ERK2 and modulates its activity. *Journal of Biological Chemistry* 2004;279:17329-37.

[198] Kimura T, Yamaoka M, Taniguchi S, Okamoto M, Takei M, Ando T, et al. Activated Cdc42-Bound IQGAP1 Determines the Cellular Endocytic Site. *Mol Cell Biol* 2013;33:4834-43.

[199] McNulty DE, Li ZG, White CD, Sacks DB, Annan RS. MAPK Scaffold IQGAP1

Binds the EGF Receptor and Modulates Its Activation. *Journal of Biological Chemistry* 2011;286:15010-21.

[200] Blagoev B, Kratchmarova I, Ong SE, Nielsen M, Foster LJ, Mann M. A proteomics strategy to elucidate functional protein-protein interactions applied to EGF signalling. *Nat Biotechnol* 2003;21:315-8.

[201] Roy M, Li ZG, Sacks DB. IQGAP1 is a scaffold for mitogen-activated protein kinase signalling. *Mol Cell Biol* 2005;25:7940-52.

[202] Sambrook J, Russell DW. Calcium-phosphate-mediated Transfection of Eukaryotic Cells with Plasmid DNAs. *CSH protocols* 2006;2006.

[203] Du LL, Novick P. Purification and properties of a GTPase-activating protein for yeast Rab GTPases. *Methods in enzymology* 2001;329:91-9.

[204] Sato M, Sato K, Fonarev P, Huang CJ, Liou W, Grant BD. *Caenorhabditis elegans* RME-6 is a novel regulator of RAB-5 at the clathrin-coated pit. *Nature cell biology* 2005;7:559-69.

[205] Su X, Kong C, Stahl PD. GAPex-5 mediates ubiquitination, trafficking, and degradation of epidermal growth factor receptor. *The Journal of biological chemistry* 2007;282:21278-84.

[206] Semerdjieva S, Shortt B, Maxwell E, Singh S, Fonarev P, Hansen J, et al. Coordinated regulation of AP2 uncoating from clathrin-coated vesicles by rab5 and hRME-6. *The Journal of cell biology* 2008;183:499-511.

[207] Korolchuk VI, Banting G. CK2 and GAK/auxilin2 are major protein kinases in clathrin-coated vesicles. *Traffic* 2002;3:428-39.

[208] Ji H, Wang J, Nika H, Hawke D, Keezer S, Ge Q, et al. EGF-induced ERK activation promotes CK2-mediated disassociation of alpha-Catenin from beta-Catenin and transactivation of beta-Catenin. *Mol Cell* 2009;36:547-59.

[209] Gibbs JB, Schaber MD, Allard WJ, Sigal IS, Scolnick EM. Purification of Ras Gtpase Activating Protein from Bovine Brain. *Proceedings of the National Academy of Sciences of the United States of America* 1988;85:5026-30.

[210] Er EE, Mendoza MC, Mackey AM, Rameh LE, Blenis J. AKT Facilitates EGFR

Trafficking and Degradation by Phosphorylating and Activating PIKfyve. *Sci Signal* 2013;6.

[211] Ji HT, Wang J, Nika H, Hawke D, Keezer S, Ge QY, et al. EGF-Induced ERK Activation Promotes CK2-Mediated Disassociation of alpha-Catenin from beta-Catenin and Transactivation of beta-Catenin. *Mol Cell* 2009;36:547-59.

[212] Xia K, Zhang S, Bathrick B, Liu S, Garcia Y, Colon W. Quantifying the kinetic stability of hyperstable proteins via time-dependent SDS trapping. *Biochemistry* 2012;51:100-7.

[213] Kluger R, Alagic A. Chemical cross-linking and protein-protein interactions-a review with illustrative protocols. *Bioorganic chemistry* 2004;32:451-72.

[214] Delprato A, Merithew E, Lambright DG. Structure, exchange determinants, and family-wide rab specificity of the tandem helical bundle and Vps9 domains of Rabex-5. *Cell* 2004;118:607-17.

[215] Scheffzek K, Ahmadian MR, Kabsch W, Wiesmuller L, Lautwein A, Schmitz F, et al. The Ras-RasGAP complex: structural basis for GTPase activation and its loss in oncogenic Ras mutants. *Science* 1997;277:333-8.

[216] Kuhlbrandt W. Cryo-EM enters a new era. *Elife* 2014;3:e03678.

[217] Bai XC, McMullan G, Scheres SH. How cryo-EM is revolutionizing structural biology. *Trends Biochem Sci* 2015;40:49-57.

[218] Nogales E. The development of cryo-EM into a mainstream structural biology technique. *Nature methods* 2016;13:24-7.

[219] Ward JH, Jordan I, Kushner JP, Kaplan J. Heme regulation of HeLa cell transferrin receptor number. *The Journal of biological chemistry* 1984;259:13235-40.

[220] Roux KJ, Kim DI, Burke B. BioID: a screen for protein-protein interactions. *Current protocols in protein science / editorial board, John E Coligan [et al]* 2013;74:Unit 19 23.

[221] Reddy RJ, Gajadhar AS, Swenson EJ, Rothenberg DA, Curran TG, White FM. Early signalling dynamics of the epidermal growth factor receptor. *Proceedings of the National Academy of Sciences of the United States of America* 2016;113:3114-9.

[222] Taylor MJ, Perrais D, Merrifield CJ. A high precision survey of the molecular dynamics of mammalian clathrin-mediated endocytosis. *Plos Biol* 2011;9:e1000604.

[223] Hu JH, Troglio F, Mukhopadhyay A, Everingham S, Kwok E, Scita G, et al. F-BAR-containing adaptor CIP4 localizes to early endosomes and regulates Epidermal Growth Factor Receptor trafficking and downregulation. *Cell Signal* 2009;21:1686-97.

[224] McNulty DE, Li Z, White CD, Sacks DB, Annan RS. MAPK scaffold IQGAP1 binds the EGF receptor and modulates its activation. *The Journal of biological chemistry* 2011;286:15010-21.

[225] Bashour AM, Fullerton AT, Hart MJ, Bloom GS. IQGAP1, a Rac- and Cdc42-binding protein, directly binds and cross-links microfilaments. *The Journal of cell biology* 1997;137:1555-66.

[226] Starling GP, Yip YY, Sanger A, Morton PE, Eden ER, Dodding MP. Folliculin directs the formation of a Rab34-RILP complex to control the nutrient-dependent dynamic distribution of lysosomes. *Embo Rep* 2016;17:823-41.

[227] Sigismund S, Woelk T, Puri C, Maspero E, Tacchetti C, Transidico P, et al. Clathrin-independent endocytosis of ubiquitinated cargos. *Proceedings of the National Academy of Sciences of the United States of America* 2005;102:2760-5.

[228] Sigismund S, Algisi V, Nappo G, Conte A, Pascolutti R, Cuomo A, et al. Threshold-controlled ubiquitination of the EGFR directs receptor fate. *The EMBO journal* 2013;32:2140-57.

[229] Phillips MJ, Voeltz GK. Structure and function of ER membrane contact sites with other organelles. *Nature reviews Molecular cell biology* 2016;17:69-82.